Behavior of Stiffened Compression Flanges of Trapezoidal Box Girder Bridges

by

Reagan Sentelle Herman, B.S., M.S.

Dissertation

Presented to the Faculty of the Graduate School of

The University of Texas at Austin

in Partial Fulfillment

of the Requirements

for the Degree of

Doctor of Philosophy

The University of Texas at Austin

August 2001

Dedication

To Jerry

for his patience and love

The Dissertation Committee for Reagan Sentelle Herman
Certifies that this is the approved version of the following dissertation:

Behavior of Stiffened Compression Flanges of Trapezoidal Box Girder Bridges

Committee:

Karl H. Frank, Supervisor

Eric B. Becker

John E. Breen

Sharon L. Wood

Joseph A. Yura

Acknowledgements

The financial support of the Texas Department of Transportation, which made this research project possible, is greatly appreciated. The assistance of Texas Department of Transportation personnel is also appreciated.

Many people have made significant contributions to the execution and completion of this work. I am grateful to my doctoral advisor, Dr. Karl H. Frank, for his advice and support of this research. I also appreciate the help and guidance of my doctoral committee, Drs. Joseph A. Yura, Eric B. Becker, John E. Breen and Sharon L. Wood.

My sincere thanks are extended to all the staff members at Ferguson Structural Engineering Laboratory, and particularly Regina Forward, Blake Stassney, and Mike Bell, for their assistance and support. I am indebted to Chris Gilchrist, Charles Barnes, Sergio Brena, Keith Thompson, Andrea Schokker, Jeff West, Brad Koester, Robert Barnes, David Jauregui, Scott Civjan, Jenny Tanner, and many other fellow graduate students for their friendship and willingness to lend a hand when it was needed.

I am deeply thankful to my parents and sisters for their love and support. Without the encouragement of my family I would not be where I am today. To my husband, Jerry, I give my deepest thanks for his patience and love. Completion of this work would not have been possible without his support.

Behavior of Stiffened Compression Flanges of Trapezoidal Box Girder Bridges

Publication No._____

Reagan Sentelle Herman, Ph.D.

The University of Texas at Austin, 2001

Supervisor: Karl H. Frank

Steel trapezoidal box girder systems are seeing increased use based on their high torsional stiffness and aesthetic appearance. This dissertation research is part of a study sponsored by the Texas Department of Transportation investigating various aspects of design and behavior of trapezoidal box girder bridge systems. The design equations contained in the bridge specifications of the American Association of State Highway and Transportation Officials (AASHTO) for the steel compression flange of box girders are different in form than other bracing-type equations and design equations contained in other box girder specifications. This dissertation research investigated the basis and validity of the AASHTO design equations and the general behavior of stiffened compression flanges of steel box girder bridges.

The basis of the design equations in the AASHTO specifications was researched and documented. The validity of the equations was investigated using eigenvalue finite element analyses results. A new formulation of the plate buckling coefficient equation, which corrects an error in the current formulation, is proposed. During the finite element study, it was noted that alternate stiffener designs, utilizing torsionally stiff longitudinal stiffeners, could result in significant increases of the elastic buckling strength of stiffened plates. An experimental program was undertaken to test the performance of plates stiffened with torsionally weak stiffeners, typical of current stiffener designs, as well as torsionally stiff longitudinal stiffeners. Both steel and concrete longitudinal stiffeners were tested.

The results of the experimental program revealed that the basis of the AASHTO design equations did not predict the experimental behavior of the stiffened plates tested. The assumption that longitudinal stiffeners of sufficient size will form straight nodal lines, about which the plate will buckle, was not supported by the results of the experimental tests. Many factors, including initial imperfections, stiffener eccentricity, overall girder bending, and second order effects have been shown to contribute to producing stiffener displacement. The AASHTO design equations result in conservative estimates of the capacity of slender stiffened plates but may indicate unconservative capacities for some stockier plate geometries. A modified design approach, which includes the influence of factors such as initial imperfections and stiffener eccentricity, should be considered for incorporation into the AASHTO specifications.

TABLE OF CONTENTS

LIST OF TABLES

LIST OF FIGURES

Chapter 1

Introduction

1.1 Overview

Box girder systems are seeing increased use because of their high torsional stiffness and aesthetic appearance. Engineers are typically less familiar with the design of steel box girders than more common steel plate girder bridges. A research project was sponsored by the Texas Department of Transportation (TxDOT) to examine several issues unique to box girder structures. This dissertation research, on the behavior of the steel compression flange of continuous box girder bridges in the negative moment region, was part of this TxDOT sponsored study.

Increased use of trapezoidal box systems in the United States in general, and Texas in particular, is due in large part to an increased interest in bridge aesthetics. The closed girders have a pleasing, clean appearance, since many bracing members and stiffeners are hidden within the girder. The closed box girder cross-sections provide a streamlined and slender appearance.

The closed shape of the box girders offers maintenance advantages as well as a pleasing appearance. The closed boxes have fewer potential corrosion issues, since the inside of the box remains dry and protected from the elements. Furthermore, the box systems do not require extensive use of external diaphragms between girders, so there are subsequently fewer places where water and debris can build-up and cause increased maintenance requirements. Inspection of the interior of box sections can be facilitated by using sections at least five feet in depth (Hall 1997).

In addition to the attractiveness of the box shape based on aesthetic and maintenance concerns, the closed shape offers significant structural advantages. Box girders have significantly higher torsional stiffness than comparable I-girder bridges, due to their closed shape. Steel trapezoidal box girder systems are subsequently an attractive alternative where long curved spans are required. The increased torsional stiffness leads to better transverse load distribution, which in turn leads to more efficient designs. Furthermore, the number of girders required to support a specified deck width can also be reduced using steel boxes. A drawback to steel trapezoidal box girder bridges is the fact that they are fracture critical.

Box girder designs have been widely acknowledged as being attractive, but have been perceived as more expensive than comparable I-girder bridges (Hall 1997). Advances in steel welding and fabrication procedures have reduced the fabrication cost of steel box girders. As familiarity with the fabrication and construction of box systems continues to increase, additional cost reductions should be realized.

1.2 Dissertation Overview

Steel trapezoidal box girder systems offer many structural, maintenance, and aesthetic advantages. However there are several stability issues that must be considered when designing box girders. One of the areas of concern is buckling of the bottom steel compression flange of box girders. The steel bottom flange of a continuous box girder is in compression in the negative moment region near interior supports, and consequently stability of the bottom flange is an issue of concern. The design equations currently contained in the bridge specifications of the American Association of State Highway and Transportation Officials (AASHTO) for stiffened flanges are different in formulation than other bracing-

design approaches, and are different from formulations contained in some other specifications.

This dissertation will address issues related to the behavior and design of the bottom steel flange of trapezoidal box girder bridges in compression. The research program completed contains both experimental and computational components. The basis of the AASTHO design equations was researched and is documented in this dissertation. An error in the formulation of the plate buckling coefficient equation was identified and an improved formulation is proposed. The validity of the AASHTO design equations was investigated using the results of eigenvalue finite element analyses. An alternate method of providing bottom flange stability through use of a composite bottom flange is discussed, and different stiffener designs that increase the elastic buckling capacity of the plate are explored. The expected magnitude of initial plate and stiffener imperfections and existing imperfection tolerances were researched. The impact of initial imperfections on stiffened plate behavior is discussed.

An experimental program was undertaken to test the performance of plates stiffened with torsionally weak stiffeners, typical of current stiffener designs, as well as alternate stiffener configurations that provide significant torsionally stiffness. Both steel and concrete longitudinal stiffeners were tested. The results of the experimental program are discussed and compared with finite element results. Additional finite element analyses that further explore the stiffened plate behavior seen in the experimental tests are discussed. Based on the results of the experimental tests and subsequent finite element analyses, a recommendation is made for consideration of an analysis approach different than that currently forming the basis of the AASHTO provisions.

1.3 Steel Box Girder Bridge Systems

Steel box girder systems used in North American construction generally consist of a pair of open steel U-shaped girders with a composite concrete deck that acts as the top flange of the box, as shown in Figure 1.1. Each steel trapezoidal box section consists of two top flanges, two webs, and a bottom flange. In negative moment regions, at interior piers in continuous spans, the bottom flange of the steel box girder is in compression. A limit state for design of the steel compression flange is buckling of this steel plate. Design of the bottom steel flange of trapezoidal box girders is based on work done by early pioneers of mechanics, including Timoshenko and Gere (Timoshenko 1961), on the behavior of plates in compression.

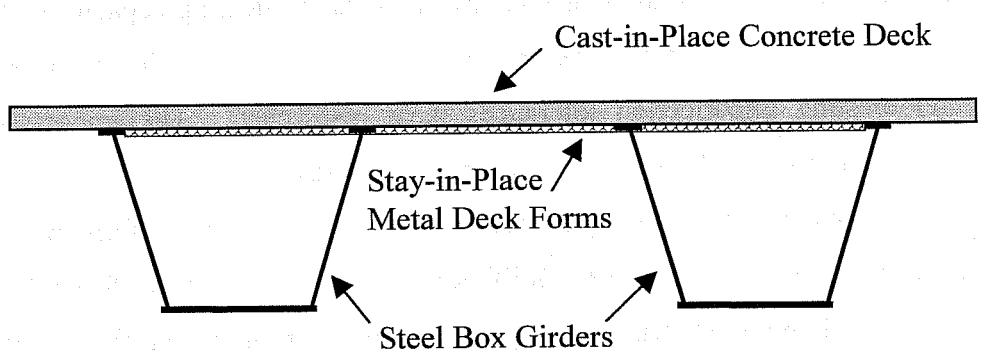

Figure 1.1 Cross-Section of Trapezoidal Box Girder System

There are several approaches available to ensure the steel compression flange element has adequate buckling capacity, including modifying the plate geometry and using longitudinal stiffeners. The buckling capacity of the flange is a function of the width, b, of the bottom flange and its thickness, t:

$$\sigma_{cr} \propto \frac{1}{(b/t)^2} \tag{1.1}$$

Therefore, decreasing the width of the flange or increasing its thickness increases the stability of the flange. However the width of the bottom flange may be set based on other factors, such as desired box size for the specified roadway width. Thus, the only traditional options to increase the buckling capacity of the flange are to increase the thickness of the plate, or add a longitudinal stiffener.

Increasing the thickness of the plate will always increase the stability of the bottom flange plate, but it is often not the most economical approach, based on the total weight of material used. It is often advisable to instead add a longitudinal stiffener to the plate. Using equally spaced longitudinal stiffeners is the most efficient way to proportion the steel material to resist the applied loads. The US practice for shorter spans, less than 200 ft., bridges is to use an unstiffened flange or a flange with a single longitudinal stiffener.

Longitudinal stiffeners commonly used in US highway construction are steel, tee-shaped stiffeners that are welded to the bottom flange of the girder. Flat plate stiffeners are sometimes used for longitudinal stiffeners of plates in compression, but are not as convenient for plates of the size used in typical box girder bridges, since they are more susceptible to torsional buckling. Furthermore, providing the required stiffener moment of inertia is also accomplished more efficiently using structural shapes rather than plate stiffeners. Zee-shaped bolted stiffeners are used heavily in the aircraft industry and welded tee-shaped stiffeners are the norm in North American bridge construction.

Generally either an unstiffened bottom flange or a flange with a single longitudinal stiffener, which bisects the width of the plate as shown in Figure 1.2, has been used in box girder bridges constructed in Texas. There are many steel

trapezoidal box girder bridges that have been recently constructed or are currently under design or construction in Texas. There are no known instances where multiple longitudinal stiffeners were used on the bottom flange of any of these structures. The preference of Texas Department of Transportation engineers is for designs utilizing unstiffened flanges, or at most a single longitudinal stiffener. Flanges with multiple stiffeners were subsequently not tested during this research program.

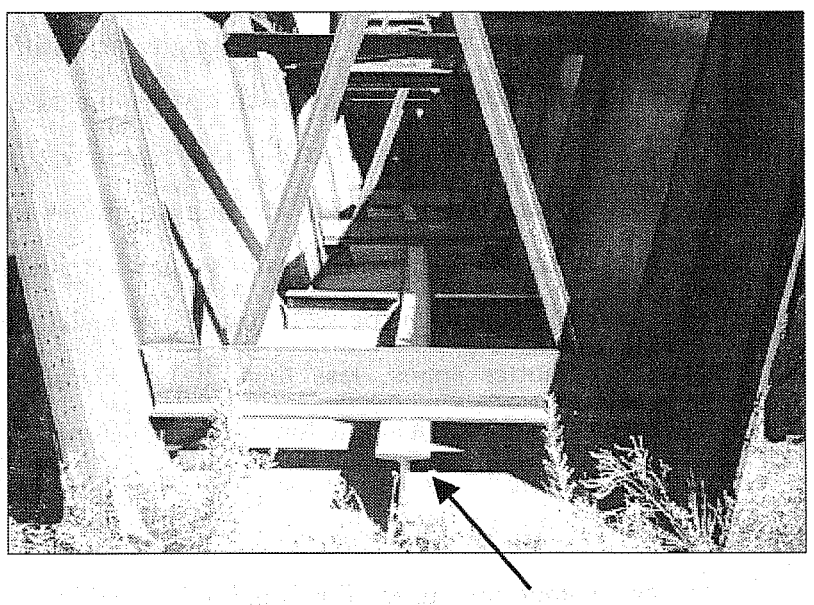

Figure 1.2 Compression Flange Longitudinal Stiffener

A survey of the Departments of Transportation (DOT) of various states was done using an e-mail list server sponsored by the AASHTO / National Steel Bridge Alliance Steel Bridge Collaboration. Kentucky DOT reports use of only unstiffened flanges in trapezoidal girder bridges to date. Illinois DOT has not used trapezoidal boxes for quite a few years based on cost studies, but reports use of both single and multiple longitudinal stiffeners in past designs. New York DOT often uses unstiffened flanges, but has designed bridges with one or two

longitudinal stiffeners. Colorado DOT has been making extensive use of box girder systems of late. They report use of stiffened flanges with more than one longitudinal stiffener in some of their structures. The Canadian steel box design specifications are analogous to those used in the US. The literature reports use of two to four longitudinal stiffeners on the bottom flanges of Canadian box girder bridges (Korol 1984).

Incorporation of stiffeners can render a more economical structure by placing the material where it can most efficiently resist the applied forces. The plate can be kept relatively thin while its stability is increased by inclusion of the longitudinal stiffener. The buckling capacity of the bottom flange plate of the box girder can be increased up to fourfold by using an appropriate longitudinal stiffener. The weight of the longitudinal stiffener is usually much smaller than the weight increase involved with simply increasing the plate thickness to handle the compressive forces (Timoshenko 1961).

For comparison, the capacity of a 60 in. wide by 0.5 in. thick compression flange was calculated using an unstiffened flange and a longitudinal stiffener sufficient to produce buckling of the flange into two waves transversely. The capacity of the flange, F_n, was calculated using the AASHTO LRFD Bridge Design Specification assuming a steel yield strength of 50 ksi. As shown in Figure 1.3, the capacity of the slender unstiffened flange is 7.28 ksi. When an ST5x12.7 longitudinal stiffener is added to the plate, the capacity is increased fourfold to 29.1 ksi. In order to obtain the same capacity as the stiffened plate with an unstiffened flange, the plate thickness must be doubled to 1 in.

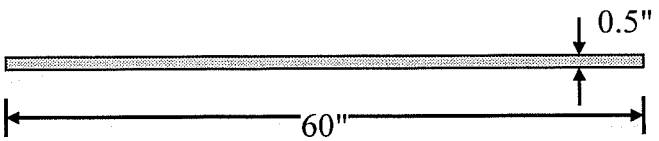

60" x 0. 5" Unstiffened Plate
F_n = 7.28 ksi
Plate Area = 30 in^2

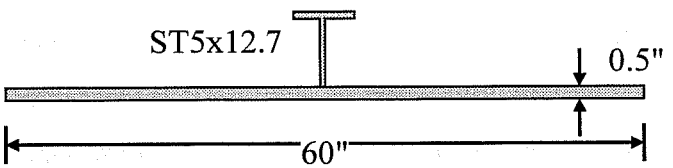

60" x 0.5" Plate with ST5x12.7 Longitudinal Stiffener
F_n = 29.1 ksi
Plate Area = 30 in^2, Stiffener Area = 3.73 in^2
Plate + Stiffener Area = 33.7 in^2

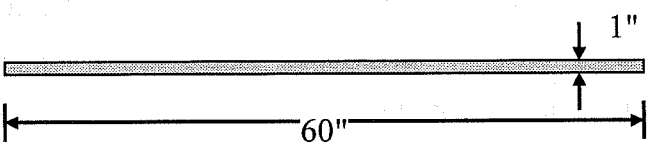

60" x 1" Unstiffened Plate
F_n = 29.1 ksi
Plate Area = 60 in^2

Figure 1.3 Unstiffened vs. Longitudinally Stiffened Flange

The cross-sectional areas of the unstiffened and stiffened flanges are also shown in Figure 1.3. Comparing the unstiffened and stiffened flanges with equal capacity, the stiffened flange has a total area of 33.7 in^2, while the unstiffened flange has a total area of 60 in^2. The area, and weight, of the compression flange

using the unstiffened design is almost 80% larger than the area of the stiffened flange design. Utilizing a stiffened flange instead of an unstiffened flange can decrease the weight of the compression flange significantly, however the added fabrication cost of welding the stiffener to the plate offsets some of the material savings.

1.4 North American vs. European Construction

In North America, the trend has been to use two or more boxes to form the bridge section rather than a single box configuration. Single box configurations are commonly used in Europe. Using twin or multiple boxes, the box girders are smaller in cross section, and the web and flange elements used have typically not been as slender as the plate panels used in the large European box girders.

The large boxes that have been constructed in Europe and Japan commonly use multiple longitudinal stiffeners, and closely spaced transverse stiffeners, on the bottom flange of the box. Compression flanges using five or more longitudinal stiffeners are commonplace in European designs and bridges with as many as 20 longitudinal stiffeners are referenced in the literature (ASCE 1974). In the United States the trend has been to use few or no longitudinal stiffeners. In Texas in particular, the preference of the Department of Transportation is for unstiffened flanges, or at most a single longitudinal stiffener.

The fabricators commonly involved with steel box production in Texas have also expressed a strong preference for unstiffened flanges. In a recent survey, a large supplier of steel boxes to the state of Texas stated that "it would always be preferable to thicken the bottom flange rather than adding bottom flange WT stiffeners. These stiffeners are very expensive especially when involved in a field bolted splice, which many times is the case (Chen 2000)." Based on this knowledge of the resistance to the use of heavily stiffened designs,

alternate methods that provide adequate bottom flange stability, without multiple stiffener use are attractive.

1.5 General AASHTO Requirements

The AASHTO specification contains requirements for cross-section layout of composite box girders. These requirements are presented in Section 6.11.1.1.1 of the LRFD Bridge Design Specifications. The same requirements, with slightly modified wording, are also contained in the AASHTO Standard Specifications. These requirements apply to simple and continuous bridges with span lengths up to 350 ft supported by two or more composite box sections. "The distance center-to-center of flanges of adjacent boxes, "a", taken at the midspan, shall neither be greater than 120 percent nor less than 80 percent of the distance center-to-center of the flanges in each adjacent box, w," as illustrated for two-girder in Figure 1.4. Additionally, for nonparallel box sections, "the distance center-to-center of adjacent flanges at supports shall neither be greater than 135 percent nor less than 65 percent of the distance center-to-center of the flanges of each adjacent box." Also, the distance center-to-center of flanges of each individual box, w, shall be the same.

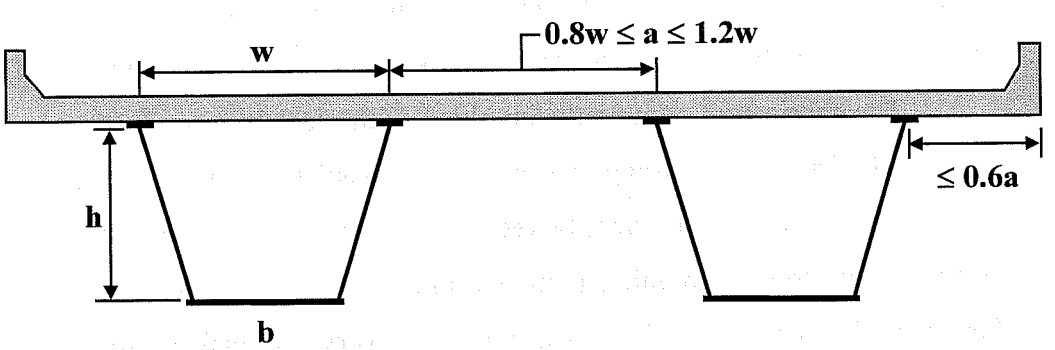

Figure 1.4 Box Layout

The cantilever overhang of the deck slab, including the curb and parapet, is also limited. The overhang "shall not be greater than 60 percent of the average distance between the centers of top steel flanges of adjacent box sections, "a", or 6.0 ft." The specifications permit the webs to be either perpendicular to the bottom flange or inclined to it. The inclination of web plates shall not exceed 1 to 4, as illustrated in Figure 1.5. Inclined webs are used to reduce the width of the bottom flange, b, thereby increasing its buckling capacity.

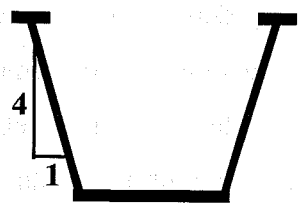

Figure 1.5 Web Inclination Limit

The basis of the limitations on box layout specified in Article 6.11 is discussed in the commentary to the specification. The commentary states that the limitations specified are necessary because the provisions concerning lateral distribution of loads, secondary distortional bending stresses, and the effectiveness of the bottom flange plate are based on extensive study of multiple box girder bridges that conform to these limitations. Reasonable limits were placed on the distance between girders, "a," and width of the girders, w, based on the criteria used in the studies forming the basis of the code provisions. The limitations allow for some flexibility of layout in design while maintaining correlation with the geometry used in the box girder studies (Mattock 1967). The extent to which conclusions drawn from these studies are valid for box girder bridges not conforming to the specified limitations is uncertain (Mattock 1967). Bridges that do not conform to these limitations should be investigated using one of the available methods of refined structural analysis. Bridges outside of the

limitations presented have been constructed in the US. A recent example is the Storrow Drive Connector Bridge in Boston, Massachusetts completed in 1999. The Storrow Drive Bridge supports a 76 ft. wide roadway using a single-cell trapezoidal girder (Kumarasena 2001).

Both the requirements for spacing between adjacent boxes and the web inclination limitation can influence the bottom flange width of the box girder in the absence of a refined analysis procedure. As already discussed, the stability of the bottom flange is directly dependant on its width. The total roadway width is typically dictated by road geometry requirements and is set before the type of bridge superstructure is selected. The geometry of the box and the geometry of the full bridge cross-section impact the width of the bottom flange. Figure 1.4 shows the full cross-section and relative dimensions for a bridge with two girders. The typical steel trapezoidal box girder design in North America is designed uses two girders. The road width is the sum of the overhangs, box widths, and the spacing between the boxes. The width of the parapets is disregarded in the following calculations.

To minimize the width of the bottom flange, the width of the box must be minimized. To minimize the box width, the overhang width and spacing between boxes must be maximized to obtain the desired road width. Thus, the selected condition would be:

$$\text{road width} = 2(0.6 \times 1.2\text{w}) + 2\text{w} + 1.2\text{w} \tag{1.2}$$

$$\text{w} = \frac{\text{road width}}{4.64} \tag{1.3}$$

The minimum bottom flange width would then be obtained using the maximum allowed web inclination, which results in

$$b = w - 2\left(\frac{h}{4}\right) \tag{1.4}$$

$$b = \frac{\text{road width}}{4.64} - \frac{h}{2} \tag{1.5}$$

Using a larger h can result in smaller bottom flange width. However, the height of the boxes is typically limited by other considerations. Taller boxes require taller piers in interchange construction. Larger web height also results in lower web bending and shear buckling capacity. Figure 1.6 shows the layout of the box and bridge cross-sections using a 34 ft. roadwidth and 6 ft. box height, and minimized width 52 in. bottom flange.

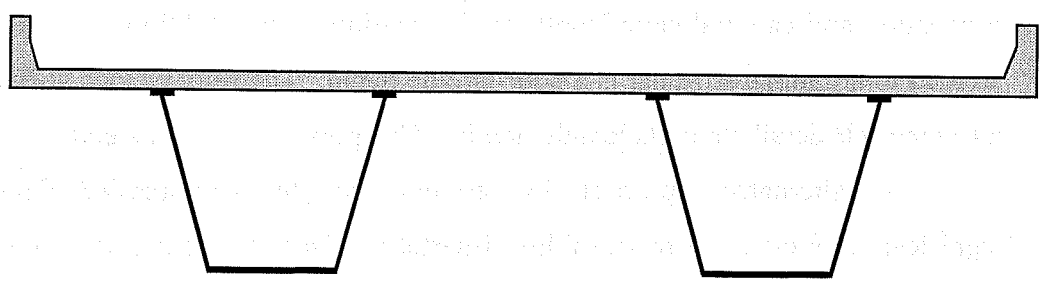

Figure 1.6 Box Layout with Minimum Bottom Flange Width

The minimum bottom flange width available to the designer using AASHTO is tied to the overall geometry considerations and cannot always be reduced simply to increase the buckling capacity of the flange without considering the overall geometry of the bridge. Consequently the only available options available to the designer to increase the capacity of the bottom flange may be to increase the thickness of the plate, add traditional longitudinal stiffeners, or utilize some other stiffening approach. An alternate stiffening approach that is of

significant interest is use of a composite bottom flange. A composite bottom flange is formed by adding a concrete slab to the steel bottom flange, producing a composite steel-concrete panel. Use of a composite bottom flange offers better fatigue properties than welded longitudinal stiffeners, takes advantage of concrete's compressive strength, and can eliminate the plate buckling failure mode.

1.6 Composite Bottom Flange

The usual approaches to prevent buckling of the bottom steel flange are to increase the thickness of the flange or add longitudinal stiffeners to the flange. Simply increasing the thickness of the flange to handle the compressive stress can result in a significant increase in the amount of material required and weight of the box. Adding a longitudinal stiffener increases the complexity of the design procedure, and can add significantly to fabrication costs. Additionally, the fully welded longitudinal stiffener is a poor fatigue detail. The fully welded stiffener is a Category B detail along its length, and is a Category E detail at its ends.

An alternative approach for strengthening the compression flange of significant interest at the onset of this dissertation research was use of a composite steel-concrete flange. Use of a bottom concrete slab in the negative moment region, in addition to the concrete used in the traditional bridge deck, is called a double-composite design. Figure 1.7 shows a negative moment section for a double-composite box girder bridge design. The concept of using steel bridges with "double-composite" action has been considered for both plate and box girder bridges. A typical cross-section of a double composite plate girder bridge in the negative moment region is shown in Figure 1.8.

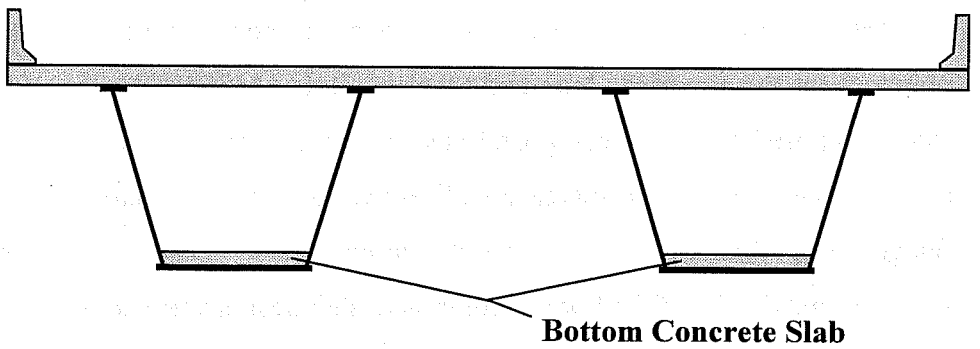

Figure 1.7 Double-Composite Box Girder Design

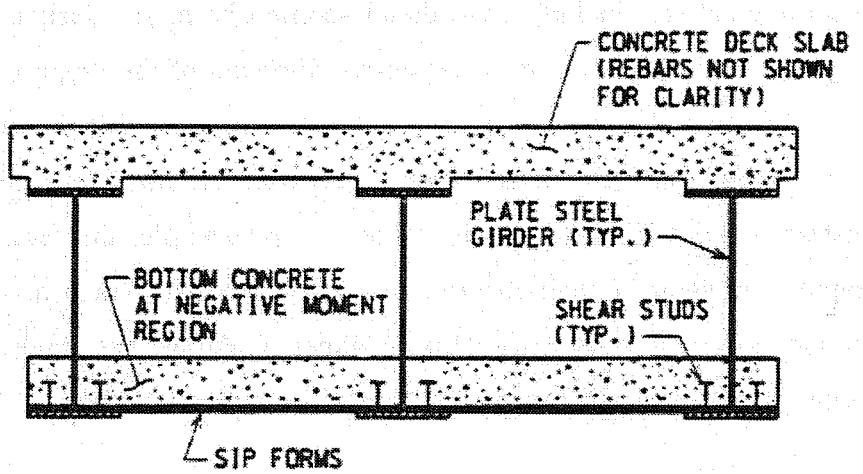

Figure 1.8 Double-Composite Plate Girder (Sen 1999)

There are a few examples of double-composite bridges that have been constructed internationally, including the Pont d'Illarsaz, Switzerland (Johnson 1986), at least three examples in Germany (Sen 1999), and the Ciervana Bridge in Spain (Sen 1999). No example of a constructed structure with a composite bottom flange was found in the United States. However, use of concrete bottom slabs at negative moment regions for double-composite action has been proposed in the United States. Such a proposal was made in a study that presented

conceptual and preliminary designs for innovative short and medium span bridges prepared for the American Iron and Steel Institute (AISI) (J. Muller 1996). This study proposed use of a composite steel-concrete bottom slab for a single-cell steel box girder design to increase stiffness while avoiding increasing the bottom flange plate thickness. A conceptual/preliminary design is presented, but specifics and details of the bottom composite slab design were not explored.

The double-composite preliminary design presented in the study by J. Muller was of a wide single box girder supporting a road width adequate for two lanes of traffic. The study included a weight and cost comparison of six different design alternatives, including the double-composite action design. The double-composite design was the most expensive alternate of the proposed alternatives, and was the only design more expensive than the "typical" LRFD Design.

Use of composite bottom flanges has also been considered in the design of constructed bridges in the United States. For example, the feasibility and the economy of using a steel-concrete composite bottom flange at the main pier locations of Boston's Storrow Drive Connector Bridge was investigated at the onset of the final design, but was ruled out (Kumarasena 2001).

1.6.1 Florida Concept Study

A report prepared for the Florida Department of Transportation entitled "Development of a New Concept for Florida's Bridges" also proposed use of steel bridges with double-composite action (Sen 1999). The report provides results of an initial study on the use of double-composite design based on "existing tools and design methods." The study recommends use of a concrete bottom slab in the negative moment region to replace relatively costly steel with less costly concrete. Additionally, the study states that inclusion of the bottom concrete slab can make more efficient use of the bottom flange steel. This more efficient use is enabled

by the concrete slab fully bracing the steel flange. Another benefit listed in the study is reduction in the number of internal cross frames as a result of the bracing of the steel flange provided by the concrete slab. The study also mentions that use of double-composite action results in a favorable distribution of moments in the bridge due to the increased stiffness over interior piers (Sen 1999).

A principal goal of the Florida study was to evaluate the potential economy of a double-composite design as compared with more conventional composite girder design. Trial three span designs using both double-composite and conventional design approaches were completed. The double-composite options include both a plate girder design and a box girder design. The trial designs showed significant cost savings using the double-composite approach, and the study concludes that "the double-composite bridge concept appears to be a viable and economical bridge alternative (Sen 1999)." Though the Florida study found the double-composite design to be a favorable alternative based on trial designs results, a thorough examination of the details associated with double-composite design was not completed.

1.6.2 Lehigh Composite Bottom Flange Study

A comprehensive study of composite bottom flanges was sponsored by the US Department of Transportation and performed by researchers at Lehigh University (Yen 1986). This study was undertaken specifically to investigate the use of composite steel-concrete compression flanges in the negative moment regions of continuous steel box girder bridges. The study by Yen et al. included preliminary analyses of several bridge designs to assess the modifications and improvements to the prior design with the inclusion of double-composite action. Experimental tests were performed on panel and box girder specimens to demonstrate the increase in capacity, and change in failure mode, accompanying

the addition of plain concrete to the steel flange. No reinforcement was used in the concrete slabs in any of the tests performed. The researchers presented a design procedure for composite bottom flanges, and proposed that rules and guidelines be introduced to the AASHTO specifications for composite bottom flanges (Yen 1986).

The Lehigh researchers found that incorporation of a composite bottom flange enabled the reduction or elimination of haunches in the negative moment region of existing steel box girder designs. They found that bearing of concrete slabs on box girder diaphragms was "essential to the development of the full strength of the composite compression flange." Even though shrinkage and creep may result in a gap between the diaphragms and the slab, they concluded that "within the practical range of component member dimensions shrinkage and creep are not likely to present concerns of behavior of composite compression flanges (Yen 1986)."

Though not expressly stated, the composite panel specimens constructed for the study seemed to be designed to fail at four times the capacity of the bare steel plate. This capacity is analogous to the capacity of a steel plate with a longitudinal stiffener that forces two half-waves transversely in the buckled shape of the plate permitting use of a plate buckling coefficient of 4. The failure load of two of the panel specimens reached or surpassed the apparent ultimate design capacity (four times the capacity of the bare steel). Failure modes included crushing of the concrete and yielding of the steel plate in compression, and cracking of the concrete. A third specimen was designed with larger stud spacing, and the predicted failure mode was local buckling between two rows of stud connectors. The specimen did fail at a lower load due to local buckling between the connectors. Another panel specimen was designed to explore what happened with a very minimal number of supplied shear connectors. This specimen also

failed at a lower load than the specimens with an adequate number of shear connectors.

This study also included testing of box girder segments with composite bottom flanges to examine the influence of moment gradients on the performance of the composite flange. Segments failed by upward buckling (towards the concrete slab) of the bottom flange in three of the tests. The tests indicated no significant difference under either different moment gradients or concrete strength under the prevailing failure mode.

In the fourth box girder segment test one end of the concrete slab was made to bear on the cross member of the diaphragm by grouting. The other end of the concrete slab was blocked against the flanges of the diaphragm to prevent lifting of that end of the slab. This addition enabled direct transmission of forces between concrete slabs in neighboring girder segments and further ensured full composite action. The failure mode in the fourth test was downward buckling of the steel flange plate, as predicted (Yen 1986). As in the panel specimen tests, the box girder segment tests showed that the composite slab had a higher capacity than the bare steel plate.

The researchers conclude that it is feasible to use steel-concrete composite compression flanges in box girders. However, results from their bridge design alternatives identified a significant potential problem with composite compression flanges. They found that the weight of the wet concrete on the bare steel flange produced significant displacements that could be considered unacceptable. They suggested use of longitudinal stiffeners to control plate deflections under the weight of the wet concrete. Unfortunately, the main point of using the composite flange would seem to be to eliminate the need for longitudinal stiffeners. If a longitudinal stiffener is required to control plate deflections under the concrete weight, then it seems reasonable to simply increase the size of the specified

longitudinal stiffener to meet the required capacity of the compression flange, and not include the concrete at all. In this situation a cast-in-place concrete composite flange does not seem an attractive alternative.

The researchers do discuss the alternative of using precast concrete planks to form the composite flange. They do not however discuss the complexities that may be involved with forming precast concrete planks to match the geometry of the box, which may be horizontally and vertically curved. Their designs and discussion are limited to straight box girders.

The report also stresses the fact that the strength of the composite flange depends on the end conditions of the concrete slab. They found that if the slab did not bear against transverse diaphragms or the webs of the box, that it was possible to get bending of the composite panel that resulted in cracking of the concrete slab. With either cast-in-place or precast concrete, it may be difficult to guarantee bearing of the concrete against the box diaphragms and webs.

There is another item of concern that is not discussed regarding erection of boxes with composite bottom flanges. If the precast planks are installed prior to erection, or if the cast-in-place concrete is placed prior to erection, the composite slab will likely be subjected to tensile forces during the erection procedure. The girder segments are typically lifted from two points near the ends of the section, putting the mid-section of the girder segment in positive bending and the bottom flange in tension. The magnitude of tensile forces in the concrete would have to be investigated to assess whether the concrete slab may be cracked during the erection procedure. The impact of such cracking was not assessed in the study.

The study states that additional research is needed to confirm the adequacy of the fatigue strength of the composite flange. Additionally, a more extensive study of the effects of creep and shrinkage of the concrete in composite panels was recommended. The recommended research, regarding the effects of concrete

shrinkage and creep in composite panels, would be most appropriately undertaken by concrete materials researchers. Further investigation was also recommended regarding the applicability of the composite bottom flanges with horizontally curved box girders. However, the details of concern identified in this study, along with the items mentioned in the above discussion, cause significant concern regarding the practical, common application of this design approach to steel box girder designs.

1.7 Dissertation Scope Outline

This dissertation will address issues related to the behavior and design of stiffened steel compression flanges of trapezoidal box girder bridges. The research program completed investigated the basis of the AASHTO design equations and other code approaches. The validity of the AASHTO equations was investigated using eigenvalue finite element analyses. An experimental program was undertaken to test the performance of plates stiffened with torsionally weak stiffeners, typical of current stiffener designs, as well as alternate stiffener configurations that provide significant torsionally stiffness. The results of the experimental program are discussed and compared with finite element results. Additional finite element analyses that further explore the stiffened plate behavior seen in the experimental tests are discussed. Based on the results of the experimental tests and subsequent finite element analyses, a recommendation is made for consideration of an analysis approach different than that currently forming the basis of the AASHTO provisions.

Chapter 2 of this dissertation presents background information on stiffened plate design, including the AASHTO compression flange design equations and the basis of their development. Chapter 3 discusses initial imperfections, residual stresses, and their impact. Chapter 4 presents an analytical

study of plates in compression, and explores advantages of torsionally stiff longitudinal stiffeners. Eigenvalue analyses of the experimental test plates are also presented in Chapter 4. Chapter 5 describes the experimental program that was completed, and the results of this program are presented in Chapter 6. An analysis of the test results is presented in Chapter 7. Chapter 8 discusses other issues related to compression flange behavior including stiffener eccentricity, impact of moment gradients, and transverse stiffener details. Use of a strut-based analysis approach is also discussed in this chapter. Chapter 9 presents conclusions and future research needs.

Chapter 2

Background

2.1 Use of Longitudinally Stiffened Plates

Stiffened plates have been used in bridges for well over a century. British bridge builders made early use of stiffened plates in the 1840's and 50's. Famous tubular bridges such as the Conway Tubular Bridge, competed in 1848, and the Britannia Bridge, completed in 1850, included stiffened steel plates (Alinia 2001, Hutchison 2001). Bridge designers of this era visited shipbuilding operations and benefited from the experience of the shipbuilding industry. At this time stiffened plates were designed by simple mechanics of materials formulas and designs were checked with model tests. Designers found that their formulas were reasonably accurate in tension, but that the behavior of plates in compression was much more difficult to predict. They found that the unrestrained plates in compression failed at lower than expected loads due to buckling of the plates (Ryall 1999, Singer 1998). The buckling behavior of stiffened plates has thus been a subject of interest to engineering researchers for many years.

The development of the linear theory of plate buckling began with Saint-Venant in the late 19th century, who established the differential equation of buckling of a plate loaded in its plane in 1870, and with Bryan, who applied the strain energy criterion to the solution of the plate buckling problem. (Bleich 1952, ECCS 1986) Important progress was made by Reissner and by Timoshenko, who applied the ideas of Rayleigh and Ritz to stability problems of plates (Bleich 1952). The evaluation of critical buckling stresses has been undertaken by many other researchers. Timoshenko, Gere, and Bleich performed early analytical research on stiffened plates in the early to mid-1900s, and

participated in extending the theory to the analysis of stiffened plates. The requirements used in North American practice (AASHTO 1996, AASHTO 1998, Ontario 1991) have been based on Timoshenko and Gere's Theory of Elastic Stability (Timoshenko 1961). German and Swiss specifications have also been based on elastic buckling theory (Wolchuk 1980).

The AASHTO specifications have contained specific provisions for design of the bottom compression flange of a box girder since the 10th Edition of the Standard Specifications for Highway Bridges (AASHO 1969). The design of unstiffened and longitudinally stiffened bottom flanges in compression in the AASHTO Specifications is based on elastic plate buckling theory. A transition curve is used between the elastic and plastic range. This transition curve is based on an assumed correlation between column and plate buckling behavior (Wolchuk 1980). The same requirements for unstiffened and longitudinally stiffened flanges as those in AASHTO are contained in the Ontario Highway Bridge Design Code (Ontario 1991).

Up to at least the early 1980s, the German general highway bridge specification, DIN 1073, has not contained specific requirements for steel box girder bridges. The design of plate elements in compression is based on the provisions for stability of plate elements: DASt Richtlinie 12. These provisions are based on elastic buckling theory. Previously the Engessner transition curve, used in the AASHTO specification, was used in the inelastic zone, but has since been replaced by a straight line between the elastic and plastic zones (Wolchuk 1980). Stiffened compression flanges are designed considering the individual stiffeners with an associated width of flange plate as elastic struts. Strut out-of-straightness is assumed equal to the maximum permitted tolerance in the design procedure (Wolchuk 1980).

As discussed above, design of compression flanges in AASHTO is based on buckling theory. The load at which the plate buckles can be defined based on small deflection behavior in terms of its out-of-plane bending. Analysis of the plate energy shows that the elastic postbuckling response of the simply-supported plate is stable, and there is a strength reserve above the buckling capacity of the plate (Timoshenko 1961).

Using the critical load of a plate based on elastic plate buckling theory for design purposes has been questioned. Especially in European countries, where larger box girders with more slender plates are used, several other design approaches are not based on elastic plate buckling theory. Alternate limit state methods, using strut or orthotropic approaches, have instead been used. Recent variations of these methods have included non-linear theory that makes direct inclusion of the effects of initial imperfections, plasticity, and postbuckling stability.

The early design approaches that prevailed in Europe are based on "column" or "strut" behavior. This is the basis for design of stiffened compression plates used in Britain. In this design philosophy the compression flange is replaced by a series of unconnected column struts consisting of a stiffener and an associated width of plate. This approach does not actually realistically model the real behavior of the stiffened plate, since the support provided by the stabilizing membrane effect in the transverse direction of the plate is not adequately considered, but this simplification is conservative (ECCS 1986). The stiffened compression flange is replaced by a series of struts consisting of a stiffener and associated plate width. Consequently, at ultimate load the deformed shape of each strut is not the same as the actual shape of a compressed plate at ultimate load. Furthermore, the struts are assumed to fail at the same time in the same shape, which also does not occur when a stiffened plate

fails in compression. Failure is assumed to occur when the plate yields or buckles between stiffeners, or when the stiffener fails in compression or yields. Early approaches did not distinguish between the direction in which the plate displaced, and consequently did not consider if the stiffener was placed in tension or compression at its outstand. Strut based approaches can make consideration of the discrete characteristics of the stiffener by use of an effective width as a correction to the analysis (ECCS 1986).

There are many variations of the column behavior approach, including the Merrison rules method, interaction diagram method, effective width and effective yield methods. The Merrison rules were the result of a committee of inquiry, under the chairmanship of Merrison, appointed after the collapse of several steel box girder bridges in the late 1960s and early 1970s. The Merrison rules consider each stiffener strut, or stiffener with associated width of flange plate, separately. The strength of the entire flange is obtained by multiplying the ultimate stress of the strut by the total area of the flange plate including the stiffeners.

Though influenced by the Merrison Rules, the recommendations of the Merrison committee were not entirely adopted into the British specification (Wolchuk 1980). The design of the bottom compression flange in the British Specification is based on the ultimate plate strength with consideration of imperfections and residual stresses using a strut-based approach. Longitudinally stiffened bottom flanges are designed by consideration of the sum of individual stiffener-struts. The effective width of the plate acting with the stiffener is generally taken to be smaller than the stiffener spacing (Wolchuk 1980). A common issue of these column or strut based approaches is a complex procedure for determining the effective length of the stiffener. In these approaches the contributions of "plate" behavior versus "column" behavior must be established.

It has been difficult to quantitatively evaluate the interaction between "plate" and "column" behavior (Wolchuk 1980).

Another approximate approach used to predict the ultimate strength of stiffened plates in compression is the orthotropic plate approach. In this design approach, the stiffened compression flange is replaced by an orthotropic plate that is obtained by smearing the rigidity of both longitudinal and transverse stiffeners out over the plate. The stiffened plate is treated as an equivalent orthotropic plate and an elastic large deflection analysis or non-linear large displacement theory is used. Using the orthotropic plate approach, the effect of the transverse continuity of the plate between the webs of the box girder is considered to give additional stability to the longitudinal stiffeners. In this approach, the stiffened plate has sinusoidal deflections that are not necessarily representative of actual stiffened plate behavior. Collapse is reached when the mean membrane stress along the unloaded edges reach yield. Plate buckling between stiffeners is generally considered using an effective width approach. With the orthotropic approach the stability provided by the plate in the transverse direction is included directly, rather than through an effective length like the strut approach. A problem with this approach though is that with the smeared plate approach, the actual softening behavior of the stiffeners and stiffened plate is not taken into account (ECCS 1986).

All ultimate load approaches, such as the strut and orthotropic plate approaches must be calibrated against test results. The strut approach is easier to codify (ECCS 1986), and as mentioned is the basis of British specifications, but the resulting code requirements are not necessarily simple to understand, particularly for someone more versed in traditional buckling approaches.

2.2 Proposed Design Specifications for Steel Box Girder Bridges

The last major attempt to improve box girder design specifications in the United States was conducted by the firm of Wolchuk and Mayrbaurl under a Federal Highway Administration (FHWA) contract. This work resulted in the Proposed Design Specifications for Steel Box Girder Bridges published in 1980 (Wolchuk 1980). The proposed specifications apply to straight girder bridges with a single steel box cross section, consisting of one or more cells, with an orthotropic steel plate or composite concrete deck, and to short and medium-span multi-box bridges with composite concrete decks. This work provides a dramatically different approach for design of longitudinally stiffened flanges in compression from the approach in the AASHTO specification. The Proposed Design Specifications were not adopted by AASHTO.

The proposed requirements for compression flanges are based on a strut approach that includes the effects of geometric imperfections and residual stresses. Residual stresses, in particular, were considered very important and their effect was given additional weight. A procedure was introduced for the design of stiffened flanges, which combined the effects of stiffener buckling with the effects of local plate buckling between stiffeners to obtain the total strut strength. The approach used was different from previous British and German specifications that treat plate buckling and stiffener buckling separately.

This report recommended changes in the requirements for both unstiffened and stiffened flanges. The proposed strength curve for unstiffened flanges was based on tests and computer-generated results from Britain. The curve chosen for the proposed specification was developed from the tests and computer "tests" corresponding to lightly welded plates (Wolchuk 1981).

The numerical methods of Little (Little 1976) were chosen as the basis for determining the design strength of stiffened compression panels. Little's method

is a second-order iterative computer method for analysis of inelastic column struts. The method considers the interaction between local buckling of the plate between stiffeners and the overall buckling of the stiffened plate. In development of the requirements for stiffened plates, values of plate imperfection between stiffeners and stiffener imperfections were assumed. The sensitivity of the approach to the assumed imperfection and residual stress was tested, and the approach was found to be suitable for practical design purposes (Wolchuk 1981).

The proposed requirements for stiffened flanges in compression are presented in an interaction diagram, shown in Figure 2.1. This chart-based approach hampers direct comparison with AASHTO capacity equations, and hinders automated calculation of capacity using spreadsheet or programming based approaches. The strut capacity is a function of λ_{col}, the column slenderness, and λ_{pl}, the plate slenderness. The strength of the flange is obtained by multiplying the ultimate strength of the strut by the total area of the flange.

The Proposed Design Specifications for Steel Box Girder Bridges were not adopted by AASHTO. Recent revisions proposed to the AASHTO Specifications (Yoo 2001) have been based on the traditional specification formulation, not the approaches recommended by Wolchuk.

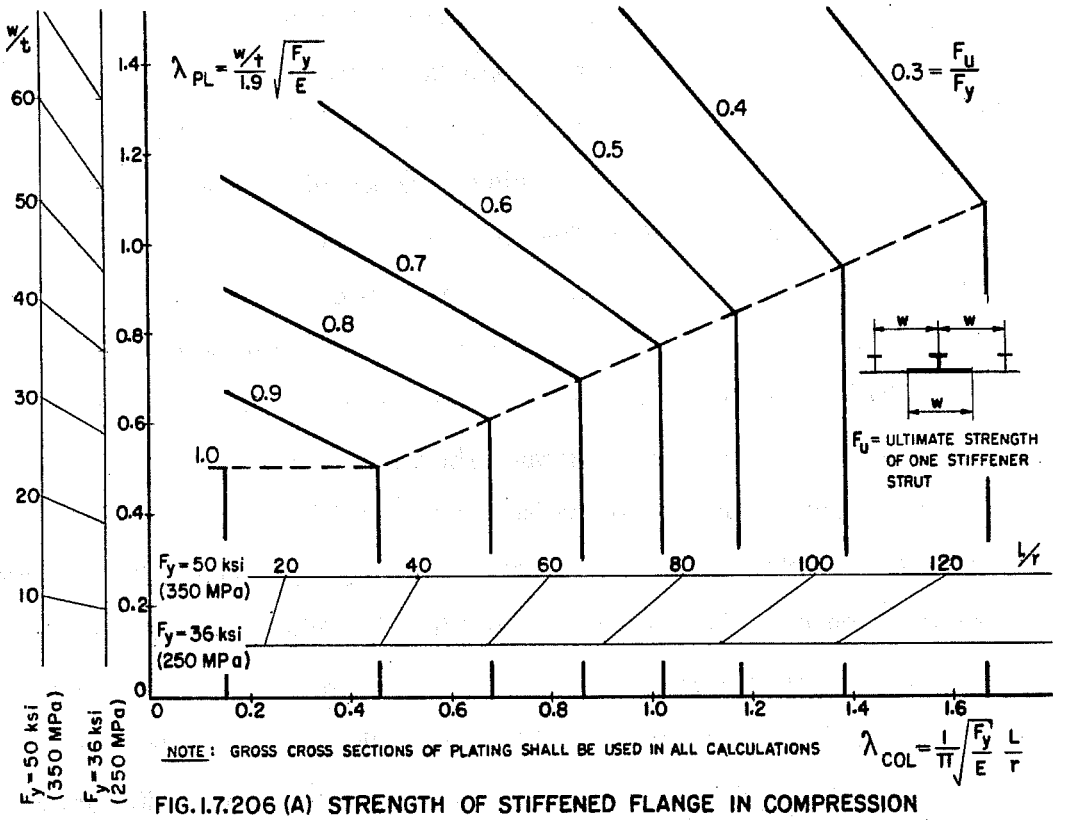

Figure 2.1 Strength of Stiffened Flange in Compression (Wolchuk 1980)

2.3 AASHTO Bridge Design Specifications

The AASHTO bridge design specifications are contained in the Standard Specifications for Highway Bridges and LRFD Bridge Design Specifications. The AASHTO Standard Specifications contain both Service Load Design Method, or Allowable Stress Design (ASD), and Strength Design Method, or Load Factor Design (LFD) based methods (AASHTO 1996). A third, newer specification is the AASHTO Load and Resistance Factor Design (LRFD) Specification (AASHTO 1998). The buckling provisions contained in AASHTO bridge design specifications for compression flanges of steel box girders are based

on the elastic buckling behavior of stiffened plates, not the approach recommended by Wolchuk.

2.3.1 Unstiffened Flanges

The ASD and LFD portions of the Standard Specifications contain essentially the same requirements for unstiffened compression flanges. The difference between the Standard Specification and LRFD approach is the assumption of a modulus of elasticity, E, of approximately 29,000,000 psi for steel in the Standard Specification. The LRFD specification equations did not include a specified value for E to make it simpler to convert the equations to metric units. The equations for design of the compression flange are given in the LRFD presentation format below, with their code reference numbers.

$$\text{If} \quad \frac{w}{t_f} \le 0.57\sqrt{\frac{kE}{F_{yc}}}, \text{ then :}$$

$$F_n = R_b R_h F_{yc} \qquad (6.11.2.1.3a\text{-}1)$$

$$\text{If} \quad 0.57\sqrt{\frac{kE}{F_{yc}}} < \frac{w}{t_f} \le 1.23\sqrt{\frac{kE}{F_{yc}}}, \text{ then :}$$

$$F_n = 0.592\, R_b R_h F_{yc}\left(1 + 0.687\sin\frac{c\pi}{2}\right) \qquad (6.11.2.1.3a\text{-}2)$$

for which :

$$c = \frac{1.23 - \frac{w}{t_f}\sqrt{\frac{F_{yc}}{kE}}}{0.66} \qquad (6.11.2.1.3a\text{-}4)$$

$$\text{If } \frac{w}{t_f} > 1.23\sqrt{\frac{kE}{F_{yc}}}, \text{ then :}$$

$$F_n = 26{,}200\, R_b R_h k \left(\frac{t_f}{w}\right)^2 \qquad (6.11.2.1.3a\text{-}3)$$

where:

F_{yc} = specified minimum yield strength of the compression flange (KSI)

w = larger of the width of compression flange between longitudinal stiffeners or the distance from a web to the nearest longitudinal stiffener (IN)

t_f = thickness of the compression flange (IN)

R_b, R_h = flange-stress reduction factors specified in Article 6.10.4.3

For unstiffened compression flanges, the code stipulates that the flange width between webs, b, be substituted for w and that the buckling coefficient, k, equal four to give the nominal bending resistance.

The R_b and R_h factors are not considered in the following discussion. The R_b factor is a postbuckling strength reduction factor that accounts for nonlinear stress variations caused by flexural buckling of slender webs. The R_h factor accounts for nonlinear variation of stresses caused by yielding of lower strength steel in the webs of hybrid girders. The values of R_b and R_h are not relevant to the topic under discussion, and are assumed to have a unit value in all calculations.

A graph of the unstiffened flange design equations is shown in Figure 2.2, using E equal to 29,000 ksi and F_{yc} equal to 50 ksi. The three regions defined by the design equations are divided using dashed lines at the transitional w/t values.

For stocky flanges, the capacity is limited by the yield stress of the flange since the plate will yield before buckling. For slender flanges, the capacity is given by the elastic buckling stress of a steel plate simply supported along its edges. The slender plate will buckle before reaching the yield stress. For flanges that are neither stocky nor slender, the capacity is determined by using a transition equation, which connects the capacity curves for the stocky and slender flanges.

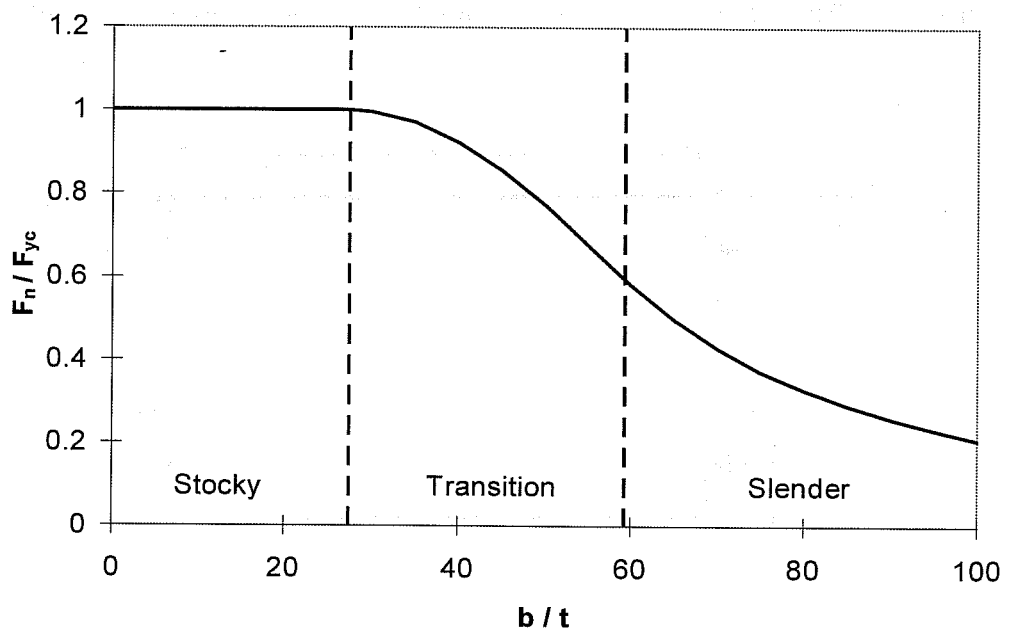

Figure 2.2 Unstiffened Flange Capacity

The bottom flange of the box girder can be modeled as a plate simply supported along its edges. Boundary conditions provided by the typical box girder to the stiffened compression flange are such that it is realistic, and safe, to assume simply supported edges (Yoo 2001, Kasparova 1983). The webs of the box girder and the continuity of the bottom flange, and transverse stiffeners if present, provide the edge support for each section of the bottom flange plate.

Timoshenko and Gere present an analysis of buckling of simply supported rectangular plates under uniform compression in one direction. A plate of width b and length "a" under uniform compression is shown in Figure 2.3. The deflection surface of a uniformly compressed square plate is presented in Figure 2.4. The magnitude of the compressive force per unit length of the edge is denoted as N_x. The critical, buckling, value of N_x can be found through integration or energy methods. The critical value of N_x for small deflections is given in Equation (2.1).

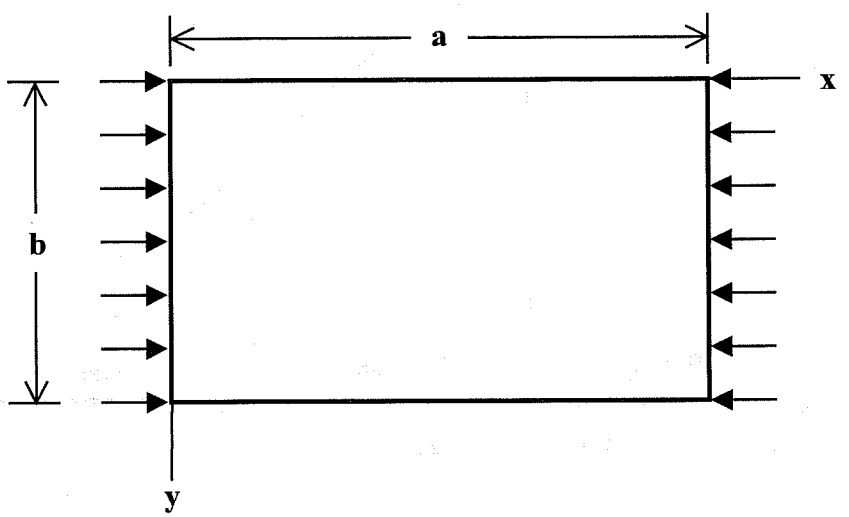

Figure 2.3 Simply Supported Compressed Plate

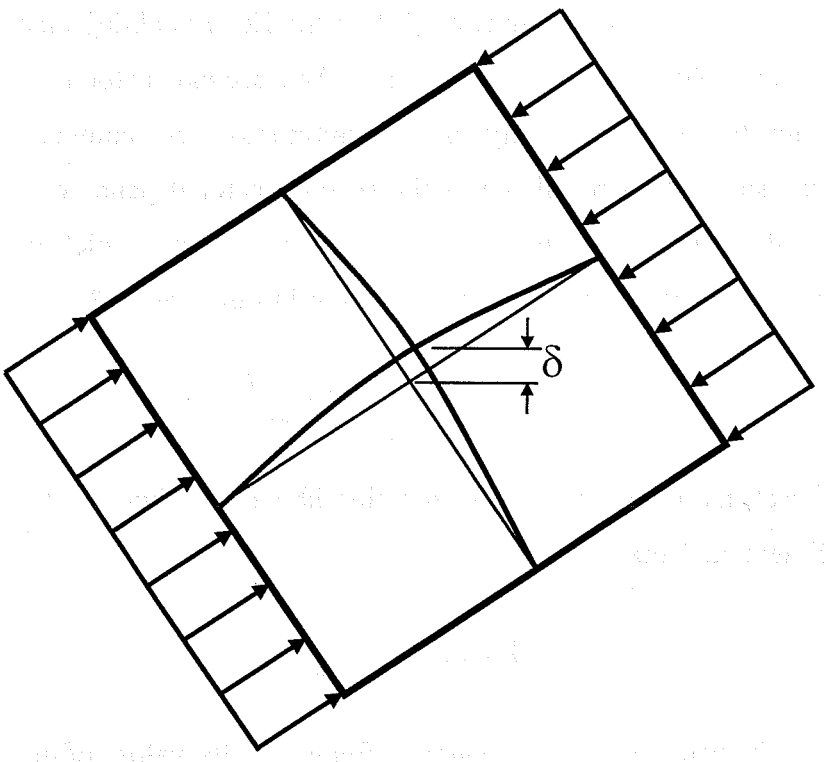

Figure 2.4 Deflection Surface of Square Plate

$$(N_x)_{cr} = \frac{\pi^2 D}{a^2}\left(m + \frac{1}{m}\frac{a^2}{b^2}\right)^2 \qquad (2.1)$$

In Equation (2.1), "a" is the plate length, b is the plate width, m is the number of half-waves into which the plate buckles along its length, and D is the flexural rigidity of the plate. The flexural rigidity is defined as

$$D = \frac{Et^3}{12(1-\nu^2)} \qquad (2.2)$$

where E is the elastic modulus, t is the plate thickness, and ν is Poisson's ratio.

The first factor in Equation (2.1) is the Euler buckling load for a plate strip with a unit width and a length of "a". The second factor is a proportion that indicates the greater stability of the continuous strip compared to that of an isolated strip. The magnitude of the second factor depends on the aspect ratio, a/b, of the plate and m, the number of half-waves into which the plate buckles. Equation (2.1) can be rearranged to the form in Equation (2.3):

$$(N_x)_{cr} = \frac{\pi^2 D}{b^2}\left[m\frac{b}{a} + \frac{1}{m}\frac{a}{b}\right]^2 \tag{2.3}$$

The bracketed expression in the equation above is defined as the plate buckling coefficient, k. Thus,

$$k = \left(m\frac{b}{a} + \frac{1}{m}\frac{a}{b}\right)^2 \tag{2.4}$$

The equation for k is plotted in Figure 2.5 for values of m = 1 through m = 5. For each value of m, the curves are plotted using solid and dashed lines. Solid lines are used where the curve gives the overall minimum value of k for a given aspect ratio, a/b. Dashed lines are used where a curve does not give the limiting value of k.

For each value of m, there is a non-linear relationship between the buckling coefficient, k, and a/b. The value of k is large for small values of a/b, then decreases as a/b increases becoming a minimum of four where a/b=m, and then increases as a/b continues to increase. The critical value of the buckling coefficient and the number of half-waves into which the plate will buckle for any aspect ratio, a/b, is found from the solid line portion of the graph.

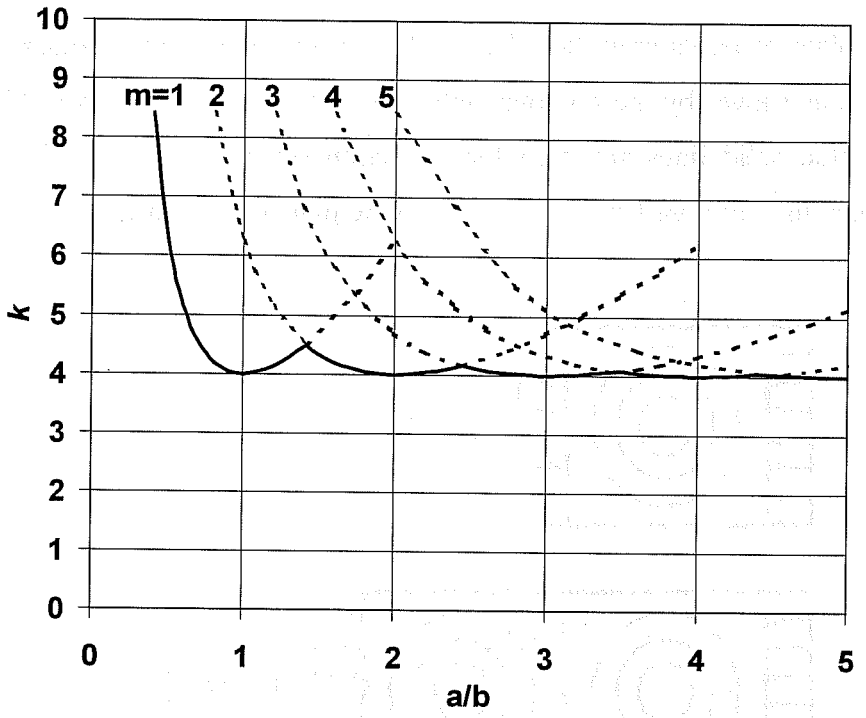

Figure 2.5 Buckling Coefficcient vs. Plate Aspect Raio

The region of the plot where a/b < 1, and the cusps between integer aspect ratios show that plates with certain length to width ratios actually have a plate buckling coefficient larger than the minimum of four. However, the aspect ratios of plates used for compression flanges of boxes are greater than one, and long plate elements will buckle in the lowest energy configuration, where k equals four.

As shown in Figure 2.5, when a/b=m the value of the k factor has the minimum value of four. When a/b=m, the critical load is simply:

$$(N_x)_{cr} = \frac{4\pi^2 D}{b^2} \qquad (2.5)$$

For plates where a/b=m, the plate buckles in half-waves over square panels of the plate, as shown by the contour plots of the deflection surfaces in Figure 2.6. In the plot, solid lines are used for deflection out of the plane of the paper, and dashed lines are used for deflection into the plate of the paper.

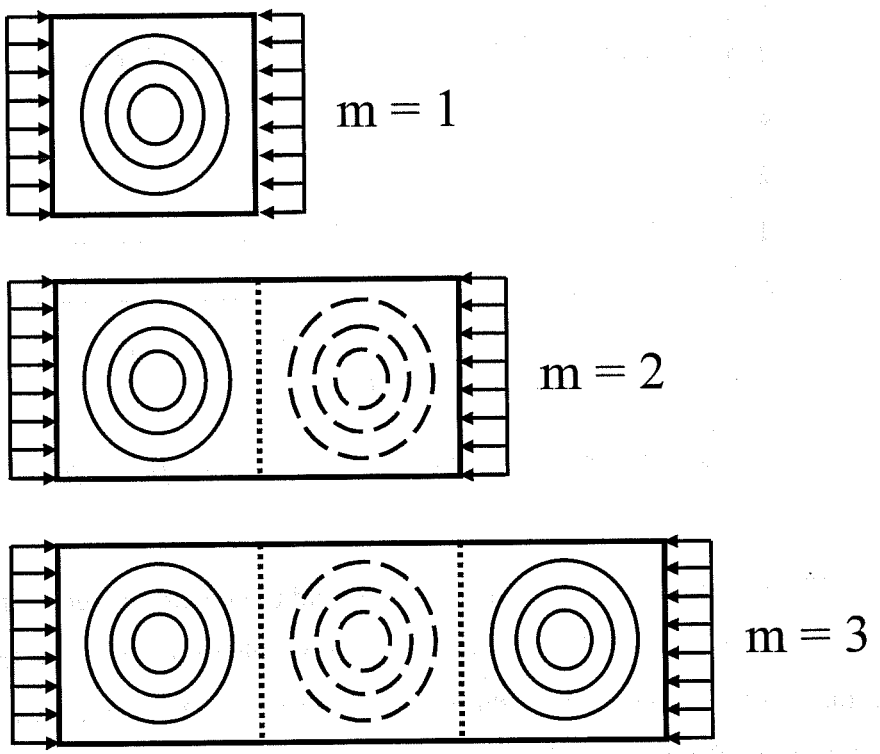

Figure 2.6 Buckling of Plate in Compression on Square Panels

The AASHTO bridge design equations for slender unstiffened flanges are drawn directly from Equation (2.5) where the plate buckling coefficient has the minimum value of four. The AASHTO LRFD equations include values of 29,000 ksi for the elastic modulus of steel and 0.3 for poisson's ratio, resulting in the form shown in Equation (2.6). The format of this equation is modified slightly for

presentation in the AASHTO specification, but the resulting capacity for slender unstiffened flanges is the same as that shown in Equation (2.6).

$$\sigma_{cr} = \frac{(N_x)_{cr}}{t} = \frac{4\pi^2}{b^2 t}\left(\frac{Et^3}{12(1-\nu^2)}\right) = \frac{4\pi^2}{b^2}\left(\frac{29{,}000t^2}{12(1-0.3^2)}\right) = 104{,}800\left(\frac{t^2}{b^2}\right) \qquad (2.6)$$

2.3.2 Flanges Stiffened Longitudinally

Though slightly different in their approach, the ASD, LFD, and LRFD specifications contain the same requirements for compression flanges stiffened longitudinally. One slight difference is an explicit note in the ASD specification that states, "In solving these equations a value of k between two and four generally should be assumed." This recommendation was not transferred to the LFD specification, and subsequently the LRFD specification, when these codes were formulated. Subsequently, if a designer uses the current formulation of the LFD or LRFD specification and chooses a design where the value of the buckling coefficient is less than two, the designer may obtain unrealistically low design capacities. If a stiffener is used that results in a buckling coefficient less than one, the predicted capacity will actually be smaller than that of an unstiffened plate with the same geometry.

The design equations presented in the unstiffened flange discussion are also used for stiffened flange design in the LRFD specification. For stiffened flanges, the value of the buckling coefficient k is based on the stiffener size and spacing, and the plate thickness, using the code equations presented below.

k = buckling coefficient specified as:

If n = 1, then:

$$k = \left(\frac{8I_s}{wt_f^3} \right)^{\frac{1}{3}} \leq 4.0 \qquad (6.11.2.13a\text{-}5)$$

If n = 2, 3, 4, or 5, then:

$$k = \left(\frac{14.3I_s}{wt_f^3 n^4} \right)^{\frac{1}{3}} \leq 4.0 \qquad (6.11.2.1.3a\text{-}6)$$

where:

n = number of equally spaced longitudinal compression flange stiffeners

I_s = moment of inertia of a longitudinal stiffener about an axis parallel to the bottom flange and taken at the base of the stiffener (IN^4)

The design equations for flanges stiffened longitudinally again have the stocky, transition, and slender flange regions as described in the unstiffened flange design. For stocky flanges, the capacity is limited by the yield stress. For slender flanges, the capacity is limited by the bucking stress. A transition curve gives the capacity of flanges that are neither stocky nor slender.

The buckling capacity of plates with longitudinal stiffeners, derived by Timoshenko and Gere, considering buckling of the plate and bending of the reinforcing ribs is

$$\sigma_{cr} = \frac{\pi^2 D}{b^2 t} \cdot \left(\frac{(1+\beta^2)^2 + (n+1)\gamma}{\beta^2 (1 + (n+1)\delta)} \right) \qquad (2.7)$$

where D is the flexural rigidity of the plate, t is the plate thickness, β is the plate aspect ratio (a/b), "a" is the plate length, b is the plate width, and n is the number of stiffeners. The values of γ and δ are as follows,

$$\gamma = \frac{EI_s}{bD} \tag{2.8}$$

$$\delta = \frac{A_s}{bt} \tag{2.9}$$

where I_s is the moment of inertia of the longitudinal stiffener about an axis parallel to the plate taken at the bottom edge of the stiffener, and A_s is the cross-sectional area of a longitudinal stiffener. The simplifying assumptions used in obtaining this expression are appropriate for longer plates, where the aspect ratio is at least 2, and assume equally spaced longitudinal stiffeners. The expression is conservative for shorter plates.

The plate width, b, can be expressed in terms of the spacing, w, of the longitudinal stiffeners and number of longitudinal stiffeners, n:

$$b = (n+1)w \tag{2.10}$$

Using this expression in Equation (2.7), the critical stress can be written as follows.

$$\sigma_{cr} = \frac{\pi^2 D}{w^2 t} \cdot \left(\frac{(1+\beta^2)^2 + (n+1)\gamma}{(n+1)^2 \beta^2 (1+(n+1)\delta)} \right) \tag{2.11}$$

The second factor in this expression is the buckling coefficient, k, therefore

$$\sigma_{cr} = k \frac{\pi^2 D}{w^2 t} \tag{2.12}$$

$$\text{where } k = \frac{(1+\beta^2)^2 + (n+1)\gamma}{(n+1)^2\beta^2(1+(n+1)\delta)} \tag{2.13}$$

The minimum critical stress occurs when k is a minimum. To find the minimum value of k, the derivative of k with respect to β^2 can be set equal to zero. The critical value is

$$\beta_{cr} = \sqrt[4]{1+(n+1)\gamma} \tag{2.14}$$

Substituting β_{cr} into Equation (2.13) determines the minimum value of k:

$$k_{min} = \frac{2\left(\sqrt{1+(n+1)\gamma}+1\right)}{(n+1)^2(1+(n+1)\delta)} \tag{2.15}$$

Therefore a long plate will buckle into half-waves of length b x β_{cr} and the critical stress can be found by substituting k_{min} into Equation (2.12).

Using the expression for k_{min}, the values of γ, and consequently I_s from Equation (2.8), necessary to give specified values of k_{min} were established (Mattock 1967). Using these values of I_s and k_{min}, approximate expressions for I_s were developed for inclusion in the AASHTO code. Development of the code equations was apparently based on an iterative procedure in which a value of k was assumed, and a reasonable value of δ was used to back out the required stiffener moment of inertia. Reasonable values of δ were likely assessed using the tabulated results presented by Timoshenko and Gere for various values of the buckling coefficient. The values of δ implicitly assumed in the AASHTO formulation were calculated and compared to actual values of δ occurring in final stiffened plate configurations. The assumed values were found to be reasonable and conservative for the stiffened plate configurations.

The assumed values of k used to formulate the required moments of inertia were compared to the values of k calculated using Timoshenko and Gere's

formulation. The procedure of assuming a value of k then computing the moment of inertia of each stiffener gives results consistent with those based on the theory of elastic stability for plates with 1 to 3 longitudinal stiffeners with buckling coefficients between approximately 2 to 4. For plates with buckling coefficients less than 2, the procedure is overly conservative. For plates with 4 to 5 longitudinal stiffeners, the proposed procedure results in overly conservative buckling coefficients for all stiffener sizes.

Design alternatives for stiffening of a slender 120" x 1" plate using the AASTHO LRFD equations were explored. Several options are shown in Figure 2.7. The figure shows that the design capacity for the unstiffened plate is 7.28 ksi. By the inclusion of one longitudinal stiffener with an I_s of 480 in^4, which results in a buckling coefficient of 4, the capacity is 29.1 ksi. To reach this same capacity, two longitudinal stiffeners with an I_s of 252 in^4, can also be used.

If two longitudinal stiffeners are used and sized so that the buckling coefficient is 4, the required stiffener moment of inertia is 2860 in^4. With this configuration the plate will actually yield before the buckling stress is reached. Two stiffeners were sized so that the buckling stress equaled the yield stress of the plate. The required I_s was 1270 in^4 for this case. Using the AASHTO buckling coefficient equations, multiple stiffener configurations are available to provide the needed flange capacity.

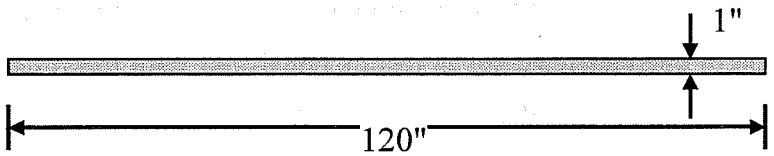

120" x 1" Unstiffened Plate, $F_y = 50$ ksi
$F_n = 7.28$ ksi

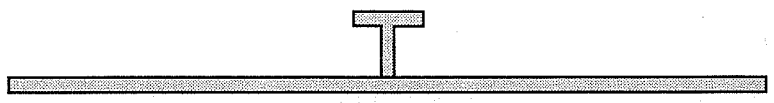

Plate with One Stiffener
$I_s = 480$ in^4 $k = 4$ $F_n = 29.1$ ksi

Plate with Two Stiffeners
$I_s = 252$ in^4 $k = 1.78$ $F_n = 29.1$ ksi

Plate with Two Stiffeners
$I_s = 2860$ in^4 $k = 4$ $F_n = 65.5$ ksi » $F_y = 50$ ksi

Plate with Two Stiffeners
$I_s = 1270$ in^4 $k = 3.05$ $F_n = 50.0$ ksi

Figure 2.7 Stiffener Design Alternatives

2.3.3 Flanges Stiffened Longitudinally and Transversely

The LRFD specification and LFD portion of the Standard Specifications do not contain additional requirements for flanges stiffened both longitudinally and transversely. The ASD portion of the AASHTO Standard Specifications does contain requirements for compression flanges stiffened longitudinally and transversely. If the plate aspect ratio, a/b, exceeds three, transverse stiffeners are not necessary and the capacity is calculated using the requirements for compression flanges stiffened longitudinally.

Using both transverse and longitudinal stiffeners, the layout of the stiffened plate is as shown in Figure 2.8. The centerlines of the stiffeners are shown in this figure. The plate width, b, longitudinal stiffener spacing, w, and transverse stiffener spacing, a, are labeled in the figure.

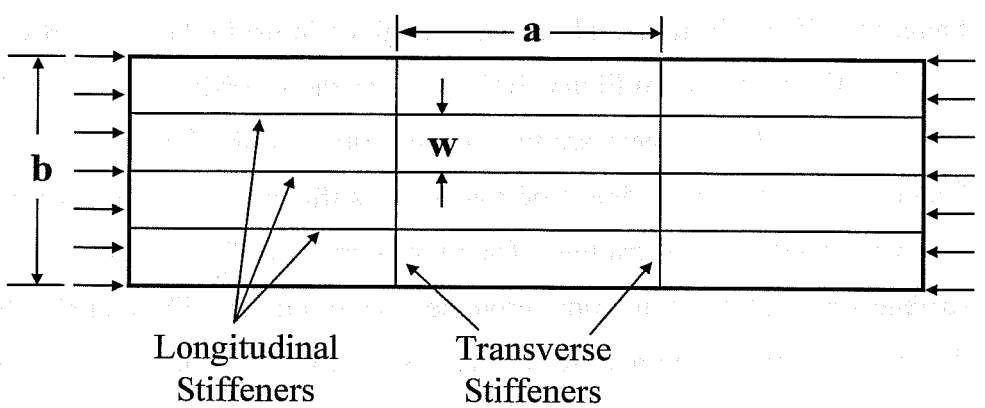

Figure 2.8 Layout of Longitudinal and Transverse Stiffeners

The Standard Specification code equation reference numbers are used in the following discussion. For flanges stiffened both longitudinally and transversely, a required minimum stiffness for longitudinal stiffeners, is specified:

$$I_s = 8t_f^3 w \qquad (10\text{-}80)$$

The required moment of inertia is the same as for flanges stiffened longitudinally with a single longitudinal stiffener with a k value of four. The required moment of inertia is not dependent on the number of stiffeners.

The requirements for flanges stiffened longitudinally and transversely contain a modified buckling coefficient, k_1, which varies with the spacing of transverse stiffeners and number of longitudinal stiffeners. The value of k_1 is

$$k_1 = \frac{\left[1 + (a/b)^2\right]^2 + 87.3}{(n+1)^2 (a/b)^2 [1 + 0.1(n+1)]} \qquad (10\text{-}83)$$

The maximum value of this k_1 buckling coefficient is limited to four. When k_1 has its maximum value, the transverse stiffeners must have a spacing, "a", equal to or less than 4w.

The specification includes two figures related to box girder compression flanges to aid the designer. Note that F_y is given in psi in the ASD Specification. The first figure is labeled Figure 10.39.4.3A in the specification, and is shown in Figure 2.9. Note that there are two sets of curves in the figure. The curves for flanges with both longitudinal and transverse stiffeners are at the bottom of plot, below the lowest y-axis gridline. The set of curves for flanges without transverse stiffeners are in the second more prominent set of curves. The plot clearly shows the dramatic increase in required stiffener size when multiple (n>1) stiffeners are used.

The second design aid is labeled Figure 10.39.4.3B in the specification, and is shown in Figure 2.10. There are also two sets of curves in this figure. The set of curves that spans from the lower left to upper right of the plot are used to select the transverse stiffener size. The second set of curves, labeled a/b, is used to establish the transverse stiffener spacing.

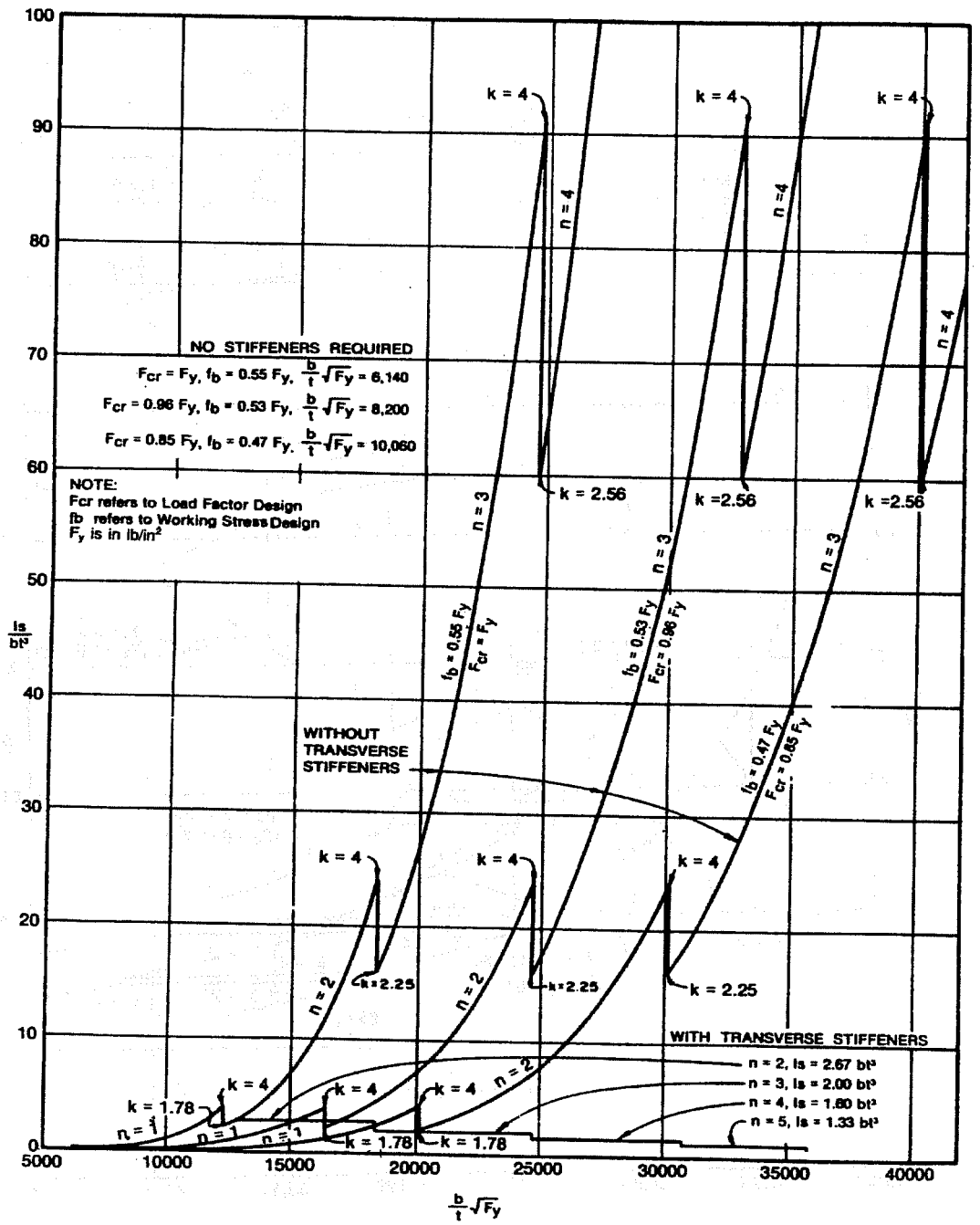

Figure 2.9 ASD Longitudinal Stiffener Design Aid

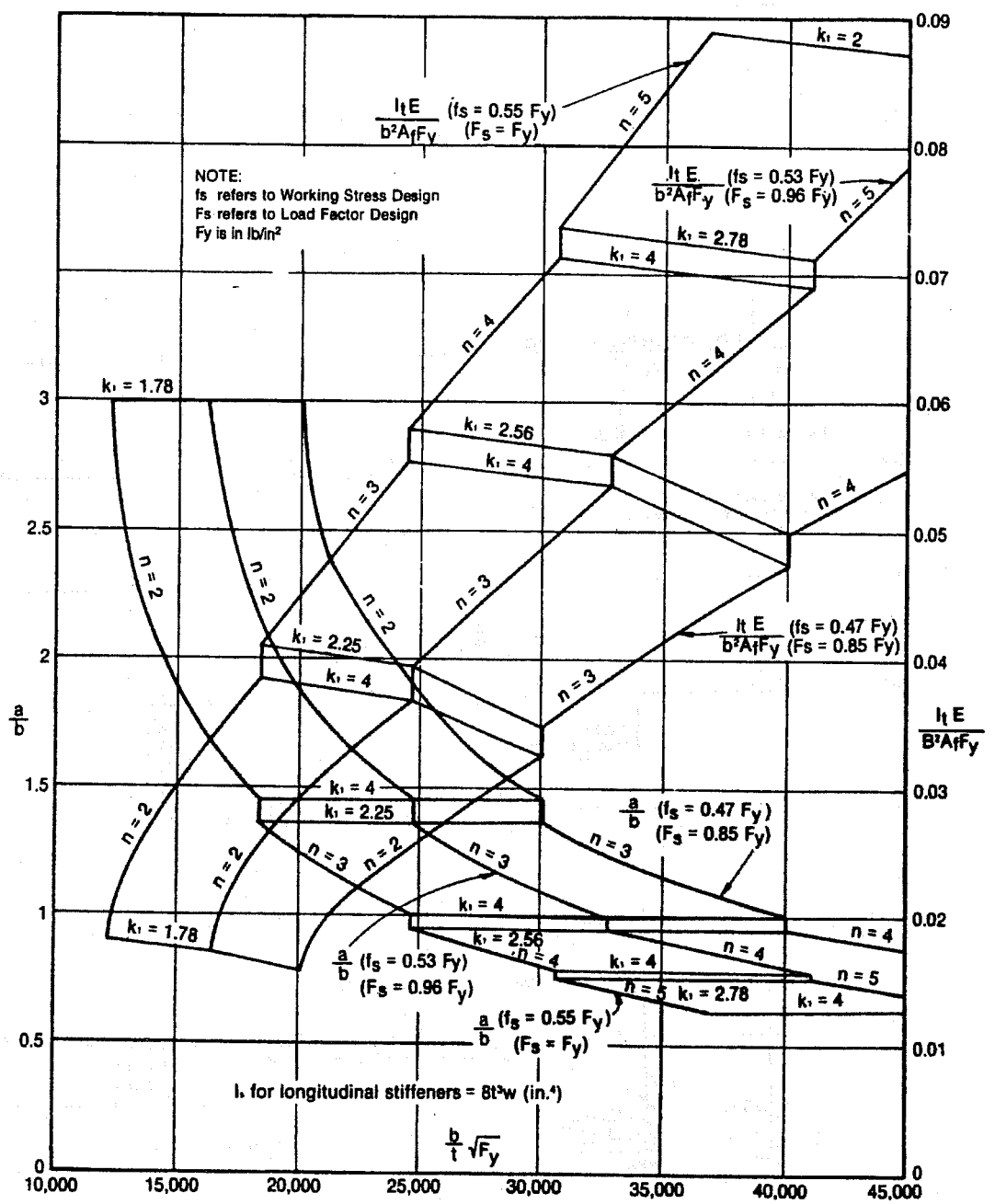

Figure 2.10 Spacing and Size of Transverse Stiffeners

Using Figure 2.9, the designer can discern the required number of stiffeners and stiffener size to reach a desired stress level for a specified compression flange with a known slenderness, b/t, and yield strength, F_y. The figure shows requirements for plates with both longitudinal and transverse stiffeners and for plates with only longitudinal stiffeners. The figure shows a preference for use of the smallest number of longitudinal stiffeners possible. It is possible to use several smaller stiffeners to reach the desired buckling stress level. However, the design aid does not show this alternative in the curves presented. For example, for the longitudinal stiffener without transverse stiffeners, only the option of using one stiffener is shown up to the level of

$$\frac{b}{t}\sqrt{F_y} = 12{,}280 \qquad (2.16)$$

It is possible to use two smaller stiffeners rather than a single longitudinal stiffener to reach the desired buckling stress level for plates whose $\frac{b}{t}\sqrt{F_y}$ are less than 12,280. Fabrication costs increase with the addition of each stiffener, and the approach in North America has been to use as few stiffeners as possible to meet the required capacity needs. Subsequently the design aid shows the option that provides the desired stress level using the fewest number of stiffeners.

Figure 2.9 also shows the significant increase in the required longitudinal stiffener size when multiple longitudinal stiffeners are used without transverse stiffeners. For example, for a flange with a $\frac{b}{t}\sqrt{F_y}$ of 20,000 and sufficient transverse stiffeners, an allowable stress of 0.55Fy can be used by providing a longitudinal stiffener with an I_s of $2.00bt^3$. For the same flange with no transverse stiffeners, a longitudinal stiffener with an of I_s of $26.5bt^3$ must be provided to reach the same allowable stress. The required longitudinal stiffener moment of

inertia with sufficient transverse stiffeners is less than one-thirteenth that required when transverse stiffeners are not used. As the number of longitudinal stiffeners is increased, the disparity between the stiffener size required with and without transverse stiffeners increases.

Using Figure 2.10 the designer can determine both the required size and spacing of transverse stiffeners to reach the desired stress level for a compression flange with a specified slenderness and strength. The value of $\frac{b}{t}\sqrt{F_y}$ for the flange is used to enter the chart. Based on the desired capacity, the number of stiffeners and required aspect ratio (transverse stiffener spacing) can be read from the set of a/b curves. The a/b curves are the set of curves that span between the upper left and lower right of the plot. This figure layout also shows a preference for using the fewest number of longitudinal stiffeners required for the desired buckling stress level. The figure displays the penalty for using a larger number of longitudinal stiffeners at the step points where the curves for different numbers of longitudinal stiffeners intersect. The required relative transverse stiffener size to reach the desired stress level can be determined from the second set of curves.

The code also stipulates in Section 10.39.4.4.7 the requirements for transverse stiffener attachment stating, "the transverse stiffeners need not be connected to the flange plate but shall be connected to the webs of the box and to each longitudinal stiffener." Thus the specification allows the transverse stiffeners to be raised to clear the longitudinal stiffener for ease of construction.

The Specifications in the ASD portion of the AASHTO code for flanges stiffened both longitudinally and transversely are also based on work by Timoshenko and Gere. The buckling coefficient for flanges stiffened both longitudinally and transversely was obtained by considering one panel of the

flange between transverse stiffeners (Mattock 1967). The buckling coefficient is calculated using Equation (2.13), which is repeated below in (2.17).

$$k = \frac{(1+\beta^2)^2 + (n+1)\gamma}{(n+1)^2\beta^2(1+(n+1)\delta)} \tag{2.17}$$

For flanges stiffened both longitudinally and transversely, a specified longitudinal stiffener stiffness of

$$I_s = 8t^3w \tag{2.18}$$

is used. This stiffness corresponds to the requirement for flanges stiffened only longitudinally with a single longitudinal stiffener and a buckling coefficient of four. Using $8wt^3$ for I_s and 0.3 for poisson's ratio, the value of γ can be calculated.

$$\gamma = \frac{EI_s}{bD} = \frac{E\left(8\frac{b}{(n+1)}t^3\right)}{b\left(\frac{Et^3}{12(1-\nu^2)}\right)} = \frac{87.3}{n+1} \tag{2.19}$$

Therefore,

$$(n+1)\gamma = 87.3 \tag{2.20}$$

Using a conservative value of 0.1 for δ and the above expression for $(n+1)\gamma$ in Equation (2.17) results in the following equation for the k_1 plate buckling coefficient contained in the AASHTO ASD code:

$$k_1 = \frac{\left(1+(a/b)^2\right)^2 + 87.3}{(n+1)^2(a/b)^2[1+0.1(n+1)]} \tag{2.21}$$

The value of k_1 is limited to a maximum of four in the code. To use the maximum k_1 coefficient, the transverse stiffener spacing, "a," must be equal to or

less than 4w. If transverse stiffeners are present but "a" is greater than 3b, the capacity is calculated using the equations for flanges stiffened only longitudinally.

Proportioning of the transverse stiffeners was based on work by Timoshenko and Gere on buckling of continuous beams on elastic supports. The transverse stiffeners are assumed to provide discrete points of lateral resistance to each unit width column. The longitudinally stiffened plate is modeled as an equivalent group of unit width columns (Mattock 1967) arranged side by side each other, as shown in Figure 2.11. If N_{cr} is the buckling load for the plate, then the buckling load for each unit width column is N_{cr}/b, where b is the plate width. The buckling load of each unit width column will be referred to as P_{cr}.

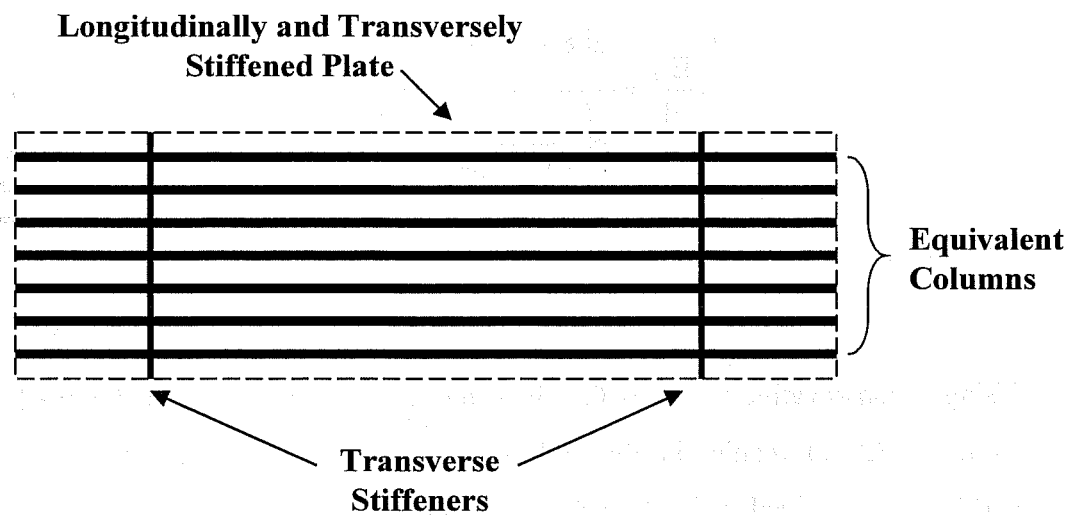

Figure 2.11 Stiffened Plate - Equivalent Group of Columns

The transverse stiffeners are modeled as elastic supports to the equivalent columns, as shown in Figure 2.12.

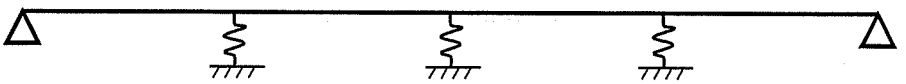

Figure 2.12 Support of Equivalent Columns by Transverse Stiffeners

A column that is laterally supported by elastic supports of rigidity α at intervals of "a" will behave as if the supports are rigid when "a" is equal to or greater than

$$\alpha = \frac{P_{cr}}{\eta a} \tag{2.22}$$

where P_{cr} is the buckling load for a column of length "a", and η is a numerical factor that approaches 0.25 as the number of spans increases (Timoshenko 1961). Therefore the required minimum support rigidity has a limiting value of:

$$\alpha = \frac{4P_{cr}}{a} \tag{2.23}$$

Therefore the minimum stiffness of the transverse stiffeners required to support each unit width of the column is

$$\alpha = \frac{4N_{cr}}{a\,b} \tag{2.24}$$

The buckling load of the plate can then be expressed as

$$N_{cr} = A_f f_{su} \tag{2.25}$$

where A_f is the cross-sectional area of the plate and longitudinal stiffeners and f_{su} is the stress in the plate at elastic buckling. Using an allowable stress approach,

$$f_{su} = \frac{f_s}{0.55} \tag{2.26}$$

where f_s is the stress in the flange at service load. Thus the required support rigidity is

$$\alpha = \frac{4\left(\frac{f_s}{0.55}\right)A_f}{a\,b} \tag{2.27}$$

The support rigidity supplied to the unit width columns by the transverse stiffener will be a minimum for the unit width column located at the midspan of the transverse stiffener (Mattock 1967).

Assuming that the same restraining force, p, is supplied to each of the unit width columns by the transverse stiffener, and conservatively using the stiffness provided to the column located at the midspan of the transverse stiffener, then the stiffness provided will be

$$\alpha = \frac{p}{\Delta} = \frac{384EI_t}{5b^4} \tag{2.28}$$

where Δ is the midspan deflection of the transverse stiffener due to the uniformly distributed load from the equivalent columns, and I_t is the moment of inertia of the transverse stiffener about its centroid.

There is a degree of conservatism inherent in this approach since the critical column at the midspan of the plate is used to calculate the required stiffness. However, since in the AASHTO specifications the transverse stiffeners have to be attached only to the longitudinal stiffener, and not to the flange plate, there is only a resistance to lateral movement provided at the points of attachment between the transverse stiffeners and longitudinal stiffener, not across the full width of the flange plate. Furthermore this approach does not consider the presence of initial imperfection in the transverse stiffener, which would indicate a

larger stiffness requirement. The transverse stiffener requirement should be reviewed with inclusion of these factors.

Equating the provided and required stiffness in Equations (2.27) and (2.28),

$$\frac{384EI_t}{5b^4} = \frac{4f_s A_f}{0.55a\,b} \tag{2.29}$$

Transposing these expressions and substituting (n+1)w for b, the value of I_t can be found:

$$I_t = 0.1(n+1)^3 w^3 \frac{f_s}{E} \cdot \frac{A_f}{a} \tag{2.30}$$

This is the transverse stiffener requirement contained in the ASD portion of the AASHTO code (Mattock 1967).

2.4 Proposed Requirements for Plates with Multiple Stiffeners

Chai Yoo, Byung Choi, and Elizabeth Ford, researchers at Auburn University, have recently completed an investigation of the AASHTO requirements for plates with multiple longitudinal stiffeners (Yoo 2001, Ford 2000). This is one aspect of the AASHTO LRFD code that has warranted additional attention, as the LRFD specification requirements do not address flanges with both longitudinal and transverse stiffeners, and can lead to extremely large stiffener sizes when multiple stiffeners are used. The Auburn researchers assert that the LRFD code equations give a reasonable required moment of inertia, I_s, when the number of stiffeners is less than or equal to two, but that the equation requires unreasonably large values for I_s when multiple stiffeners are used.

The Auburn researchers attribute the over-conservatism in the LRFD requirements to two fundamental assumptions. The first of these is that the analytical model used in the development of the equations assumes an infinitely

long plate strip. They observe that an infinitely long plate strip will never be subjected to uniform compressive stresses over its entire length since the stress in the bottom flange is not uniform, and varies sharply at intermediate supports. The simplifying assumptions used in obtaining the AASHTO code equations do lead to the underlying expectation of very large aspect ratios.

The second point that is questioned is the assumption that the plate buckling coefficient, k, can be less than 4. This implies that the longitudinal stiffener will not remain straight, which is contradictory to the idea that a nodal line will form along the stiffener. The researchers state that they will use a longitudinal stiffener with the minimal required rigidity for formation of a nodal line along the stiffener and that by so doing produce an anti-symmetric buckling mode and yield a better design (Ford 2000).

The Auburn researchers have proposed replacing the required moment of inertia of longitudinal stiffeners for compression flanges stiffened longitudinally, and compression flanges stiffened longitudinally and transversely, with the requirement shown below.

$$I_s = 0.3\alpha^2\sqrt{n}\, w t_f^3 \qquad (2.31)$$

where $\alpha = a/w$

The proposed equation is significantly influenced by the transverse stiffener spacing, a. The researchers make no new recommendations on the required size of transverse stiffeners, so it is assumed the recommendations currently in the AASHTO specifications are considered adequate.

The paper by Yoo et al includes a table showing current stiffener requirements and those obtained using the proposed equation for various values of α, n, w, and t_f. Parts of the first four rows of this table are presented in Table 2.1. The stiffened plate configurations shown in Table 2.1 were checked using a finite

element eigenvalue analyses (ABAQUS). The proposed stiffener sizes when a/w equals 1 were found slightly inadequate to cause anti-symmetric buckling. The stiffener sizes proposed were found to be adequate to cause anti-symmetric buckling when a/w equals 5.

The AASHTO LRFD stiffener requirements assuming k=4, for compression flanges stiffened only longitudinally were calculated. The AASHTO requirement for I_s was added to the data from Yoo and is shown in Table 2.1. This enables comparison of the proposed requirements with the current AASHTO requirements. It is apparent that the AASHTO LRFD requirement does not vary with the a/w ratio since no transverse stiffeners are required for the design equations for compression flanges stiffened only longitudinally.

Table 2.1 Compression Flanges Stiffened with Only Longitudinal Stiffeners

a/w	n	w (in)	tf (in)	I_s - AASHTO LRFD (in^4)	I_s - Proposed (in^4)
1	1	80	0.75	270	10.13
5	1	80	0.75	270	253.13
1	3	80	0.75	12,247	17.54
5	3	80	0.75	12,247	438.43

The data show that for single stiffeners when a/w equals 1, the proposed stiffener size is significantly less than the current AASHTO requirement for compression flanges stiffened longitudinally. For single stiffeners the proposed equation is analogous to the AASHTO requirement when a/w equals 5. Though not presented in the paper, for values of a/w greater than 5.16, the proposed

equation actually indicates a larger stiffener size requirement for a single longitudinal stiffener than that currently required by the code.

For the cases in Table 2.1 where n equals 3, it can be seen that regardless of the transverse stiffener spacing, the proposed stiffener size is significantly less than the AASHTO requirement. For small a/w values there is a significant reduction in the required moment of inertia for multiple stiffeners by use of the proposed formula when compared to the current AASHTO requirements for compression flanges stiffened only longitudinally. As a/w approaches infinity, the proposed equation indicates that stiffeners larger than that currently required by the code are necessary.

As already discussed, the ASD portion of the AASHTO Standard Specifications contains requirements for compression flanges stiffened longitudinally and transversely. Comparison of the proposed equation to the AAHSTO ASD requirements was not made in the report by Yoo et al. The AASHTO ASD requirements for flanges stiffened both longitudinally and transversely use a modified buckling coefficient, k_1. The table below shows the required value of a/w to obtain k_1 equal to 4, and the non-dimensional stiffener requirement of AASHTO ASD and Yoo et al. When k_1 equals to 4, there is a match point where the results of the AASTHO equation and the proposed equation can be appropriately compared. At larger transverse stiffener spacings, the approach currently used by the code is to hold the required moment of inertia constant, while varying the buckling coefficient. The approach used by Yoo et al is to hold the buckling coefficient equal to 4, and vary the required moment of inertia. Thus, for larger transverse stiffener spacings, it is inappropriate to directly compare the moment of inertia required by AASHTO to that recommended by the proposed equation.

Table 2.2 Compression Flanges Stiffened Longitudinally and Transversely

n	a/w	k_1	AASHTO ASD I_s/wt^3	Proposed I_s/wt^3
1	4	4	8	4.8
2	4	4	8	6.79
3	4	4	8	8.31
4	3.87	4	8	8.99
5	3.73	4	8	9.33

For the one match point where the k_1 factor in the code equals 4, just as the proposed equation assumes k equal to 4, the proposed equation and the current equation contain comparable stiffness requirements. The AASHTO approach (hold I, vary k) and the proposed approach (hold k, vary I) lead to different stiffener configurations, and subsequently different capacities, away from the match point compared above.

In the work by Yoo et al the assumption that the value of the plate buckling coefficient can be less than 4 is dismissed. A plate buckling coefficient less than 4 reflects the presence of a small stiffener that does not force anti-symmetric buckling. Stiffeners that do not force anti-symmetric buckling can still significantly increase the buckling capacity of the compression flange. Finite element analyses results that will be discussed in Chapter 4 have verified this contribution of stiffeners smaller than that required to force anti-symmetric buckling in eigenvalue analyses.

2.5 Cold Formed Steel Design Manual

The Cold Formed Steel Design Manual of the American Iron and Steel Institute (AISI) contains design equations for uniformly compressed elements with one intermediate stiffener. The capacity equations in the AISI manual were compared to the design provisions contained in the AASHTO LRFD Bridge Specification.

The AISI formulation contains separate equations for determination of the plate buckling coefficient in the AISI code transition region and determination of the coefficient for slender flanges. No intermediate stiffener is required for stocky flanges. The AISI design equations for slender and transition flanges are presented below.

For $S < b_o/t < 3S$

$$k = 3(I_s/I_a)^{1/2} + 1 \leq 4$$

$$I_a/t^4 = [50(b_o/t)/S]-50$$

For $b_o/t \geq 3S$

$$k = 3(I_s/I_a)^{1/3} + 1 \leq 4$$

$$I_a/t^4 = [128(b_o/t)/S]-285$$

where:

k = buckling coefficient

b_o = plate width

S = $1.28\sqrt{E/f}$

I_s = Moment of inertia of stiffener about its own centroidal axis parallel to the element to be stiffened

I_a = Adequate moment of inertia of the stiffener, so that each component element will behave as a stiffened element

E = Elastic modulus

f = Member stress

The AISI plate buckling coefficients were compared to those in AASHTO. In this comparison, F_y was used for f in the AISI equations. The AASHTO requirements are based on the moment of inertia of the stiffener about the base of the stiffener. To enable direct comparison of the AISI and AASHTO requirements, use of plate stiffeners was assumed. Therefore the AISI I_s (centroidal) is equal to 1/4 of the AASHTO I_s (about base of stiffener).

The buckling coefficients obtained using the AISI equations, and the buckling coefficient based on the AASHTO equation for single stiffeners are plotted vs. I_s/I_a in Figure 2.13 and Figure 2.14. These plots show a weakness of the AAHTO formulation previously mentioned. The AASHTO formulation gives unrealistically low predictions for the strength of the stiffened plate when small stiffeners are used, and can actually indicate that the stiffened plate has less capacity than an unstiffened plate of the same geometry. The buckling coefficient in the AASHTO formulation goes to zero, instead of to one: the buckling coefficient of the unstiffened plate.

The buckling coefficients based on AISI and AASHTO agree extremely well in the transition region, where $S < b_o/t < 3S$. The AISI formulation appropriately goes to one, the capacity of the unstiffened plate, for small stiffener sizes. For slender plates, where $b_o/t > 3S$, AISI predicts larger buckling coefficients than AASHTO for a given stiffener size. The AISI equations indicate that smaller stiffeners contribute more significantly to the buckling capacity for slender plates than do the AASHTO capacity equations.

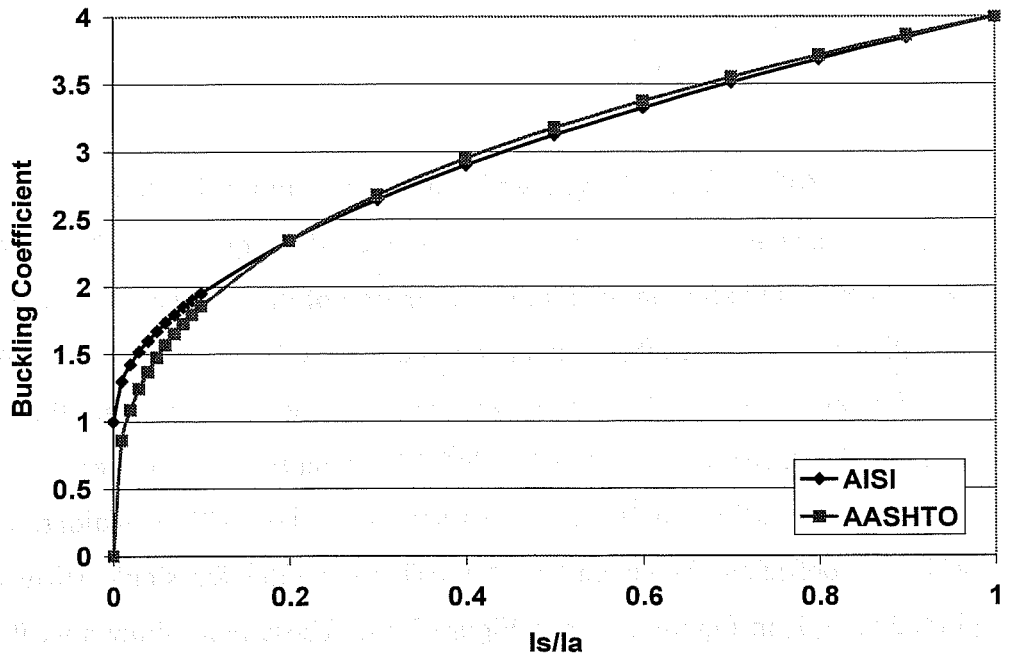

Figure 2.13 AISI vs. AASHTO: S < bo/t < 3S

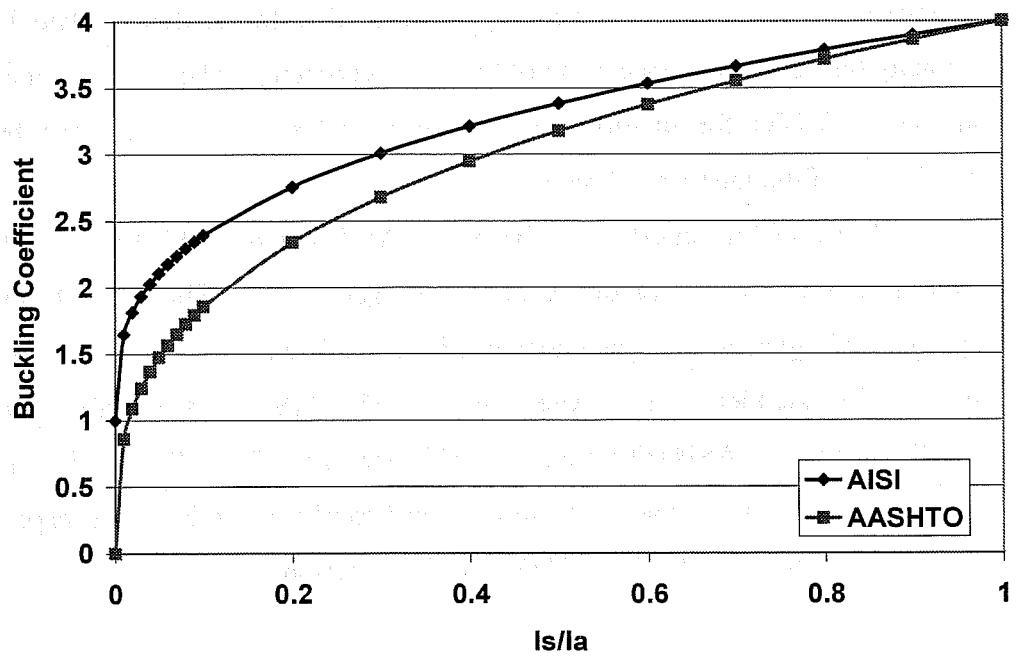

Figure 2.14 AISI vs. AASHTO: bo/t > 3S

Based on the AISI formulation of the buckling coefficient in the transition region, a proposed replacement for the AASHTO buckling coefficient equation for flanges with single longitudinal stiffeners was developed. The AISI equation for k in the transition zone is

$$k = 3(I_s/I_a)^{1/2} + 1 \leq 4 \tag{2.32}$$

The size of an adequate stiffener was calculated using the AASHTO equation assuming a buckling coefficient of 4. The size of the adequate stiffener based on AASHTO is

$$I_{adequate} = 8wt^3 \tag{2.33}$$

Substituting the above expression for $I_{adequate}$ for I_a in Equation (2.32), yields the equation below for the buckling coefficient.

$$k = \left(\frac{9I_s}{8wt^3}\right)^{\frac{1}{2}} + 1 \tag{2.34}$$

The proposed equation is graphed with the current AASHTO requirement in Figure 2.15. The equations show close agreement for buckling coefficients between 2 and 4. For small stiffeners, producing buckling coefficients less than 2, the proposed equation predicts a larger buckling coefficient then the current equation. The proposed equation appropriately approaches 1, the buckling coefficient of the unstiffened plate, when I_s/wt^3 approaches zero.

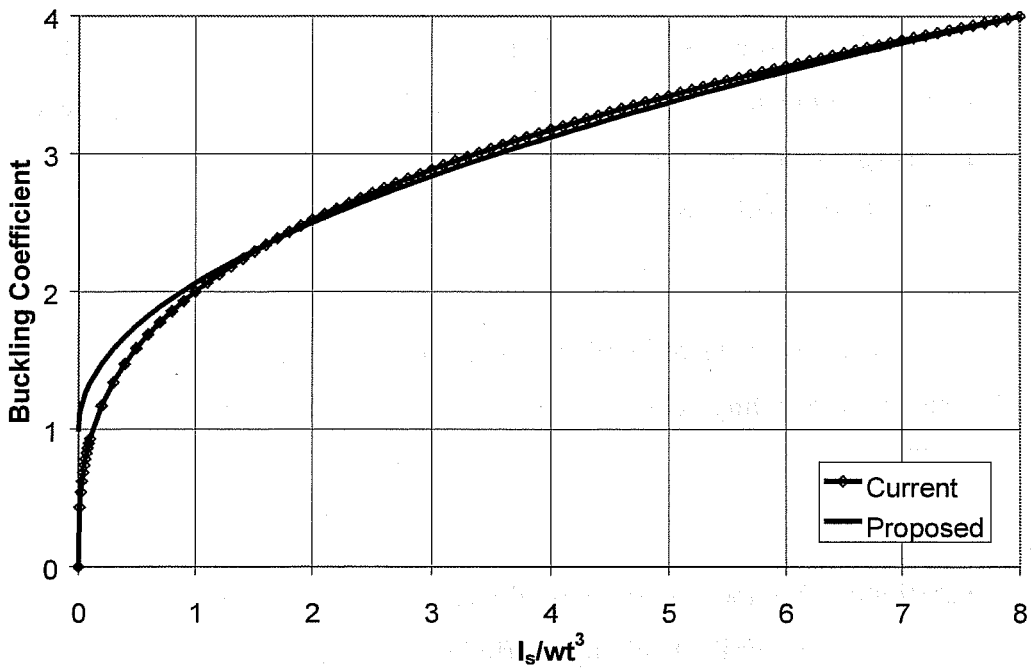

Figure 2.15 Current and Proposed Equation for Buckling Coefficient of Plate with Single Longitudinal Stiffener

A new equation for the buckling coefficient of plates with 2 to 5 longitudinal stiffeners was also developed based on the AISI formulation. The size of an adequate stiffener was calculated from the AASHTO buckling coefficient equation for plates with multiple stiffeners using a k value of 4.

$$I_{adequate} = \frac{64}{14.3} wt^3 n^4 \qquad (2.35)$$

Substituting the above expression for $I_{adequate}$ for I_a in Equation (2.32), yields the equation below for the buckling coefficient.

$$k = \left(\frac{2I_s}{wt^3 n^4} \right)^{\frac{1}{2}} + 1 \qquad (2.36)$$

The proposed equation is graphed with the current AASHTO requirement in Figure 2.16 for two longitudinal stiffeners (n=2). The equations again show close agreement for buckling coefficients between 2 and 4. For small stiffeners, where the buckling coefficient is less than 2, the proposed equation again predicts a larger buckling coefficient then the current equation. The proposed equation approaches 1, the buckling coefficient of the unstiffened plate, as is appropriate when I_s/wt^3 approaches zero unlike the AASHTO equation. Similar agreement is seen between the current and proposed equation when 3, 4, or 5 longitudinal stiffeners are used.

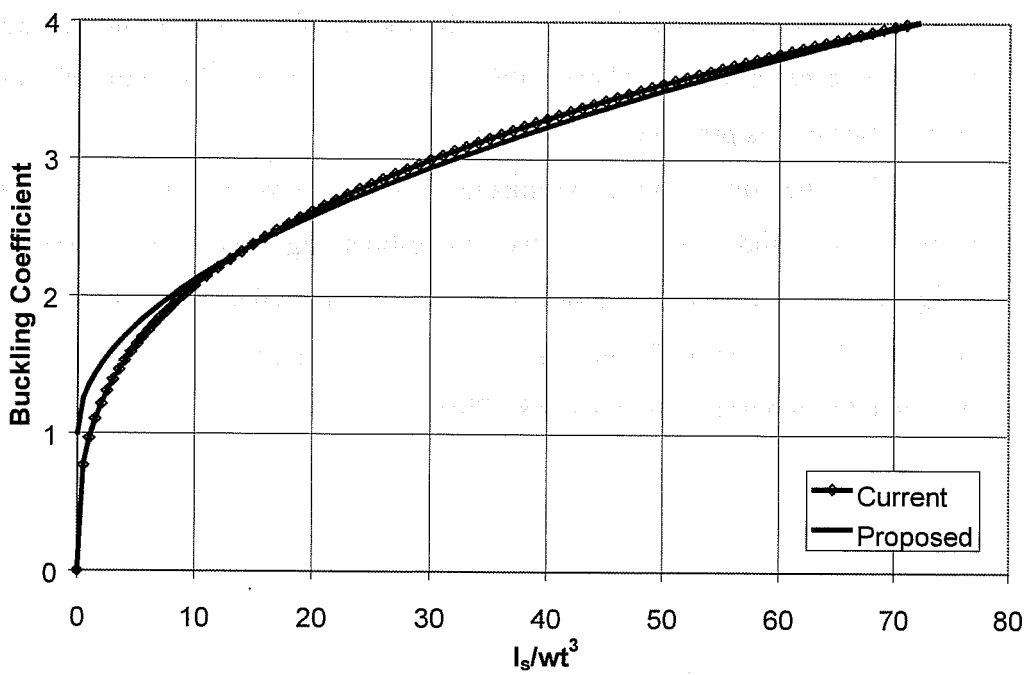

Figure 2.16 Current and Proposed Equation for Buckling Coefficient of Plate with Two Longitudinal Stiffeners

Based on the formulation of the buckling coefficient presented in the AISI Cold Formed Steel Design Manual new buckling coefficient equations were developed for the AASHTO specification. The proposed equations approach a buckling coefficient of 1, the capacity of the unstiffened plate, as the stiffener size decreases. The current formulation in the AASHTO specification illogically goes to zero as the stiffener size is decreased.

2.6 Analytical and Experimental Program

The basis of the design approach used in AASHTO for compression flanges of box girder bridges is elastic plate buckling theory. The basis of the design approach used in the Proposed Design Specifications for Steel Box Girders presented by Wolchuk is a strut approach. The approach recommended by Wolchuk makes direct consideration of the magnitude of initial imperfections and residual stresses in predicted capacities. A discussion of initial imperfections and residual stresses is presented in Chapter 3.

An analytical and experimental research program was undertaken to evaluate the validity of eigenvalue (plate-buckling) and strut approaches for design of box girder compression flanges. An analytical study of compression flange buckling was performed, and is discussed in Chapter 4. The subsequent experimental program is discussed in Chapter 5.

Chapter 3

Initial Imperfections and Residual Stresses

3.1 Introduction

The magnitude of initial imperfections and residual stresses have been directly considered in the development of some design approaches, including that contained in the Proposed Specifications for Steel Box Girder Bridges (Wolchuk 1980). Initial imperfections, particularly stiffener out-of-straightness, were found to significantly affect the response of the stiffened plates tested in the experimental program of this dissertation research. A study of initial imperfections, and imperfection tolerances and their history was completed and is documented in this chapter. There are more specified tolerances for webs than for box girder flanges, but the reasons for the specification of the specific web tolerances was not clear, and was researched.

The impact of residual stresses was also found to be important for certain plate geometries in the analysis procedure comparison presented in Chapter 8. A short discussion of residual stresses is presented at the end of this chapter.

3.2 Initial Imperfections of Plates and Stiffeners

All plates have initial out-of-flatness and all stiffeners have some degree of out-of-straightness. The manufacturing and fabrication process, including the welding of stiffeners to the plate, can increase the magnitude of the out-of-flatness of the plate and the out-of-straightness of the stiffener. The fundamental effect of the geometric imperfections is to produce out-of-plane plate deflections with the initial application of load. The out-of-plane deflections grow as more load is applied. Figure 3.1 shows the general impact of initial imperfections on an

unstiffened plate, where P is the applied load and P_{cr} is the elastic buckling load of the plate. Figure 3.1 was generated based on finite element results and a figure presented by the European Convention for Structural Steelwork (ECCS 1986).

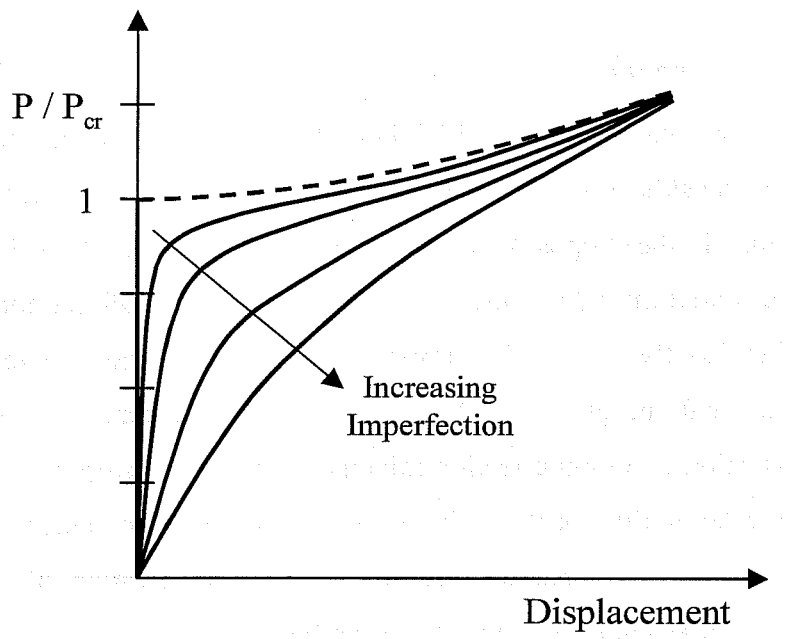

Figure 3.1 Effect of Imperfection on Elastic Response of Plate in Compression

The effects of the out-of-flatness reduce the initial stiffness of the plate. Therefore with larger initial imperfections there are larger plate displacements at low loads. However, as shown in the figure, with any level of imperfection, the plate still approaches the path of the ideal plate at higher levels of strain. A plate with significant imperfections will undergo large displacements to approach the path of the ideal plate. At a given load level below the buckling load, the displacements are substantially larger for larger initial imperfections. The larger displacements that occur at lower loads are important, particularly for an element of a bridge that is subject to cyclical loading.

Much literature on plate buckling makes reference to initial imperfections, but the conclusions on the impact of imperfections have varied. At one extreme

the significance of the initial imperfections has been questioned. Consequently the effect of residual stresses has been neglected in some analytical studies (Singer 1998, Fukumoto 1974, Korol 1984). Linear elastic buckling theory does not include the effects of initial imperfections existing in plates and stiffeners.

The other extreme is that the impact of the initial imperfections is extremely important. The latter viewpoint is one that has been supported by the European Convention for Constructional Steelwork, Merrison, Wolchuk, Frieze, Little, and others. The experiments conducted as part of this dissertation research found the presence of certain initial imperfections significantly influenced the behavior of the stiffened test plates.

3.2.1 American Specifications - Variation from Flatness

The specifications of the American Society for Testing & Materials (ASTM) include dimensional tolerances for steel plates and shapes. ASTM A6 contains tolerances on out-of-flatness and out-of-straightness of steel plates and structural shapes. The American Welding Society's Bridge Welding Code (AWS D1.5), a joint publication of the American Welding Society (AWS) and AASHTO, also contain dimensional tolerances for welded elements and girder webs. The AASTHO LRFD Bridge Construction Specifications contain tolerance limits for orthotropic-deck bridge members.

The tolerance requirements of the American Bureau of Shipping (ABS) were also researched. The American Bureau of Shipping Rule Requirements for Materials and Welding 2001 was reviewed. This publication contains maximum permissible under thickness tolerances for hull steel plates, and out-of-roundness for boilers and pressure vessels, but does not specify out-of-flatness or out-of-straightness tolerances for plates and stiffeners.

The tolerance requirements provided by ASTM and AWS are referenced by other specifications for steel structures. The Load and Resistance Factor Design Manual of Steel Construction (AISC 1994) plate provisions are a subset of the requirements presented by ASTM. The Texas Standard Specifications for Construction of Highways, Streets and Bridges (TXSS 1993) refer to both ASTM A6 and AWS D1.5.

The basis for the out-of-flatness tolerances in ASTM A6 and AWS D1.5 is not apparent. It has been surmised that the requirements in ASTM A6 are based on tolerances that can be reasonably obtained using standard production procedures. The theoretical basis, if any, for the out-of-flatness requirements for webs in the AWS Bridge Welding code was not found.

There is significant confusion regarding the appropriate method of measuring plate out-of-flatness to meet the specified tolerances in some American specifications. Hence, there is confusion over what the out-of-flatness tolerances actually mean. Some have interpreted certain tolerance requirements to be a deviation from plate-centerline requirement, while others have interpreted the same requirement as being an out-to-out tolerance, or sum of the worst peaks and valleys across the plate. Both of these methods of measuring plate imperfection are shown in Figure 3.2. The magnitude of Δ_1, the deviation from plate centerline, is significantly different from Δ_2, the sum of the peak and valley measurements for the imperfection in the figure.

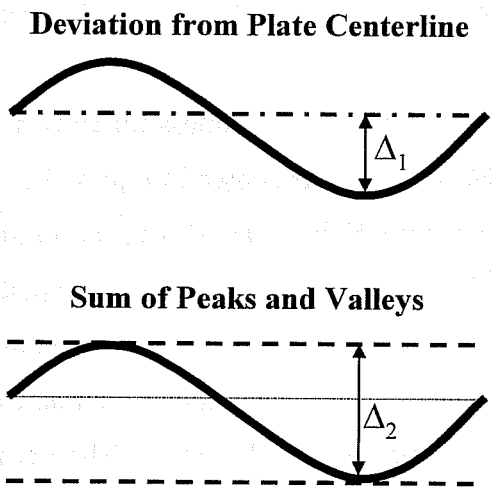

Figure 3.2 Methods of Measuring Initial Imperfection

3.2.1.1 ASTM A6 (2000) - Plate Out-of-Flatness

The ASTM tolerances for steel plate out-of-flatness are contained in the ASTM A6/A6M Standard Specification for General Requirements for Rolled Structural Steel Bars, Plates, Shapes and Steel Piling. The specific basis for selection of the out-of-flatness and out-of-straightness tolerances in ASTM is not known. An informal survey of structural engineering professors, Texas Department of Transportation personnel, TxDOT contacts, and review of related literature revealed no concrete history on the source of any of the tolerances. It is believed by some surveyed that the plate and shape fabrication tolerances were derived from actual flatness and straightness measurements that were reasonably obtainable using common production practices.

ASTM Specification A6 was issued in 1949. The specifications pertaining to steel plate prior to 1949 do not appear to contain out-of-flatness requirements (ASTM 1946). The out-of-flatness of plates and camber tolerances for plates and structural shapes have been specified in ASTM A6 since at least 1958 (ASTM A6-58). The out-of-flatness tolerances for plates are generally 1/16 in. more

stringent in the current standards than the tolerances used in the 1950's and 1960's.

The permitted variations in flatness for carbon steel plates are presented in Table 13 of ASTM A6, which is shown in Figure 3.3. For plates with a specified minimum tensile strength higher than 60 ksi, the limits in the table are increased by 50%. The specified thickness, or weight, of the plate and the width of the plate are used to enter the table, and the permitted variation from a flat surface of the plate is read from the table. The permitted variation from a flat surface across the width of the plate is specified in the table. The permitted variation from a flat surface along the length must not exceed the tabular amount for plates up to 12 ft. in length, or in any 12 ft. of length for longer plates.

The specification does not clearly explain how to measure the variation from a flat surface of a plate. The specification states that the plate must be in a horizontal position on a flat surface when flatness is measured, but there is no additional guidance on the procedure for measuring the variation. From the title of the table, "Permitted Variations from a Flat Surface," it is obvious that the plate should be measured with respect to a flat surface, but it is not clear if the out-of-flatness should be measured from a plane passing through the centerline of the plate, from a plane adjacent to the surface of the plate, or by using some other method.

TABLE 13 Permitted Variations From a Flat Surface for Carbon Steel Plates

NOTE 1—When the longer dimension is under 36 in., the permitted variation from a flat surface shall not exceed ¼in. When the longer dimension is from 36 to 72 in., incl, the permitted variation from a flat surface shall not exceed 75 % of the tabular amount for the specified width, but in no case less than ¼ in.

NOTE 2—These permitted variations apply to plates that have a specified minimum tensile strength of not more than 60 ksi or comparable chemical composition or hardness. The limits in this table are increased 50 % for plates that have a higher specified minimum tensile strength or comparable chemical composition or hardness.

NOTE 3—This table and these notes cover the permitted variations from a flat surface for circular and sketch plates, based upon the maximum dimensions of such plates.

NOTE 4—Where "..." appears in this table, there is no requirement.

NOTE 5—Plates must be in a horizontal position on a flat surface when flatness is measured.

Specified Thickness, in.	Specified Weight, lb/ft²	Permitted Variations from a Flat Surface for Specified Widths Given in Inches, in.[A,B]										
		To 36, excl	36 to 48, excl	48 to 60, excl	60 to 72, excl	72 to 84, excl	84 to 96, excl	96 to 108, excl	108 to 120, excl	120 to 144, excl	144 to 168, excl	168 and Over
To ¼, excl	To 10.2, excl	9/16	3/4	15/16	1 1/4	1 3/8	1 1/2	1 5/8	1 3/4	1 7/8	...	...
¼ to ⅜, excl	10.2 to 15.3, excl	½	5/8	3/4	1 5/16	1 1/8	1 1/4	1 3/8	1 1/2	1 5/8	...	...
⅜ to ½, excl	15.3 to 20.4, excl	½	9/16	5/8	5/8	3/4	7/8	1	1 1/8	1 1/4	1 7/8	2 1/8
½ to ¾, excl	20.4 to 30.6, excl	7/16	½	9/16	5/8	5/8	3/4	1	1	1 1/8	1 1/2	2
¾ to 1, excl	30.6 to 40.8, excl	7/16	½	9/16	5/8	5/8	5/8	3/4	7/8	1	1 3/8	1 3/4
1 to 2, excl	40.8 to 81.7, excl	3/8	½	½	9/16	9/16	5/8	5/8	5/8	1 1/16	1 1/8	1 1/2
2 to 4, excl	81.7 to 163.4, excl	5/16	3/8	7/16	½	½	½	½	9/16	5/8	7/8	1 1/8
4 to 6, excl	163.4 to 245.1, excl	3/8	7/16	½	½	9/16	9/16	5/8	3/4	7/8	7/8	1
6 to 8, excl	245.1 to 326.8, excl	7/16	½	½	5/8	11/16	3/4	7/8	7/8	1	1	1
8 to 10, excl	326.8 to 409.0, excl	½	½	5/8	11/16	3/4	13/16	7/8	15/16	1	1	1
10 to 12, excl	409.0 to 490.1, excl	½	5/8	3/4	13/16	7/8	15/16	1	1	1	1	1
12 to 15, excl	490.1 to 613.0, incl	5/8	3/4	13/16	7/8	15/16	1	1	1	1	1	...

[A] *Permitted Variation from a Flat Surface for Length*—The longer dimension specified is considered the length, and the permitted variation from a flat surface along the length shall not exceed the tabular amount for the specified width for plates up to 12 ft in length, or in any 12 ft for longer plates.

[B] *Permitted Variation from a Flat Surface for Width*—The permitted variation from a flat surface across the width shall not exceed the tabular amount for the specified width.

Figure 3.3 Permitted Variations from Flat Surface (ASTM A6)

In Figure 3.4 two potential plate cross sections are shown. The method of measuring the out-of-flatness of even the simple half wave shape is not clear. Two alternate methods of measuring the out-of-flatness of this plate are shown. Measuring the variation from a flat surface touching the edges of the plate width is one option. Another option is measuring the variation from a plane passing through the cross-section of the plate. With a more complex shape, like that shown on the right in Figure 3.4, there are even more potential options for measuring the plate variation. Again the plate could be referenced to an actual flat surface placed next to the extreme edges of the plate. Or the variation from different planes passing through the cross-section could be used. The specification does not clearly state how to make this measurement, and the correct way to measure out-of-flatness of different plates is an issue of current debate.

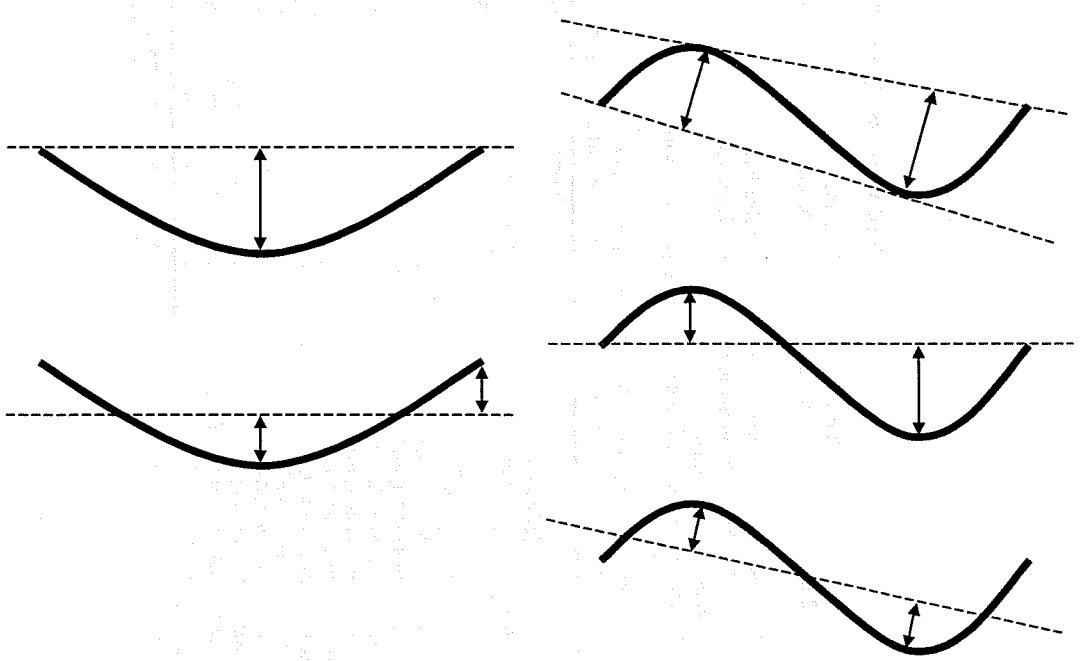

Figure 3.4 Variations from Flat Surface

ASTM A6 also contains limits on the allowable waviness of steel plates. The allowable waviness of a plate is based on the number of waves along the length of a plate. The waviness tolerances provide stricter limits on the plate out-of-flatness when multiple waves occur along the length of the plate. The waviness limits are contained in Table 15 of ASTM A6, which is shown in Figure 3.5. The permitted variation in waviness is a function of the permitted variation from a flat surface of the plate and the number of waves along the length of the plate. For a plate with multiple waves along the length of the plate, the permitted variation in waviness is less than that for a plate with fewer waves along the length.

The specification contains more explicit wording regarding how waviness is measured than it does regarding how flatness is measured. Waviness is defined as the "maximum deviation of the surface of the plate from a plane parallel to the surface of the point of measurement and contiguous to the surface of the plate at each of the two adjacent wave peaks ... as measured in an increment of less than 12 ft of length (ASTM A6)." Waviness is thus the deviation of the surface from a plane that does not cut through the plate, but is adjacent to the surface of the plate.

TABLE 15 Permitted Variations in Waviness for Plates

NOTE 1—Waviness denotes the maximum deviation of the surface of the plate from a plane parallel to the surface of the point of measurement and contiguous to the surface of the plate at each of the two adjacent wave peaks, when the plate is resting on a flat horizontal surface, as measured in an increment of less than 12 ft of length. The permitted variation in waviness is a function of the permitted variation from a flat surface as obtained from Table 13 or 14, whichever is applicable.

NOTE 2—Plates must be in a horizontal position on a flat surface when waviness is measured.

Permitted Variation from a Flat Surface (from Table 13 or 14), in.	Permitted Variation in Waviness, in., When Number of Waves in 12 ft is						
	1	2	3	4	5	6	7
5/16	5/16	1/4	3/16	1/8	1/8	1/16	1/16
3/8	3/8	5/16	3/16	3/16	1/8	1/16	1/16
7/16	7/16	5/16	1/4	3/16	1/8	1/8	1/16
1/2	1/2	3/8	5/16	3/16	3/16	1/8	1/16
9/16	9/16	7/16	5/16	1/4	3/16	1/8	1/8
5/8	5/8	1/2	3/8	1/4	3/16	1/8	1/8
11/16	11/16	1/2	3/8	5/16	3/16	3/16	1/8
3/4	3/4	9/16	7/16	5/16	1/4	3/16	1/8
13/16	13/16	5/8	7/16	5/16	1/4	3/16	1/8
7/8	7/8	11/16	1/2	3/8	1/4	3/16	1/8
15/16	15/16	11/16	1/2	3/8	5/16	1/4	3/16
1	1	3/4	9/16	7/16	5/16	1/4	3/16
1 1/8	1 1/8	7/8	5/8	1/2	3/8	1/4	3/16
1 1/4	1 1/4	15/16	11/16	1/2	3/8	5/16	1/4
1 3/8	1 3/8	1 1/16	3/4	9/16	7/16	5/16	1/4
1 1/2	1 1/2	1 1/8	7/8	5/8	1/2	3/8	1/4
1 5/8	1 5/8	1 1/4	15/16	11/16	1/2	3/8	5/16
1 3/4	1 3/4	1 5/16	1	3/4	9/16	7/16	5/16
1 7/8	1 7/8	1 7/16	1 1/16	13/16	9/16	7/16	5/16
2	2	1 1/2	1 1/8	7/8	5/8	1/2	3/8
2 1/8	2 1/8	1 5/8	1 3/16	7/8	11/16	1/2	3/8
2 1/4	2 1/4	1 11/16	1 1/4	15/16	11/16	9/16	3/8
2 3/8	2 3/8	1 13/16	1 5/16	1	3/4	9/16	7/16
2 1/2	2 1/2	1 7/8	1 7/16	1 1/16	13/16	9/16	7/16
2 5/8	2 5/8	2	1 1/2	1 1/8	13/16	5/8	7/16
2 3/4	2 3/4	2 1/16	1 9/16	1 1/8	7/8	5/8	1/2
2 7/8	2 7/8	2 3/16	1 5/8	1 3/16	15/16	11/16	1/2
3	3	2 1/4	1 11/16	1 1/4	15/16	11/16	9/16
3 1/8	3 1/8	2 3/8	1 3/4	1 5/16	1	3/4	9/16

Figure 3.5 Permitted Variations in Waviness (ASTM A6)

Figure 3.6 shows possible wave patterns along the length of a plate. Two planes are shown by dashed lines next to each wave pattern. The first plane in each of the figures is tangent to the surface at the point of measurement. The second plane is adjacent to the highest neighboring wave peak. Since the specification states that "a plane parallel to the surface of the point of measurement and contiguous to the surface of the plate at *each* of the two adjacent waves" should be used to make the measurement, the measurement from each of the adjacent wave peaks should be checked, and the larger variation, from the higher peak, must pass the specification.

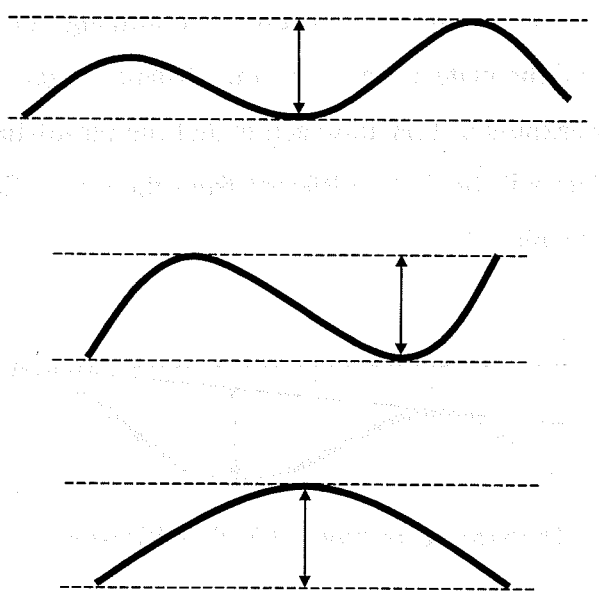

Figure 3.6 ASTM Procedure for Measurement of Waviness

The permitted variations in waviness requirements state that for a plate with one wave along its length, the permitted variation in waviness equals the permitted variation from a flat surface. This statement, equating the waviness and out-of-flatness, implies that the out-of-flatness should be measured using the same standard established for measuring waviness. Hence, the out-of-flatness of the

plate would be the sum of the peak and valley measurements, or an out-to-out measurement of the plate deflected shape.

In practice, the parallel plane approach to measuring out-of-flatness and plate waviness is not used. Based on discussions with TxDOT representatives, and those versed in the specification, it has been learned that the following approach is commonly used to measure plate out-of-flatness. The plate is laid flat on a horizontal surface. A 12 ft. straightedge is placed on the plate touching the plate in at least two locations, as shown by the solid straight line in Figure 3.7. The dashed line of the parallel plane approach is also shown in the figure. The straightedge is placed in the position maximizing the distance between the straightedge and the plate surface, and this distance is reported as the plate out-of-flatness. A weakness of this approach is that the out-of-flatness measured on one face of the plate will likely be different from the out-of-flatness measured on the other face of the plate.

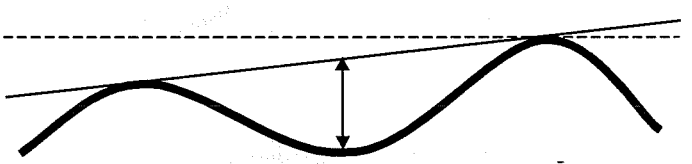

Figure 3.7 Approach Commonly Used to Measure ASTM Out-of-Flatness

3.2.1.2 ASTM A6 (2000) - Stiffener Out-of-Straightness

The ASTM A6 specification also contains guidelines for the permitted variation in straightness of plates and structural shapes. The permitted variations in straightness of structural shapes both vertically (camber) and horizontally (sweep) are discussed. The positions for measuring camber and sweep of a W shape presented in ASTM A6 are shown in Figure 3.8. The camber and sweep of other structural shapes are measured using the same approach as that shown for

the W shape. The permitted camber variation is pertinent to this discussion of initial imperfection since structural shapes are used as longitudinal stiffeners on the bottom flanges of box girders. The out-of-flatness of the stiffened plate is impacted by the out-of-straightness, or camber, of the longitudinal stiffener welded to it. The out-of-straightness of the longitudinal stiffener affects the behavior of the stiffened plate under load.

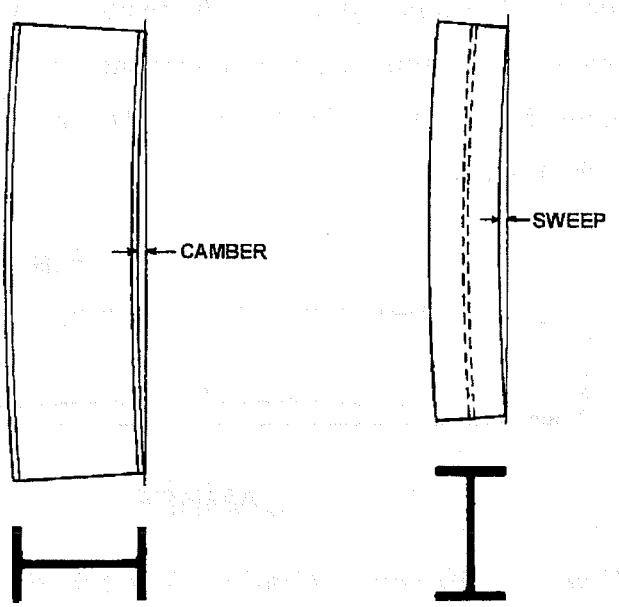

Figure 3.8 Measuring Camber and Sweep of W Shape (ASTM 2000)

The permissible variance in straightness for most standard shapes in ASTM A6 has been the same since at least 1958 (ASTM A6-58). The same camber tolerances are applicable to S and M beams, C and MC channels, angles, tees, and zees, and are specified in Table 21 of ASTM A6. For these structural shapes, when the nominal size is under 3 in. the permitted camber variation is 1/4 in. in any 5 ft., or 1/4 in. times the number of feet of total length divided by 5.

For these structural shapes with nominal size over 3 in., the permitted variation is 1/8 in. times the number of feet of total length divided by 5 ft. A permitted variation of 1/8 in. in 5 ft. of length is equal to a tolerance of L/480, where L is the length of the stiffener.

The permitted camber of universal mill, sheared, special-cut and gas-cut plates is specified in Tables 11 and 12 of ASTM A6. This camber is of interest since plate stiffeners are also used as longitudinal stiffeners. The camber of a plate stiffener is shown in Figure 3.9. The camber is measured with the plate in a flat position, and the permitted variation for plates up to 2 in. thick is 1/8 in. times the number of feet of length divided by 5. This again is a tolerance of L/480, where L is the length of the stiffener.

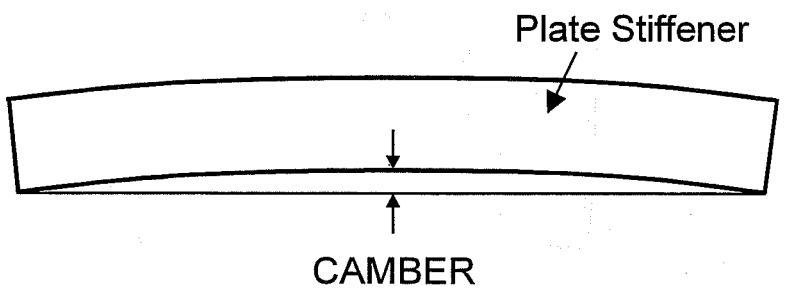

Figure 3.9 Measuring Camber Along Length of Plate Stiffener

3.2.1.3 AISC Manual of Steel Construction

The AISC specifications specify rolling and cutting tolerances in the Mill Practice Section of Part 1 of the Manual of Steel Construction. In very old AISC specifications, such as the Fourth Edition released in 1943, tighter tolerances were in place for the plate geometries addressed. The tolerances for certain plate geometries were half that contained in the current AISC specification. The requirements for plate out-of-flatness in the AISC specification are currently a subset of the ASTM A6 specification.

The camber tolerances contained in the current edition of the AISC LRFD specification are also a subset of the ASTM A6 specification. The AISC tolerance for structural shapes has been essentially the same since the AISC 1943 Specification. The camber tolerances for plates used in the current AISC specification have also been the same since 1943, for the specified plate geometries addressed in 1943.

3.2.1.4 AWS D1.5

The AWS dimensional tolerance requirements are contained in Sections 3.5 and 9.19 of the ANSI/AASHTO/AWS D1.5-95 Bridge Welding Code. Section 3.5 contains general requirements, which apply to welded structural members. This section includes permissible variations in straightness of welded beams or girders, regardless of cross section, where there is no specified camber or sweep, and for girders with specified camber and/or sweep. The specification states that the tolerances apply to welded beams or girders. It does not state that each element of the girder fall within the specified tolerance, and the fact that Section 9.19 contains permissible variations from flatness of webs of girders implies that the general requirements for welded girders are not to be applied to the individual elements of each girder. There are no requirements included in the specification for bottom flanges of box girder bridges. Since the specifications of the American Welding Society (AWS) do not contain out-of-flatness tolerances for the bottom flanges of box girder bridges, the Texas Department of Transportation (TxDOT) has at times applied the web out-of-flatness requirements of AWS to check the bottom flange elements of box girders (Gilmer 2001).

The specifications of the American Welding Society (AWS) have contained tolerances on the variation from flatness of webs since the Fifth Edition

of the Standard Specifications for Welded Highway and Railway Bridges issued in 1956. The tolerances issued in 1956, shown in Figure 3.10, were in place up to at least 1966. The specifications contained an allowable deviation from flatness of girder webs along the length of the web, as shown in Figure 3.10. Specifications since 1972 have not specified that the deviation from flatness be measured simply along the length, but that the deviation should be measured in any position of maximum variation.

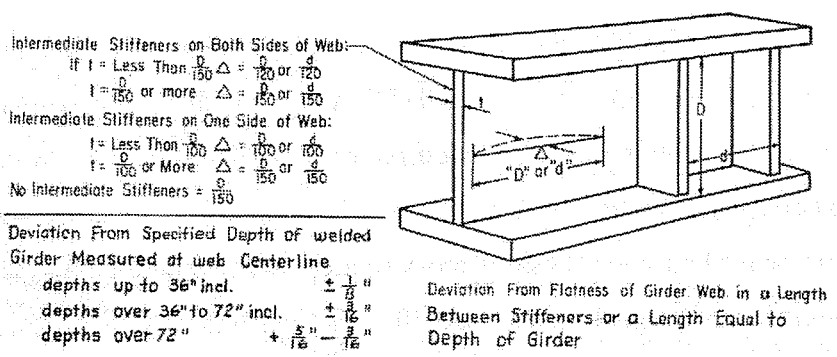

Figure 3.10 Deviation from Flatness of Girder Web (Blodgett 1966)

The same deviation from flatness requirement specified in 1956 for webs with no intermediate stiffeners is still used in the current AWS Bridge Welding Code (AWS 1956, AWS 1995). The current AWS Bridge Welding Code contains less stringent tolerances for webs with intermediate stiffeners than was contained in older specifications. The deviation from flatness requirements for webs contained in the 1995 AWS Bridge Welding Code are presented in Figure 3.11. The variable D is the web depth, t is the panel thickness, and d is the least panel dimension, as shown in Figure 3.12.

buckling under anticipated construction or service conditions, and are also intended to ensure the aesthetic quality of the bridge (AASHTO 2001)." This statement ties the web tolerance to the buckling capacity of the web, but the basis for this statement is not supported by any references regarding the history of these tolerances, furthermore the out-of-straightness of the web does not affect its buckling capacity. It is reasonable that the requirements for flatness of exterior girder webs are based on aesthetic requirements, as will be stated in the commentary.

For many configurations, the AWS Bridge Welding Code specifications for webs with intermediate stiffeners are less stringent than the requirements for webs without intermediate stiffeners. If d = D, the permitted web out-of-flatness may be more than twice as large as that permitted for webs without intermediate stiffeners. No analytical basis for permitting larger out-of-flatness for webs with intermediate stiffeners has been found. As will be discussed, the Swiss specifications contain the same web out-of-flatness of D/150 for all webs, regardless of whether they have intermediate stiffeners or not.

The AWS specification states that "web distortion of twice the allowable tolerance shall be satisfactory when occurring at the end of a girder which has been drilled, or subpunched and reamed either during assembly or to a template for a field bolted splice, provided, when the splice plates are bolted, the web assumes the proper dimensional tolerances (AWS D1.5)." Thus even larger imperfections are allowable prior to connecting the splice plates, so long as the stated requirements are met in the web of the constructed girder. Extending this statement to bottom flanges, larger imperfections would be permitted for the bottom flange prior to field bolting, so long as the tolerances were met after completion of the connection. In practice, internal diaphragms with bottom flange transverse stiffeners connected to the webs of the box and to the

longitudinal stiffener are installed near field splice locations to shore up the cross section of the box next to the splice.

From an informal survey, it has been confirmed that the web out-of-flatness of some bridges has been measured with respect to a straightedge placed adjacent to the surface of the web plate. This approach measures the sum of the peak and valley out-of-flatness. The web tolerance of other girder bridges has been measured with respect to an estimated centerline. This estimated centerline was marked by pulling a string between web peaks, and then pushing the string over to the approximate centerline of the member at points A and B shown in Figure 3.13. The offset is then measured between the string and the web plate. This sort of approach is not accurate or repeatable and should not be used.

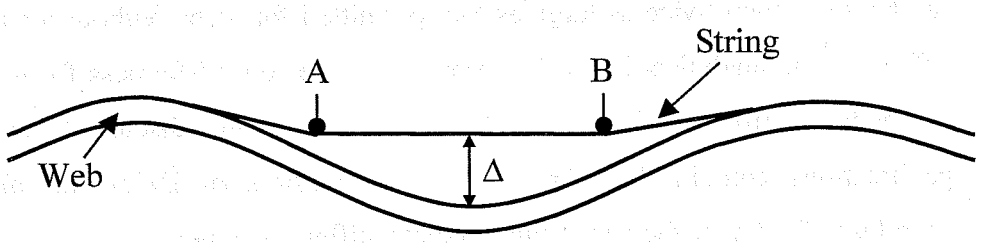

Figure 3.13 Measuring Offset from Estimated Centerline

The AWS D1.1 Structural Welding Code also contains variation from flatness tolerances for webs. Though AWS D1.1 is not a document referenced by AASHTO, many requirements contained in AWS D1.1 Bridge Welding Code, which is a joint publication of AWS and AASHTO. The variation from flatness requirements in AWS D1.1 for cyclically loaded nontubular structures are exactly the same as the web requirements contained in AWS D1.5.

AWS D1.1 contains more specific information regarding measurement of the variation in web flatness. The text specifies that the variations from flatness of girder webs be determined by measuring the offset from the actual web

Intermediate stiffeners on both sides of web

Interior girders—

where D/t <150 — maximum variation = d/115

where D/t ≥ 150 — maximum variation = d/92

Fascia girders—

where D/t <150 — maximum variation = d/130

where D/t ≥ 150 — maximum variation = d/105

Intermediate stiffeners on one side only of web

Interior girders—

where D/t <100 — maximum variation = d/100

where D/t ≥ 100 — maximum variation = d/67

Fascia girders —

where D/t <100 — maximum variation = d/120

where D/t ≥ 100 — maximum variation = d/80

No intermediate stiffeners—maximum variation = D/150

Figure 3.11 Variation from Flatness of Girder Webs (AWS D1.5)

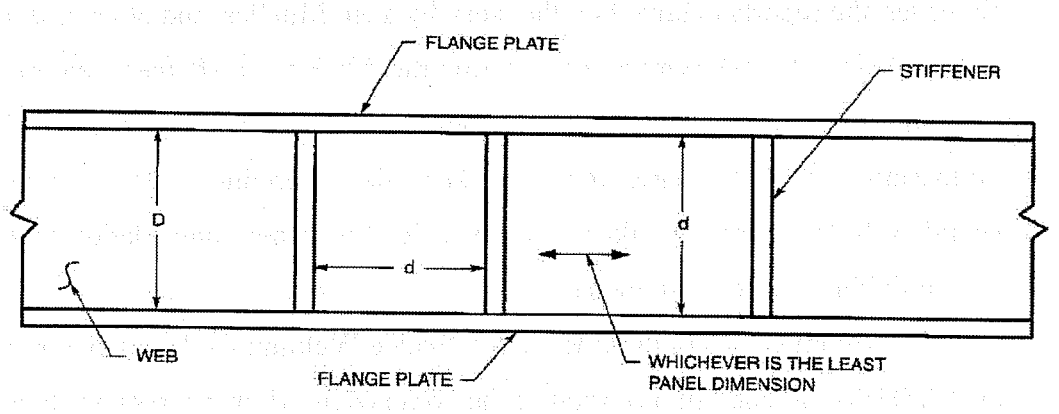

NOTES:
1. D = DEPTH OF WEB
2. d = LEAST PANEL DIMENSION

Figure 3.12 Flatness of Girder Web -Dimensions (AWS D1.5)

The current requirements for webs with intermediate stiffeners were established with the release of the first edition of the AWS D1.1 Structural Welding Code in 1972. The specifications since 1972 contain separate requirements for fascia girders and interior girders, which was not the case in older AWS specifications. The allowable variation from flatness for webs of interior girders with intermediate stiffeners on both sides of the web is approximately 30% greater than the limit used prior to 1972. The allowable variation from flatness for webs of interior girders with intermediate stiffeners on one side of the web is approximately 50% greater than the limit used prior to 1972. It is not known why the tolerance limits were loosened from the requirements in earlier specifications.

There is a belief based on oral history that the specifications for interior girders in the AWS Bridge Welding Code may have been altered from that contained in older AWS specifications based on fatigue tests of girder webs conducted by Yen, Muller and others at Lehigh University in the 1960's. However, the reports obtained on the work by Yen, Mueller, and other researchers at Lehigh do not make reference to altering the AWS out-of-flatness requirements (Corrado 1965, Yen 1966a, Yen 1966b, Mueller 1967, Parsanejad 1970). Furthermore their concerns regarding secondary bending stresses caused by lateral web deflections would not seem to lead to a recommendation to loosen web initial imperfection tolerances.

A commentary on the AWS D1.5 Bridge Welding Code is being prepared by AASHTO. A copy of a portion of the commentary draft addressing flatness of girder webs was obtained. The draft states "in addition to the dimensional tolerances based upon workmanship standards provided in 3.5, these requirements for the flatness of girder webs are intended to ensure that there will be no web

centerline to a straight edge. The commentary to AWS D1.1 contains a figure, shown in Figure 3.14, that identifies the variation from flatness. A straightedge is placed against the stiffeners or flanges. The offset between the straightedge and the plate is measured at the stiffener/flange and at peaks and valleys. The variation from flatness is the difference between the offset at the stiffener/flange and the offset at the peak or valley. An approach similar to this was used to measure the out-of-flatness of the plates tested as part of this dissertation research.

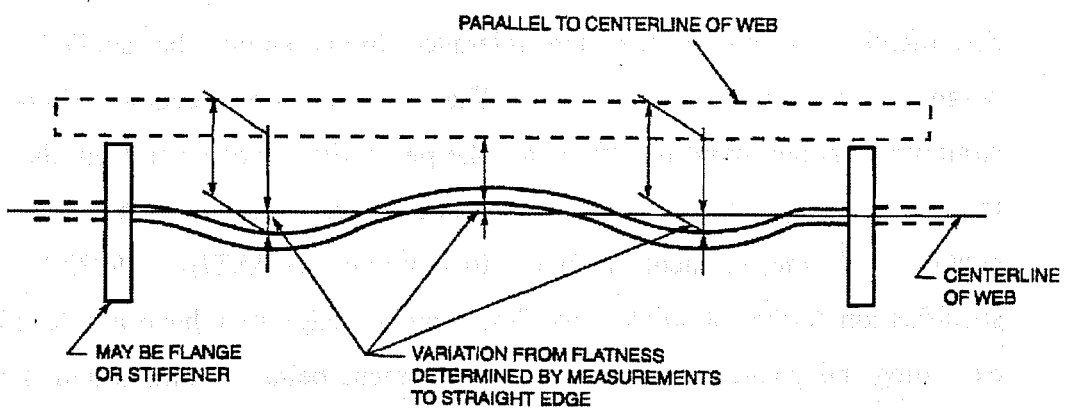

Figure 3.14 Variation from Flatness Measurement - AWS D1.1

Since the same tolerance limits exist in both AWS D1.1 and AWS D1.5, it is reasonable to assume that the same procedure would be followed in making the measurements for AWS D1.5. Consequently, the variation from flatness tolerances in AWS D1.5 are assumed to apply to the deviation from the member centerline. To ensure that this fact is clearly conveyed, a figure similar to Figure 3.14 should be included in the body of AWS D1.5.

Though it may seem that measuring or defining the out-of-flatness of a plate is simple or intuitive, this has not been found to be the case. Most of the tolerance limits in American Specifications have been in place for many years, however there is substantial confusion over how to measure the out-of-flatness to

verify the tolerance limit has not been exceeded. It is consequently recommended that figures clarifying how to measure plate out-of-flatness be included in AWS D1.5, ASTM A6, AASHTO construction specifications, and other specifications which contain dimensional tolerance limits.

3.2.1.5 AASHTO LRFD Orthotropic Deck Tolerances

The 1998 AASHTO LRFD Bridge Construction Specifications contain dimensional tolerance limits for orthotropic-deck bridge members. The Specifications stipulates that the tolerance limits should be applied to the completed but unloaded member. The deviation from detailed flatness or straightness at any point is defined as "the perpendicular distance from that point to a template edge which has the detailed straightness or curvature and which is in contact with the element at two other points. (AASTHO 1998b)". The specification further stipulates that "the template edge may have any length not exceeding the greatest dimension of the element being examined and, for any panel, not exceeding 1.5 times the least dimension of the panel (AASHTO 1998b)." The template may be placed anywhere within the boundaries of the element.

The maximum deviation from flatness or specified curvature shall not exceed the greater of:

$$3/16 \text{ in. or } \frac{D}{144\sqrt{T}} \text{ in.}$$

where D is the least boundary in inches along the boundary of the panel, and T is the minimum thickness in inches of the plate comprising the panel.

The straightness of the longitudinal stiffeners of the orthotropic panel is also specified. The maximum deviation, in mm, from detailed straightness or

curvature in any direction perpendicular to its length shall not exceed L/480, where L is the length of the stiffener between cross members, webs, or flanges.

3.2.1.6 Proposed Design Specifications for Steel Box Girder Bridges

The Proposed Design Specifications for Steel Box Girder Bridges contain proposed additions to the 1977 AASHTO Standard Specifications for Highway Bridges Steel Structures Construction Guidelines (Wolchuk 1980). The 1977 AASHTO Standard specifications contained essentially the same requirements for orthotropic-decks in the 1998 AASHTO LRFD Bridge Construction Specifications described above. The same language regarding use of a template edge and its placement was contained in the 1977 AASHTO Standard Specification, and this wording was extended to the Proposed Design Specifications.

The Proposed Design Specifications for Steel Box Girders recommended use of the AWS D1.5 web tolerances for the webs of box girders. Stricter limits were suggested for the bottom flanges of the girders. The maximum deviation from flatness of the bottom flange panel is limited to D/200, where D is the shorter dimension of the panel. For unstiffened flanges a panel is defined by the clear area of steel plate bounded by the webs. For longitudinally stiffened flanges a panel is the clear area of steel plate bounded by longitudinal stiffeners. In portions of the bottom flange not subjected to compression, the permissible deviation from flatness may be doubled, subject to approval by the Engineer.

The proposed specifications also stipulate that the maximum deviation from detailed straightness or curvature for longitudinal stiffeners shall be less than L/500, where L is the smaller of the transverse flange stiffener spacing or the value L_o, which is the "actual buckling length" defined in the specification. A template edge of length L must be used to measure the deviation. For

longitudinal stiffeners in portions of the box not subjected to compression, the allowable out-of-straightness is increased to L/250.

3.2.1.7 TxDOT Standard Specification

Item 441 of the Texas Department of Transportation's Standard Specifications for Construction of Highways, Streets and Bridges contains workmanship requirements for steel structures (TxDOT 1993). The tolerance requirements in Item 441 specify that fabrication and rolling tolerances shall be in accordance with ASTM A6 and tolerances for fabricated girders shall be in accordance with Welding Code D1.5.

Item 441 does make one additional requirement which states "flanges of completed girders shall be free of kinks, short bends and waviness that depart from straightness or the specified camber by more than 1/8 inch in any ten (10) feet along the flange (TxDOT 1993)." However, based on discussions with TxDOT engineers, this requirement was developed for application to the flanges of plate girders, not box girders. Fabricators have been checking out-of-flatness against this 1/8 in. in 10 ft. tolerance, however, regular exceptions to this out-of-flatness tolerance have apparently been made.

3.2.2 Swiss Codes

The Swiss Code for Steel Structures SN 161 does not contain an out-of-straightness (camber) tolerance for tees or plates. The same web tolerance contained in the AWS Bridge Welding code for webs with no intermediate stiffeners is used for all webs in the Swiss SN 161 Code. This web out-of-flatness is web depth over 150.

The Swiss Steel Handbook contains permitted out-of-flatness for plates. For plates up to 50 mm in thickness, the out-of-flatness is limited to 0.003 times

the plate width. For plates up to 1000 mm in length, the out-of-flatness is limited to 7 mm. For plates above 1000 mm in length and under 2857 mm in length, the out-of-flatness is limited to 0.007L. For plates above 2857 mm in length, the out-of-flatness is limited to 20 mm.

3.2.3 NORSOK Standard

The NORSOK Standard published by the Norwegian Technology Standards Institution contains fabrication tolerances for plate panels, such as those used for the webs and bottom flanges of box girders. The allowable out-of-flatness of box girder plates is 0.5% (1/200) of the panel dimension, with a maximum allowable deviation of 10 mm. When multiple stiffeners are used, the allowable out-of-straightness is 0.5% of the width between stiffeners, with a maximum deviation of 5 mm. The allowable out-of-straightness, or camber, of a plate stiffener is 0.15% of the plate width, with a maximum deviation of 10mm. Note that the out-of-straightness of the stiffener is not based on the geometry of the stiffener, but of the plate it is used to stiffen.

3.2.4 British Specifications - Interim Design and Workmanship Rules

The tolerance provisions contained in the Interim Design and Workmanship Rules, or Merrison Rules, were reported to be detailed, elaborate, and restrictive but the exact tolerances limitations were not cited (Wolchuk 1980). The Merrison Rules described how to measure the out-of flatness of a plate. The plate panel flatness was to be measured using a special adjustable scanning device, which was constructed of a bar with two prongs that could be positioned at a specified gage length. The two prongs were to be placed in contact with the measured panel, and a moveable dial gage measured the deviation from a straight

line between the two prongs. The scanning device was always positioned parallel to the longer side of the panel, at any location across the width of the plate. The permissible variation from flatness was given by a formula that is a function of the plate width, plate thickness, and gage length (Wolchuk 1980).

The Merrison tolerance provisions prescribed different tolerances when the maximum deviation of the stiffener was towards the inside of the box versus, when the deviation was away from the inside of the box (Wolchuk 1980). A point that will be discussed later is an observance of the impact of the direction of the stiffener out-of-straightness. No other proposed tolerances reviewed make different tolerance recommendations based on the direction of the out-of-straightness. The tolerances obtained using the Merrison rules were quite small and were found to be overly restrictive. The tolerances could not reasonably be met using standard practice, and would have significantly increased fabrication costs. Consequently the proposed recommendations were not followed (Wolchuk 1980).

3.2.5 Canadian Field Investigation of Box Girder Imperfections

Thimmhardy, Korol and Cheung have conducted a field investigation of geometrical imperfections of girders after fabrication and in situ steel box girder bridges (Thimmhardy 1988). This investigation was performed in Canada, where the design approach and box girder bridge designs are comparable to United States practice. In Canada and the United States the trend has been to use multiple box girders to form the bridge section rather than the single box configuration more commonly used in Europe.

Data collected in the field investigations were based on measurement of panel out-of-flatness. Panel dimensions were defined as shown in Figure 3.15. Note that Figure 3.15 shows the out-of-plane deviations of the plate using straight

stiffeners. However as shown at the bottom right of the figure, the stiffener also has an initial out-of-straightness. Based on the out-of-plane deviations measured, the researchers recommended obtainable tolerance levels for plate panels and longitudinal stiffeners. Their proposed limits are b/165 for plate panels, where b is the spacing between longitudinal stiffeners and a/500 for stiffeners, where "a" is the stiffener length. The researchers commented that most of the bridges investigated in Canada would not meet the b/200 plate tolerance proposed in some European countries, but would generally comply with the proposed a/500 stiffener limit (Thimmhardy 1987).

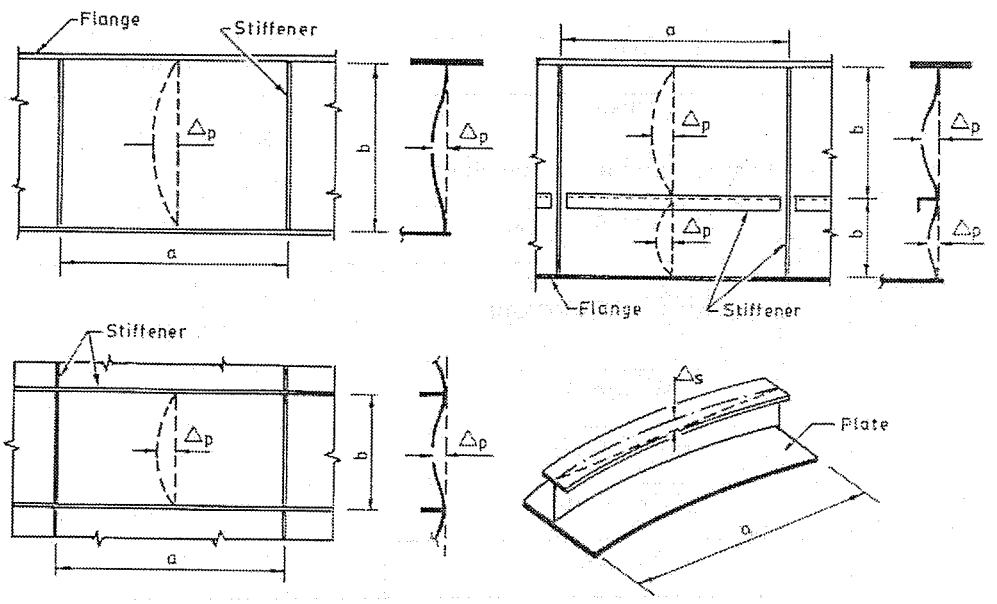

FIG. 1. Out-of-plane deviations.

Figure 3.15 Out-of-Plane Deviations (Thimmhardy 1987)

Thimmhardy et al make comments regarding European tolerances and their ability to be met in practice. They cite a survey by Massonnet who found that even the most liberal of plate tolerances specified in Europe was commonly

exceeded in steel box girder bridges constructed in the countries concerned (Thimmhardy 1987).

3.2.6 Comparison of Out-of-Flatness and Out-of-Straightness Tolerances

The plate out-of-flatness and stiffener out-of-straightness tolerances presented above are summarized in Table 3.1 and Table 3.2, respectively. The tolerances are presented using the plate width, b, stiffener spacing, w, plate thickness, t, and stiffener length, L.

Table 3.1 Plate Out-of-Flatness

Specification	**Tolerance**
ASTM A6 (assuming one half-wave shape)	b/64 to b/192
AWS D1.5 (webs)	b/150
AASHTO Orthotropic	$\frac{w}{144\sqrt{t}}$
Wolchuk	b/200 or w/200
Swiss Webs	b/150
Swiss Plates	~ b/140 - b/333
Norsok	w/200
Thimmhardy	w/165

Table 3.2 Stiffener Out-of-Straightness

Specification	Tolerance
ASTM A6	L/480
AASHTO Orthotropic	L/480
Wolchuk	L/500
Norsok	b/670
Thimmhardy	L/500

Using the stiffener spacing, w, to represent both unstiffened plate width and stiffened panel widths, the tolerances range from w/64 to w/333. A tolerance of w/200 (b/200) appears to be reasonable. The stiffener tolerances range from L/480 to L/500. A tolerance of L/500 appears to be reasonable. These tolerances will be used in Chapter 7 to check the initial imperfection of the experimental test plates.

A point of concern is that Thimmhardy et al found that Canadian bridges, which are similar to United States box girder bridges, regularly failed to meet a w/200 tolerance. Based on the results of their survey, a less conservative out-of-flatness tolerance of w/165 was recommended.

In practice, steel box girder fabricators must consider the interaction between plate out-of-flatness and stiffener out-of-straightness. The stiffened plate must meet both plate out-of-flatness and stiffener out-of-straightness requirements. Due attention must be paid to the initial out-of-flatness and initial out-of-straightness of box girder components to ensure the final constructed box conforms to established requirements, particularly since plate and stiffener stock may not meet the specified tolerances of the fabricated unit.

It should be noted that it is not common practice to measure the out-of-straightness of the longitudinal stiffener along the length of the stiffener. For a

compression flange without transverse stiffeners, the length over which the out-of-straightness measurement should be made is not clear to the inspector. Furthermore, the stiffener length that should be used to check a given tolerance is not apparent. The issue of measuring the stiffener out-of-straightness is also complicated by the camber of the box girder. The camber introduced into the plate from the cambering of the overall girder will contribute to the displacement of the stiffener under load. However, the camber of the girder should be isolated from the stiffener out-of-straightness in terms of checking the plate for conformance with fabrication tolerances.

The NORSOK specification tolerance listed above specifies the permissible out-of-straightness of the longitudinal stiffener based on the width of the flange, rather than the length of the stiffener. Measuring imperfections across the width, rather than along the length, of the flange is the common procedure. By measuring the imperfection across the width of the plate at multiple locations along the length of the flange, it is possible to obtain the relative out-of-straightness of the stiffener. However, even using this approach the specific length over which the stiffener should be evaluated is not clear to the inspector in flanges without transverse stiffeners.

3.2.7 Out-of-Flatness and Plate Behavior Under Load

There have been concerns expressed regarding what variation from flatness parameter is most important to the response of a web or flange plate under load. The question is whether the variation from flatness of a web plate with respect to the centerline of the plate, or the sum of the worst peak and valley on the plate surface are most indicative of the response of the loaded plate.

It should again be noted that some out-of-flatness tolerances have been established for purely aesthetic reasons. A person looking at the bowed web or

flange of a steel girder bridge does not observe the deviation from the plate centerline, they notice the disparity between the peaks and valleys along the plate surface. Thus, aesthetically, it is important to address the sum of the peak and valley measurements in the establishment of acceptable aesthetic tolerances. However, when these tolerances are included in a specification, the aesthetic tolerances can be presented in terms to agree with the presentation of non-aesthetic tolerances.

The question remains whether the deviation from plate centerline, or sum of peak and valley measurements is important with respect to plate behavior. For compression flanges, the measurement of longitudinal ripples along the length of the plate is of interest. Finite element analyses, which included various initial imperfections, were constructed using ABAQUS in an attempt to answer this question. Analyses of square plates and plates with an aspect ratio, a/b, of 2 showed that the softest plate response was seen when initial imperfections were of the same shape as the first buckling mode of the plate. A conclusive link between the method of specifying the imperfection, sum of peaks and valleys or deviation from centerline, and the softness of the plate response could not be made from this analysis.

A practice commonly used in analytical investigations, which was followed in the analytical program presented in Chapter 4, is including initial imperfections of the same shape as the first buckling mode of the plate in the finite element model to produce the softest response. The softest plate response is seen when the initial imperfection was in the shape of the first buckling mode even when compared to somewhat larger initial imperfections of other shapes.

To further investigate whether the deviation from centerline of the plate, or the sum of maximum positive and negative plate deviations most affect the response of the plate, plate imperfections were input to the finite element model

of the test setup used in the experimental program. The test plate in the finite element model has an aspect ratio, length/width of 2.9, and a thickness of 3/16 in. The imperfections shown in Figure 3.16 were input to the model. The mirror images about a horizontal axis of Imp. 1 - up and Imp. 3 - up were also studied. These cases were labeled Imp. 1 - down and Imp. 3 - down respectively.

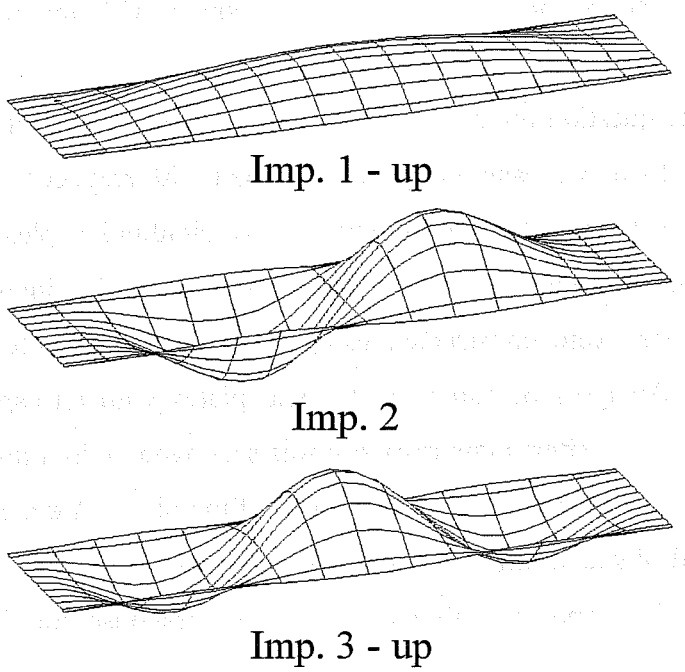

Figure 3.16 Initial Imperfections of FEM "Test" Plate

The magnitude of the initial imperfection was specified using the variation from flatness of the plate from the nominal centerline of the plate. The same magnitude of imperfection, 0.12 in., was input for each imperfection. This imperfection level is approximately b/210, where b is the plate width.

The final displaced shapes of the plates from an elastic large displacement analysis with the different initial imperfections are shown in Figure 3.17. The load-displacement response with each imperfection is presented in Figure 3.18.

The displacements in the middle of the plate and in the middle of one end panel are traced for Imperfections 1 and 3. The displacements at the middle of the half-waves in Imp. 2 are also plotted. Note that for the slender plates studied, this level of imperfection results in essentially a linear load-displacement response in all but one curve shown in Figure 3.18.

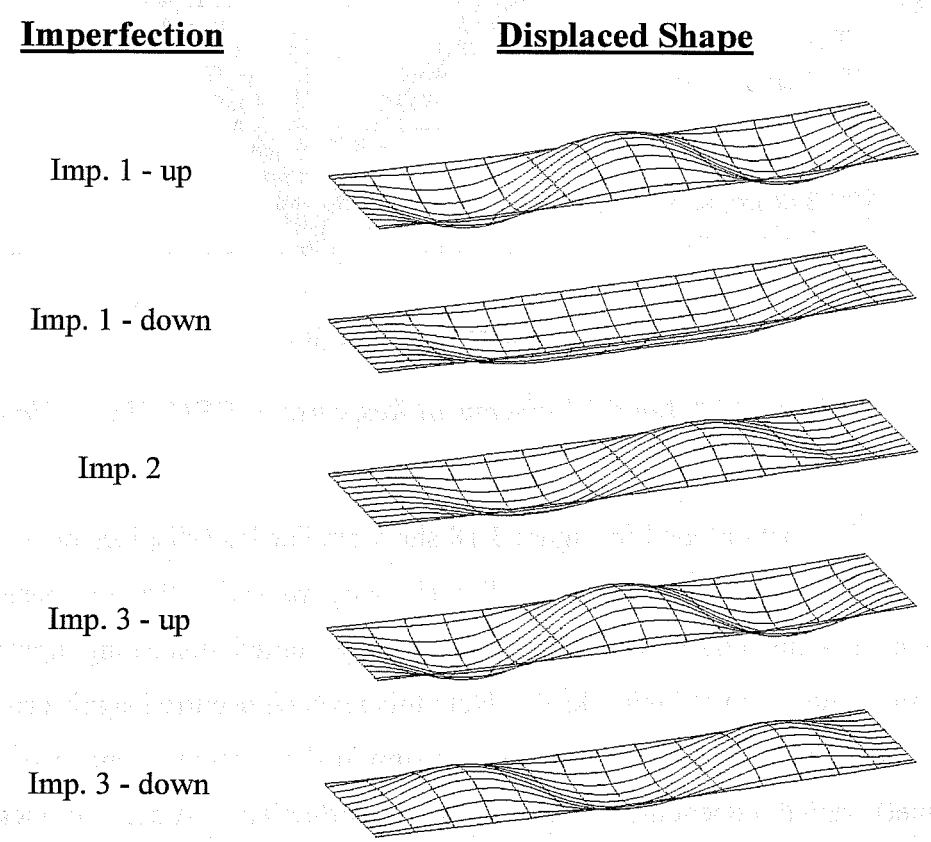

Figure 3.17 Displaced Shape of Plates with Varying Initial Imperfections

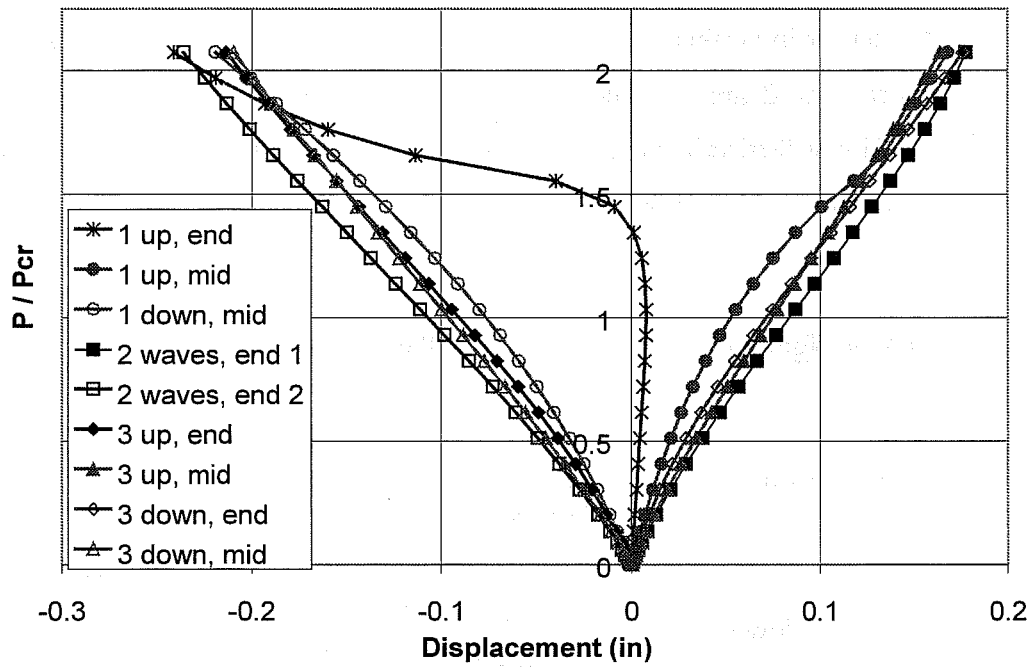

Figure 3.18 Load-Displacement Response of FEM "Test" Plate

The data plotted in Figure 3.18 show similar load-displacement responses for most of the curves. The only line showing markedly different behavior was "Imp. 1 - up, end" where the plate initially started displacing upward, then reversed direction at higher loads. Note this reversal occurred significantly above the buckling load. The location of maximum displacement (end panel vs. mid panel) varied depending on the initial imperfection. Also, the locations of positive displacement vs. negative displacement varied with the initial imperfection. However, specifying the initial imperfection magnitude based on deviation from nominal plate centerline resulted in comparable maximum displacements regardless of the shape of the initial imperfection. Based on these results, flatness tolerances related to load-displacement response should be made

based on the deviation of the plate from the nominal plate centerline, as indicated by the AWS D1.1 Structural Welding Code.

3.2.8 New Approaches for Measuring Plate Out-of-Flatness

There are "high tech" methods available for measuring plate out-of-flatness. Research conducted at the University of Texas on measuring the out-of-flatness of structural steel plates investigated using a manual rotating beam laser level for measuring the out-of-flatness of steel plates (Tamura 1993). The study was specifically investigating the impact of plate out-of-flatness on loss of bolt tension in bolted connections. The laser used was able to establish horizontal and vertical planes so nominally horizontal and vertical surfaces could be measured. The procedure developed resulted in measurements with an accuracy of 0.01 inches. However, use of the approach developed required significant amounts of time to measure each horizontal and vertical surface (Tamura 1993). Based on the amount of time required to use this method it is not appropriate for performing full web and flange inspections of steel girder bridges.

There are also tools that have been developed specifically for measuring floor flatness. One of these tools, the "FloorPro" produced by Ytteberg Scientific, is a self-propelled, rolling precision inclinometer device that travels 40 feet per minute (FloorPro 2001). The FloorPro includes software that analyzes the out-of-flatness data it collects and checks the data against tolerance limits. The FloorPro and similar tools have been developed for use on flat, horizontal surfaces, and are subsequently not appropriate for use on girder webs or on the bottom flange of girders with significant vertical rise. However, tools such as these could perhaps be modified to meet the needs of the bridge industry if there is a demand for them.

3.2.9 Simple Approach for Measuring Plate Out-of-Flatness of Bottom Flange

The most reasonable method for measuring plate out-of-flatness currently is still using a straightedge or a string. The inspector should first eye the plate and identify the areas with the largest out-of-flatness. For webs of plate girders, the straightedge or string can be stretched between the stiffeners and or flanges. The offset between the straightedge and web plate at the flange/stiffener should be measured. Then the imperfection at the worst peaks and valleys on the plate surface should be measured. The difference between the offsets and peaks/valleys can then be used with the plate thickness to calculate the deviation from the plate centerline.

Measuring the out-of-flatness of the flanges and webs of trapezoidal box girders is a little more difficult than checking plate girders. In this instance, a simple device such as that shown in Figure 3.19 can be used. The device consists of a string stretched between two end rods of the same height, h. In practice, it may be helpful to mount magnets to the bottom of the rods, so that the rods will stay in place at the desired location as the measurements are made. When measuring the out-of-flatness of a plate, the two end rods would be placed at the ends of the area being measured. Typically, for a bottom flange plate the end rods would be positioned on either edge of the width of the plate, adjacent to the box webs, or adjacent to the web/stiffeners on stiffened flanges. The offset at the worst peaks and valleys should be measured. Using the known end rod height, the plate thickness and the measured offsets, the variation from flatness of the plate from the nominal centerline can be determined.

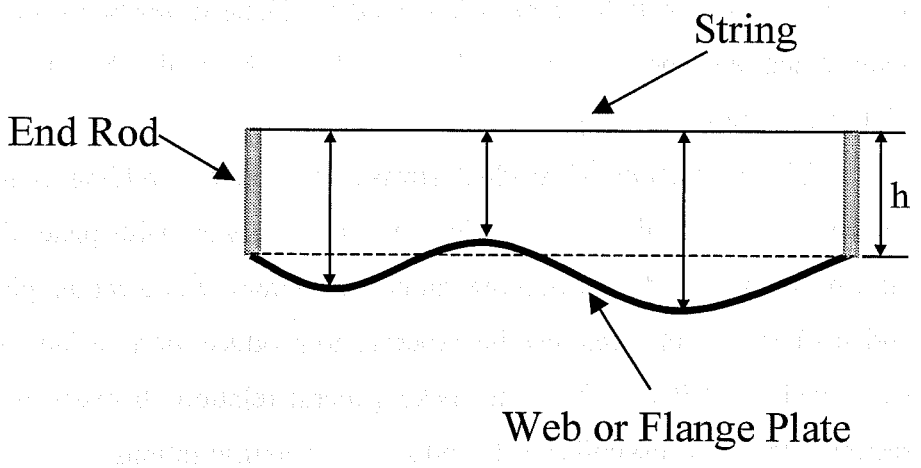

Figure 3.19 Measuring Plate Out-of-Flatness

3.3 Residual Stresses

Residual stresses are stresses that remain in structural members after fabrication. In welded sections, the residual stresses result from uneven cooling of portions of the section after welding. The areas of the section that cool slowly develop residual tension that is balanced by residual compression in other portions of the member. Residual stresses can have an effect on the yielding process and hence may effect the strength of a welded member.

Many researchers have indicated that the effects of compressive residual stresses in stiffened plates may be significant (Wolchuk 1980, ECCS 1986, Dwight 1969, Maeda 1975, Skaloud 1984). It has also been argued that the effect of welding residual stresses on stiffened plate performance is not known and too uncertain to be included calculations (Wolchuk 1980). The influence of residual stresses from welding in slender plate panels may not significantly affect the flange capacity (Ghavami 1994), however the impact of residual stresses in stockier plates, such those in the transition zone of the AASHTO design equations, is thought to be significant (Wolchuk 1980, ECCS 1986). Pronounced

residual stress effects have been indicated by Skaloud for plates buckling about longitudinal stiffeners, but less effect was found for global buckling of stiffened plate panel (Skaloud 1984).

The prediction of residual stresses caused by welding is not an exact science. The magnitude of residual stresses can vary with plate size, stiffener size, weld size, welding procedure, and other factors. For a certain plate thickness and stiffener, a large weld can be expected to produce more residual stress than a small weld, but it is difficult to make general relations between weld size and residual stress for dissimilar plate and stiffener configurations.

Compressive stresses in stiffened plates are generally assumed to have a distribution similar to that shown in Figure 3.20. The stiffeners have tensile residual stresses adjacent to the flange, and are believed to carry relatively little compressive residual stress away from the flange plate. As noted, the magnitude of the residual stress in a particular stiffened plate is not at all certain. Assumed residual compressive stress magnitudes of 3.6 to 10 ksi have been used in the development of capacity equations (Wolchuk 1980, Dwight 1973).

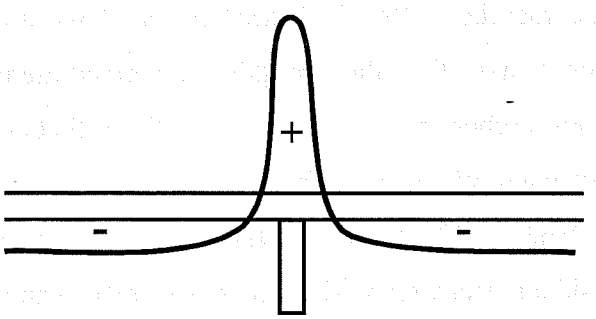

Figure 3.20 Assumed Residual Stress Distribution in Plate

The effects of residual stresses are included in the AASHTO specification by setting a limit of $0.6F_y$ on use of the elastic buckling capacity, and by use of the Engessner transition curve above this $0.6F_y$ limit. The Proposed Design

Specifications for Steel Box Girder Bridges, and some European specifications, directly include assumed residual stress magnitudes in calculating the capacity of stiffened compression flanges (ECCS 1986). The impact of residual stresses is considered in this dissertation in the comparison of finite element analysis, AASHTO, and strut approach capacities for stiffened flanges. The results of this comparison are presented in Chapter 8 and indicate flange capacities smaller than the AASHTO design capacity for certain plate geometries.

3.4 Conclusions

An investigation of initial imperfections and imperfection tolerances was undertaken. The tolerances contained in several different specifications were compared and tolerance limits were selected for application to the plates tested in the experimental program. A brief review of research on the impact of residual stresses on stiffened plates was completed. The impact of residual stresses is included in the strut-based analysis procedure presented in Chapter 8.

Chapter 4

Analytical Program

4.1 Stiffened Plate Buckling Investigation Using FEA

The stiffened plate study was begun with eigenvalue buckling estimates. All finite element analysis (FEA) was performed using the program ABAQUS. ABAQUS is a commercial finite element package developed by Hibbitt, Karlsson, & Sorenson, Inc. This package is capable of performing numerous analysis types, including eigenvalue and large displacement analyses. Eigenvalue estimates for stiff shell collapse analyses are usually accurate when the response prior to buckling is essentially linear; when the collapse is not catastrophic; and when the structure's response is elastic (HKS 1995). In the eigenvalue procedure, an arbitrary load magnitude can be used, since the amplitude of the response is directly proportional to the magnitude of the load.

4.1.1 Finite Element Model

A convergence study was undertaken to select an appropriate level of mesh refinement for both the eigenvalue buckling prediction and the subsequent load-displacement study. Finite element models (FEM) of the unstiffened plate and models of the plate with various size stiffeners were developed. The full plate was modeled throughout this research, as opposed to modeling a portion of the plate with symmetry boundary conditions, because even though the plate geometry is symmetric, the deformed shape of the stiffened plate may not be symmetric. The study indicated that the finite element results did converge, and the results were used to select the appropriate level of mesh refinement for the subsequent analyses.

Several 8-noded and 9-noded elements were considered for use in the study. Finite element models were constructed using several different element types, and the results using the different element types were compared. The ABAQUS S8R5, an 8 noded element, did not give good results for the doubly curved shapes obtained in the more complex buckling modes. The ABAQUS S8R and S9R5 gave comparable results. The 8-noded S8R shell element was selected for use throughout the rest of the study based on the FEA results and conversations with FEA experts. Comparable finite element models were often built using the S9R5 during investigations of the FEA results to check for any differences in results.

Initially a general beam section, in which the beam section behavior is specified directly by inputting section properties, was used to model the stiffener. During the mesh convergence study, the general beam section did not behave well as the buckled shape of the plate became more complicated. Features of the general beam section caused local problems that resulted in unreasonable buckling modes in which individual shell elements responded independently. Subsequently, as suggested in the ABAQUS reference material, an I-shaped beam element was selected from the available elements to model the stiffener. The width and thickness of one flange of the I-section were set equal to zero to model the tee-shape of the stiffener.

Figure 4.1 shows the finite element model of the plate with the applied load. The length and width of the plate are also labeled in this figure. Figure 4.2 shows the finite element model with a tee-shaped longitudinal stiffener constructed of shell elements. Analyses were performed both with loads applied to the ends of the longitudinal stiffener and with no loads at the ends of the stiffener. The presence of load at the ends of the stiffener did not impact the eigenvalue results. In each of the subsequent figures presented in this section the

same viewpoint will be used, with the loaded edges of the plate in the same position as shown in Figure 4.1 and Figure 4.2. The plate is compressed in one direction by a uniform load along two edges. The load was actually input as point loads along the edge nodes of the plate. Since second-order elements, which use quadratic interpolation along their edges, are used in this analysis, the appropriate loads were applied to the edge nodes according to Simpson's integration rule.

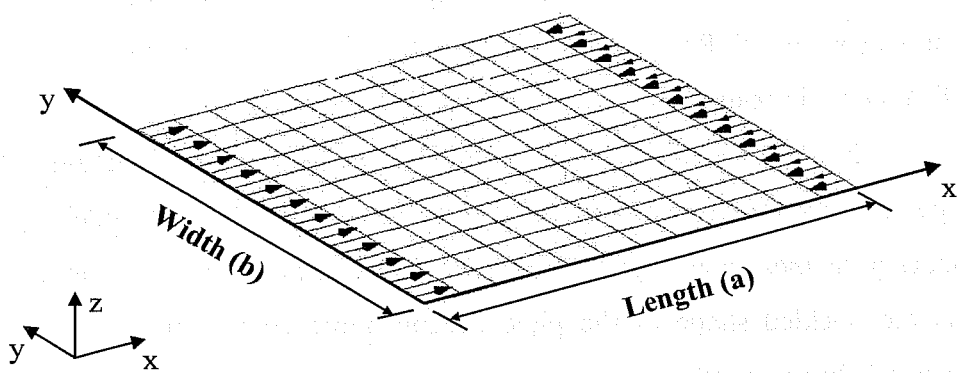

Figure 4.1 Finite Element Mesh with Applied Load

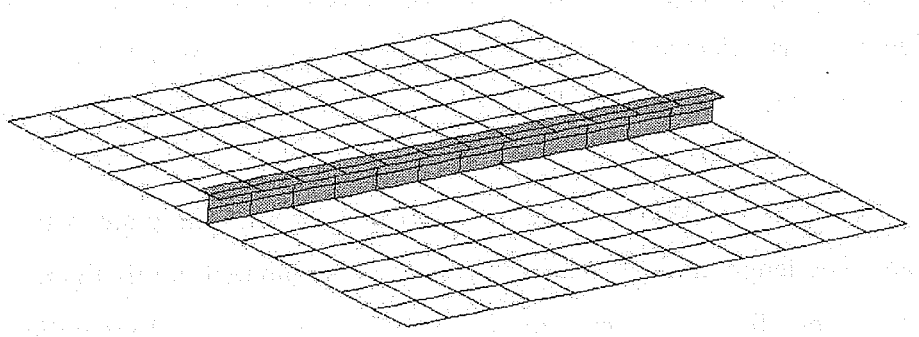

Figure 4.2 Finite Element Model with Shell Element Stiffener

To model the simply supported edge condition of the plate, the edges of the plate were restrained from moving out-of-plane (z-direction). All plate edges

were also restrained from in-plane twisting using the appropriate rotation restraint on the edge nodes of the plate. To prevent rigid body translation of the plate in the x-direction, movement in the x-direction was restrained at the middle of length a on the unloaded edges of the plate. To prevent rigid body translation in the y-direction, movement in the y-direction was restrained at one node in the middle of one unloaded plate edge.

4.1.2 Buckled Shapes of Unstiffened and Stiffened Plates

A longitudinal stiffener significantly increases the buckling capacity of a plate by causing a change in the buckled shape. A large stiffener will force a straight nodal line, and the plate will buckle about the stiffener. The buckled shapes of the first three modes of the unstiffened plate are shown in Figure 4.3. In the first mode the plate buckles in one half wave along the length and across the width of the plate. The second buckling mode of the plate has a full wave along the length of the plate, and the third buckling mode has one and a half waves along the length of the plate.

The first three buckled shapes of the plate with a small stiffener are shown in Figure 4.4. A small stiffener is one that does not stop the out-of-plane displacement of the plate at the stiffener. The first buckling mode of the plate with a small stiffener is the same in appearance as that of the unstiffened plate. In the second mode, there is a very slight depression of the plate along the longitudinal stiffener in the middle of the bows in the second mode. In the third buckling mode, the impact of the longitudinal stiffener is even more noticeable. The plate displaces less along the stiffener.

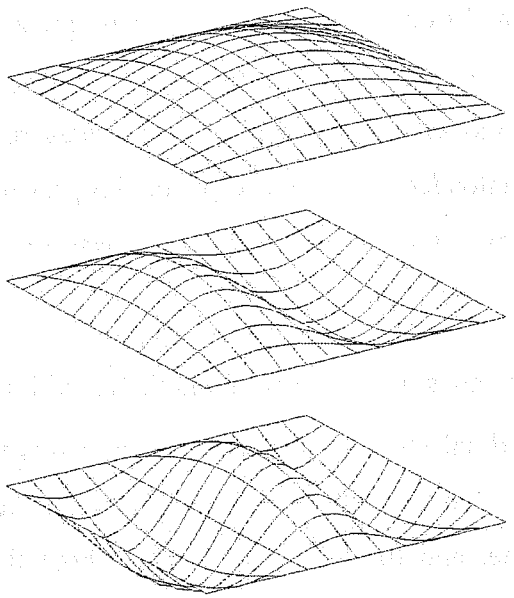

Figure 4.3 First Three Buckling Modes of Unstiffened Plate

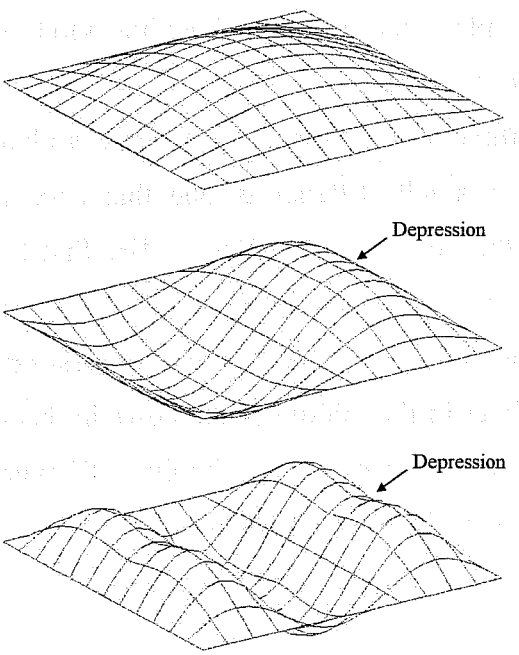

Figure 4.4 First Three Buckling Modes of Plate with Small Stiffener

A large stiffener prevents movement of the plate along the stiffener. The nodes along the longitudinal stiffener are prevented from moving out-of-plane by the stiffener. The shapes of the first three buckling modes of the plate with the centerline of nodes prevented from moving out-of-plane are shown in Figure 4.5. The buckled shape of the plate in each of the modes is much more complex than the buckled shapes of the unstiffened plate and plate with a small stiffener. In the first mode, the plate buckles in an anti-symmetric shape with full waves along the length and across the width of the plate. The second mode shape is an anti-symmetric shape with three half-waves along the length of the plate. The third mode shape is symmetric with three half-waves along the length of the plate.

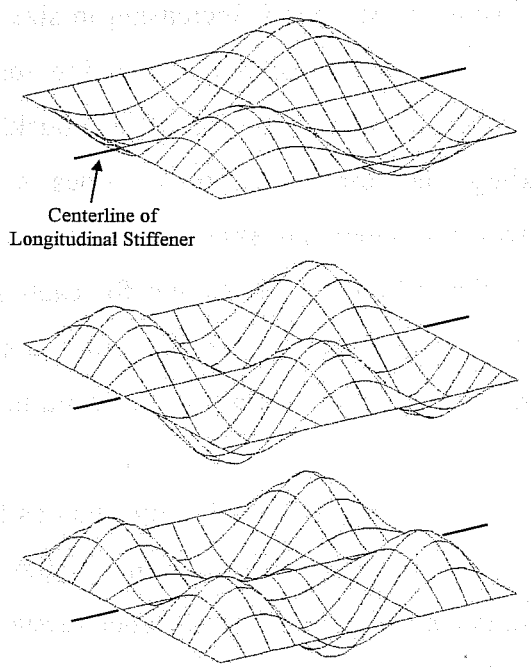

Figure 4.5 First Three Buckling Modes of Plate with Centerline Nodes Fixed Out-of-Plane

Buckling of the plate into the more complex shapes shown in Figure 4.5 requires more energy than buckling into the less complex shapes shown in Figure

4.3 and Figure 4.4. Therefore higher loads are required to buckle into the more complex shapes. Consequently, the buckling stress of the plate with a large stiffener that forces a nodal line will be higher than that of the unstiffened plate or plate with a small stiffener.

4.1.3 Unstiffened and Longitudinally Stiffened Plates

The first step in the finite element analysis (FEA) was to look at an unstiffened plate. After modeling the unstiffened plate, a very small longitudinal stiffener, which did not significantly alter the buckled shape of the plate, was then added to the plate. The ABAQUS I-Section beam element was used to model the stiffener. Next a series of stiffeners, increasing in size, were added to the plate. The inclusion of stiffeners increased the buckling load of the plate, and the addition of larger stiffeners caused the shape of the buckled plate to change.

The buckling loads for the first three modes of the unstiffened plate and the plate with various stiffeners are shown in Table 4.1. The moment of inertia about the base of the stiffener, I_s, is shown for each stiffener. The table also contains the buckling load obtained when the nodes along the center of the plate, where the longitudinal stiffener is placed, are restrained against moving out of plane.

A review of the data in Table 4.1 shows that as the size of the stiffener is increased, the buckling load approaches a limit. Figure 4.6 shows a chart of the moment of inertia about the base of the stiffener versus the normalized buckling load of the plate. The buckling loads were normalized with respect to $P_{ref} = 80.6$ k/in, which is the first mode-buckling load of the plate with the centerline nodes fixed against moving out-of-plane. The capacity of the plate with the centerline nodes fixed against moving out-of-plane is the last entry in Table 4.1. Figure 4.7 also contains a plot of the data in Table 4.1, with a reduced x-axis scale.

Table 4.1 Buckling Load of 72 in. x72 in. x1 in. Plate

Stiffener		Mode 1	Mode 2	Mode 3
Type	I_s (in^4)	(k/in)	(k/in)	(k/in)
Unstiffened	0	20.2	31.5	55.9
WT2x6.5	5.60	24.1	45.4	79.2
WT5x11	58.3	69.7	95.0	102
WT8x13	147	105	109	110
WT9x17.5	250	108	111	112
WT13.5x57	2020	114	114	115
WT22x167.5	15,400	117	117	120
Centerline Nodes Fixed Out-of-Plane	N/A	80.6 = P_{ref}	94.3	112

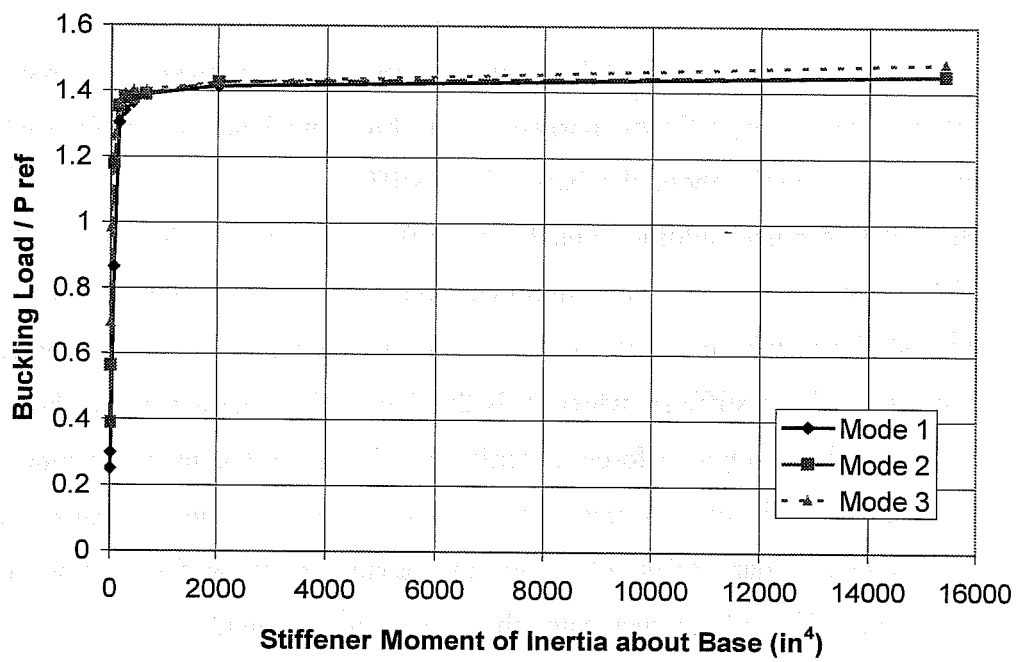

Figure 4.6 Buckling Load vs. Stiffener Moment of Inertia

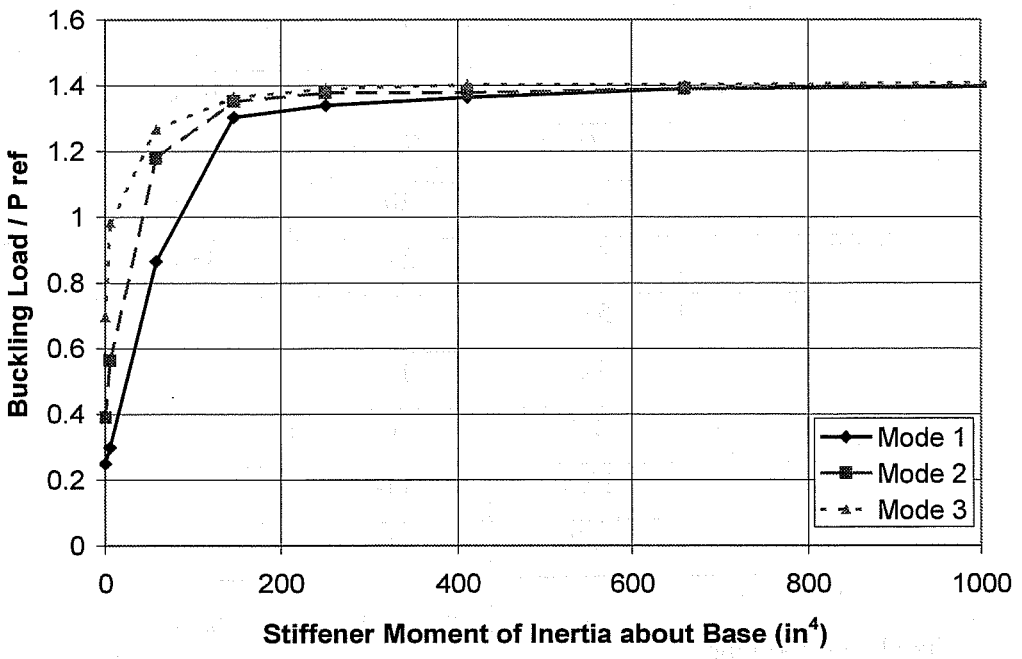

Figure 4.7 Buckling Load vs. Stiffener Moment of Inertia - Reduced Scale

As the data in the tables and figures show, increasing the moment of inertia causes a significant increase in the buckling load of the plate when the moment of inertia about the base of the stiffener is in the 0 to 200 in^4 range. Beyond this range, adding even larger stiffeners, whose I_s is between 200 and 1000 in^4, does not result in as significant increases of the buckling load. Using a huge stiffener, whose I_s was 15,400 in^4 produces a negligible increase in capacity compared with a stiffener whose I_s is 2020 in^4. At a certain point, the stiffener becomes stiff enough to force a significant change in the buckling mode of the plate. Above this size, increasing the moment of inertia does not cause a change in the buckled shape of the plate, and the capacity of the stiffened plate does not increase significantly by increasing the size of the stiffener.

The next step in the analysis was to examine plates with larger aspect ratios. As previously discussed, the aspect ratio, a/b, of the test plate is the length

of the plate, "a", over the width of the plate, b. Plates with aspect ratios between 2 and 7 were examined. Only integer aspect ratios were investigated in this study, because as discussed in Chapter 2 plates with integer aspect ratios give the lower limit of the plate buckling coefficient. Table 4.2 contains the first mode buckling loads of plates with aspect ratios of 1, 2, 3, 4, and 7. Figure 4.8 plots the same data for aspect ratios of 1, 4 and 7, again normalized with respect to P_{ref} = 80.6 k/in. The data for aspect ratios 2 and 3 are not shown since these curves are essentially the same as that of the plate with an aspect ratio of 4, and reduced the clarity of the plot.

Table 4.2 First Mode Buckling Load (k/in)

Stiffener Type	Aspect Ratio (b=72", t=1")				
	a/b=1	a/b=2	a/b=3	a/b=4	a/b=7
Unstiffened	20.2	20.2	20.2	20.2	20.2
WT2x6.5	24.1	24.0	23.9	23.8	23.3
WT5x11	69.7	46.3	47.3	46.0	46.1
WT8x13	105	74.1	72.7	70.3	67.1
WT9x17.5	108	96.4	95.0	94.8	85.9
WT13.5x57	114	111	113	114	116
Centerline Nodes Fixed Out-of-Plane	80.6 (P_{ref})				

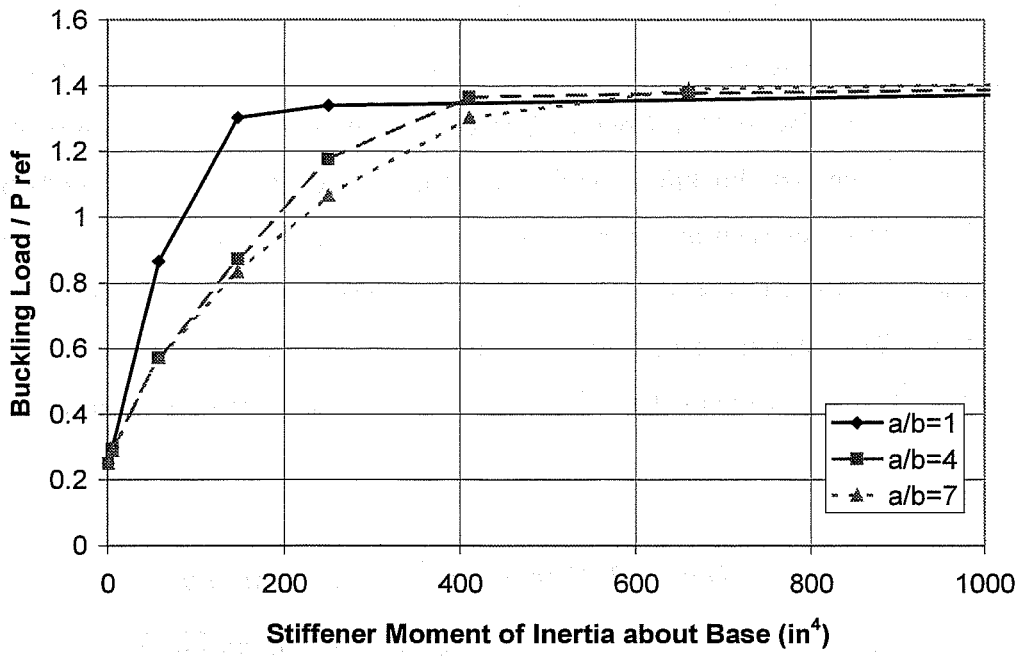

Figure 4.8 Effect of Aspect Ratio on Buckling Load

The data in Table 4.2 show that for the unstiffened plate, the buckling load of the first mode is always 20.2 k/in. When stiffened with small stiffeners, the plates with larger aspect ratios have less buckling capacity than plates with smaller aspect ratios. The study also showed that it took a larger stiffener to reach the limit capacity for plates with larger aspect ratios, as shown in Figure 4.8. The limit capacity is reached by forcing a marked change in the buckled shape of the plate. The largest stiffener in the last row of Table 4.2 was adequate to cause a significant change in the buckled shape of each of the plates. The capacity of the plate with the largest stiffener was comparable regardless of the aspect ratio of the plate. The limit capacity for the unstiffened plate is also the same regardless of aspect ratio.

The unstiffened plate buckled shape is repeated on the left in Figure 4.9, and the buckled shape from an eigenvalue analysis of the plate with the centerline

nodes fixed from moving out-of-plane is shown on the right in Figure 4.9. When a large enough stiffener is used, the buckled shape of the plate will change from the simple one-half wave shape to the more complex shape. Throughout this report, a stiffener that is large enough to cause this marked change in the buckling shape is called an adequate stiffener. Much more energy is required to buckle the plate into the more complex shape, and consequently the buckling load of the adequately stiffened plate is much larger than that of the unstiffened plate.

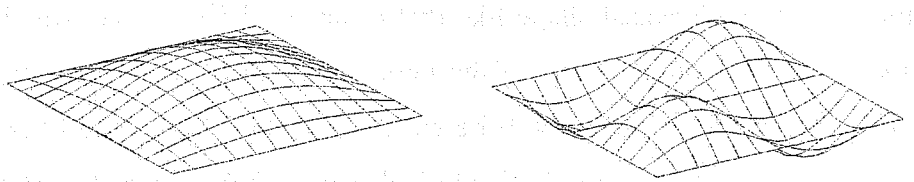

Figure 4.9 Unstiffened Plate vs. Adequately Stiffened Plate

The data in Table 4.2, and similar additional FEA runs, show that there is not a length effect on the capacity of the unstiffened plate or the capacity of a plate stiffened with an adequate stiffener. The capacities of the unstiffened plate and plate with a large stiffener, respectively, are essentially the same regardless of the aspect ratio of the plate. As has been discussed, based on the eigenvalue analyses long unstiffened plates will buckle on square panels at the same buckling load as a plate with an aspect ratio of 1. For plates with large stiffeners, a nodal line is formed along the stiffener and the plate buckles on either side of the stiffener. Each square panel of the stiffened plate will buckle in the anti-symmetric shape shown in Figure 4.9 at the same buckling load. There is, however, a length effect with respect to what stiffener size is required to force a marked change in the buckled shape of the plate. Larger stiffeners are required to force a change in the buckling mode of plates with larger aspect ratios.

4.1.4 Large Displacement Analysis

The next step in the investigation of stiffened plate capacity was conducting a load-displacement study using FEA. The results presented in this section are for a square 72 in. x 72 in. x 1 in. plate. The nature of the load-displacement response varies with location across the surface of the plate. In the following discussions, the displacement at the node in the FEM showing the largest displacement is presented.

A variety of initial geometric imperfections were investigated in this study. First, a displaced shape like that of an unstiffened plate was input to the model. An exaggerated view of the initial shape of the plate is shown in Figure 4.10. This displaced shape will be called the "One Half-Wave Shape." Figure 4.11 and Figure 4.12 show the load-displacement behavior of the plate with two different stiffeners and different magnitudes of initial imperfection. The load is again normalized with respect to P_{ref}, the first mode buckling load for a plate with its centerline nodes fixed out-of-plane.

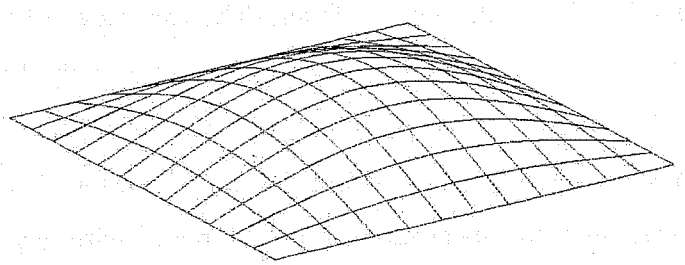

Figure 4.10 Initial Imperfection: One Half-Wave Shape

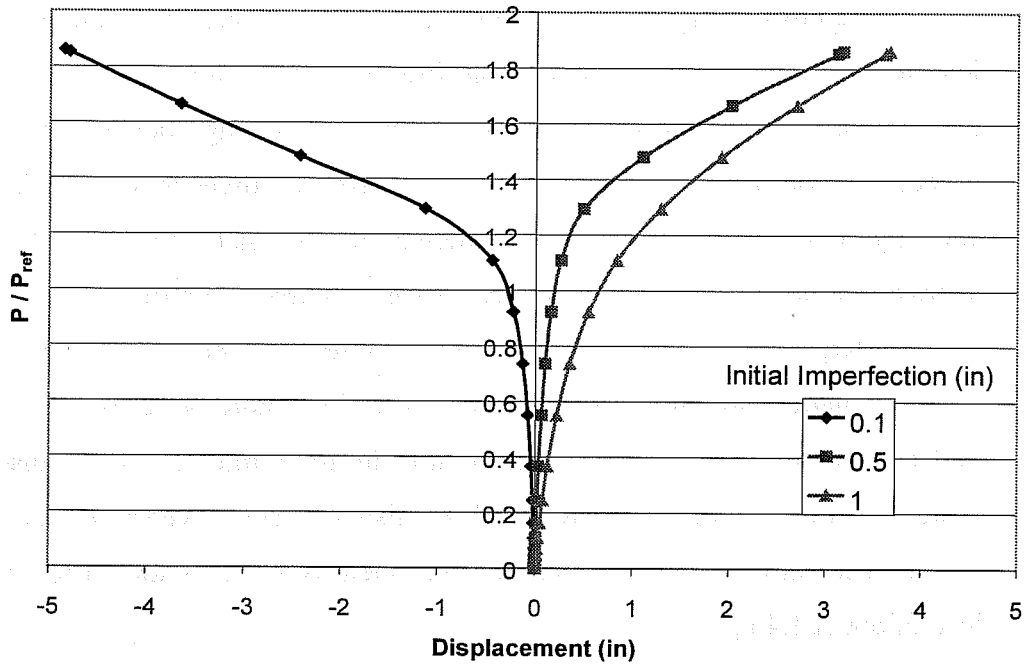

Figure 4.11 Load vs. Displacement with WT 8x13 Stiffener (I_s=147 in^4)

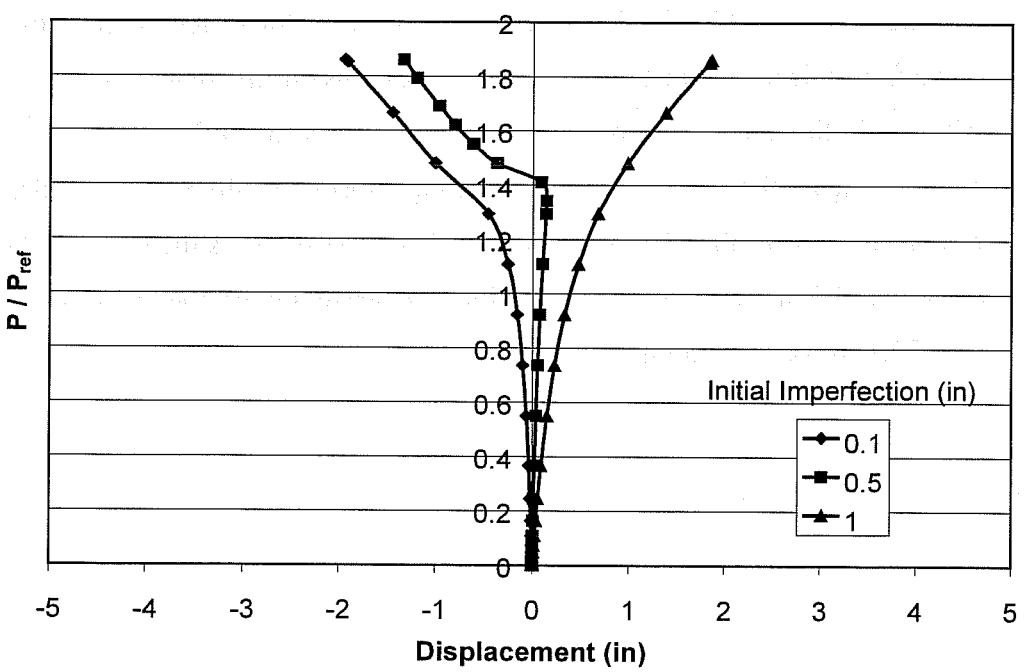

Figure 4.12 Load vs. Displacement with WT 9x17.5 Stiffener (I_s=250 in^4)

The plots in Figure 4.11 and Figure 4.12 show a very stiff response at low load levels. Then there is a noticeable loss of stiffness above P_{ref}, at a load of approximately 1.2 to 1.4 P_{ref}. The plots also show the significant post-buckling capacity of the plate. Comparing the two stiffeners, there is less displacement with the larger stiffener, but the softening of the plate occurs at the same approximate load level. There is a less dramatic change in stiffness for the plate with the largest initial imperfection, which was equal to the plate thickness. The most dramatic softening response was seen in Figure 4.12 with an initial imperfection of 0.5 in. The node at this location initially began displacing upward, but as the load was increased the displacements reversed direction, and produced a sharp knee on the load-displacement plot. This knee occurred at a load of about 1.4 P_{ref}.

Another initial imperfection input to the finite element model was the full-wave symmetric shape shown in Figure 4.13. The load displacement response of a plate with a WT 9x17.5 stiffener with the full-wave symmetric initial imperfection is shown in Figure 4.14. The response of the plate is again very stiff with the initial application of load, then softens at a load of approximately 1.3 to 1.4 P_{ref}. Again the significant post-buckling capacity of the plate is evident. The displaced shape of the plate with the WT 9x17.5 stiffener is the same as the shape of the initial imperfection. The initial imperfection of the plate was simply amplified as load was applied.

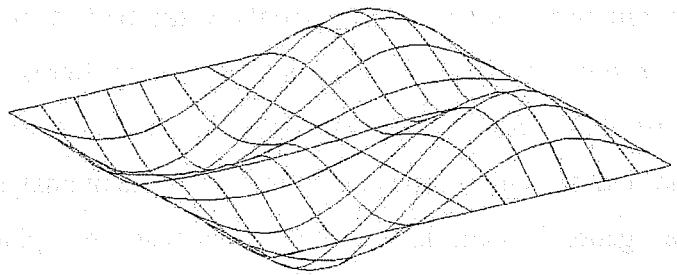

Figure 4.13 Initial Imperfection: Full-Wave Symmetric

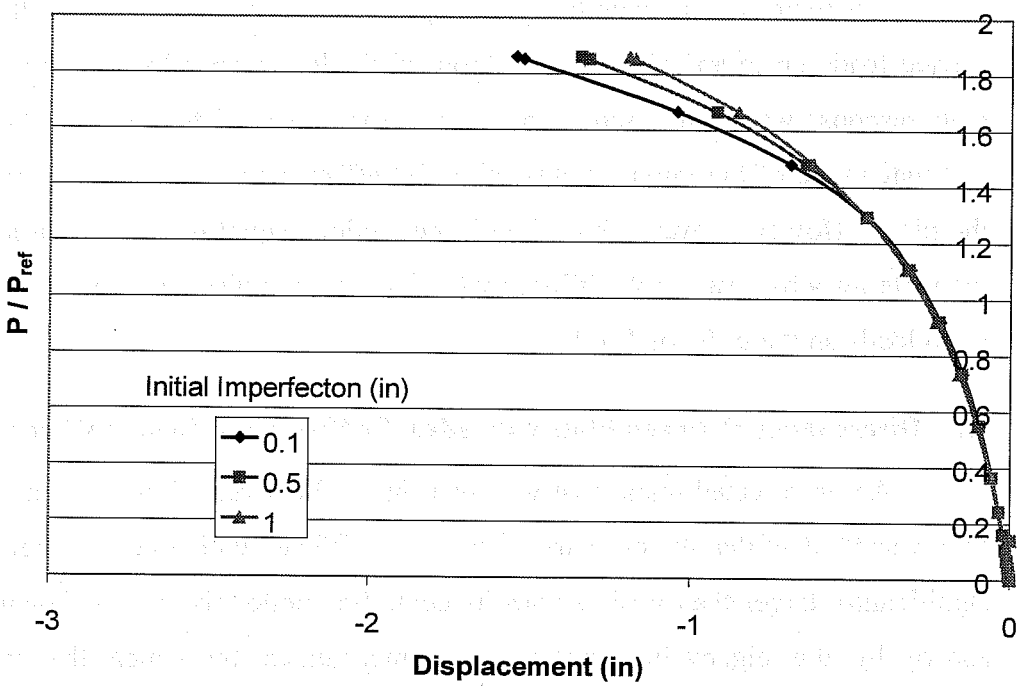

Figure 4.14 Load vs. Displacement with WT 9x17.5 Stiffener (I_s=250 in^4)

An interesting feature of the response of the plate is that with a larger initial imperfection, the displacement at higher loads was actually less than that of a plate with a smaller imperfection. With the larger initial imperfection a larger surface area of the plate seemed to participate in resisting the displacement,

resulting in smaller ultimate displacements at the node that displaced the most. As will be discussed, there were actually some problems with the use of the ABAQUS I-Beam element as a plate stiffener, and this resulted in unexpected responses in both the eigenvalue and large displacement analyses.

The general load-displacement response of plates with different imperfections was similar. The plate's response was very stiff with the initial application of load. The plate showed softening at a load of approximately 1.3 P_{ref}, and demonstrated significant post-buckling capacity.

The main finding from the load-displacement investigation is that the plate carried loads up to and above P_{ref} without difficulty. Generally softening of the plate response was seen around a load of approximately 1.3 to 1.4 P_{ref}. The shape and magnitude of the initial imperfection did affect the relative displacements of the plate. However, even with initial imperfections equal to the plate thickness, the plate response was very stiff at low load levels, and displacements were small up to loads on the order of 1.4 P_{ref}.

4.2 Discrepancy Between Plate with Ideal Stiffener and Beam Stiffener

An unexpected result that was seen in the FEA regardless of plate aspect ratio was the fact that the capacity of the plate stiffened with a large stiffener was significantly larger than a plate with its centerline nodes fixed out-of-plane. As shown by the eigenvalue analyses, the mechanism by which the stiffener significantly increases the buckling load of the test plate is by forcing a nodal line along the stiffener, thereby changing the buckled shape of the plate. The plate buckles on either side of the stiffener on the half-width of the plate. The capacity of the plate with the centerline nodes fixed against moving out-of-plane has been labeled P_{ref} and was used to normalize the results. However, the ABAQUS results

indicated that the capacity of the plate with "adequate" stiffeners was significantly larger than P_{ref}, by almost 40%.

As shown in Figure 4.6 each of the first three eigenvalues surpass the P_{ref} value by approximately 40%. A nominal increase in the capacity of the stiffened plate over P_{ref} was expected, due to the fact that the stiffener participates in carrying the applied load. Using A_s for the area of the stiffener and A_{pl} for the plate cross-sectional area, the relative area of the plate with a physical stiffener to the plate with the centerline nodes fixed out-of-plane is $(A_s+A_{pl})/A_{pl}$. The increased cross-sectional area of the stiffened plate through the stiffener's participation in carrying the applied load explains a nominal increase in the capacity of the stiffened plate over P_{ref}, but the participation of the stiffener was not enough to explain the marked increase in capacity using a stiffener. Consequently a revised model of the test plates, using shell elements for the plate and stiffener, was constructed to further evaluate the issue.

4.2.1 Finite Element Model with Shell Element Stiffeners

Finite element models were constructed using shell elements for both the plate and stiffener. The models using shell elements for the stiffeners did not show the marked increase in capacity that was seen using the ABAQUS I-Section beam element for the stiffener. The buckling loads of the plate with various stiffener sizes are presented in Table 4.3. The data in the table are plotted in Figure 4.15 and Figure 4.16.

Table 4.3 Buckling Load of 72 in. x72 in. x1 in. Plate

I_s (in^4)	Mode 1	Mode 2	Mode 3
0	20.2	31.5	56.0
20.3	47.1	80.1	81.9
37.2	65.0	82.3	92.7
49.1	74.3	83.9	95.6
67.5	84.1	89.6	97.3
106	84.5	97.3	105
230	86.3	98.5	110
860	87.1	98.7	113
15,400	95.7	105	116
Centerline Nodes Fixed Out-of-Plane	80.6 = P_{ref}	94.3	112

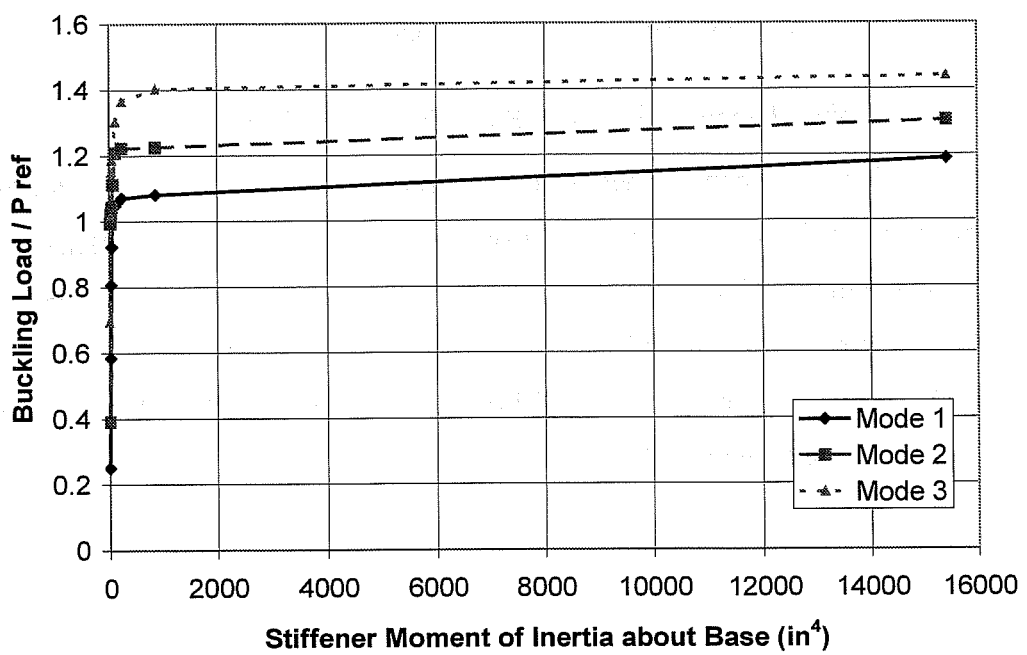

Figure 4.15 Buckling Load vs. Stiffener Moment of Inertia

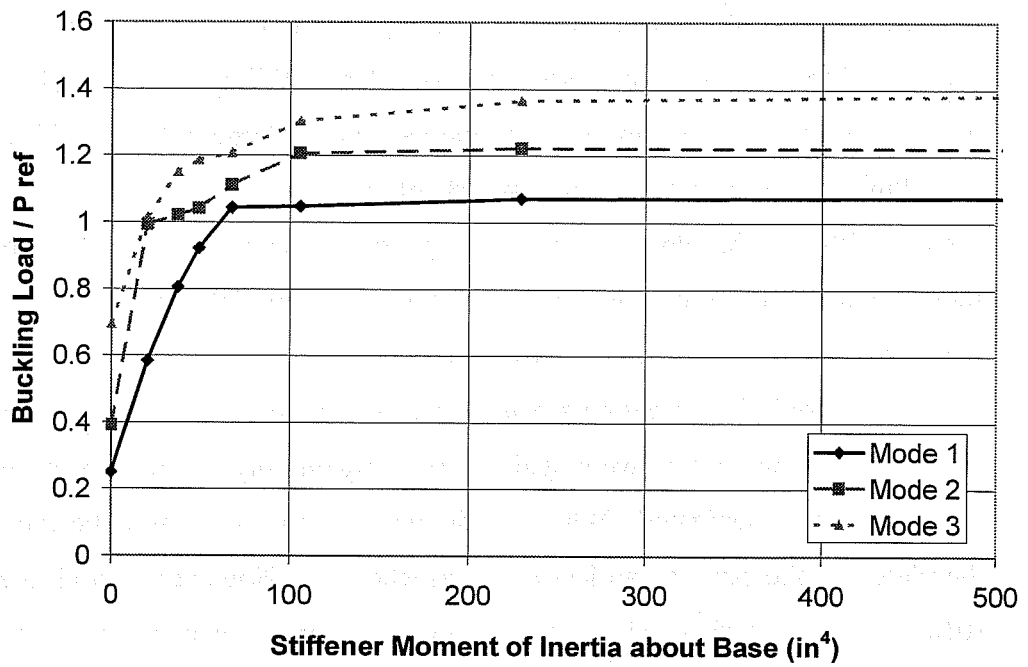

Figure 4.16 Buckling Load vs. Stiffener Moment of Inertia - Reduced Scale

The general response of the plate in the revised finite element model is the same as was seen with the previous model. The capacity of the plate is increased by inclusion of a small stiffener. With larger stiffeners, there is a significant increase in the capacity of the plate approaching a limit capacity that is connected to a marked change in the buckling shape of the plate. Once the limit capacity is reached, increasing the size of the stiffener further does not markedly increase the capacity of the plate. However, the limit capacity with the shell element stiffeners is not 1.4 P_{ref}, as was seen with the beam stiffener. The limit capacity is slightly larger than P_{ref} due to fact that the physical stiffener participates in carrying the applied load.

Referring to Figure 4.16, the buckling load increases significantly as the size of the stiffener is increased up to the stiffener with an I_s of 67.5 in^4. Beyond

this stiffener size, the impact of larger stiffener size is much less significant. The capacity of the plate does increase when very large stiffeners are used, but use of huge stiffeners is not economical. In the case of the large stiffener with an I_s of 15,400in^4, the stiffener area is almost 70% of the plate area. Instead of using such a large stiffener, that does not provide significant material savings, it would be more economical to just increase the plate area by 70% and not incur the fabrication costs of using a longitudinal stiffener.

The study investigating the impact of the plate aspect ratio was repeated, and the same conclusions were again drawn. Again only integer aspect ratios, 1, 2, 3, etc. were investigated. When an adequate stiffener was used, the capacity of the plate was the same regardless of the aspect ratio. However, as with the beam stiffener, larger stiffener sizes were required to force a change in the buckling mode of plates with larger aspect ratios.

4.3 Comparison of FEA to AASHTO Elastic Capacity

For comparison, the buckling capacity of the unstiffened and stiffened plate were calculated using the AASHTO Standard Specifications for Slender Flanges, and the formulation presented by Timoshenko and Gere. No load or reduction factors were considered in the code calculations. Table 4.4 lists the calculated capacities, along with the first buckling mode from the Finite Element Analysis.

Table 4.4 Buckling Loads (k/in) for 72"x72"x1" Plate

I_s (in^4)	FEA	Timoshenko And Gere	AASHTO Elastic Capacity
0	20.2	20.2	20.2
2.30	24.1	23.1	16.2
20.3	47.1	46.9	33.4
37.2	65.0	66.5	40.9
49.1	74.3	78.9	44.8
67.5	84.1	80.9	49.9
106	84.5	80.9	58.0
230	86.3	80.9	75.0
860	87.1	80.9	80.9
Centerline Nodes Fixed out-of-Plane	80.6	80.9	80.9

4.3.1 Comparison of FEA to Timoshenko and Gere

The buckling load for the unstiffened plate calculated by the finite element analysis agrees exactly with Timoshenko and Gere, as expected. There is also close agreement between the FEA for the plate with the centerline of nodes fixed against moving out-of-plane and Timoshenko and Gere's calculations for a plate with half the original width.

The results from the finite element analysis of the stiffened plate also compare well to the formulas from Timoshenko and Gere for small stiffeners. With larger stiffener sizes, there finite element analysis indicates larger buckling capacity than Timoshenko and Gere. The buckling capacity from Timoshenko and Gere is bounded by the capacity of the unstiffened plate and an unstiffened

plate with half the original width. However, the finite element analysis reflects the additional capacity obtained due to the participation of the stiffener in carrying the applied load. Timoshenko and Gere's analysis treats the plate with an adequate stiffener as a plate with the centerline of nodes fixed against moving out-of-plane. The FEA reveals the stiffener's participation with the plate as the plate is buckled. The stiffener increases the capacity of the plate more than is done by simply fixing the plate's centerline nodes out-of-plane.

4.3.2 Comparison of FEA to AASHTO

The buckling loads from the finite element analysis of the stiffened plate were larger than those predicted by the AASHTO elastic equation. The equations for slender plates in the AASHTO formulation are based on the theory of elastic stability. However, the formulation of the stiffener requirements in AASHTO does not consider the aspect ratio of the plate. For a given plate buckling coefficient, k, the stiffener size is dependant on the stiffener spacing, w, and the plate thickness, t. As already discussed, with longer aspect ratios, larger stiffener sizes are required to force a change in the buckling mode. The AASHTO equations are based on using the stiffener size required to force buckling in a longer plate, and subsequently indicate smaller capacities for the square plate under examination. In analyses of longer plates, there is closer agreement between the AASHTO elastic equation and finite element analysis. However, even for longer plates the finite element analysis indicates larger capacities than does AASHTO. The FEA includes the participation of the stiffener in carrying the applied load while the AASHTO equations do not take advantage of this participation. As with Timoshenko and Gere's formulation, the limit of capacity for the AASHTO equation is the capacity of an unstiffened plate with half the

original width. This conservative approach is reasonable in specifying code capacity.

Examining the AASHTO capacity, with the addition of a very small stiffener, the AASHTO equations actually indicate a drop in capacity for the plate. This is due to an error in the formulation of the AASHTO equations that has already been discussed during the presentation of the AASHTO formulas

Using the AASHTO equations, the buckling capacity of the stiffened plate approaches that of an unstiffened plate with half the original width. However, as with Timoshenko and Gere, the stiffened plate capacity predicted by AASHTO is less than that indicated by the finite element analysis. This is again due to the fact that the AASHTO equations do not take advantage of the stiffener's participation in carrying the applied load.

The second reason for the disparity between the FEA and AASHTO capacities is due to the fact that the AASHTO formulation indicates a much larger stiffener is required to cause a mode change in the buckled shape of the plate. As previously discussed, in the finite element analysis the buckled shape of the plate changed to the more complex mode with a moment of inertia of around 70 in^4 about the base of the stiffener. Increases in the stiffener size caused much less increase in capacity past this point. The AASHTO formulation also includes a stiffener size beyond which there is no increase in buckling capacity. However in the code the stiffener size required to produce maximum buckling capacity is much larger than that indicated in the FEA analysis. The AASHTO code specifies that for this 72"x72"x1" plate to have the maximum buckling capacity the stiffener must have a moment of inertia of at least 288 in^4. With stiffeners smaller than this size the capacity of the plate is discounted by the code. This is done since the code formation was developed to apply to plates with larger aspect ratios than that of the square plate. It is not common in American construction to

have transverse stiffeners on the bottom flange resulting in square plate panels. Consequently, the code equations were formulated to handle the more common condition where the aspect ratio of the plate is larger.

4.4 Large Displacement Analyses of Plate with Shell Element Stiffener

A variety of initial plate imperfections were input to the finite element models of the 72 in. x 72 in. x 1 in. plate, with both the plate and stiffener modeled using shell elements. An anti-symmetric initial imperfection, as shown in Figure 4.17, was found to produce the softest plate load-displacement response. This imperfection is the shape as that of the first buckling mode of the plate. A common approach used to attempt to maximize the effects of initial imperfection, to examine the "worst case" situation, is to input initial imperfections that are the same shape as the first buckling mode of the plate. This approach was used in the large displacement analysis conducted by Yoo et al (Ford 2000) and was also a policy followed in the preliminary analytical work done in the completion of this dissertation research. As a result of the behavior seen in the experimental program, later analytical work included stiffener out-of-straightness.

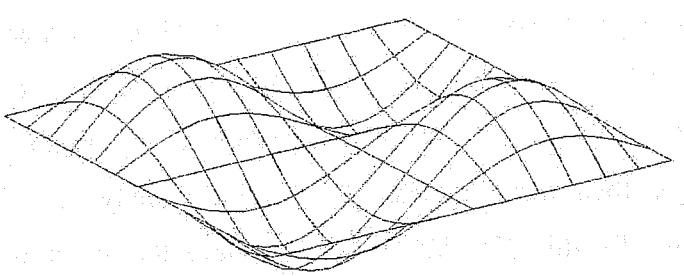

Figure 4.17 Initial Imperfection: Two Waves Anti-Symmetric

The load-displacement response of a plate with an adequate stiffener and initial imperfections in the shape of the first buckling mode is shown in Figure 4.18. The load is normalized with respect to P_{ref}, the first mode buckling mode load of a plate with the centerline nodes fixed against movement out-of-plane. As expected, Figure 4.18 shows larger displacements with larger initial imperfections. When the initial imperfection was equal to the plate thickness, the softest response was observed. The load-displacement plot was almost linear with an imperfection of this level. The main finding from the large displacement investigation was that the load-displacement response of the plate was softened by the presence of initial imperfections. The most significant plate softening was seen with initial imperfections that were the same shape as the first buckling mode of the plate.

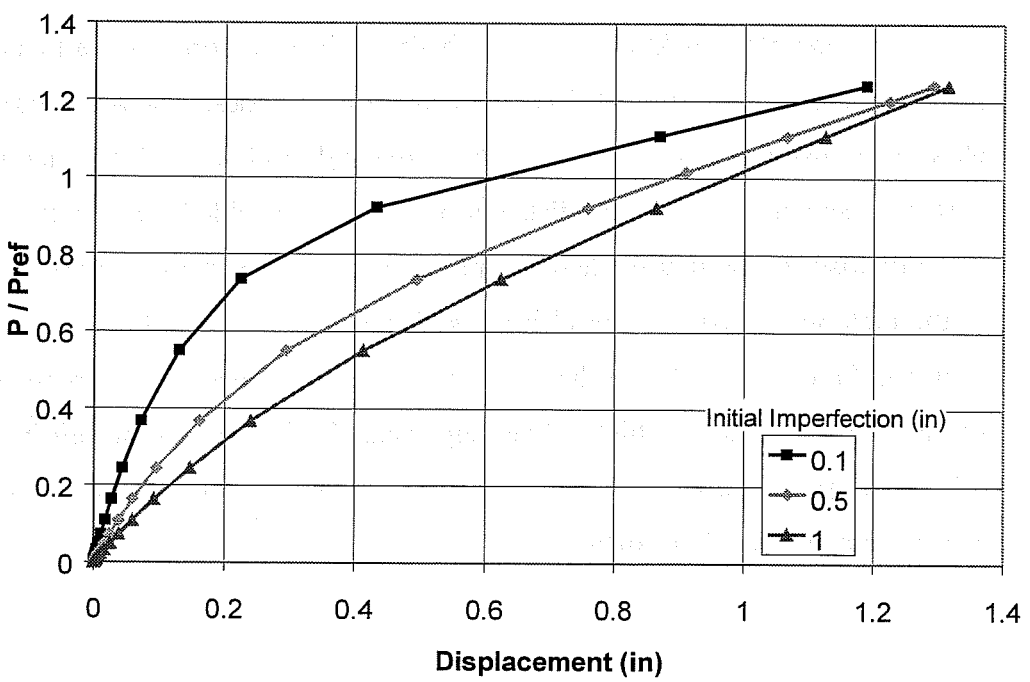

Figure 4.18 Load vs. Displacement with Initial Imperfection of Same Shape as First Buckling Mode

4.5 Source of Error using ABAQUS Beam Stiffener Element

The finite element models using shell elements for both the plates and stiffener agreed more closely with the expected results than did the ABAQUS analysis using the I-Section beam element for the longitudinal stiffener. The use of an adequate shell stiffener resulted in a plate buckling capacity comparable to that obtained by simply fixing the centerline of nodes against moving out of plane. The buckling capacity with a real stiffener is a little higher than that obtained by simply fixing the nodes since the stiffener participates in carrying the applied load. The percentage increase in capacity with the real stiffener, which carries stress, is reasonable using the shell element model.

When the ABAQUS beam element was used for the stiffener, the capacity of the plate with an adequate stiffener was approximately $1.4P_{ref}$. The capacity of the third mode of the plate using shell elements for the stiffener is also $1.4P_{ref}$. This more complex buckling shape is obtained when rotation, as well as out-of-plane movement, is restrained along the centerline of nodes. The ABAQUS beam element apparently overestimates the torsional rigidity of the tee-shaped stiffeners, and consequently predicts a more complex buckled shape with a higher buckling load for the first mode of the plate. The shape of the first buckling mode of the plate with a large beam element stiffener was generally one of the shapes shown in Figure 4.19. These shapes are more complex then the first mode shown in Figure 4.5 and have a higher buckling load. The shape on the left in Figure 4.19 is the same shape expected for the third buckling mode of a plate with the centerline nodes fixed out-of-plane.

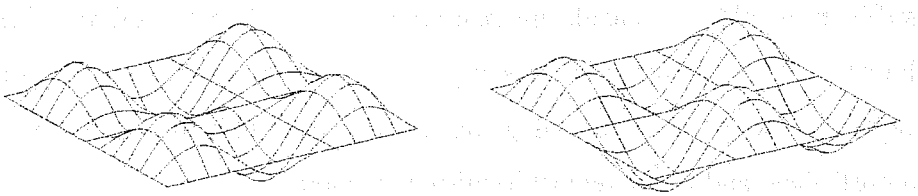

Figure 4.19 First Buckling Mode of Plate with Large Beam Stiffener

Using shell elements for the stiffener realistically modeled the torsional rigidity of the stiffener, and the finite element results using the shell elements agree with expectations. In all subsequent buckling analyses the longitudinal stiffeners were modeled using shell elements.

Though inappropriate for the tee-shaped stiffeners used in the FEA, the torsional rigidity of the ABAQUS beam element did reveal the substantial increase in the buckling load of the plate that accompanied a torsionally rigid stiffener. The traditional approach used when selecting a longitudinal stiffener for the compression flange of box girders in the US has been to use a tee-shaped stiffener. These stiffeners provide substantial moment of inertia, to stop the plate from moving out-of-plane along the stiffener. However, the FEA using the ABAQUS beam element for the stiffener revealed that a stiffener that provides adequate bending moment of inertia as well as a substantial torsional constant can significantly increase the buckling load. Utilization of a new sort of stiffener, which provided significant moment of inertia and torsional rigidity was investigated further in this study.

4.6 Evaluation of Simulated Stiffener Using Boundary Conditions

The added benefit of the torsionally stiff stiffener can most easily be revealed by using boundary conditions to represent the restraint provided by the stiffener. The boundary conditions of the centerline nodes, where a longitudinal

stiffener would be placed, are restrained to simulate the effect of the stiffener. Figure 4.20 shows the first buckling mode of an unstiffened plate, a plate with the centerline nodes fixed out-of-plane, and a plate with the centerline nodes fixed out-of-plane and fixed against longitudinal rotation.

The unstiffened plate in Figure 4.20 buckles into a simple one-half wave shape. The plate with the centerline nodes fixed out-of-plane models a plate with a stiffener with adequate moment of inertia to form a nodal line along the plate centerline. This plate buckles in an antisymmetric shape with a full wave on either side of the plate centerline. The plate with the centerline node fixed out-of-plane and fixed against longitudinal rotation models a stiffener with adequate moment of inertia to form a nodal line along the plate centerline, and with sufficient torsional rigidity to constrain rotation along the centerline of the plate. This plate buckles into three half-waves on either side of the stiffener.

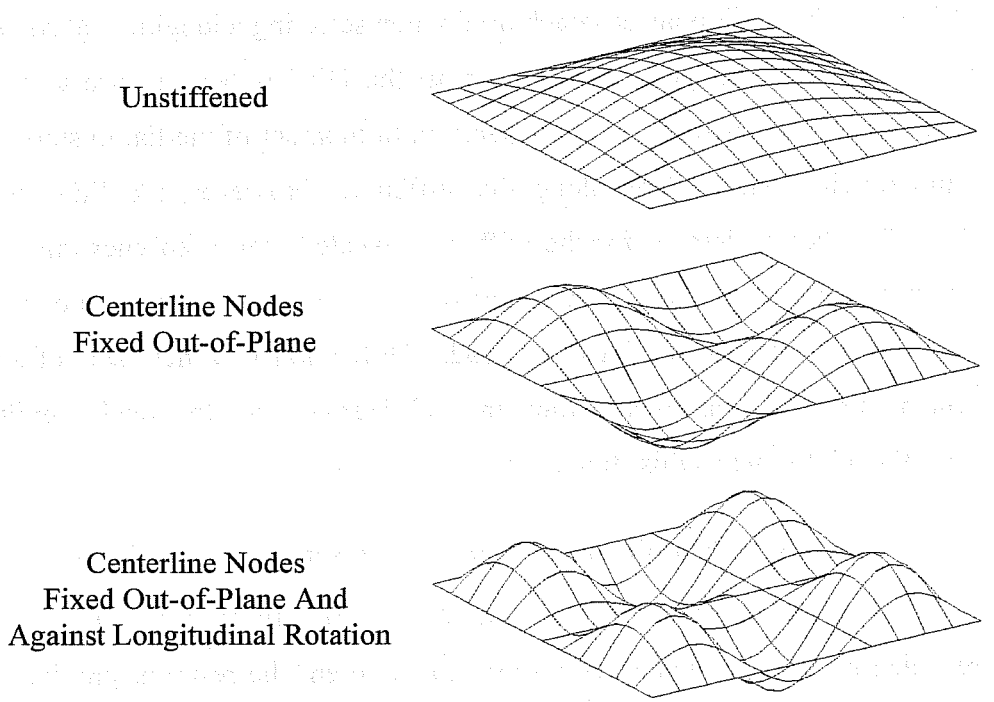

Figure 4.20 First Buckling Mode of Plate with Specified Boundary Conditions

For a plate with the centerline nodes fixed out-of-plane and fixed against longitudinal rotation, the first two buckling modes of the plate are essentially equally likely. The first two buckling modes are shown in Figure 4.21. There is less than 0.1% difference in the buckling load in these two modes. In both of these modes the plate buckles into a complex shape, with three half-waves on either side of the stiffener. The first mode has a symmetric shape about the stiffener, and in the second mode the plate buckles in an antisymmetric shape, but both have three half-waves along the length of the plate.

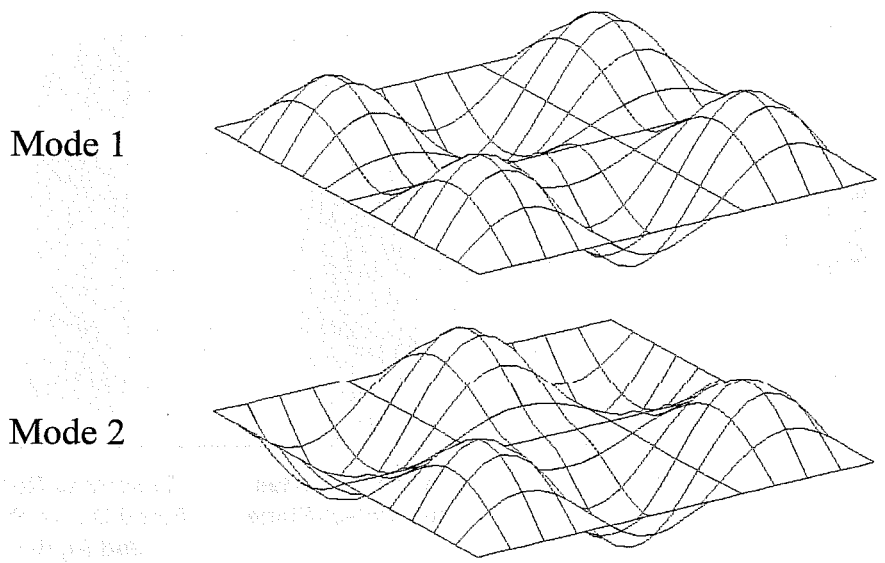

Figure 4.21 First Two Buckling Modes of Plate with Centerline Nodes Fixed Out-of-Plane and Fixed Against Longitudinal Rotation

The added complexity of the buckling mode with the centerline nodes fixed out-of-plane and fixed against longitudinal rotation results in a larger plate buckling load. The buckling loads of the unstiffened plate, the plate with the centerline nodes fixed out-of-plane, and the plate with the centerline nodes fixed out-of-plane and against longitudinal rotation are shown in Figure 4.22. The

capacity is normalized with respect to P_{ref}, the capacity of the plate with the centerline nodes fixed out-of-plane. The capacity of the plate with the centerline nodes fixed out-of-plane is 4 times the capacity of the unstiffened plate, as expected. The capacity of the plate with the centerline nodes fixed out-of-plane and against longitudinal rotation is almost 39% higher than P_{ref}. The torsional fixity produces substantial additional capacity.

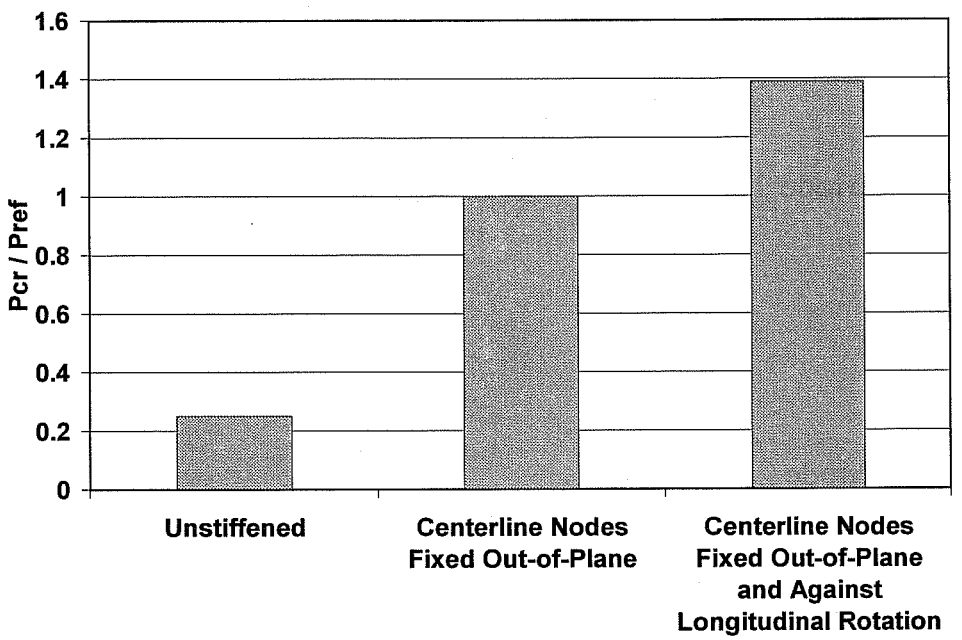

Figure 4.22 Buckling Capacity of Plate with Specified Boundary Conditions

4.7 Longitudinal Stiffener with Significant Torsional Constant

As demonstrated by restraining torsional rotation along the centerline of the plate, the buckling capacity of a plate can be significantly increased not only by using a stiffener with adequate bending moment of inertia, but also by using a

stiffener with adequate torsional rigidity. The tee-shaped longitudinal stiffeners typically used in trapezoidal steel box girders are not torsionally stiff. Open stiffeners such as a plate stiffener or a tee-shaped stiffener have very small torsional constants. Closed shapes, such as round pipes and square tubes, have substantially larger torsional constants.

The steel structural shapes most appropriate for providing significant torsional rigidity are angles and hat shapes. Figure 4.23 shows the plate with open plate and tee stiffeners, and closed angle and hat stiffeners. The closed shape of the angle and hat stiffener is provided by the legs of the stiffener and the area of the stiffened plate immediately beneath the stiffener.

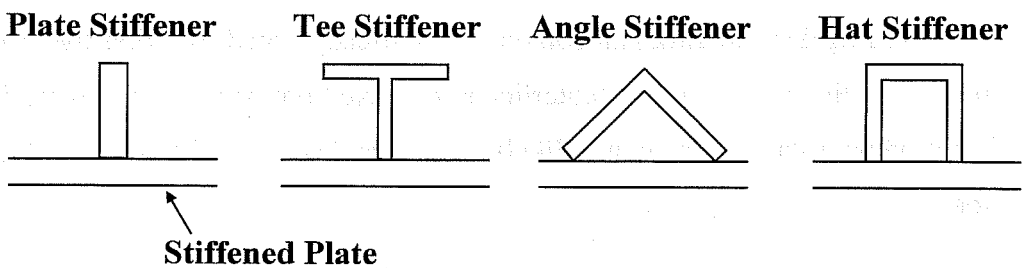

Figure 4.23 Open vs. Closed Stiffeners

The hat shaped stiffener is an attractive shape for use as a torsionally stiff longitudinal stiffener. The flange of the hat stiffener, like the flange of the tee stiffener, can effectively provide adequate bending moment of inertia about the base of the stiffener. The angle stiffener is also an appropriate shape for providing torsional rigidity. However, the angle shape is not as efficient in providing bending moment of inertia as the hat stiffener. For larger plates, a hat shaped stiffener is more appropriate to provide the required bending moment of

inertia and torsional constant. For smaller plates, an angle shaped stiffener may be sufficient to provide adequate moment of inertia and torsional stiffness.

4.8 Hat Stiffener

Finite element models incorporating hat shaped stiffeners were analyzed. Shell elements were used to model both the plate and stiffener. The buckling shape of a plate with an adequate hat stiffener is shown in Figure 4.24. The hat stiffener in this model provides adequate bending moment of inertia, so that the plate buckles about the stiffener, and also provides substantial torsional stiffness. The plate is buckled in an anti-symmetric shape with three half-waves on either side of the stiffener. The buckled shape of the plate is the same as the second buckling mode shape of the plate that had the centerline nodes fixed out-of-plane and fixed against longitudinal rotation. As already noted, the first two buckling modes for the plate with the centerline nodes fixed out-of-plane and fixed against longitudinal rotation are equally likely, with less than 0.1% difference in buckling load.

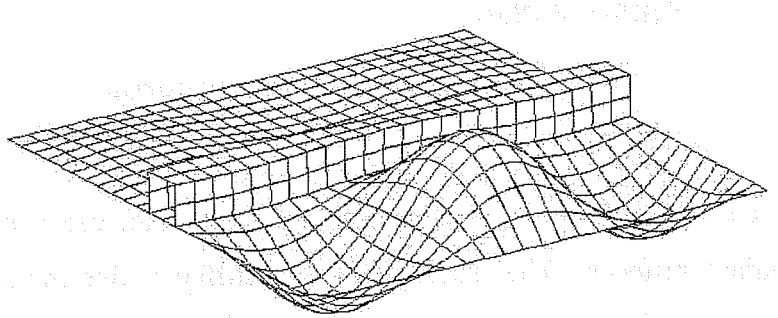

Figure 4.24 First Buckling Mode of Plate with Adequate Hat Stiffener

Finite element analysis demonstrated that with a closed stiffener that had adequate bending moment of inertia and provided adequate torsional rigidity, the elastic buckling capacity of the plate was significantly increased. To more clearly

show the impact of increasing the torsional constant of the stiffener, a series of FEA runs were performed where a stiffener was transitioned from a tee-shaped stiffener to a hat stiffener. The accompanying increase in capacity is shown in Figure 4.25. The buckling load is normalized with respect to P_{ref}, the buckling load of the plate with the centerline of nodes fixed out-of-plane. A plate with an adequate tee-shaped stiffener was initially analyzed. The web of the tee was then split in half, and the two web sections were spread apart as shown in Figure 4.25. The stiffener was transitioned from a tee stiffener, to a π shaped stiffener, and finally to a hat stiffener. Each stiffener had the same I_s or stiffener moment of inertia about the base of the stiffener. Thus the increase in plate buckling capacity is due to the increase in the torsional constant accompanying the transition from an open stiffener to a closed stiffener.

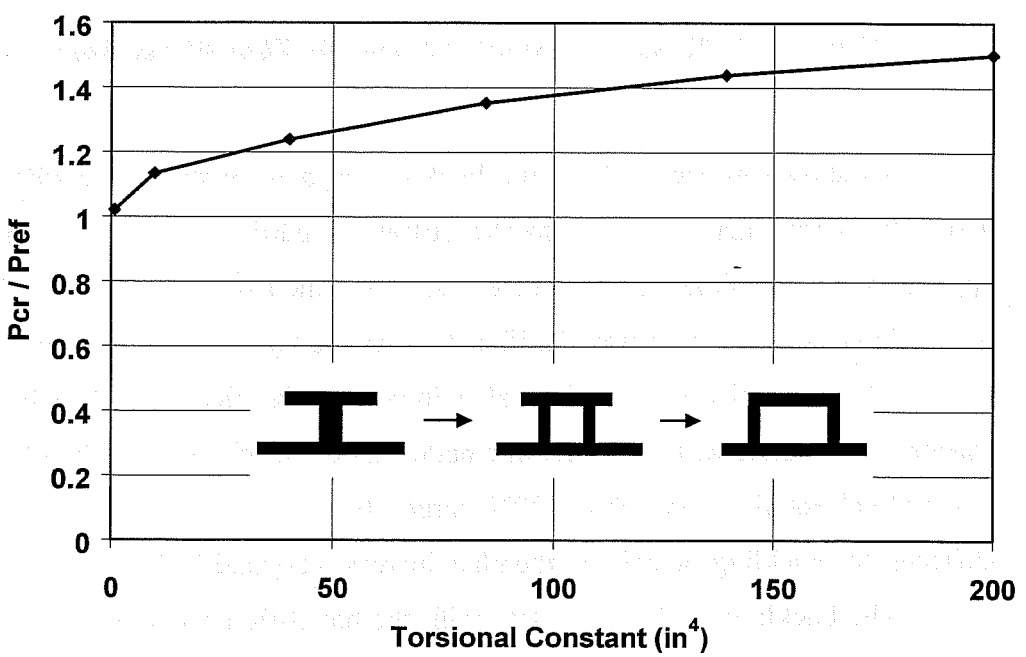

Figure 4.25 Buckling Capacity Increase with Hat Stiffener

The torsion constant of the tee-shaped element was calculated based on the sum of the $bt^3/3$ of the web and flange elements of the tee. The torsion constant of the hat-shaped stiffeners was calculated based on the enclosed area and perimeter of the section, as shown in Figure 4.26.

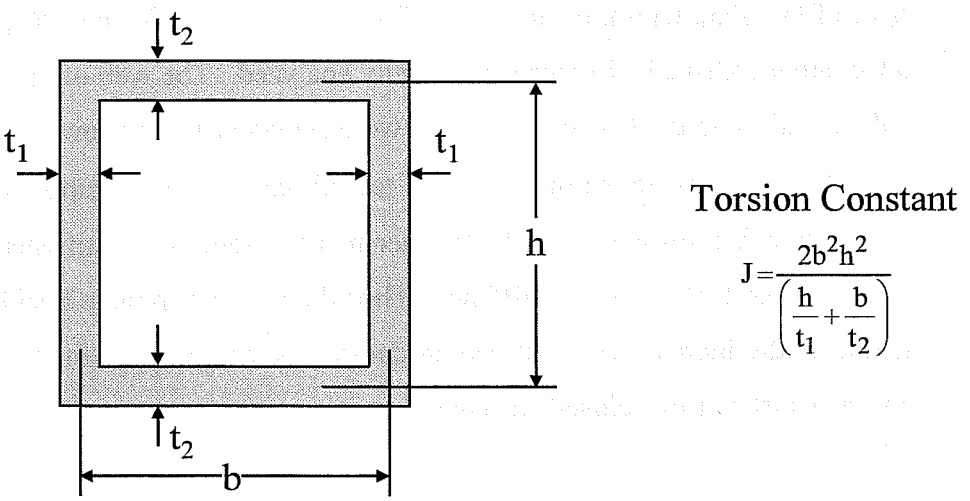

Figure 4.26 Torsion Constant of Rectangle Thin-Walled Shape

As shown in Figure 4.25, the buckling capacity with the tee-stiffener is about 3% larger than P_{ref}, due to the stiffener's participation in carrying the applied load. When the web of the tee is split and the two webs are spread apart, the torsional constant increases significantly. As the torsion constant is increased, the buckling capacity of the plate also increases significantly. The buckling capacity of the plate with the centerline nodes fixed out-of-plane and fixed against longitudinal rotation was about 39% larger than P_{ref}. With the hat shaped stiffener, the buckling capacity of the plate increases beyond 1.39 P_{ref}.

The buckling load of the plate with the hat stiffener is even greater than that of a plate with the centerline nodes fixed out-of-plane for three main reasons. First, the hat stiffener participates in carrying the applied load. This added

capacity is not captured when boundary conditions are used to model the stiffener's impact. Second, the hat stiffener actually restrains rotation over a longitudinal strip down the center of the plate, rather than just at the centerline nodes. The width of the plate contained within the webs of the hat stiffener is restrained with the hat stiffener. Furthermore, with a hat stiffener, the unsupported width on either side of the stiffener is actually less than half the plate width. As shown in Figure 4.27, the plate width between the web of the box and the edge of the hat stiffener is half the plate width minus half the stiffener width. When formulating capacity equations, it would be conservative to use distance between the web and the centerline of the stiffener. However, the finite element analysis results include the added capacity accompanying the reduction in the unsupported plate width.

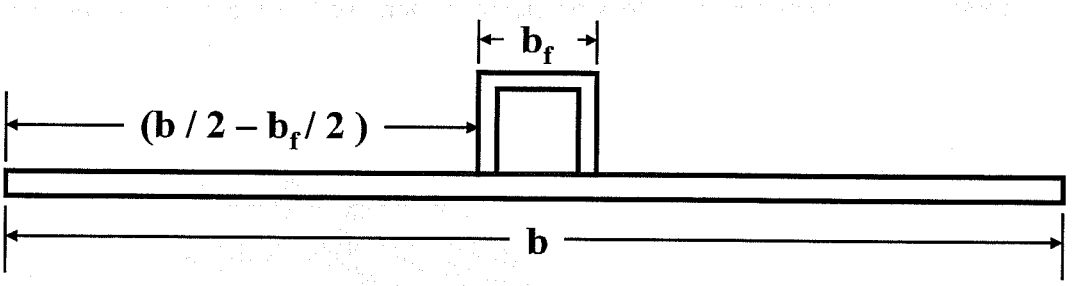

Figure 4.27 Reduced Unsupported Plate Width with Hat Stiffener

4.9 Concrete Stiffener

As previously discussed, an alternative approach to using a steel longitudinal stiffener on the bottom flange of steel trapezoidal box girders is using a composite bottom flange. As mentioned, a significant drawback to the use of a composite bottom flange is that the weight of the wet concrete on the unsupported bottom flange can produce significant, possibly unacceptable, displacements.

Consequently, it was suggested that the inclusion of longitudinal stiffeners to control plate deflections might be desirable (Yen 1986). This finding significantly reduces the usefulness of a full composite bottom flange. If it is necessary to go to the trouble and expense of welding a longitudinal stiffener to the bottom flange, the most reasonable approach would be to simply use a larger stiffener that would significantly increase the buckling capacity of the bottom flange and not use a composite flange.

An interesting combination of the composite bottom flange approach and use of torsionally stiff stiffeners is a concrete stiffener. By localizing the concrete to the middle longitudinal line of the steel plate, as shown in Figure 4.28, the weight of the concrete, and the resulting deflections, are significantly reduced. Furthermore, the solid cross section of a concrete stiffener can provide the torsional stiffness required to significantly increase the plate's buckling capacity above P_{ref}.

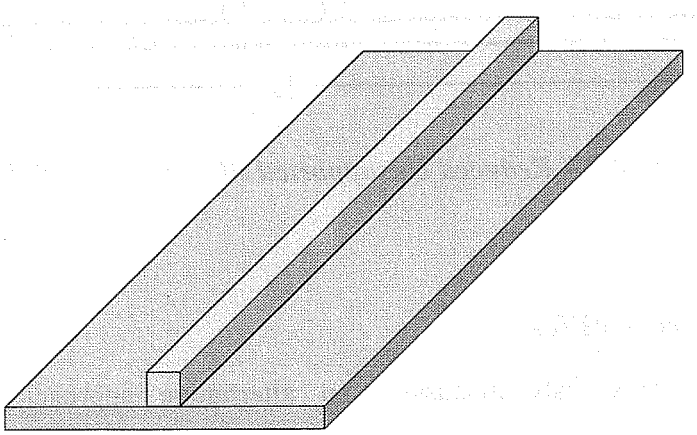

Figure 4.28 Concrete Stiffener

The concrete stiffener can be attached to the bottom flange of the box using shear studs, as shown in Figure 4.29. The concrete stiffener could be either

cast-in-place or precast. If the stiffener was precast, block outs for the shear studs would need to be provided and filled with grout in the field.

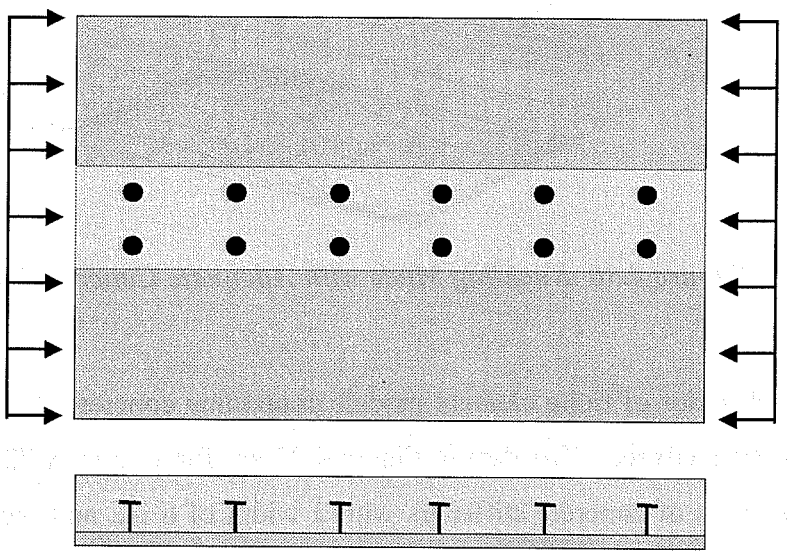

Figure 4.29 Concrete Stiffener - Shear Studs

Finite element models using a concrete stiffener were prepared. An elastic modulus of 3,270 ksi was used for the concrete. Models with the stiffener fully bonded to the steel plate, as well as models with the stiffener connected only at the shear stud locations, were analyzed. The analysis showed that with adequately spaced shear studs, the concrete stiffener performed well. The buckling mode of a concrete stiffener with adequate bending moment of inertia and torsional stiffness is shown in Figure 4.30. The plate is buckled in an anti-symmetric shape with three half-waves on either side of the stiffener, as was seen with the steel hat stiffener.

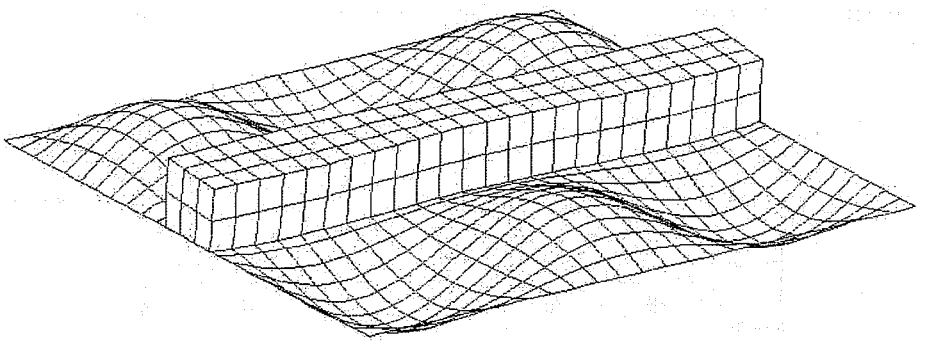

Figure 4.30 Buckling Mode with Adequate Concrete Stiffener

A series of finite element models containing concrete stiffeners of various sizes were analyzed. The data in Figure 4.31 are for a 72 in. x 72 in. x 1 in. plate with a series of concrete stiffeners with a width of 6 in., and increasing heights. The stiffener moment of inertia is calculated about an axis parallel to the plate at the base of the stiffener as recommended by Timoshenko and Gere (Timoshenko 1961). Figure 4.31 shows the same general trend that was seen with plate and tee stiffeners. With small stiffeners, the buckling capacity of the plate is greater than that of the unstiffened plate, but less than P_{ref}. As the stiffener size is increased, the plate approaches a limit capacity beyond which further increases in stiffener size are not accompanied by significant increases in buckling capacity. As expected, the limit capacity with the concrete stiffener is approximately 1.4 P_{ref}. The concrete stiffener with adequate bending moment of inertia, and a significant torsional constant results in a higher plate buckling capacity.

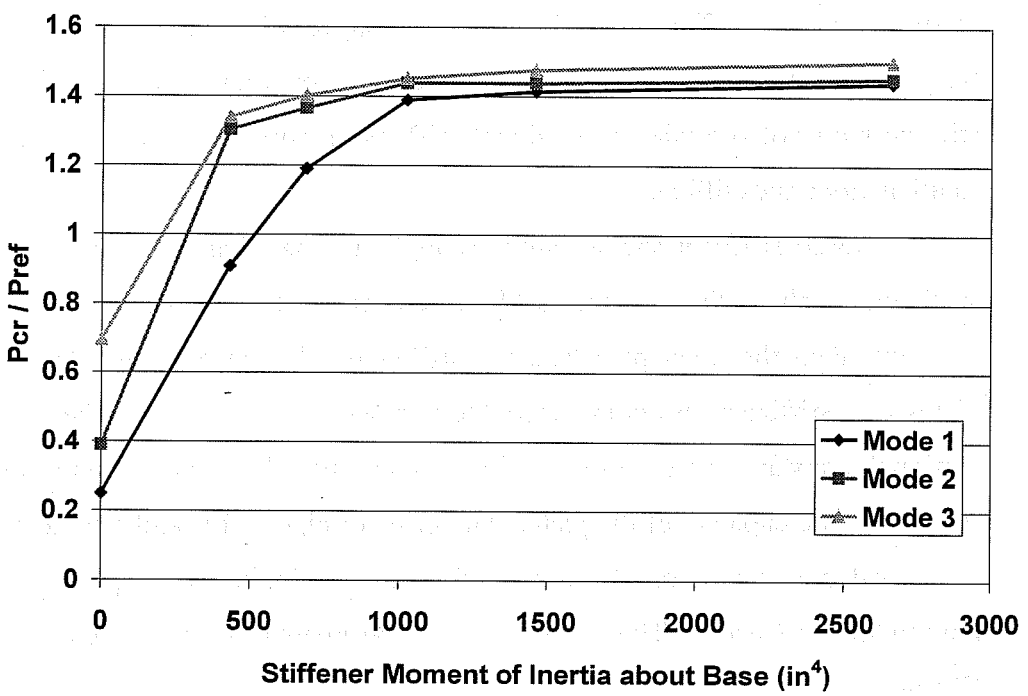

Figure 4.31 Buckling Load vs. Stiffener Moment of Inertia - Concrete Stiffener

The data presented in Figure 4.31 show that a stiffener with an I_s of approximately 1020 in^4 was required to reach the limit buckling capacity. A stiffener that is 6 in. wide and 8 in. high provides this required moment of inertia. This moment of inertia of an adequate concrete stiffener is much larger than the moment of inertia of an adequate steel tee stiffener. The main reason for the significant increase in the required moment of inertia using a concrete stiffener is the fact that concrete has a much smaller modulus of elasticity than steel.

4.10 Experimental Program

The finite element analysis results showed that the buckling capacity of a stiffened plate could be increased significantly by using a stiffener that not only provided an adequate bending moment of inertia, but also had a substantial

torsional constant. The open plate and tee shaped stiffeners commonly used as longitudinal stiffeners in the United States are torsionally weak. These open stiffeners do not provide the torsional stiffness required to restrain longitudinal rotation along the stiffener.

Closed stiffener shapes, such as angle and hat shaped sections, and solid stiffeners, such as the concrete stiffener described, have much higher torsional constants than the open plate and tee stiffeners. In the experimental program, plates with stiffeners providing adequate bending moment of inertia and adequate torsional constant were tested to investigate the effect of stiffener torsional rigidity on the capacity of the plate. The basis of eigenvalue and strut approaches were evaluated based on the test results of plates with both open and closed longitudinal stiffeners. The details of the experimental program are described in Chapter 5.

Chapter 5

Experimental Program

5.1 General

The experimental program consisted of laboratory tests to study the elastic buckling behavior of the steel compression flanges of trapezoidal box girders. Tests were conducted on eight plates with various stiffener configurations. The width, thickness and steel grade of the compression plate were the same for each test.

A scale trapezoidal box girder fabricated for elastic studies of overall girder buckling behavior was reused in this testing program. The girder was simply supported with overhanging end spans. The girder was 20 ft. in length with an 8 ft. center span and 6 ft. overhangs on each end, as shown in Figure 5.1. The girder was loaded at the ends to produce a uniform bending moment region between supports. The overall test setup is shown in Figure 5.2 and Figure 5.3.

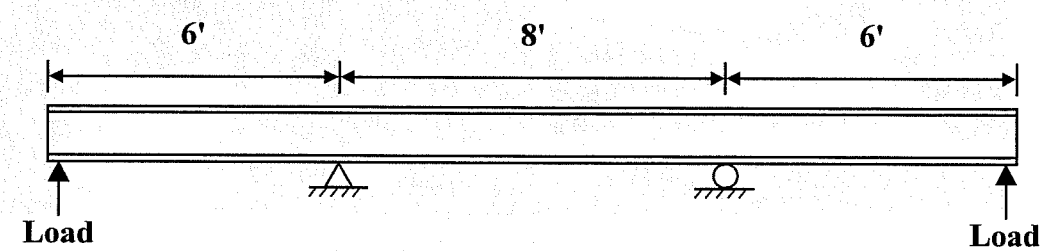

Figure 5.1 Test Setup Schematic

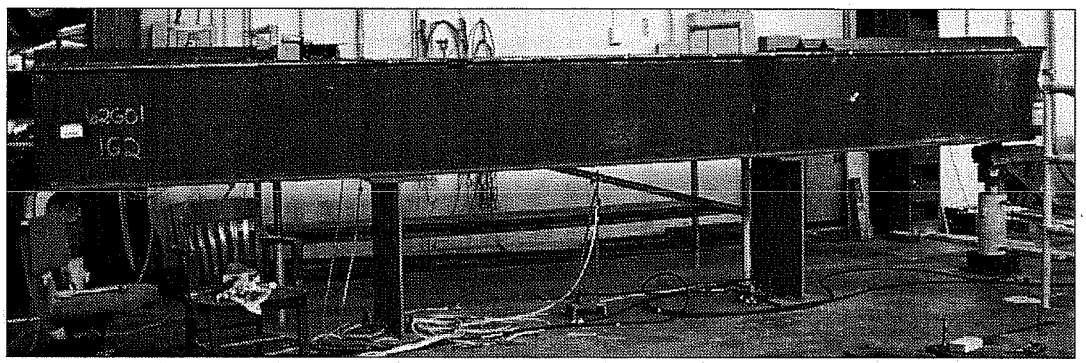

Figure 5.2 Test Setup Side View

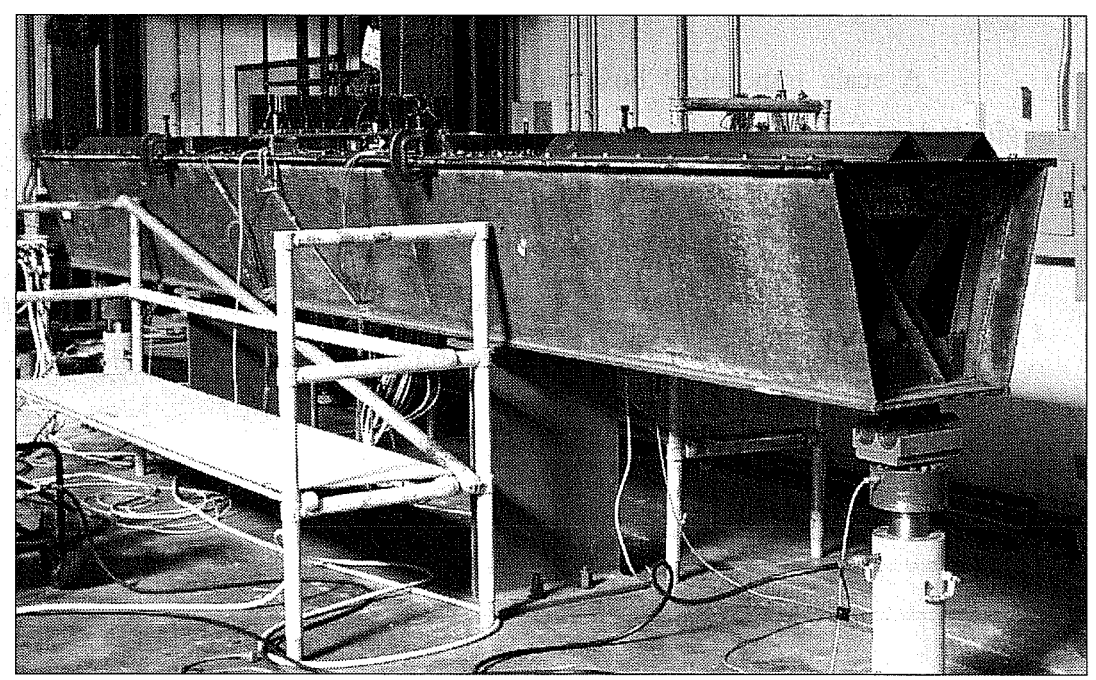

Figure 5.3 Overall Test Setup

The girder was fabricated using steel with a specified minimum yield stress of 50 ksi for the top and bottom flanges and 36 ksi for the webs. The

average measured cross sectional properties of the girder are presented in Figure 5.4.

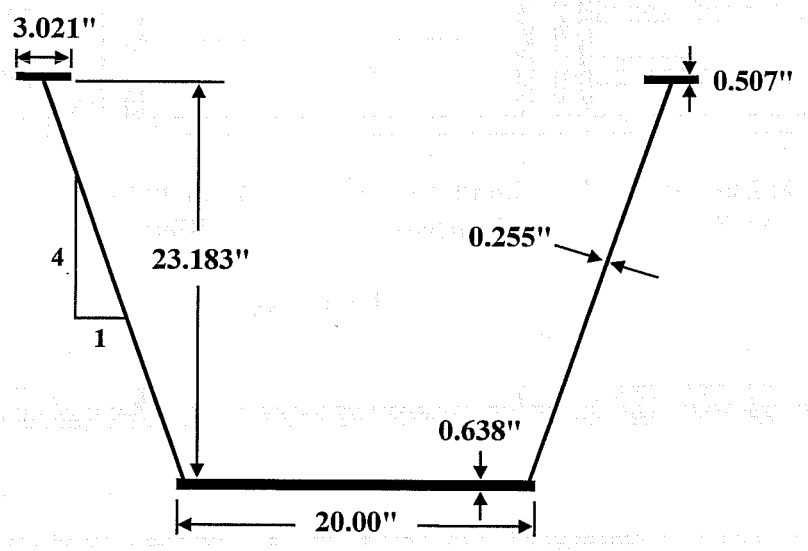

Figure 5.4 Average Girder Cross-Section Properties

Since the test setup and girder were originally constructed to test overall girder buckling in the positive moment region, the setup was designed to put the top flanges of the box girder in compression and the bottom flange in tension. To modify the test setup to meet the needs of the current testing program, thin test plates that would buckle elastically as desired were bolted to the top flanges of the existing box girder.

5.2 Test Plate and End Span Plates

A total of three plates, two end span plates and a center test plate, were used as shown in Figure 5.5. _End span plates were used, rather than leaving the end overhangs open, so that the plate force could be developed in the end spans, and then transferred to the test plate.

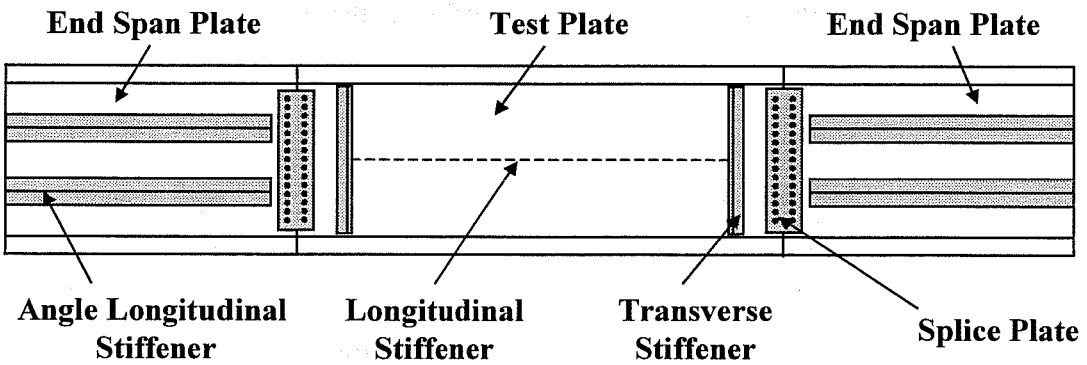

b) Plan View

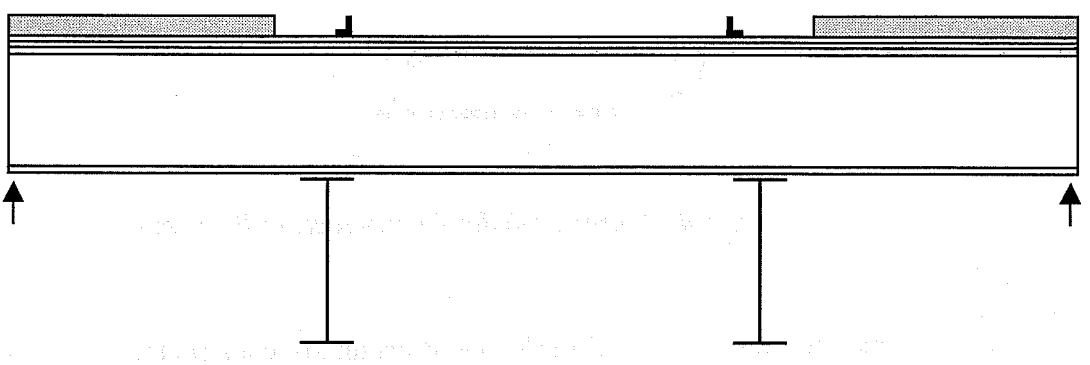

b) Elevation

Figure 5.5 Test Plate and End Span Plates

Figure 5.6 shows the girder during installation of a test plate. Both the end span and test plates were constructed of 3/16 in. thick steel plate with a specified minimum yield strength of 70 ksi. High strength steel plates were used to ensure that the plates remained elastic throughout the testing program.

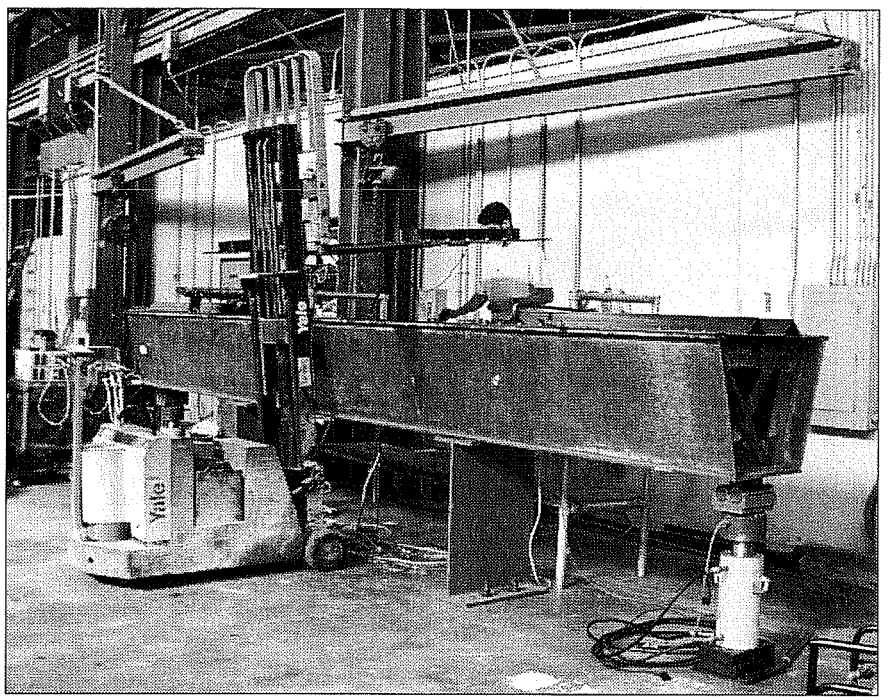

Figure 5.6 Installation of Test Plate

The test compression flange region was located in the center span of the box girder, as shown in Figure 5.5. The center span of the girder, and the test plate, were under uniform moment. Testing the plate under uniform moment is a conservative loading condition compared to the actual loading of the compression flange in a box girder structure with moment gradients near the supports. Stiffeners were added to the end span plates to ensure they did not buckle during the tests. Two angle stiffeners were welded to each end span plate as shown in Figure 5.5 and Figure 5.7.

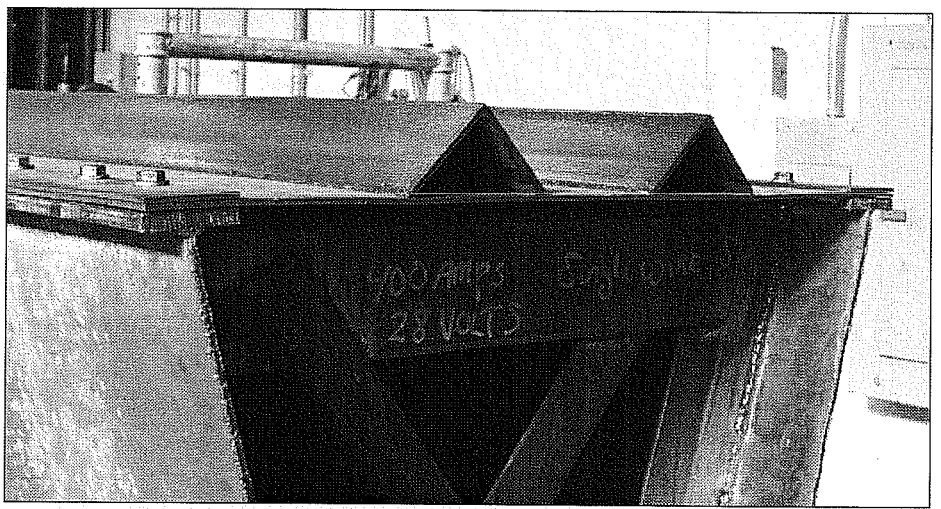

Figure 5.7 Stiffened End Plate

Each end span plate was attached to the test plate via a bolted splice connection. Figure 5.8 shows the end span plate and the splice connection. Thirty 5/8 in. A490 bolts were used in each splice connection. Since the bottom of the connection was not accessible during installation of the plates the nuts were welded to the bottom splice plates.

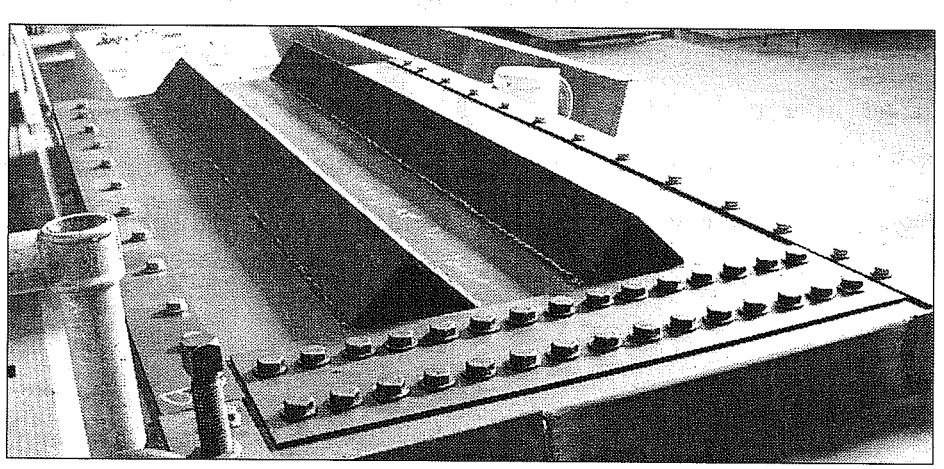

Figure 5.8 Stiffened End Plate and Splice Connection

Transverse stiffeners were installed on the test plate to define the test region of the plate, as shown in Figure 5.5. The steel 3×3×3/8 angles used for the transverse stiffeners were bolted to the test plate. A continuous steel angle was used between the top flange edge plates on both the top and bottom side of the plate. Attachment angles with a clipped leg were then welded to either end of the transverse stiffener angle on the top of the plate, as shown in Figure 5.9. These angle sections were seated directly on top of the edge plates and welded to the transverse stiffeners. The transverse stiffeners were bolted to the test plate, and the attachment angles were fastened to the top flanges of the box girder with beam clamps as shown in Figure 5.10.

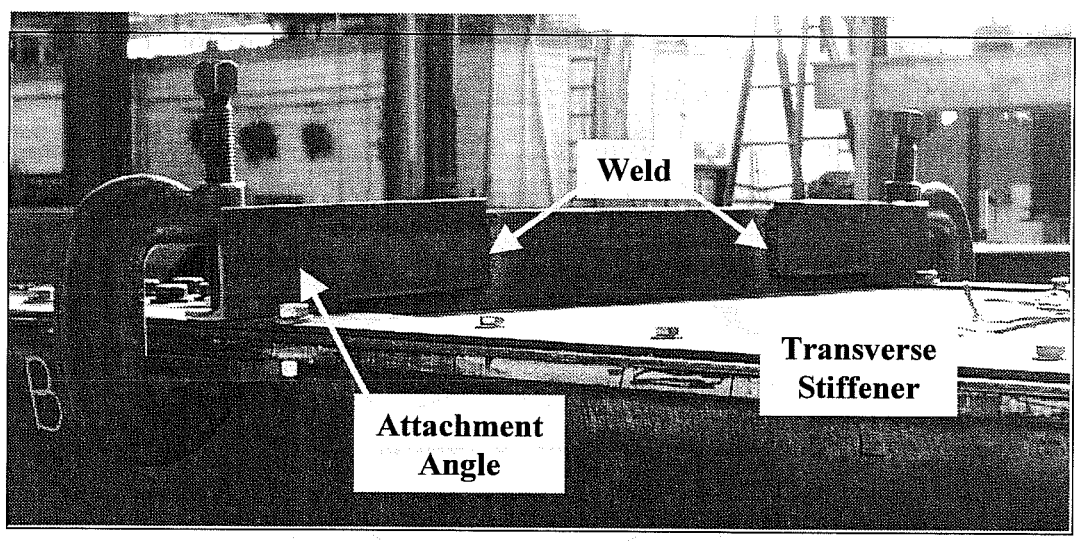

Figure 5.9 Transverse Stiffener and Attachment Angles

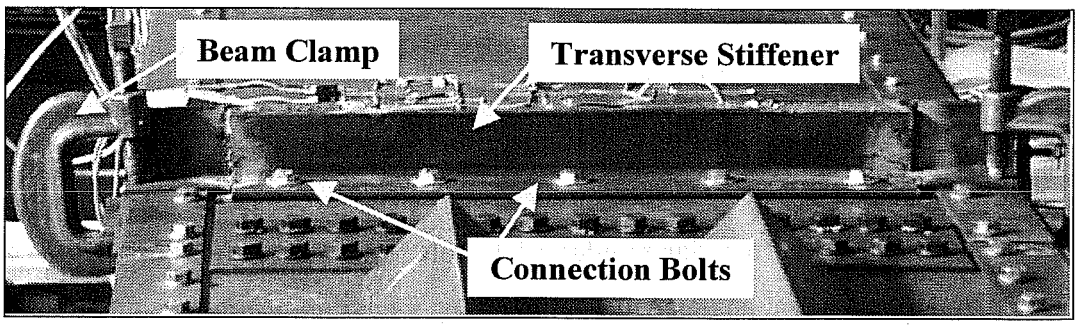

Figure 5.10 Transverse Stiffener

5.3 Attachment of Test and End Span Plates to Girder

The end span and test plates were bolted to the top flanges of the trapezoidal girder, as shown in Figure 5.11. High-strength hex head cap screws were used to bolt the plates to the girder. In the end span region, 1/2 in. bolts at a maximum of 5 in. spacing were used, and in the test span 3/8 in. bolts at a maximum of 6 in. spacing were used. The bolt spacing varied slightly along the length of the girder since the bolts were positioned to avoid the intermittent welds between the web and the top flange on the inside of the girder.

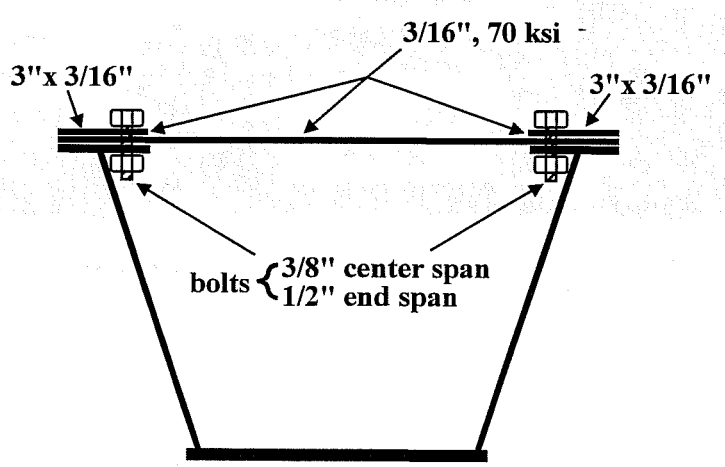

Figure 5.11 Bolted Plate Connection

Connection bolts in the center span were spaced to prevent buckling of the plate between the fasteners. An edge plate was added on top of the new compression plates on each side to ensure that the plate did not buckle locally between fasteners. The edge plates are also shown in Figure 5.11.

The plates were bolted to the top flanges on the inside edge of the top flanges. This made construction difficult, since it was not possible to access the inside of the girder after the top plate was placed on the girder. Therefore the nuts for each bolt were welded to the underside of each top flange prior to putting the top plate into place. The welds held the nuts in position and restrained them from rotating during installation of the bolts.

The top plate was bolted on the inside of the box to maintain a constant effective buckling width for the plate. If the plate was bolted on the outside edge of the flanges, the effective buckling width, b, was significantly different when the plate buckled up versus buckling down. Finite element analysis showed that this difference in effective buckling width significantly effected results. Thus the arrangement with the bolts on the inside of the top flanges was selected.

5.4 Test Plate Slenderness and Aspect Ratio

As discussed, the transverse stiffeners defined the length of the test region of the plate. The bolt lines defined the effective buckling width of the test plate. The buckling width, b, of the test plate was 29 in., as shown in Figure 5.12. Also shown in Figure 5.12 is the test plate length of 84 in that was established by the transverse stiffeners.

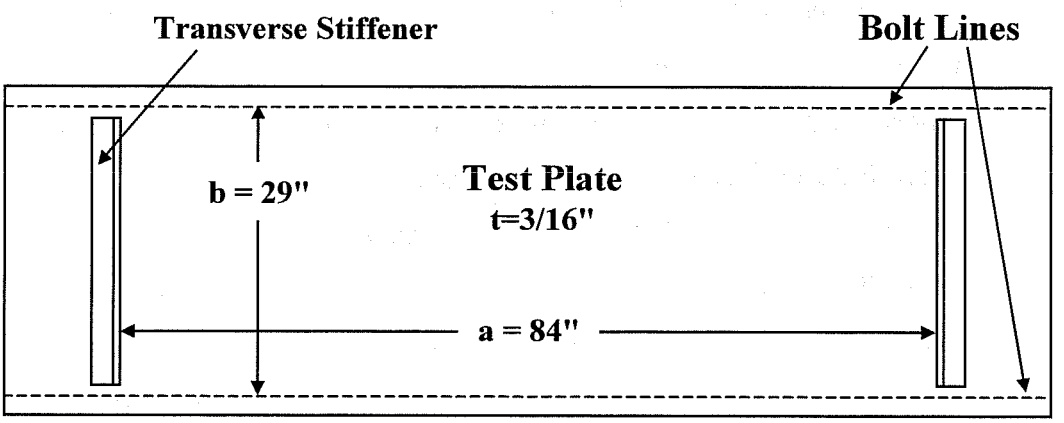

Figure 5.12 Test Plate Dimensions

The plate was originally expected to buckle between the top flanges of the box girder with an effective width of 28 in. A test plate length of a = 3b, or 84 in. was selected. Test results and finite element analysis showed that the plate actually displaced between the lines of connection bolts with an effective width of 29 in. as shown in Figure 5.12. The aspect ratio, a/b, of the unstiffened test plate was therefore 2.9.

5.5 Loading and Support System

The box girder supports were designed to approximate simple supports. The supports were 2 ft. long W36x150 beams that were oriented transversely to the box girder, as shown in Figure 5.2 and Figure 5.3. The bending resistance of the webs of the support beams provided very little rotational restraint to the girder, thereby adequately providing the desired simple support. The bottom flange of the support beam was bolted to the floor using four 1 in. diameter threaded rods. The support beams were bolted to the bottom flange of the box girder using four 1 in. diameter bolts.

Permanent internal cross-frames were installed at each support location and loading location. These cross-frames prevented lateral movement of the top flanges and enabled transfer of the load into the full girder section without local buckling of the bottom flange, web buckling, or web crippling. The girder cross section and the cross-frame at one of the load points are presented in Figure 5.13.

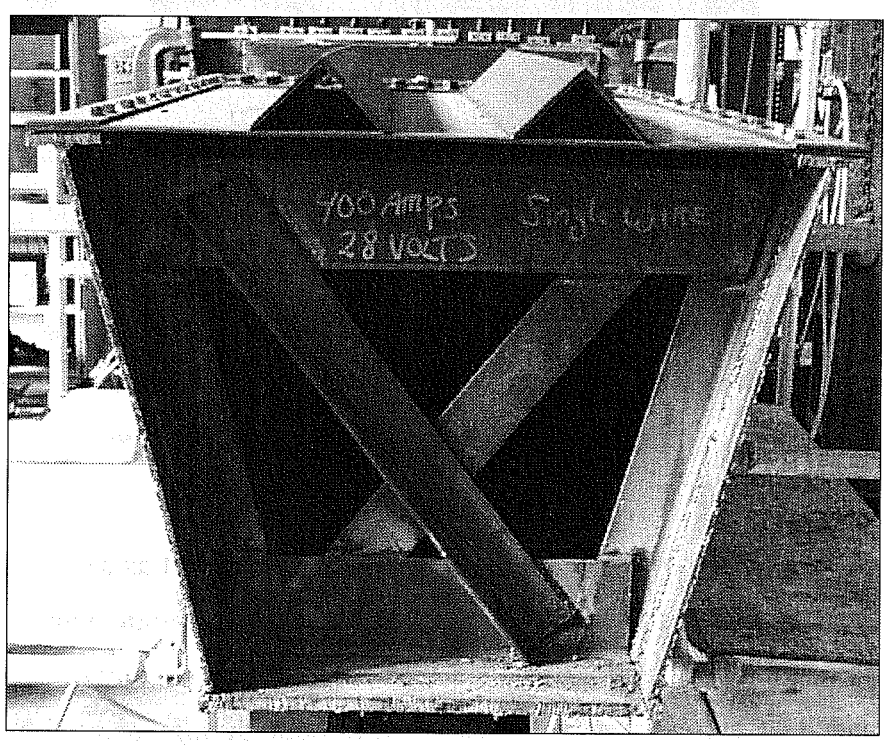

Figure 5.13 Girder Cross Section

Load was applied to the bottom flange of the box girder about 6 inches from the girder ends using hydraulic rams. Both rams were connected to a single air actuated hydraulic pump, shown in Figure 5.14, ensuring that equal loads were applied simultaneously at both load points. A roller bearing assembly was placed between the ram and the girder, as shown in Figure 5.15, so that only vertical loading was applied to the ends of the girder. A load cell was placed in series

with each ram to measure the applied load. Steel spacer plates were placed beneath the ram to ensure adequate ram stroke was available to apply the desired load.

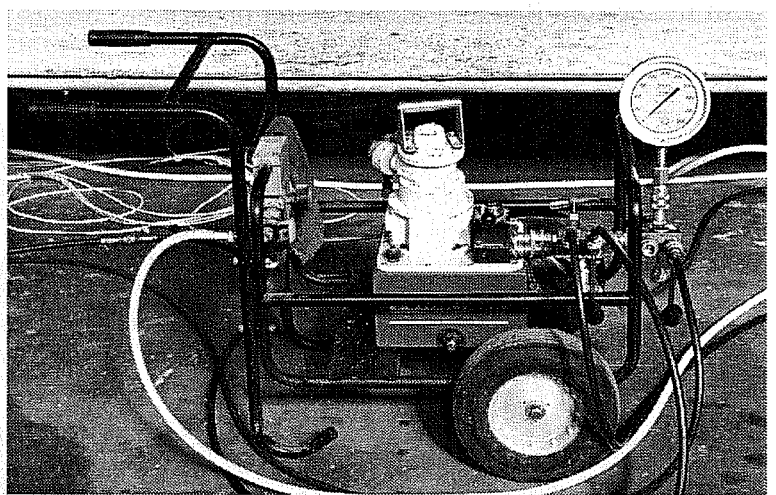

Figure 5.14 Air-Actuated Hydraulic Pump

Load was applied to the girder during the tests at as slow a rate as could reasonably be maintained using the air actuated hydraulic pump. Load was applied at a rate of approximately 5 kips per minute at each ram. The girder was unloaded at approximately the same rate, both during load cycling and final unload.

Each test plate was loaded and unloaded multiple times. The load was cycled during specific tests to examine the behavior of the plate at loads well beneath its buckling load and loads in the neighborhood of the plate's buckling load.

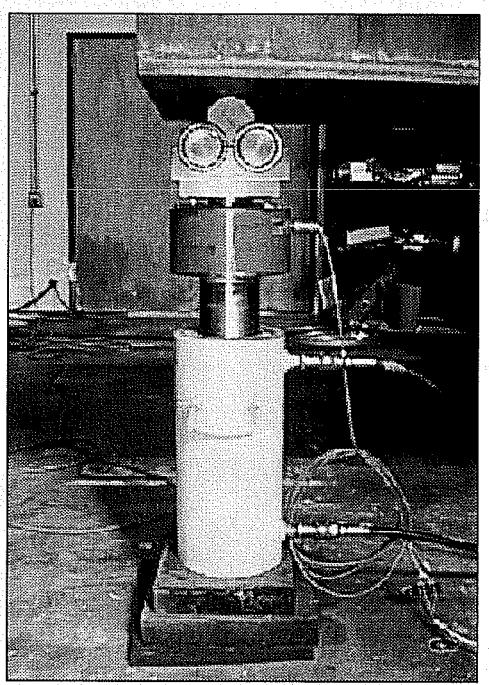

Figure 5.15 Ram, Load Cell, and Roller/Bearing Assembly (Chen 1999)

5.6 Instrumentation

5.6.1 Data Acquisition

During testing, deflections, strains, and loads were monitored using a computerized data acquisition system. The data acquisition system consisted of a Pentium class computer and a Hewlett Packard 3852A Data Acquisition/Control Unit shown in Figure 5.16. All strain gages were connected to the data acquisition system through Quarter Bridge Front End Boxes, or completion boxes, which are also shown in Figure 5.16. Each strain gage signal is connected independently to a Wheatstone bridge in a quarter-bridge arrangement within the completion boxes.

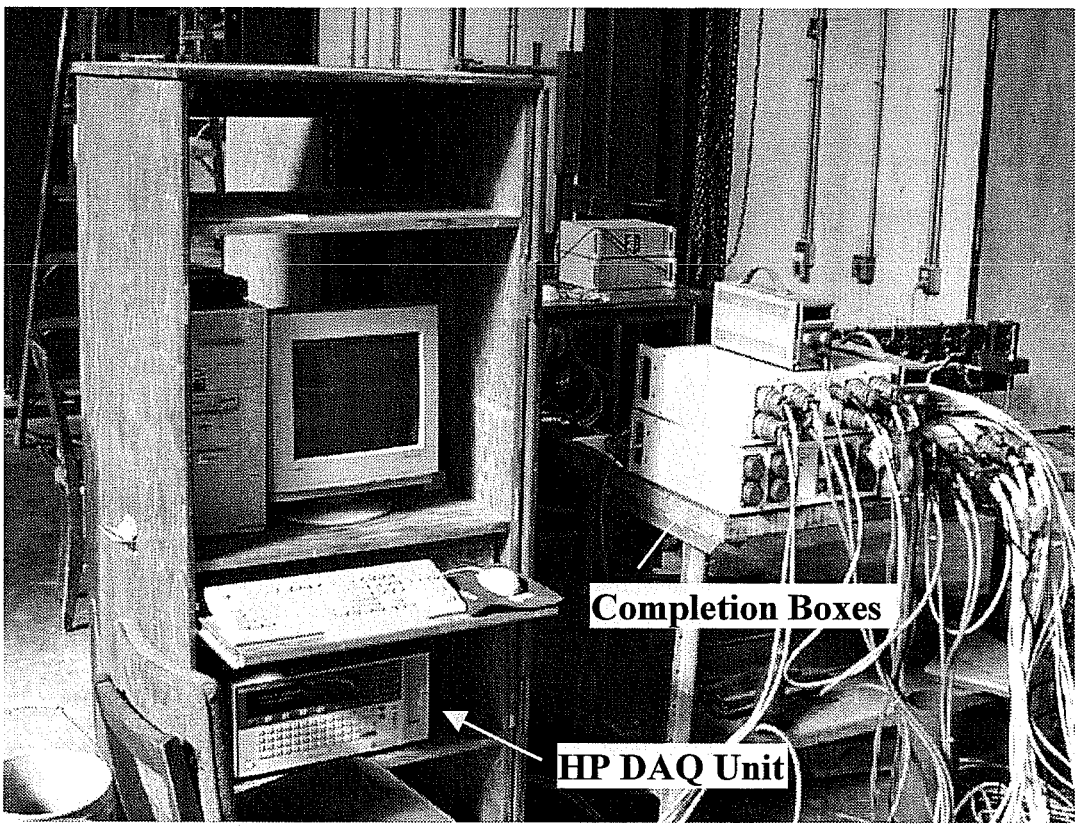

Figure 5.16 Data Acquisition System

The data acquisition control software used was a National Instruments product called Measure that is run as an add-in to Microsoft Excel. During girder loading and unloading, data was continuously collected from all instruments every 8 to 10 seconds.

5.6.2 Strain Measurement

Strains were measured in the test plate and each stiffener using electronic resistance strain gages. Gages were placed across the width and along the length of each test plate. Strain gages were also mounted to each longitudinal stiffener.

A large number of gages were installed on the first plates tested to investigate any strain variations across the width and along the length of each

plate. Gages were installed across the width of the plates to verify that the cross-section of the plate was under uniform compression. The strain gages were installed in the test region between the transverse stiffeners and edge plates on each test plate. The layout of gages on the first test plate, which was an unstiffened plate, is shown in Figure 5.17. Gages were installed on both sides of the plate in each location on each test plate.

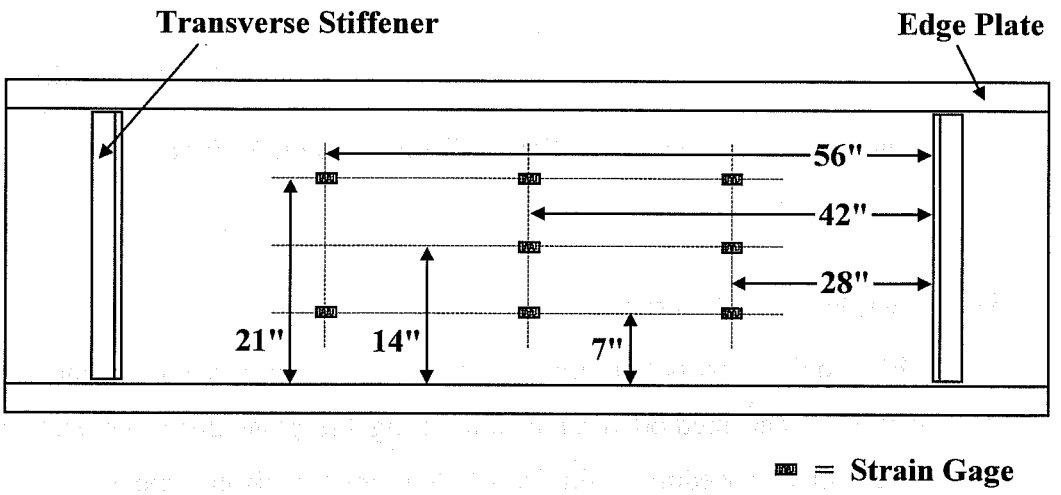

Figure 5.17 Layout of Strain Gages on Unstiffened Test Plate

Strain gages were installed in at least two locations along the length of each longitudinal stiffener. At each gage location, strain gages were attached to both sides of the stiffener. The placement of gages on each type of longitudinal stiffener tested is shown in Figure 5.18.

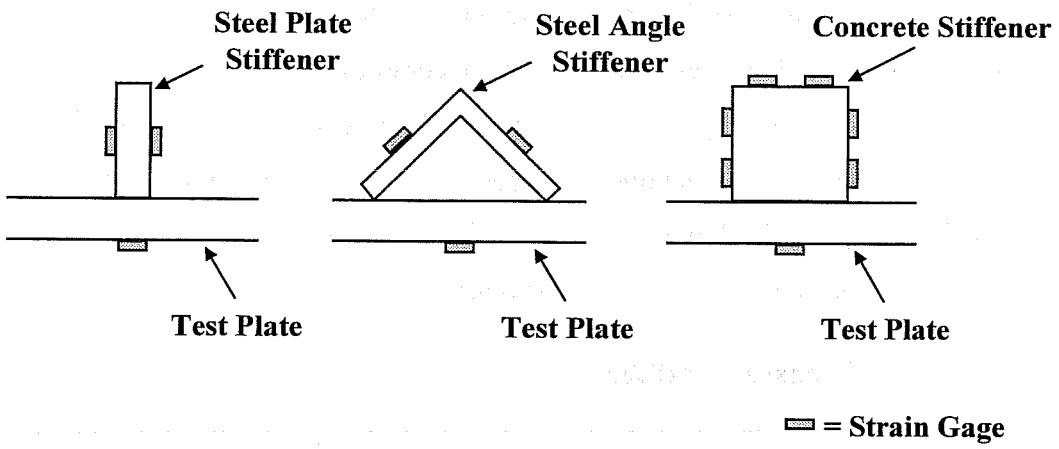

Figure 5.18 Placement of Strain Gages on Longitudinal Stiffeners

5.6.3 Displacement Measurement

Electronic linear potentiometers were used to measure the displacement of the test plate. The method used in measuring the plate displacement evolved during the testing procedure. Initially a Potentiometer Displacement Gage (PDG) was constructed to hold 11 linear potentiometers, as shown in Figure 5.19. This device was constructed from a straight length of 2x8 lumber. Channels were routed to accommodate the square body of the potentiometers. A small clamping plate was screwed into place across each potentiometer to hold it in place, as shown in Figure 5.20. This method of mounting held each potentiometer firmly in place on the PDG.

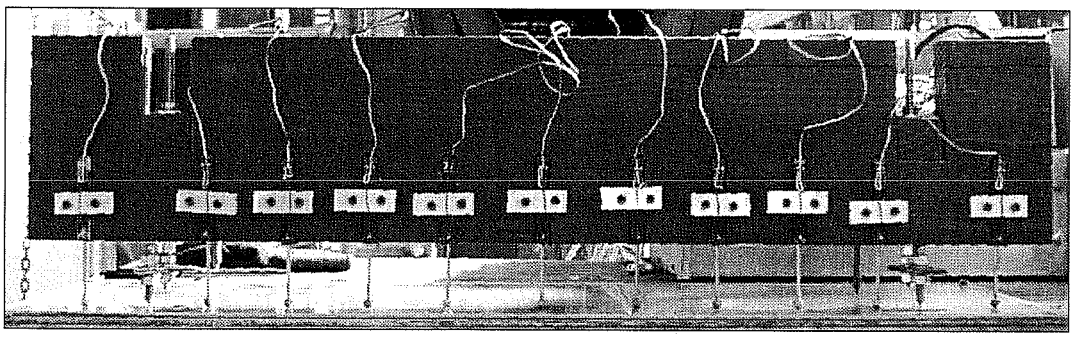

Figure 5.19 Potentiometer Displacement Gage (PDG)

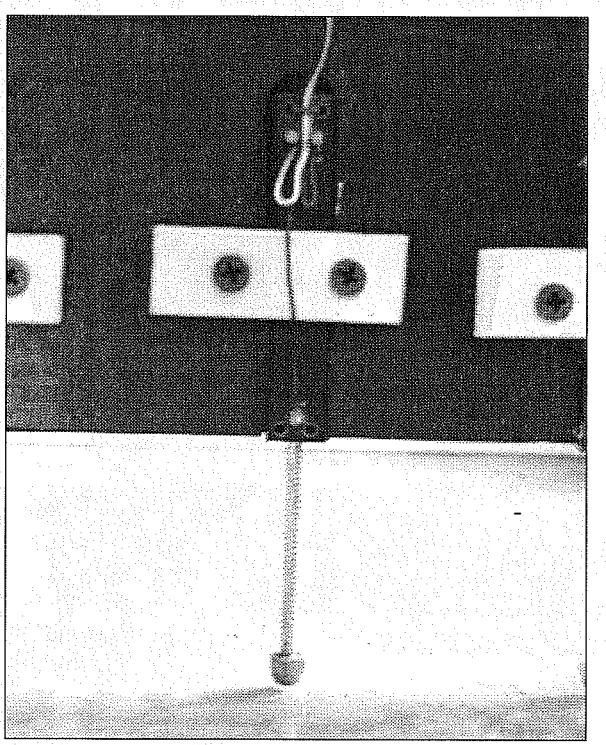

Figure 5.20 Potentiometer Mount in PDG

Prior to each use, the PDG was leveled, as shown in Figure 5.21. The PDG was leveled in both horizontal and vertical directions by adjusting the

threaded legs of the PDG. The initial readings of each potentiometer were then recorded while the PDG was seated on a flat glass plate. These initial readings were used to zero the potentiometer readings. The PDG was then used to measure the displacement of the plate at specified locations along the surface of the test plate. The PDG was used to scan the initial imperfection of the plate prior to each test. During the first tests, loading was stopped and the load was held at specified intervals while the PDG was used to scan the displaced shape of the plate. After testing, the PDG was used to scan the final shape of the plate.

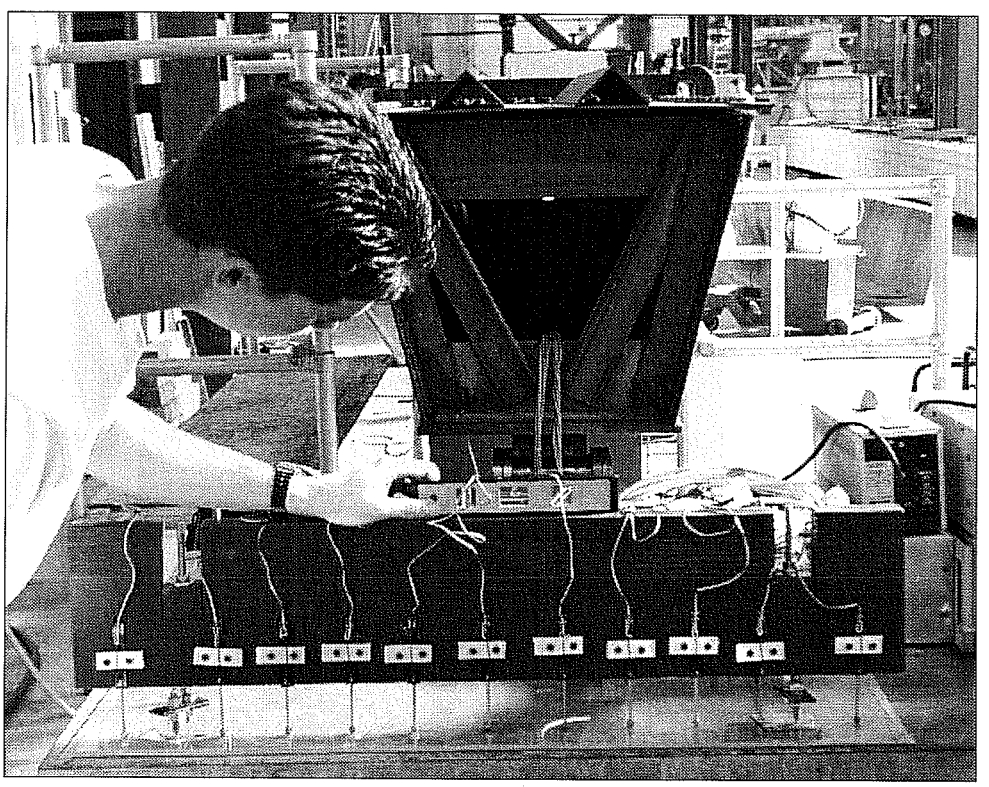

Figure 5.21 Leveling PDG Prior to Use

In early tests, a fixed potentiometer was also put in place to continuously monitor the displacement near the midpoint of the test plate during each test.

Another linear potentiometer was placed at midspan beneath the girder to measure overall girder deflection. Two electronic levels were also used in early tests to measure rotation of the top flanges at midspan of the box girder.

Use of the PDG resulted in an intricate testing procedure, since several people were required to assist in positioning the device and scanning the potentiometers during the test. Two people were required to position the device during testing as shown in Figure 5.22. The readings were sensitive to misplacement of the device, particularly if the legs of the PDG were not seated firmly against the plate. The placement of the PDG was checked carefully, and the PDG was leveled at each measurement point as shown in Figure 5.23.

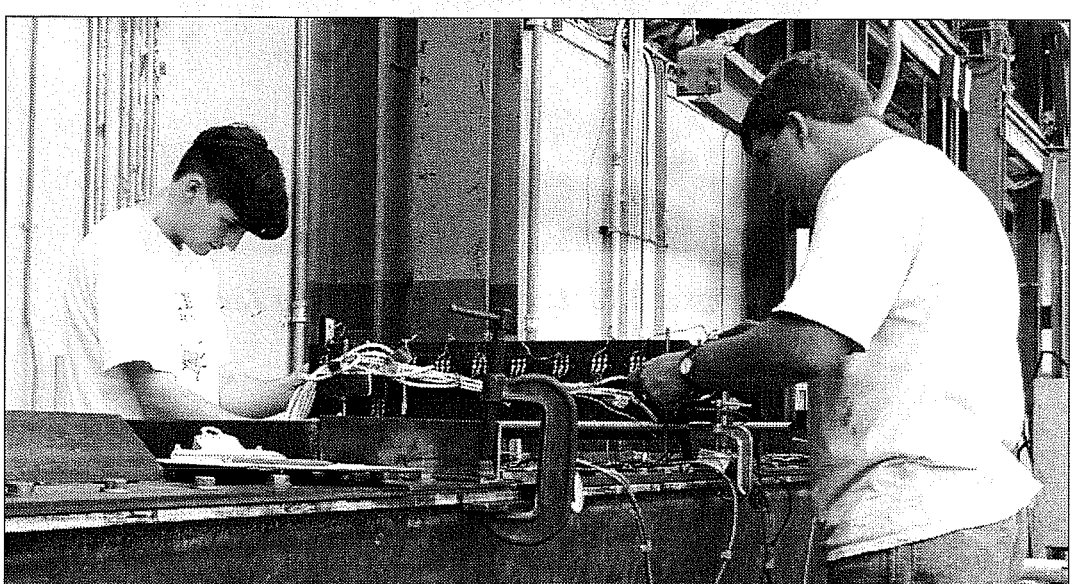

Figure 5.22 Positioning PDG During Test

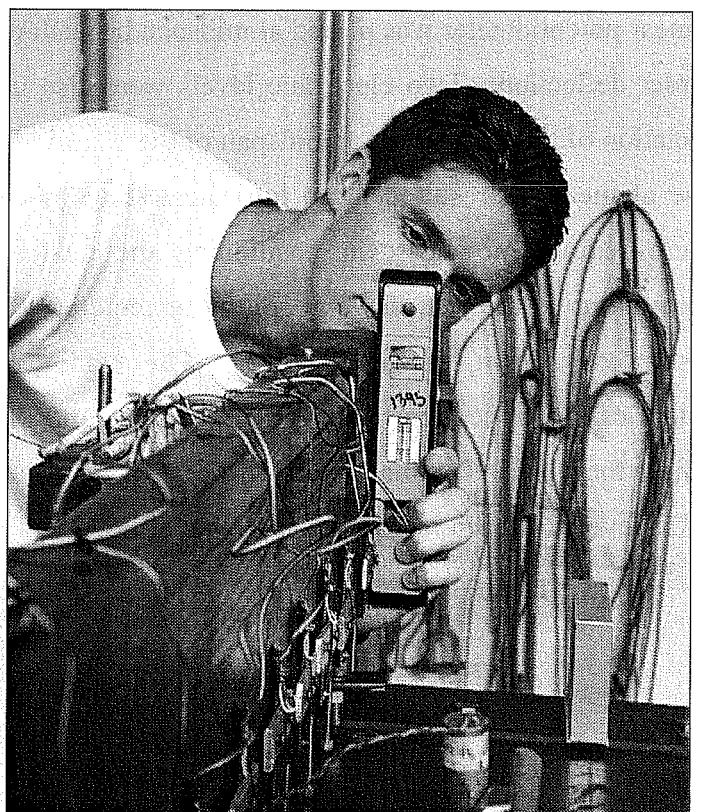

Figure 5.23 Leveling PDG During Test

It was not practical to conduct multiple passes to measure and confirm the displaced shape at each load point. During the first test, the load reduced significantly during the load hold portion of testing. Installation of new connectors on the rams aided the ability to hold the load, however there was still some load reduction over time, particularly at higher loads. Therefore due to the time and manpower needed for each pass of the PDG, and the fact that a certain load point could not be held precisely constant, only one pass of the PDG was made at each load hold. During the initial imperfection and final imperfection scans, the plate surface was scanned multiple times and the readings were averaged. This helped alleviate the impact of potential misplacement of the PDG.

The PDG device adequately served displacement measuring needs in the tests of the unstiffened plate and plates with small (inadequate) stiffeners. However as the size of the stiffener was increased, and the plate displacement consequently decreased, the PDG accuracy was not sufficient to measure the plate displacements. The PDG was still used in each test to measure both the initial imperfection prior to testing, and final imperfection after testing. However a new approach was used for measuring displacements during testing. The number and position of potentiometers in the PDG was adjusted to complement the new system used to measure displacements during the test.

An additional supply of linear potentiometers had become available in the testing laboratory, and by using this supply of potentiometers along with the potentiometers from the PDG, it was possible to continuously measure the displacement of the plate at 40 points on the plate surface, as shown in Figure 5.24. Two body styles of potentiometers were used in the new setup. The potentiometers with a square cross-section were installed on lengths of 2x4 in the same fashion used to mount them to the PDG. The potentiometers with a cylindrical body were mounted with clamps to lengths of 3/4 in. electrical conduit, as shown in Figure 5.25.

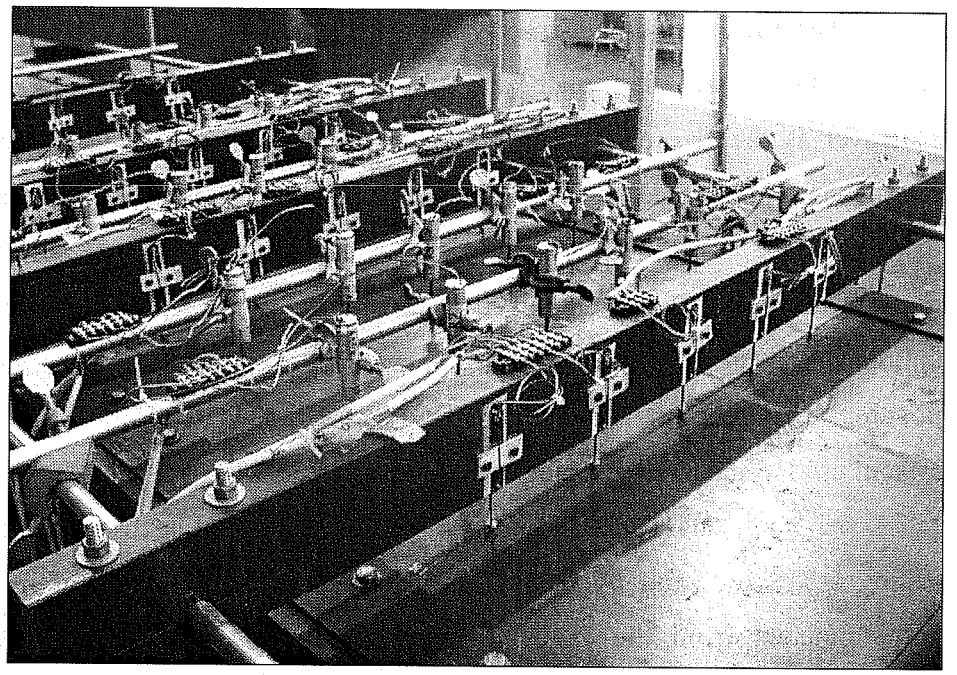

Figure 5.24 Fixed Potentiometer Displacement Frame

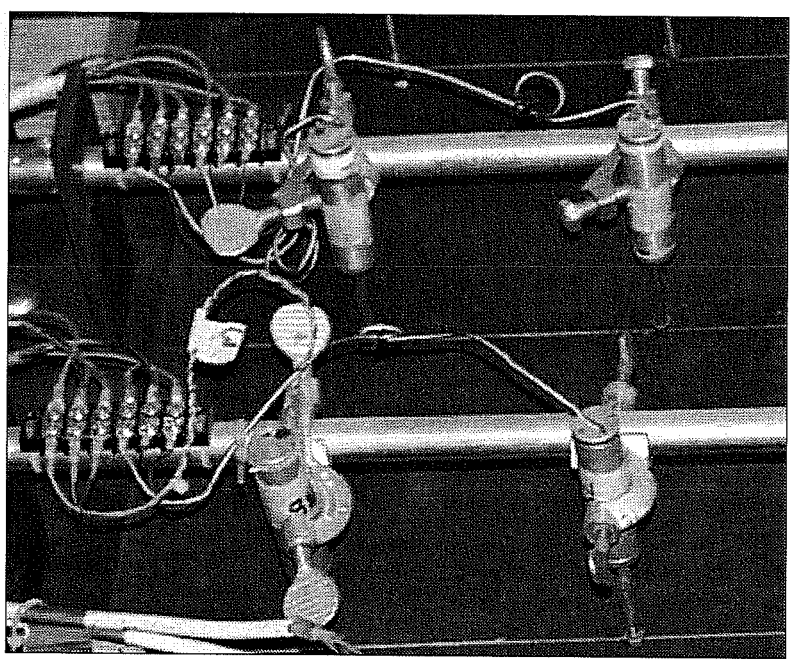

Figure 5.25 Mounting of Cylindrical Potentiometers

Both the conduits and 2x4 members to which the potentiometers were mounted were attached to a frame constructed of 3/4 in. electrical conduit. The legs of this framework were supported on sand bags. The amount of sand in the sand bag was varied to place the framework at the desired location relative to the girder. The framework in place over the box girder is shown in Figure 5.26. Seven string potentiometers were installed on the bottom of the girder to capture the overall deflection along the length of the girder. This testing setup was used for a single test, then the setup evolved to its final form as more potentiometers became available.

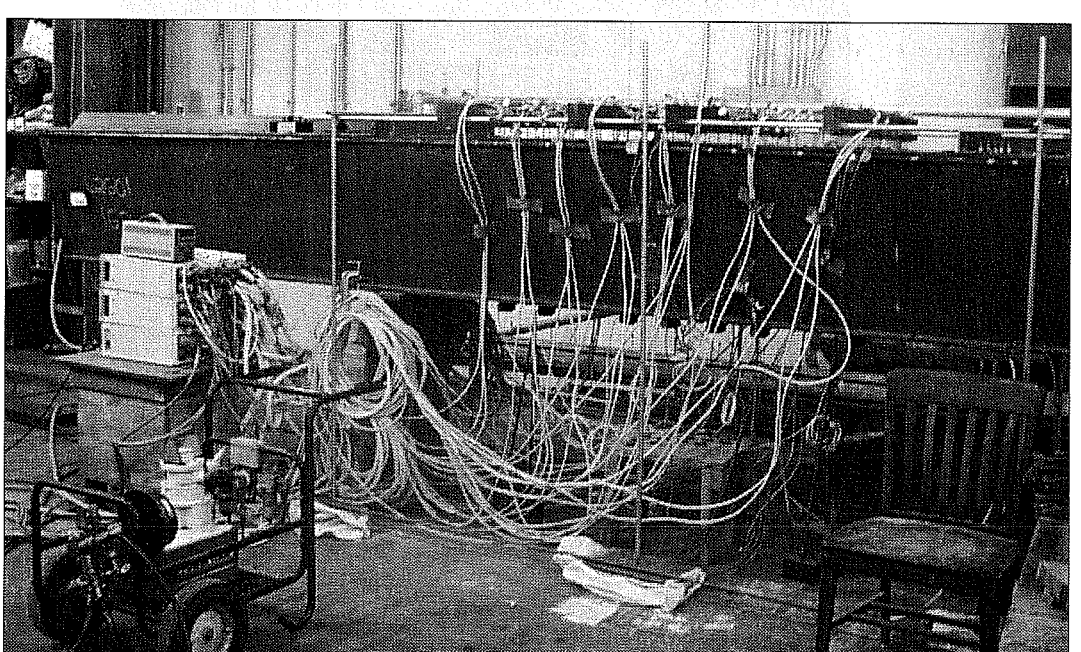

Figure 5.26 Fixed Potentiometer Displacement Frame

The final form of the test setup is pictured in Figure 5.27. When the stiffener was on the top surface of the plate, the middle longitudinal line of potentiometers were placed slightly off-center to avoid the longitudinal stiffener. For test plates without a stiffener on the top surface, the middle line of

potentiometers was placed along the centerline of the plate. This setup measures the plate displacement at 55 points on the plate's surface. Each cross member holding the potentiometers was attached directly to the box girder's top flanges using C-clamps and small bar clamps. With this setup the relative plate displacement was measured directly, and it was not necessary to subtract the overall girder deflection from the potentiometer readings.

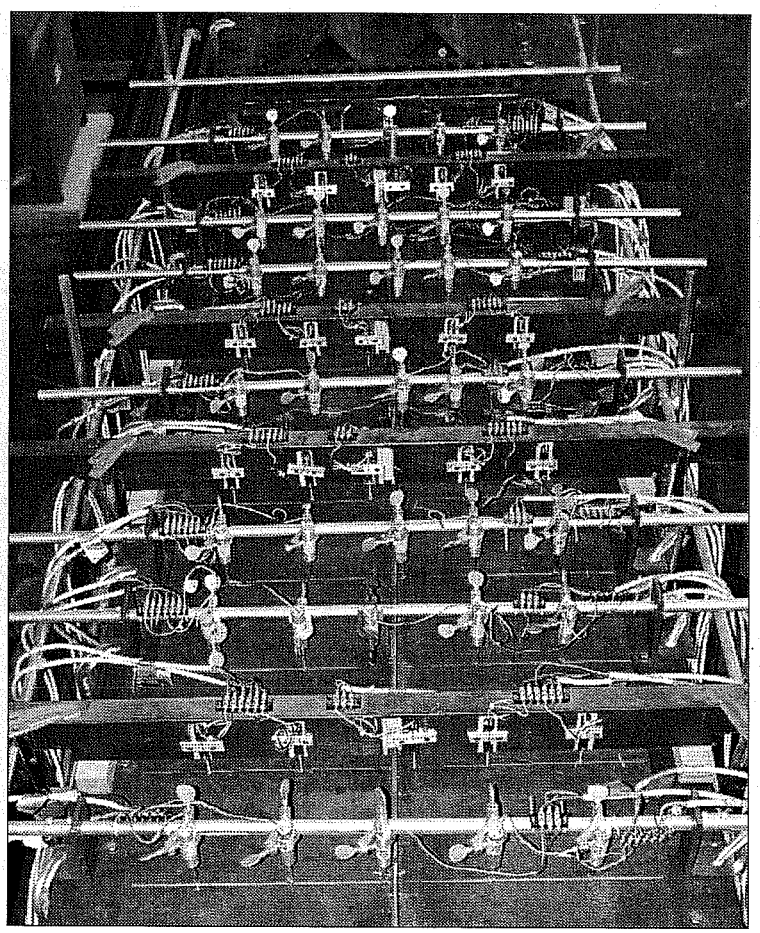

Figure 5.27 Potentiometer Setup Measuring Displacement at 55 Points

The cross members were modified slightly to accommodate the concrete stiffener in the last stiffened plate test. As shown in Figure 5.28, the centerline of

potentiometers was raised to clear the stiffener and ensure there was adequate stroke available to measure the displacements.

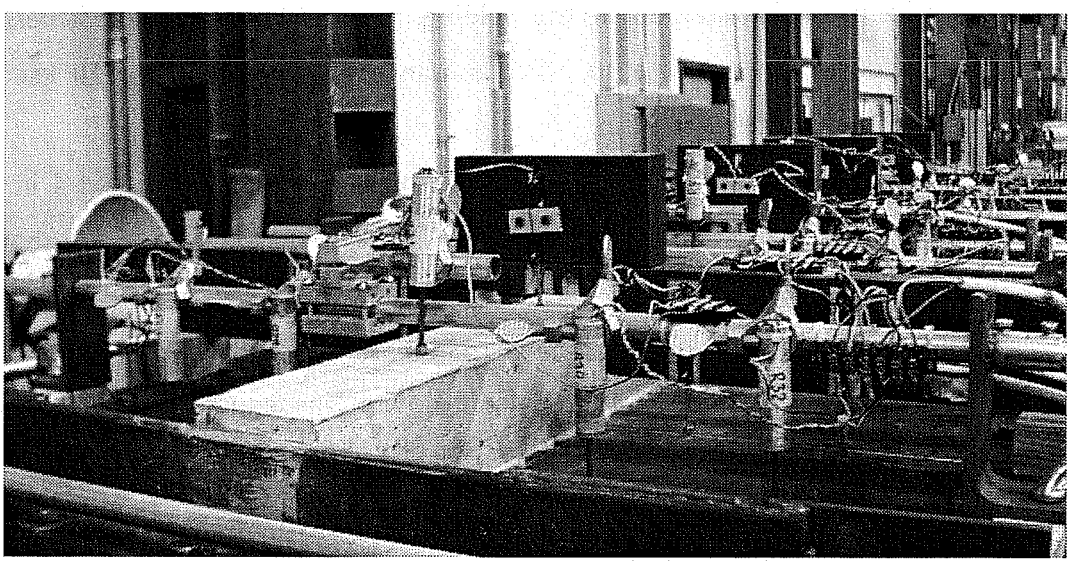

Figure 5.28 Displacement Measurement Setup for Concrete Stiffener Test

The frame initially constructed to hold the potentiometer cross members was still used in the final setup. The cross-members were not attached to this frame during testing, but the frame was used to move the entire setup out of the way to install a new test plate on the girder. Using this approach it was not necessary to detach the potentiometers and wiring, then reassemble the hookups for the next test.

5.7 Test Plate Configurations

Eight different plate configurations were tested in this study. The first test conducted was on an unstiffened plate, which will be referenced as the "unstiffened" test. Each test plate was constructed of 3/16 in. thick steel with a specified minimum yield strength of 70 ksi.

All steel longitudinal stiffeners were welded to the test plates using 3 in. long 3/16 in. intermittent staggered welds. Intermittent welds were used to minimize plate distortion due to the welding. All steel longitudinal stiffeners were constructed of steel with a specified minimum yield strength of 50 ksi. The length of each stiffener is 84 in.

The first stiffened test plate had a small longitudinal 1 in. x 1/4 in. plate stiffener welded to one side of the plate. The stiffener and plate are shown in Figure 5.29. The test plate was initially installed on the box girder with the stiffener side up. This test is referenced as the "inadequate up" test. The test plate was also studied with the stiffener side down, "inadequate down," where the stiffener was enclosed inside the box. The stiffener "up" and stiffener "down" configurations are shown in Figure 5.30.

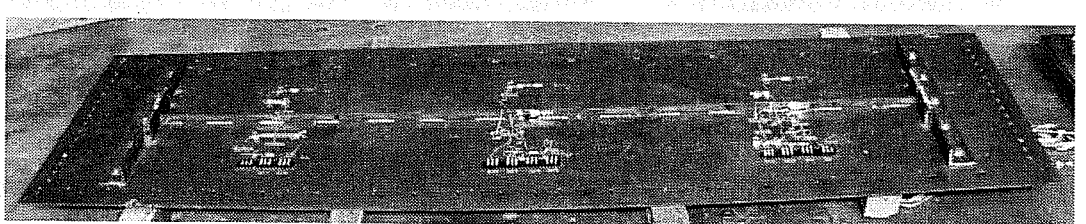

Figure 5.29 Plate with Inadequate Stiffener

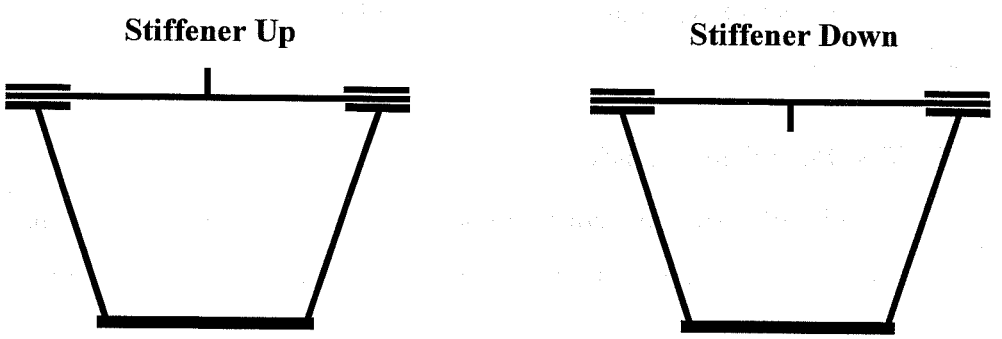

Figure 5.30 Stiffener "Up" vs. Stiffener "Down"

Transverse rotation at the ends of the longitudinal stiffener was restrained as shown in Figure 5.31. Two plates were butted against the longitudinal stiffener and welded to the transverse stiffener. Transverse rotation at the ends of the longitudinal stiffener was restrained to model the restraint provided by the continuity of longitudinal stiffeners and transverse cross-frames in actual bridge girders. Transverse rotation was restrained in the same fashion at the ends of each steel stiffener tested in this study.

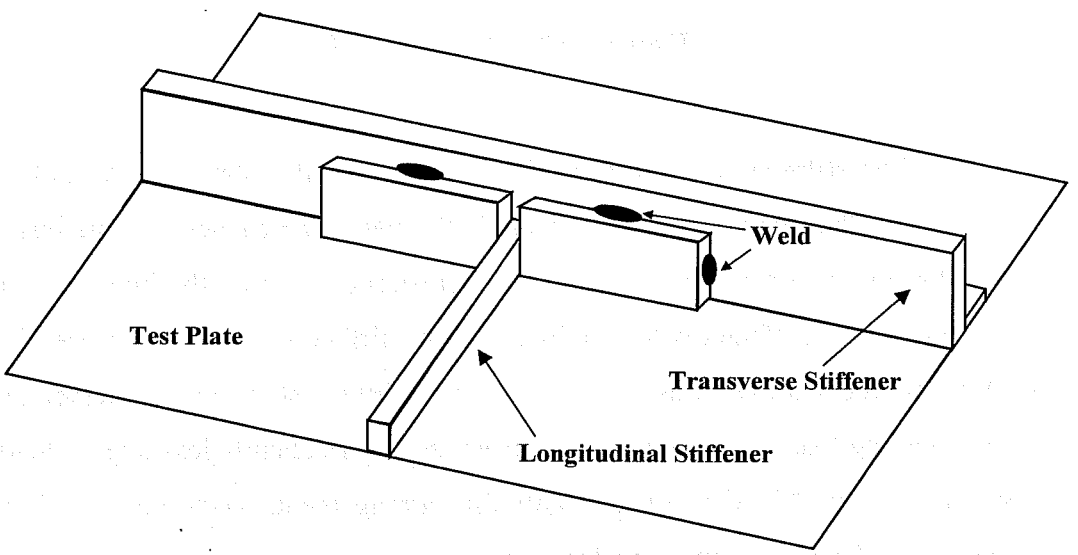

Figure 5.31 Rotational Restraint at Ends of Longitudinal Stiffener

The second stiffened test plate had a longitudinal 2 1/2 in. x 1/4 in. plate stiffener welded to one side of the plate. This stiffener was welded off-center of the steel plate, as shown in Figure 5.32. The test plate was installed with the stiffener down. The stiffener was sized to be larger than the adequate stiffener size required by AASHTO to cause plate buckling about the stiffener, permitting use of a plate buckling coefficient of 4. This test case is labeled the "adequate off-center" test.

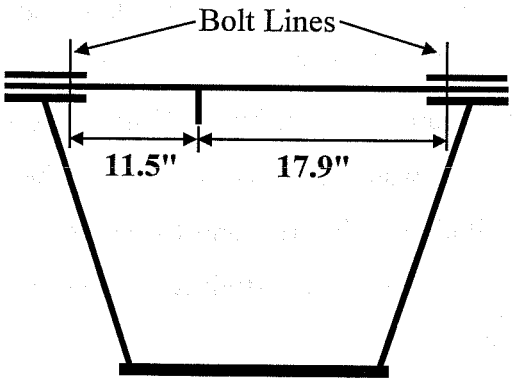

Figure 5.32 Off-Center Stiffener

The stiffener was welded off-center so that the plate would buckle at a lower load than with a centrally located stiffener. The capacity of the test setup was limited, and it was not possible to significantly surpass the buckling load of the test plates stiffened with rotationally stiff stiffeners that are discussed below. One option considered was to test each plate with the stiffeners off-center, so that the buckling load of the plate was reduced, and consequently less overall load was required to buckle the plate. With this arrangement, loads that significantly surpassed the plate's buckling load could be applied. However, use of the off-center stiffener added additional complexity to the buckling behavior of the plate and consequently complicated analysis of the results. After completion of the adequate off-center test it was decided that the rest of the plates would be tested with centrally located longitudinal stiffeners.

The next stiffened plate had a 2 1/4 in. x 1/4 in. plate stiffener welded down the middle of the length of the test plate, as shown in Figure 5.33. The test plate was installed with the stiffener down. The stiffener was sized to be larger than the adequate stiffener size required by AASHTO to cause plate buckling about the stiffener, permitting use of a plate buckling coefficient of 4. This test is

labeled the "adequate" stiffener test. After conducting the adequate stiffener test, an additional 1 in. x 1/4 in. plate stiffener was welded to the top of the plate, as shown in Figure 5.34. This configuration is referenced as the "double" stiffener test.

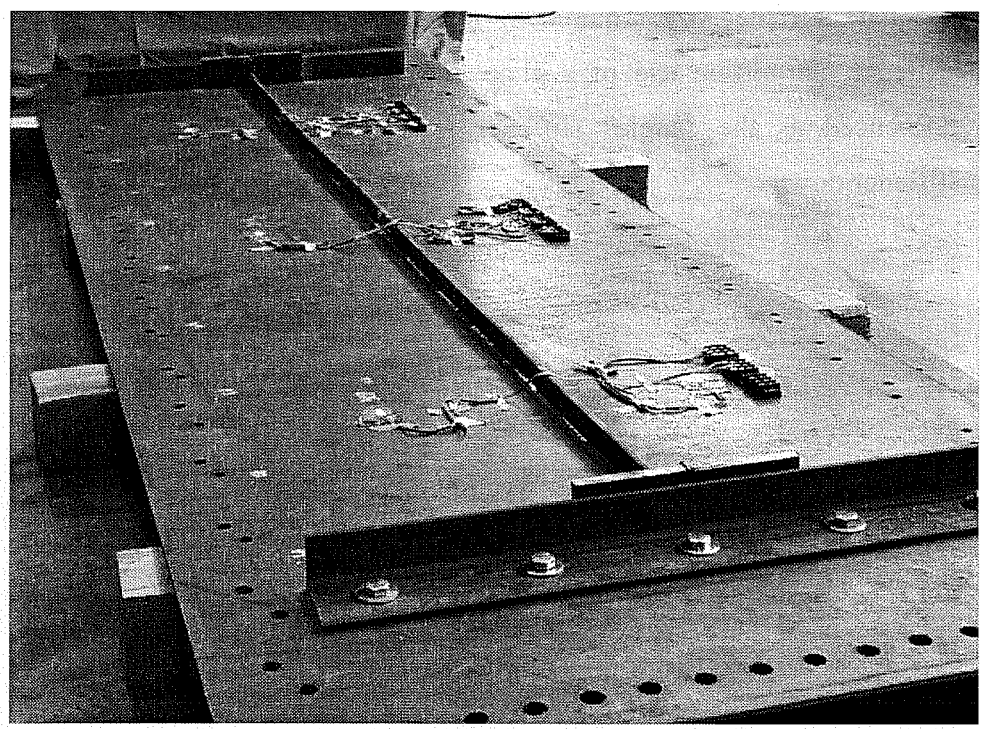

Figure 5.33 Plate with Adequate Stiffener

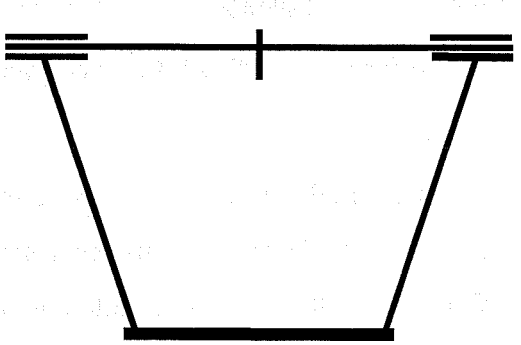

Figure 5.34 Stiffener on Top and Bottom in "Double" Plate Test

The next test plate had a 2 1/2×2 1/2×3/16 angle longitudinal stiffener, as shown in Figure 5.35. Each leg of the angle was welded to the plate using 3 in. long 3/16 in. intermittent staggered welds. A 3 in. spacing was used between each of the intermittent welds. The stiffener was sized to be larger than the adequate stiffener size required by AASHTO to cause plate buckling about the stiffener, permitting use of a plate buckling coefficient of 4. The test plate, referenced as the "angle" stiffener test, was installed with the longitudinal stiffener down.

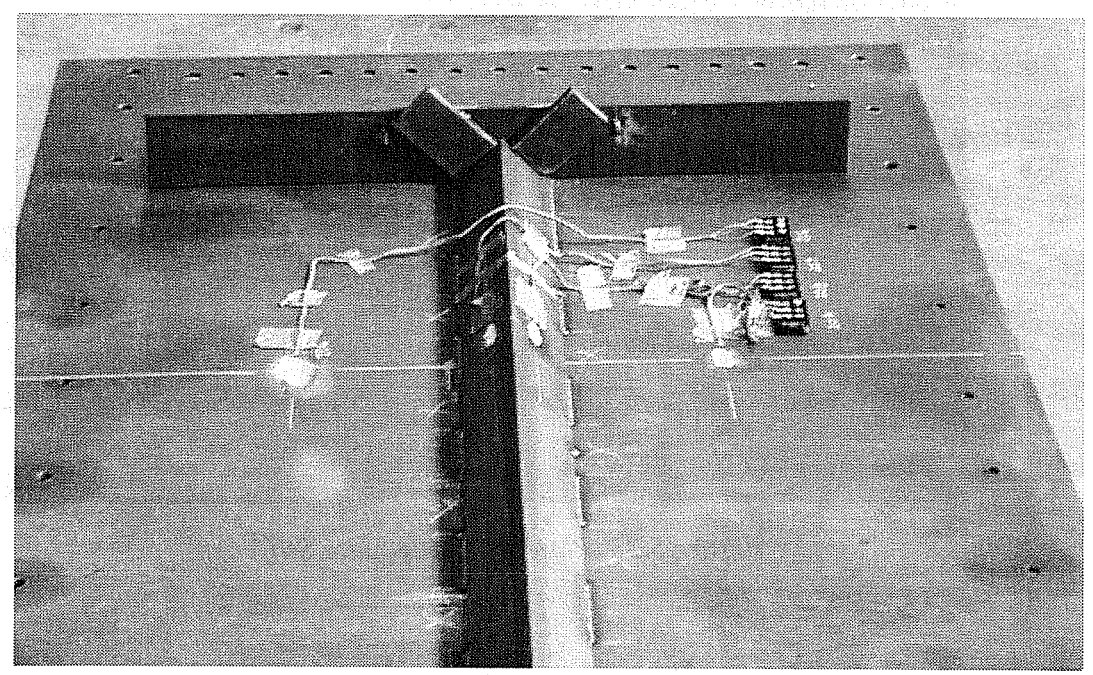

Figure 5.35 Steel Angle Stiffener

The final test plate used a cast-in-place concrete stiffener. The stiffener was sized to be larger than the "adequate" stiffener size causing buckling of the plate about the stiffener, permitting use of a plate buckling coefficient of 4. This test is referenced as the "concrete" stiffener test. A report on tests of small-scale

reinforced concrete members conducted at the University of Illinois and two former graduate students involved with similar studies were consulted for assistance in designing the concrete mix and reinforcement layout for the concrete stiffener (Gilbertsen 1980). The concrete stiffener reinforcement layout and dimensions are shown in Figure 5.36. The pitch of the rectangular spirals used for transverse reinforcement is shown in Figure 5.37. Both the longitudinal and transverse reinforcement were mechanically cleaned prior to use. The longitudinal reinforcement was cleaned using a wire wheel. The transverse reinforcement was sandblasted, both to clean it and roughen its surface. The transverse reinforcement consisted of No. 12 gage wire (0.08 in. diameter) formed into rectangular spirals. The surface of the wire was deformed using a welder's hammer prior to construction of the spirals, to help ensure bond developed between the concrete and reinforcement.

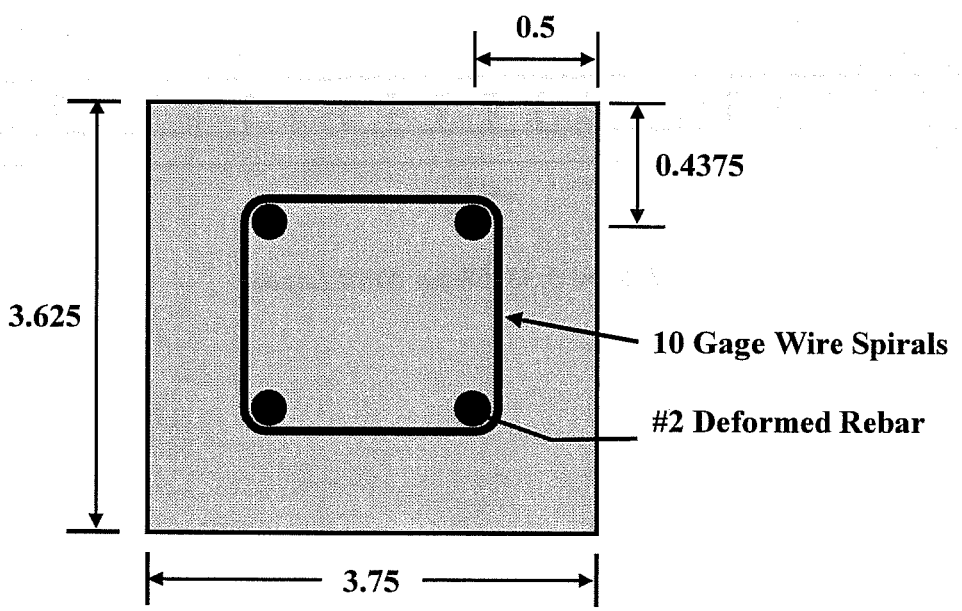

Figure 5.36 Concrete Stiffener Reinforcement and Measured Dimensions

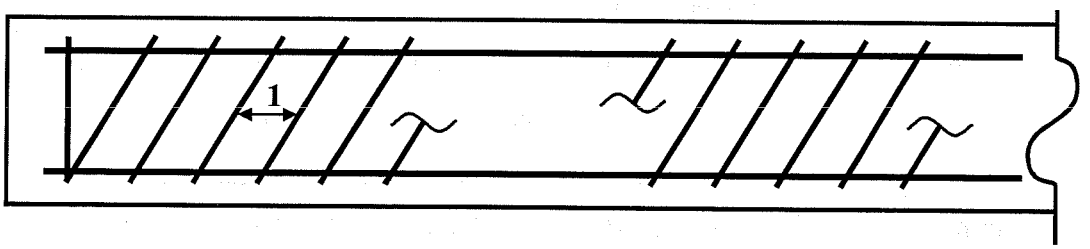

Figure 5.37 Concrete Stiffener Plan View

Shear studs were used to ensure composite action was developed between the steel plate and concrete stiffener. The shear studs consisted of 1/4 in. diameter bolts welded to the test plate. The bolts were welded to the plate at the spacing shown in Figure 5.38. A picture of the concrete reinforcing cage, blocked up using wood 2x4 pieces, and the shear studs is shown in Figure 5.39.

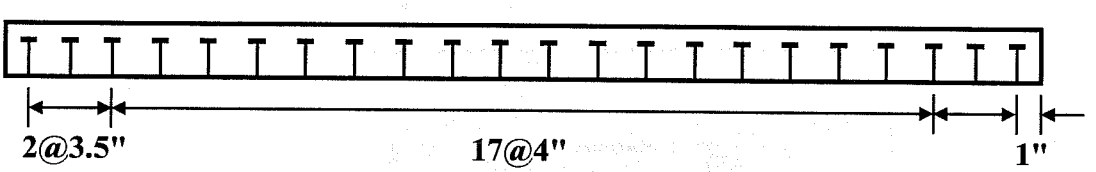

Figure 5.38 Shear Stud Layout

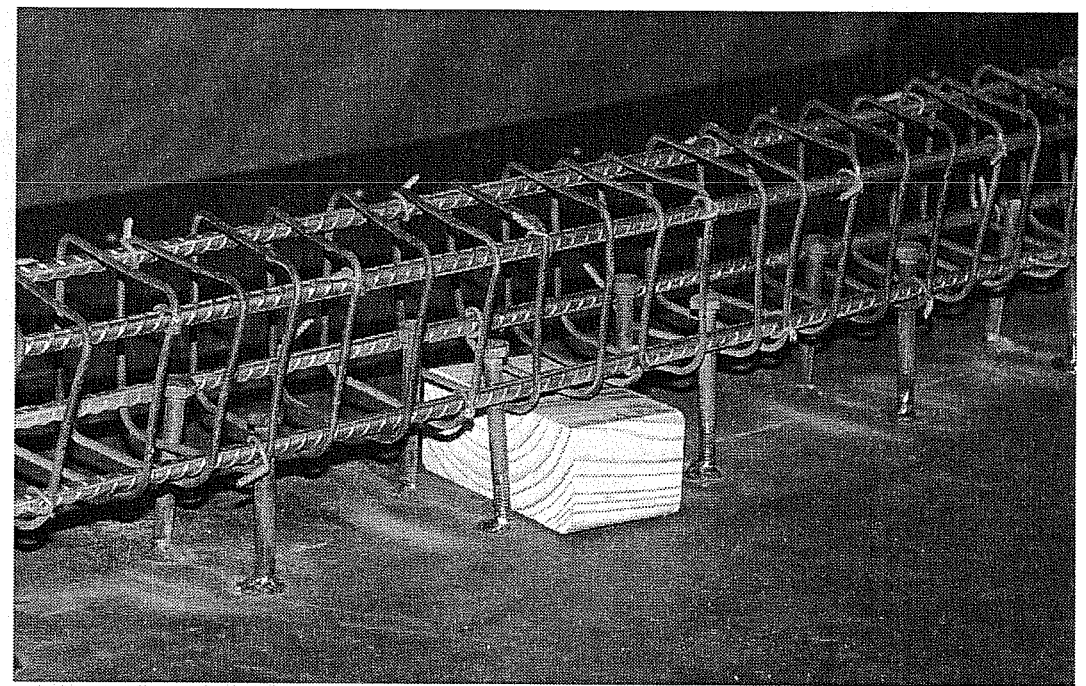

Figure 5.39 Concrete Reinforcing Cage and Shear Studs

The concrete used in the specimen was a small aggregate mix consisting of Type III cement, 3/8 in. pea gravel aggregate, and sand. The mix proportions by dry weight were 1.5:2.2:1.0 (coarse:fine:cement) with a water cement ratio of 0.53. The concrete stiffener was cast-in-place with the test plate already bolted to the trapezoidal box girder. The stiffener was cast on top of the box girder to make sure that the concrete stiffener was not cracked during installation of the test plate. The formwork for the concrete stiffener was provided by two 2x4 members along the sides of the stiffener, and the transverse stiffeners at the ends of the stiffener, as shown in Figure 5.40.

Figure 5.40 Concrete Stiffener Formwork

The concrete stiffener was consolidated using external mechanical vibration and was also rodded by hand. The concrete stiffener prior to removal of the formwork is shown in Figure 5.41. The concrete stiffener immediately prior to testing is shown in Figure 5.42. The stiffener and control specimens were cured under wet burlap and plastic for two weeks. The plate stiffened with the concrete stiffener was tested over a two-day period beginning 14 days after casting. The concrete strength and age at testing are presented in Table 5.1.

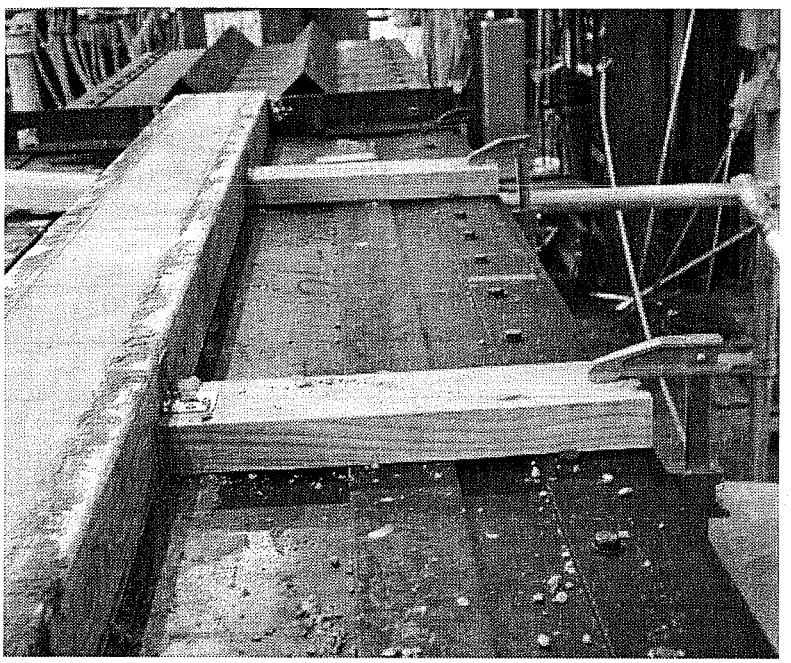

Figure 5.41 Concrete Stiffener After Casting

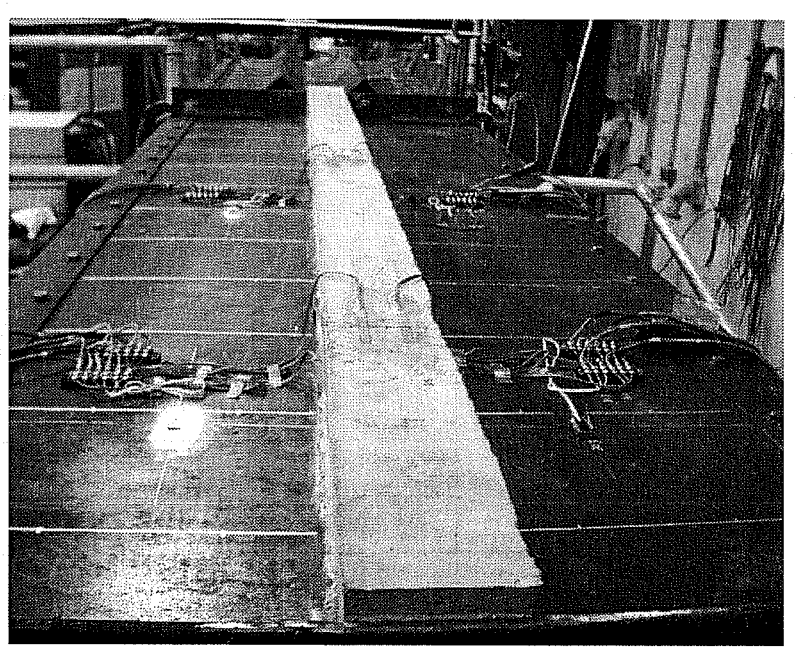

Figure 5.42 Concrete Stiffener

Table 5.1 Measured Concrete Properties

Age at Testing (days)	Compressive Strength (psi)	Splitting Tensile Strength (psi)	Modulus of Rupture (psi)	Modulus of Elasticity (psi)
9	6,060	-	-	-
15	6,180	510	330	3,950,000
30	6,290	500	520	-

5.8 Measured Test Plate and Steel Stiffener Properties

Coupons were cut from each test plate and steel stiffener. The measured static yield strength, σ_{ys}, ultimate tensile strength, σ_u, and percent elongation for each test plate are presented in Table 5.2. The same properties for each steel stiffener are presented in Table 5.3. Material that was supposedly Grade 70 was used for the test plates. However the yield strength of every test plate was substantially lower than 70 ksi. Based on the coupon tests, the plate material was not actually Grade 70 material, even though it was sold as such.

Table 5.2 Test Plate Properties

Test Plate	**σ_{ys} (ksi)**	**σ_u (ksi)**	**% Elongation**
Unstiffened and Inadequate	52.4	74.2	22
Adequate Off-Center	49.6	72.7	23
Adequate / Double	56.0	79.4	22
Angle	54.8	79.9	25
Concrete	50.6	72.5	24

Table 5.3 Steel Stiffener Properties

Stiffener	σ_{ys} (ksi)	σ_u (ksi)	% Elongation
Inadequate	58.1	79.2	26
Adequate Off-Center	51.8	75.7	24
Adequate	51.7	76.0	26
Double - Second Stiffener	58.1	78.7	25
Angle	58.3	82.5	24

The plate thickness, plate slenderness, and stiffener cross-sectional properties for each test plate are summarized in Table 5.4. The slenderness of the test plate reported in the table is w/t, where w is the stiffener spacing and t is the plate thickness. For the unstiffened test plate, w is the plate width between the bolt lines. For the stiffened test plates, w is the distance between the centerline of the stiffener and a bolt line. The results from the experimental program are presented in Chapter 6 and an analysis of the results is presented in Chapter 7.

Table 5.4 Test Plate and Stiffener Dimensions

Test Plate	Plate Thickness (in)	Plate w/t	Stiffener Properties		
			Width (in)	Depth (in)	I_s (in^4)
Unstiffened	0.1901	153	N/A	N/A	N/A
Inadequate Up/Down	0.2010	72	0.268	1.06	0.106
Adequate Off-Center	0.2015	72	0.267	2.43	1.29
Adequate	0.1913	76	0.267	2.52	1.44
Double	0.1913	76	0.271	1.24	1.61
Angle	0.2018	72	0.199	1.78	0.989
Concrete	0.1901	76	3.75	3.625	14.9

Chapter 6

Test Results

6.1 Eigenvalue Analysis of Test Setup

The eigenvalue buckling loads of the test plates will be referenced in the following discussion of test results. The eigenvalue analysis of the test setup is therefore discussed in this section prior to the presentation of test results. The experimental program and test setup were described in Chapter 5. A finite element model of the scale box girder and test plates used in the study was constructed, as shown in Figure 6.1. The girder, test plate, and supports were modeled using shell elements. Displacements were restrained at the base of each of the girder supports. Load was applied to the finite element model at the ends of the girder.

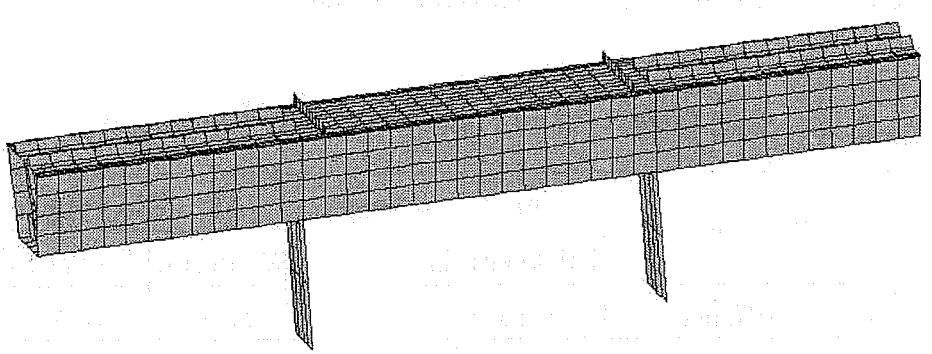

Figure 6.1 Finite Element Model of Test Setup

The finite element model was fine-tuned based on results obtained in the test of an unstiffened plate. The buckling load of the test plate was very sensitive to how the connection detail between the test plates and the top flanges of the girder was modeled. Both the method of attaching the test plate to the top flanges

of the box girder and the location of the connected nodes significantly influenced the eigenvalue buckling load. The buckling load was increased when the rotation at the edges of the test plate was constrained in the finite element model.

In the final form of the finite element model, the compression plate nodes were attached to the nodes of the top flanges using the ABAQUS "pin" multi-point constraint. The pin constraint makes the displacements of the attached nodes equal, but leaves the rotations independent of each other. The nodes of the test plate were attached to the top flanges on each edge of the test plate; at the same transverse location where the real test plate was bolted to the box girder setup. The width of the plate between the bolts was 29 in.

6.1.1 Up vs. Down Stiffener Configuration

A plate with a small stiffener was tested both with the stiffener up, on the top of the test plate, and the stiffener down, on the bottom of the test plate. The same stiffened plate was used in both of these tests. Through finite element analysis it was discovered that the buckling load with the stiffener down was about 6% greater than the buckling load with the stiffener up. The plate was tested with the stiffener both up and down to investigate this difference in capacity.

Since the steel flange of the box girder is actually a component of a girder in bending, there is a stress variation through the depth of the stiffener. With the stiffener on the top of the test plate, the stiffener is outside the box girder section and carries higher stresses than the test plate. When the stiffener is on the bottom of the test plate and is contained within the box girder the test plate stresses were higher than those in the stiffener. This difference in the stiffener stress appeared to be the reason for the difference in the buckling load of the plate with the stiffener up vs. down. The test plate with the small stiffener was tested both with

the stiffener up and the stiffener down to experimentally investigate the impact of the stiffener orientation on the capacity of the plate. The effect of stiffener orientation will be discussed further in Chapters 7 and 8.

6.1.2 Eigenvalue-Buckling Loads

The eigenvalue-buckling load with each of the test plates was computed. The loads from both the finite element analysis and the experimental program are the jack loads, P, shown in Figure 6.2. The eigenvalue buckling load, P_{cr}, is the value of P shown in Figure 6.2 that resulted in buckling of the compression test plate. For the test of the girder with the unstiffened plate mounted to the top flange the I_x is 3828 in^4 and the distance from the neutral axis of the cross-section to the centerline of the test plate is 13.10 in. The load was applied 66 in. from the support in this test. The compressive stress, σ_{pl}, in the plate is therefore:

$$\sigma_{pl} = \frac{My}{I} = \frac{66"(P) \times (13.10")}{3828\,in^4} = 0.225P \qquad (6.1)$$

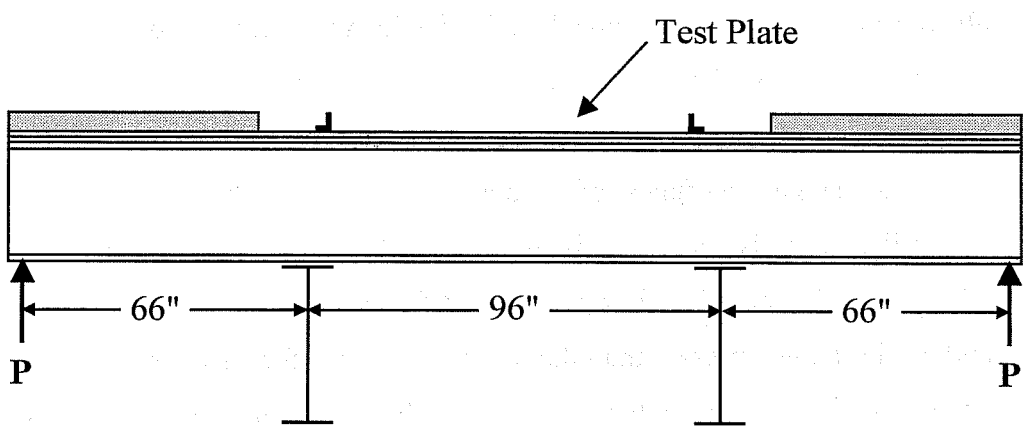

Figure 6.2 Loading of Test Setup

Eight different plate configurations were tested, as discussed in Chapter 5. The first mode buckling shapes of the test plates are presented alongside the

displaced shapes measured in the experimental tests in the following sections. The eigenvalue buckling loads for each test plate are presented in Table 6.1. The unstiffened test plate had the smallest buckling load of 19.2 kips. The buckling load for the plate with small, "inadequate," stiffeners, was 2.3 to 2.5 times that of the unstiffened plate. With an adequate stiffener, the buckling load was about 4.4 times that of the unstiffened plate. The plate with the angle stiffener had a buckling load of 1.45 times that of the adequate plate. The test plate with the concrete stiffener had the largest predicted buckling load, with a capacity of 1.54 times that of the adequate plate.

Table 6.1 Eigenvalue Buckling Load

Test Plate	P_{cr} (kips)
Unstiffened	19.2
Inadequate Up	45.0
Inadequate Down	47.9
Adequate Off-Center	60.1
Adequate	84.3
Double	90.7
Angle	122
Concrete	130

Each of the plates was installed on the box girder and tested. The initial imperfection of each test plate prior to testing was measured. Displacement, load, and strain data were collected during each test. The experimental results are presented in the following sections.

6.2 Compression Plate Tests

Eight compression plate configurations were tested. The plate configurations and their respective labels are repeated in Table 6.2. The definition of stiffener orientation is shown in Figure 6.3.

Table 6.2 Test Plate Configurations

Test	Stiffener Nominal Dimensions	Stiffener Orientation
Unstiffened	N/A	N/A
Inadequate Up	1 in. x 1/4 in. steel plate	Up
Inadequate Down	1 in. x 1/4 in. steel plate	Down
Adequate Off-Center	2 1/2 in. x 1/4 in. steel plate	Down
Adequate	2 1/4 in. x 1/4 in. steel plate	Down
Double	2 1/2 in. x 1/4 in. steel plate down 1 in. x 1/4 in. steel plate up	Up and Down
Angle	3×3×3/8 steel angle	Down
Concrete	3 3/4 in. x 3 5/8 in. concrete	Up

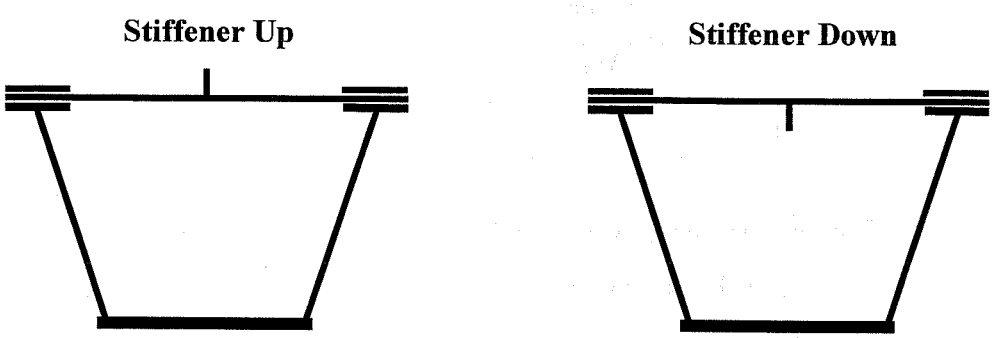

Figure 6.3 Stiffener "Up" vs. Stiffener "Down"

6.3 Stiffener Moment of Inertia

Table 6.3 contains the moment of inertia about the base of the stiffener, I_s, and the modulus of elasticity of the stiffener times I_s for each of the test plates. The table also normalizes E times I_s of each stiffener by the AASHTO LRFD requirements for an "adequate" stiffener. The AASHTO LRFD requirement for an adequate stiffener is the required stiffener size that is large enough to force a nodal line along the stiffener. The plate buckles about the stiffener, which results in a plate buckling of coefficient of 4 in the capacity equations. All test plates except the inadequate test plate had stiffeners that were significantly larger than the AASHTO "adequate" requirement. A combination of ordering plate sizes slightly larger than needed for the plate stiffeners, and then receiving delivery of even larger plate sections, resulted in a larger I_s for the adequate and adequate off-center stiffeners. The moment of inertia in the double test was purposely increased. A larger I_s than that required based on AASHTO was specified for the concrete stiffener based on finite element results. The constructed concrete stiffener was also slightly over desired size due to form shifting during casting of the stiffener.

The concrete stiffener had the largest EI_s value of all the stiffeners. The smallest moment of inertia by far was provided by the inadequate stiffener. The inadequate stiffener was expected to buckle with the test plate. The next smallest moment of inertia was provided by the angle stiffener. The table also contains the eigenvalue buckling load from the finite element analysis of the box girder and test plate. The load is the applied ram load that caused buckling of the test plate in the eigenvalue analyses.

Table 6.3 Stiffener Properties

Test Plate	I_s (in^4)	EI_s ($lb \cdot in^2$)	$(EI_s)/(E_sI_{AASHTO})$	Eigenvalue P_{cr} (kips)
Unstiffened	---	---	---	19.2
Inadequate Up	0.106	3,130	0.11	45.0
Inadequate Down	0.106	3,130	0.11	47.9
Adequate Off-Center	1.28	37,800	1.3	60.1
Adequate	1.44	42,500	1.6	84.3
Double	1.61	47,500	1.8	90.7
Angle	0.989	29,200	1.0	122
Concrete	14.9	58,800	2.3	130

6.4 Presentation of Results

6.4.1 Displacement Surfaces

Plate displacements at multiple locations along the length and across the width of the test region of each plate were measured during each test. Load-displacement plots at particular locations on the test plate are presented in the following discussion. Additionally, the displacements measured at each location are combined to form surface plots of the displaced shape of the plate.

The surface plots of the plate displacement are presented in two forms. One form is the absolute displacement of the plate with respect to a flat plane. The absolute displacement of the plate prior to testing is the initial imperfection of the plate. Surface plots showing the relative displacement of the plate are also used to present the results. The relative displacement surface plots show the

displacement of the plate with respect to its initial shape. The load at which each displacement plot was generated is shown on the plot.

The surface plots of test results were produced using the technical graphing program AXUM 6.0 by Mathsoft, Inc. The surface plot type used is a spline plot, which generates smoothed surfaces of gridded data. The program uses interpolation to fit a surface over the data grid and generates a smooth surface plot of the source data.

The load reported throughout this discussion is the applied load at each end of the girder. For convenience, in the discussion of results the behavior of the test plate will be discussed in terms of "panels". Three panels along the length of the test plate were defined. The left end panel, center panel, and right end panel of the test region are shown in Figure 6.4. As noted in Chapter 5, the test plates had an aspect ratio, length/width, of 2.9.

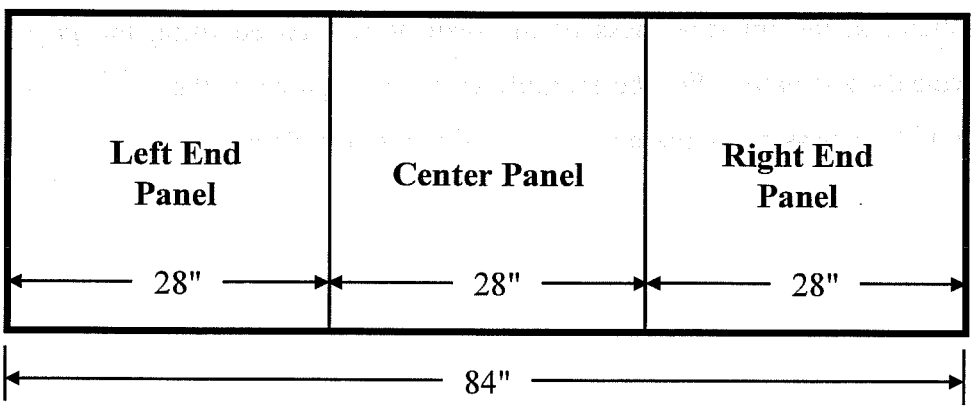

Figure 6.4 Test Plate "Panels"

6.4.2 Stress and Strain

Strains from the gages in the same location on opposite sides of the plate were averaged to obtain the axial strain in the plate. Strains from gages on either side of the stiffener were also averaged. The average stress is labeled using the numbers of all gages involved in obtaining the average. For example, if the strains from Gages 100 and 200 are averaged, the result is referenced as "100,200".

For plates with a stiffener on one side of the plate, the axial strain in the plate at the stiffener was interpolated from the readings of the strain gages mounted to the stiffener and the gage mounted to the test plate on the plate surface opposite the stiffener. Referring to Figure 6.5, the strain from Gages a and b were first averaged, producing $\varepsilon_{a,b}$. A linear strain distribution through the plate and stiffener was assumed, as is shown in Figure 6.5. The strain at the mid-thickness, $\varepsilon_{a,b,c}$, of the plate was then interpolated from $\varepsilon_{a,b}$ and ε_c. The strain, or stress, at the mid-thickness of the plate is referenced using the gages used to calculate its value. For the example shown in Figure 6.5, the stress or strain at the mid-thickness of the plate is referenced as the result from Gages a,b,c.

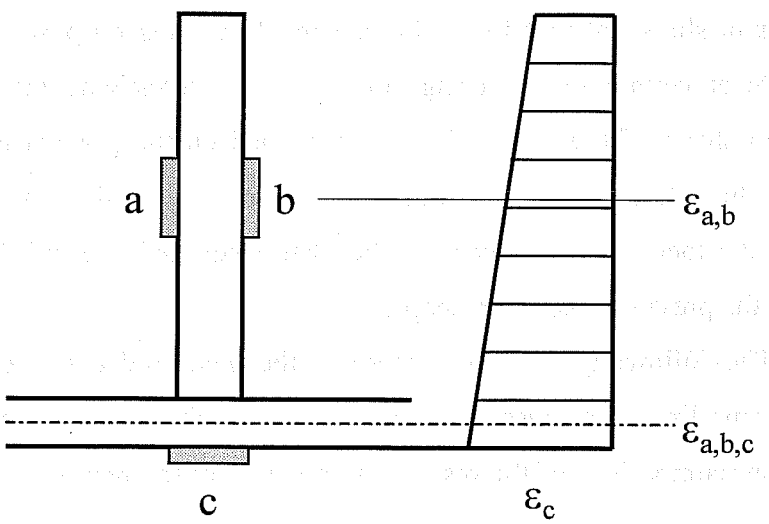

Figure 6.5 Calculating Axial Strain in Plate from Plate and Stiffener Gages

All steel strains remained in the elastic range during testing. The steel strains were converted to stress using a modulus of 29,500 ksi. The concrete strains were converted to stress using a modulus of 3,950 ksi, based on the results of cylinder tests. These same material properties were also used in the finite element analysis models.

6.5 General Behavior Throughout Testing Program

There was no noteworthy permanent strain after testing in any tests except that of the plate with the concrete stiffener. Occasionally during a load-unload cycle the displacement at certain potentiometers did not return to their initial positions after testing. This was due to the fact that there were multiple equilibrium shapes that the plate could assume under no load and low loads. It was possible to push with light hand force vertically on a local area of the plate and pop that local area down and another local area up at low loads. Both the initial shape prior to this vertical loading, and the shape afterward were

equilibrium shapes at that load. Light hand force was purposely applied to the test plate at certain loads during some tests to investigate the impact on the displaced shape of the plate. The vertical load on the plate would cause local areas of the plate to pop into other shapes at low loads. As more load was applied, the local waves induced in the plate smoothed out and the plate moved towards the previous displaced shapes.

The following discussion presents the measured data from each of the tests. Some limited discussion comparing the results between tests is made, but significant comparison of the results and analysis of the response will be made in Chapter 7.

6.6 Unstiffened Plate Test

The first plate tested was not longitudinally stiffened. The plate properties and eigenvalue-buckling load from the finite element model of the test setup are repeated in Table 6.4. As described in Chapter 5, plate displacements were measured using the Potentiometer Displacement Gage (PDG). The PDG was positioned at ten longitudinal locations during the test.

Table 6.4 Unstiffened Test Plate Properties

Plate Thickness (in)	b/t	P_{cr} (kips)
0.1901	153	19.2

The longitudinal locations of the PDG are shown in Figure 6.6 and are labeled from 1 to 10. The transverse locations of the potentiometers in the PDG are also shown in Figure 6.6 and are labeled A through I. In the following discussion, displacement at a particular point will be referred to by its longitudinal

and transverse label, so the displacement at the lower left of the plate is referenced as 1A, the displacement at the upper right of the plate is referenced as 10I. The positions of both transverse and longitudinal potentiometer locations in this test are given in Table 6.5.

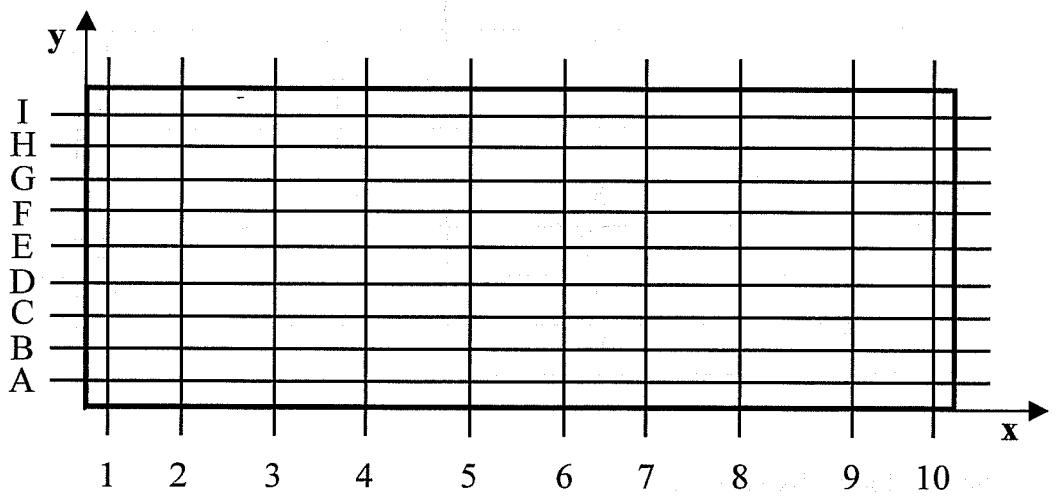

Figure 6.6 Potentiometer Locations during Unstiffened and Inadequate Stiffener Tests

Table 6.5 Longitudinal and Transverse Potentiometer Locations

Longitudinal (x)		**Transverse (y)**	
Label	Position (in)	Label	Position (in)
1	2	A	2 1/4
2	9	B	5 1/8
3	18	C	8
4	27	D	10 3/4
5	37	E	14
6	46	F	17 1/4
7	54	G	20
8	63	H	22 7/8
9	74	I	25 3/4
10	82	----	----

6.6.1 Plate Displacements

The unstiffened plate was loaded and unloaded several times. In all of the plots and discussions of the test results the load reported is the ram load applied at each end of the test girder. The maximum applied load was 40 kips. The eigenvalue buckling load of the unstiffened plate based on the finite element model of the test setup is 19.2 kips. The absolute displacement of the plate in the test to 40 kips is presented in Figure 6.7. Note the same scale is used on each of the plots contained in Figure 6.7.

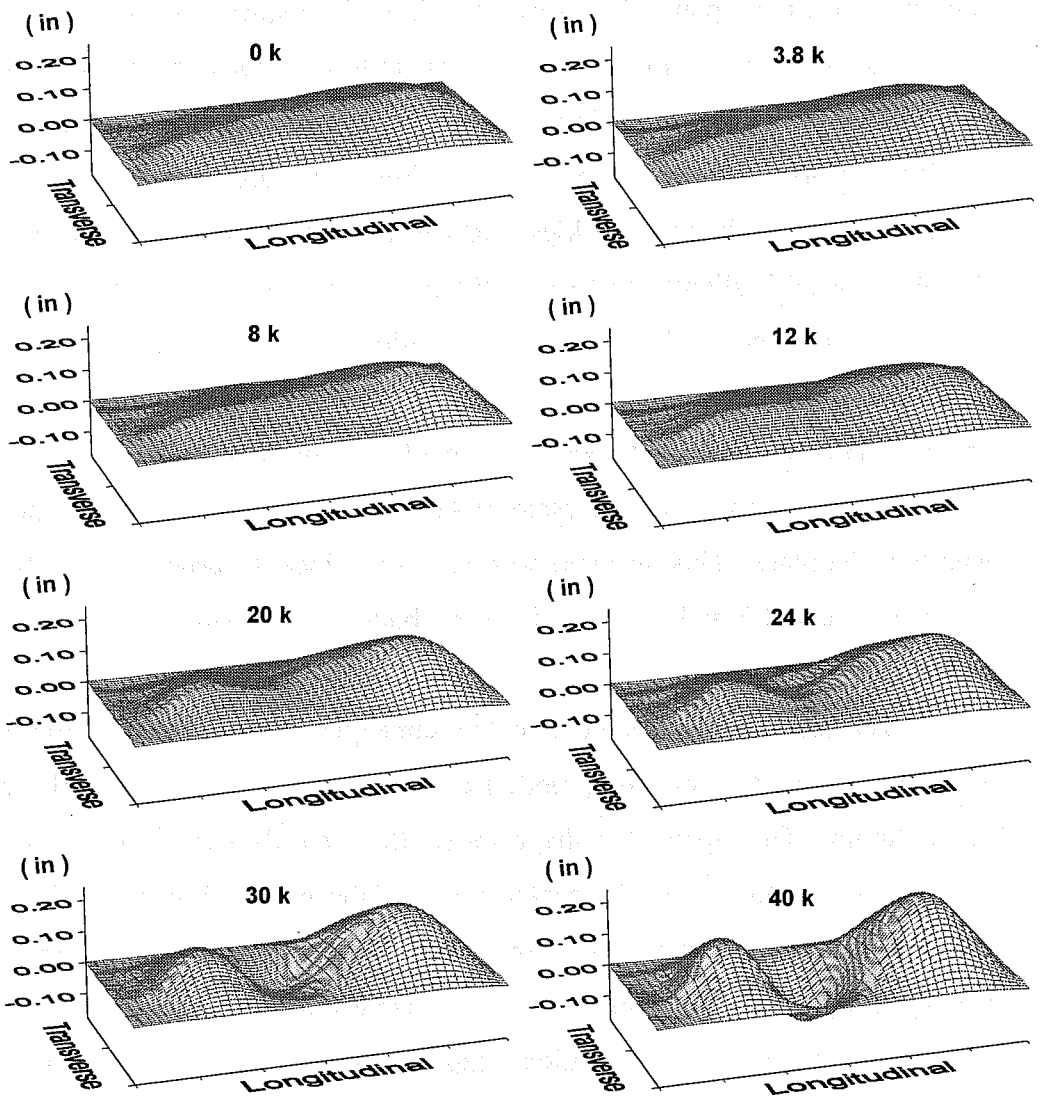

Figure 6.7 Unstiffened Plate Test - Absolute Displacement

The absolute displacement plot at a load of 0 kips shows the initial imperfection of the plate. The plate was initially displaced up along the length and across the width of the plate, with respect to the edges of the plate. As load was applied to the girder, the initial imperfection of the plate was amplified. The displaced shape of the plate is very similar in appearance to the initial imperfection up to the plot at 8 kips. However in the plot at 12 kips, the middle of the center panel is slightly depressed with respect to the centers of the end panels. As load continued to be applied, the middle of the center panel began to noticeably move downward, as the center of the end panels continued to displace upward. This response continued with the addition of more load.

The final shape of the plate at 40 kips has three half waves along the length of the plate. This response was expected, since the aspect ratio, a/b, of the test plate is about 3 and the plate therefore buckles on square panels in three half waves along its length.

The relative displacement of the same plate is presented in Figure 6.8. The shape of the first buckling mode from the eigenvalue analysis is also shown in the figure. The eigenvalue shape shows the plate displaced downward in the end panels and upward in the center panel of the plate. A buckled shape with displacement upward in the end panels and downward in the center panel is an equally likely shape. The direction of the displacements in the panels of the test plate was influenced by the initial imperfection of the real test plate. The displaced shape of the test plate recorded in the experimental tests agrees with the eigenvalue prediction.

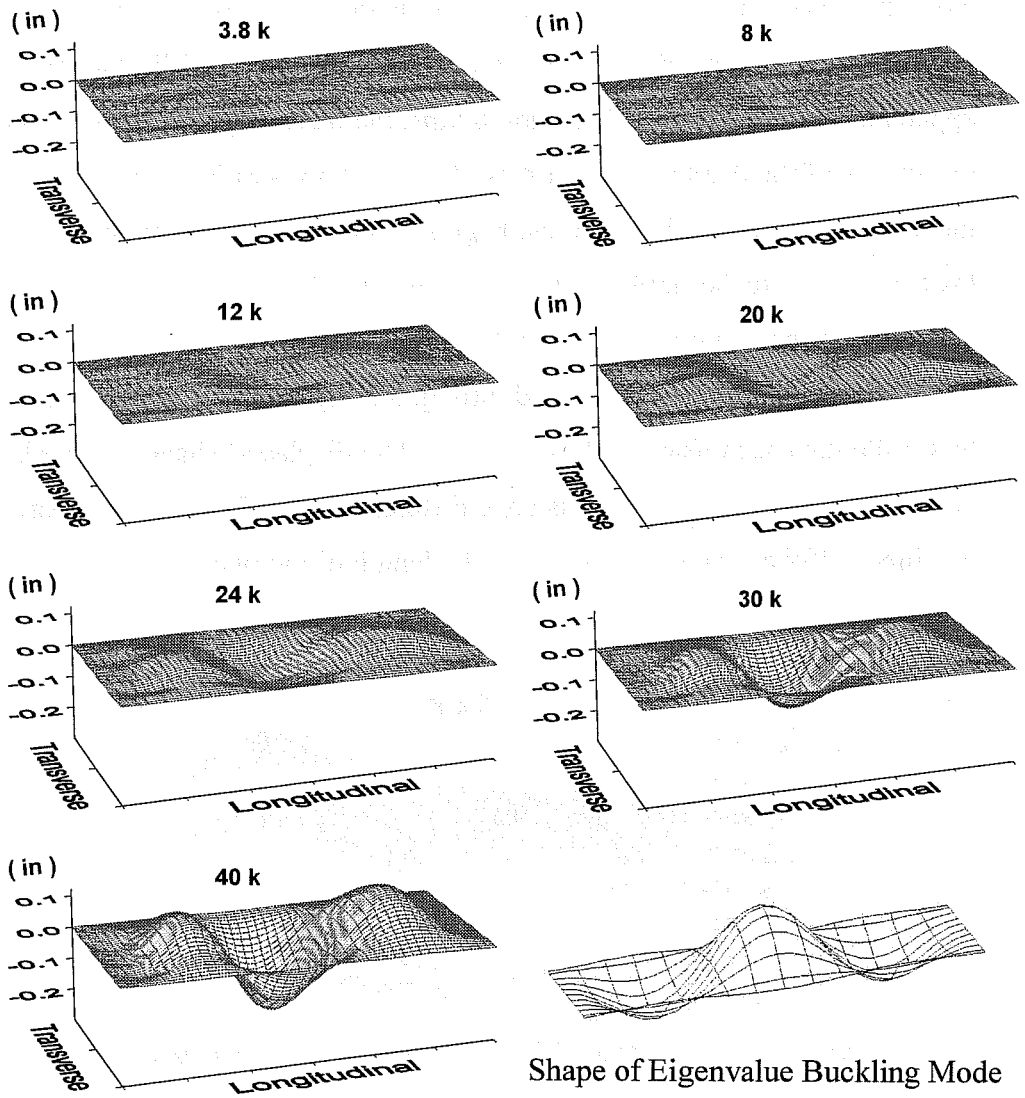

Figure 6.8 Unstiffened Plate Test - Relative Displacement

The relative displacement of the plate clearly shows three half-waves along the length of the plate. At very low loads, local areas of the plate seem to be displacing independently, and the final form of the displacement is not apparent. In the plots at 3.8 kips and 8 kips, the plate displacements are small and the shapes of the displacement at these loads are not similar to each other. When the applied load is 12 kips the plate begins to show the three half-wave shape. As load continues to be applied, the displacement shows a fairly symmetric three half-wave shape along the length of the plate.

Since the same scale is used throughout Figure 6.8 it is somewhat difficult to see the displaced shape at lower loads. The displaced shape of the plate at 12 kips is repeated in Figure 6.9 using a different scale. This figure clearly shows the three half-waves developing along the length of the plate.

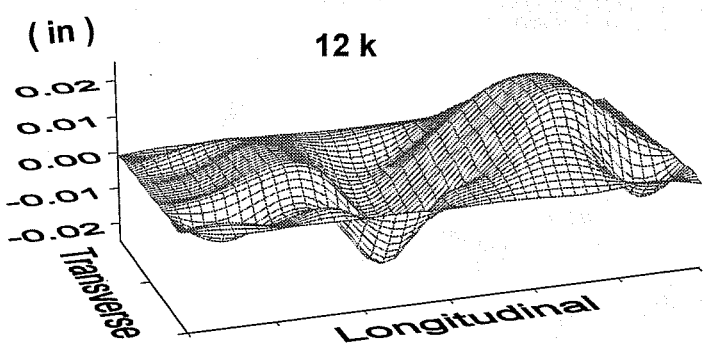

Figure 6.9 Unstiffened Test - Relative Displacement at 12 kips

The load-displacement response at eight specific locations is presented in Figure 6.10 and Figure 6.11. The locations are labeled using the convention discussed earlier in this chapter. At some locations, the plate initially moves in a certain direction, and continues to move in that direction throughout the test. At other points, the plate initially moves one way, then the displacement switches

directions as more load is applied. At location 3G, shown in Figure 6.10, the plate initially moves up slightly, then down slightly, then begins to move upward and continues moving upward throughout the test.

As shown in Figure 6.10 and Figure 6.11 the response of the plate is initially stiff. The eigenvalue buckling load based on finite element analysis is 19.2 kips. There is relatively little displacement until the applied load is near the buckling load. As more load is applied, the response of the plate softens. Each point displaces more significantly with the application of an equivalent increment of load.

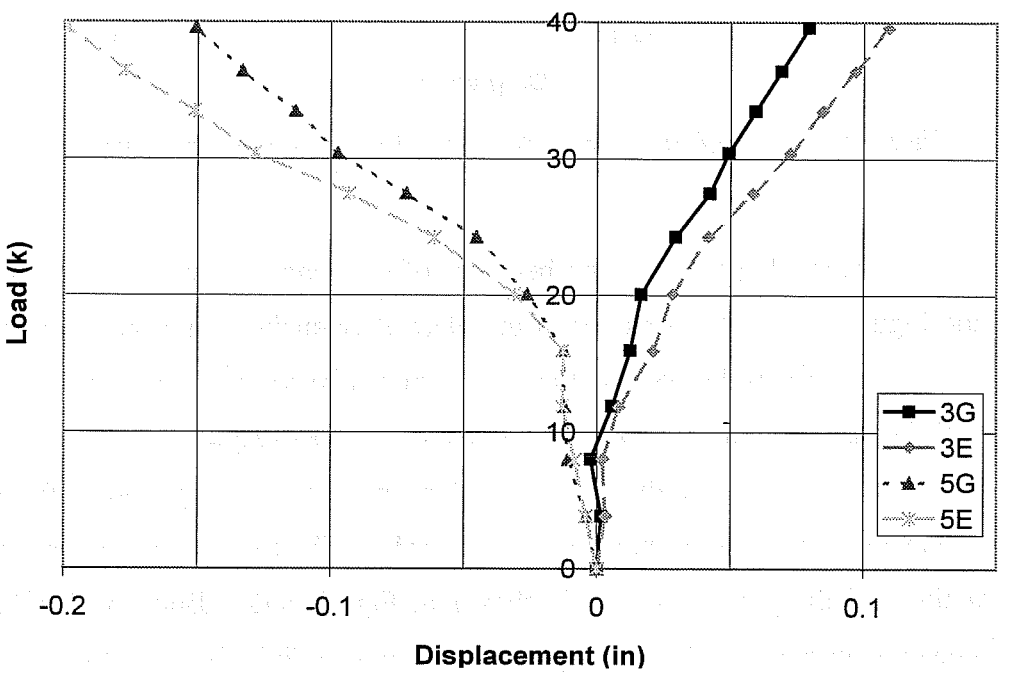

Figure 6.10 Unstiffened Test - Relative Displacements at Positions 3 and 5

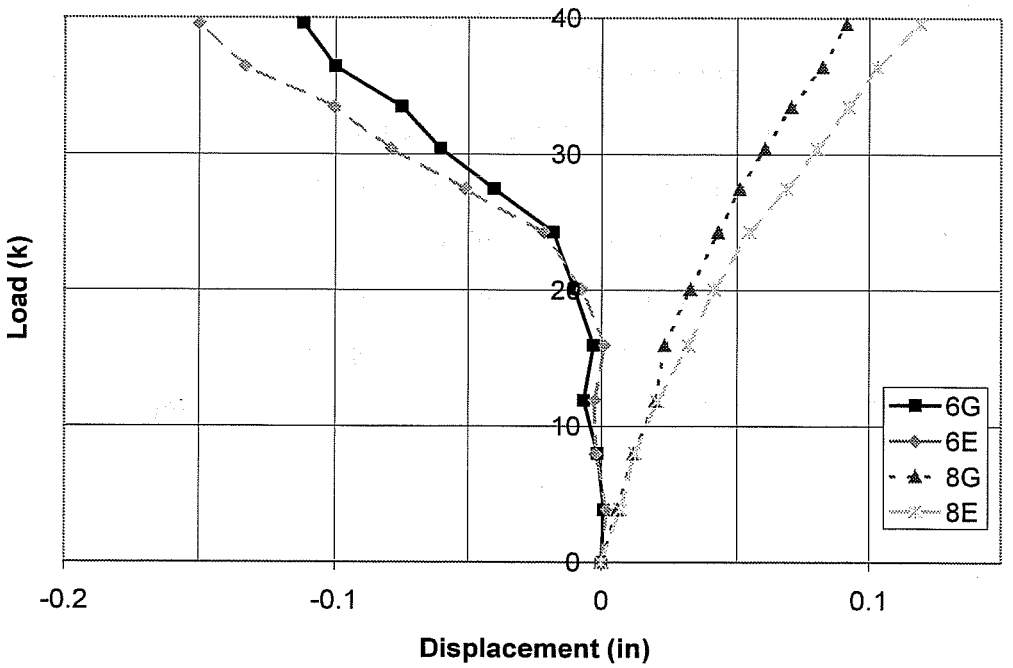

Figure 6.11 Unstiffened Test - Relative Displacements at Positions 6 and 8

The stable post-buckling behavior of the plate can be seen in Figure 6.10 and Figure 6.11. The behavior of the plate after buckling is very different from that of a compressed slender column. The plate can continue to support load after buckling, and can support loads above that of the buckling load.

In another test, the PDG was left in place at longitudinal Position 5 throughout loading and unloading of the girder. The load-displacement response at three of the potentiometers is shown in Figure 6.12. Both the loading and unloading curves are shown. Figure 6.12 shows the initially stiff response of the plate, and softening of the response around 16 to 17 kips. The figure also shows that the plate behaved very similarly on loading and unloading. The unloading curve closely retraces the loading curve. The plate returns to zero relative displacement after removal of the load.

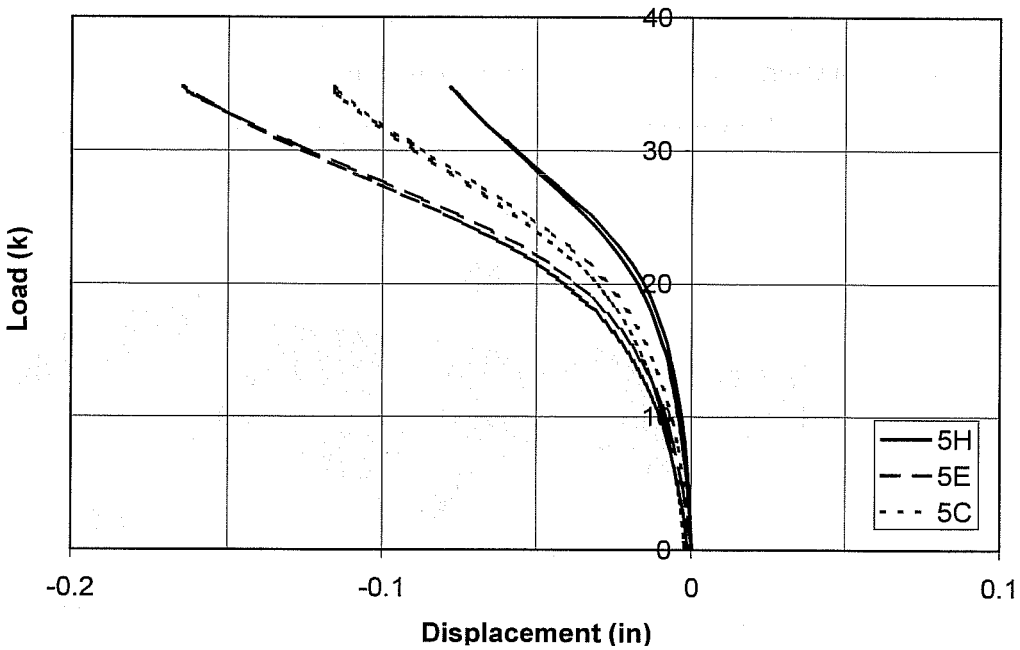

Figure 6.12 Unstiffened Test - Displacement with PDG at Position 5

The displacements from the twenty-one potentiometers at the locations of maximum relative plate deflection were averaged. The longitudinal locations of the averaged potentiometers are shown in Figure 6.13. The readings from transverse potentiometers B through H at each longitudinal line were used. The data from select potentiometers were averaged, rather than averaging the data from all potentiometers, since some potentiometers were at locations where the plate was not displacing significantly. Potentiometers that were near nodal locations of the buckling shape, and near the edges of the test region of the plate did not show significant displacement, as expected.

The load-displacement response using the averaged displacement is shown in Figure 6.14. The load is that applied by the ram to the girder. The eigenvalue buckling load of 19.2 kips is also shown on the plot. As was seen with the individual potentiometers, the plate response is initially stiff. Up to the readings

taken at 16 kips, the load-deflection curve is linear. Beyond this load-level, the plate's deflection is larger for the same increment, or even a smaller increment, of load. The plate's averaged response is stiffer below the buckling load, and softer above it.

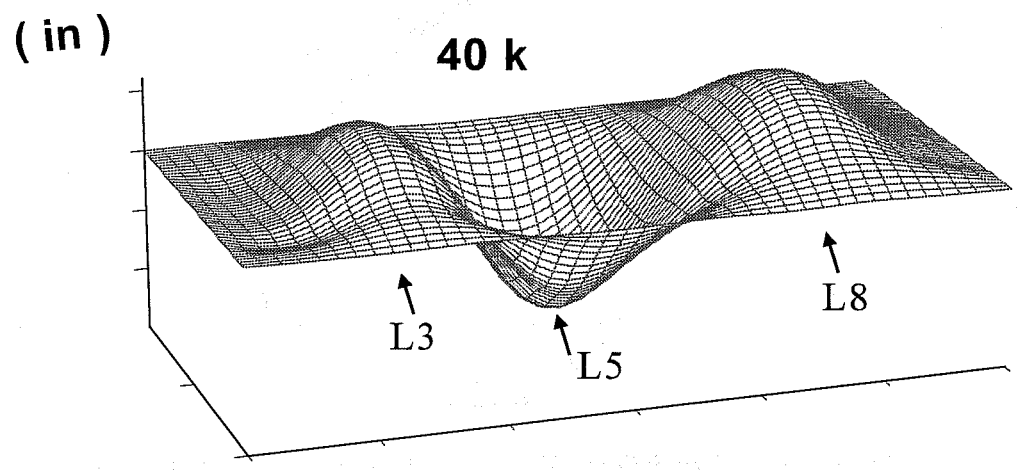

Figure 6.13 Unstiffened Test - Longitudinal Location of Averaged Readings

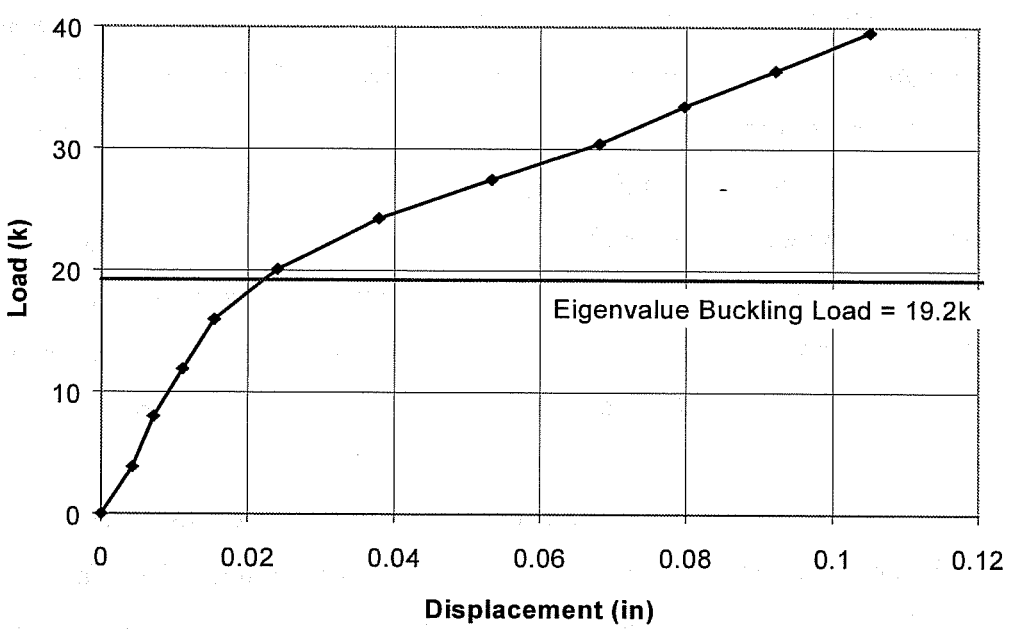

Figure 6.14 Unstiffened Test - Average Relative Displacement

6.6.2 Strain Gage Data

Strain gages were installed on both sides of the test plate, along the length and across the width the plate. The location of the strain gages and their labels are shown in Figure 6.15. Gage 209 was damaged during installation of the test plate, and data from it was not used.

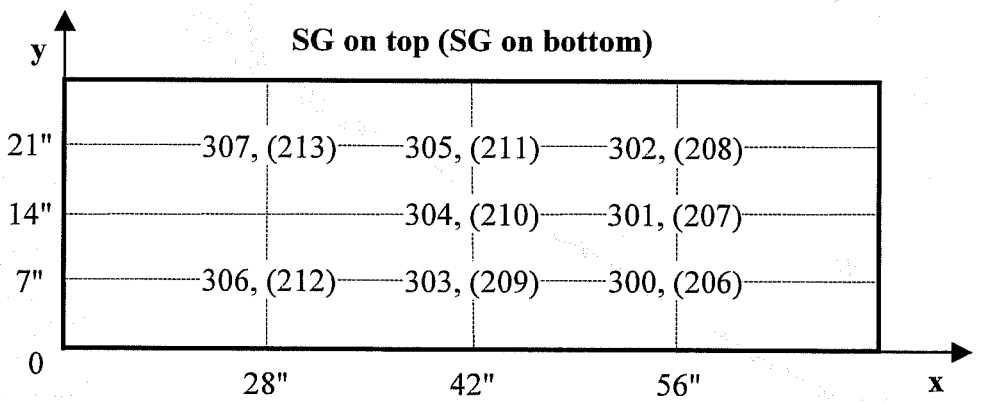

Figure 6.15 Strain Gage Map

The averaged stresses are plotted against the applied load in Figure 6.16. The stresses increase fairly linearly, as expected, with the initial application of load. Above a load of approximately 22 kips the plate was bending very significantly at the middle of the center panel. There is less support to the center panel than the end panels, and load was shed from this location at higher loads. Consequently, above 22 kips the average of Gages 210 and 304 was non-linear with respect to the application of additional load. The final relative displacement at the middle of the center panel was about twice as large as the relative displacement at the middle of the end panels.

Below the buckling load, comparable strains were seen at gages installed at different locations along the length and across the width of the plate. The fact that the strain was fairly uniform across the entire plate surface confirms that the

plate was adequately connected to the girder and that the plate was fully participating in supporting the applied loads.

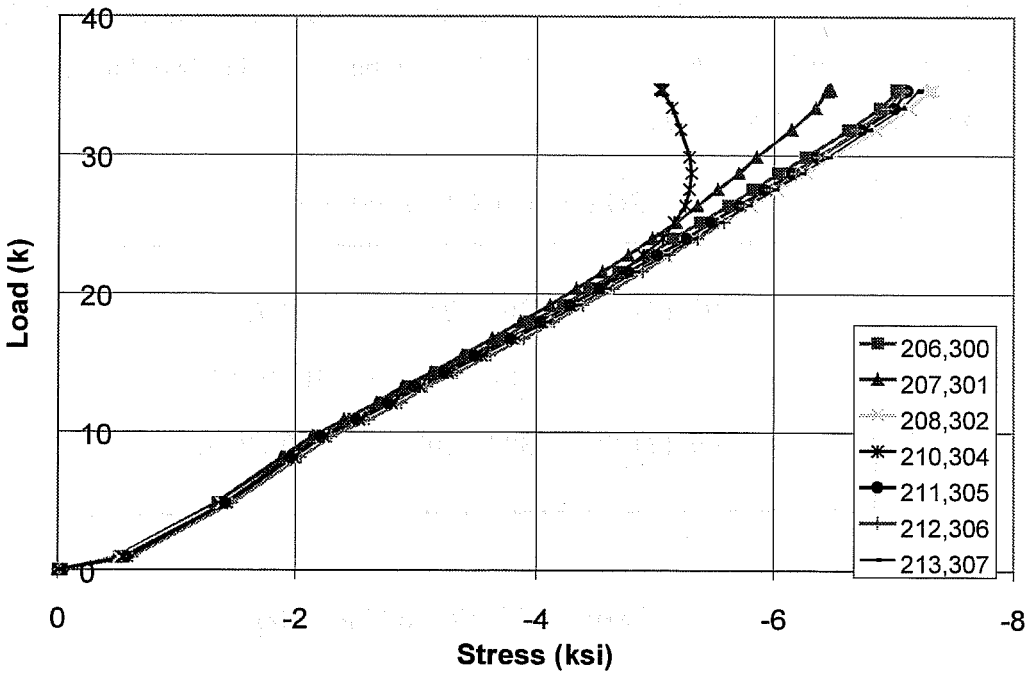

Figure 6.16 Average Stress

The average stresses across the width of the plate at one longitudinal location are presented in Figure 6.17. Initially, the averages of each set of gages track closely together. As more load is applied, and particularly when the load surpasses 15 kips, the stresses become divergent. The stresses across the width of the plate at four load levels are plotted in Figure 6.18. In this plot, the middle longitudinal line of the plate is referenced as the 0 in. transverse position. At higher loads, the stress at the middle of the plate is lower than the stresses nearer the edges of the plate.

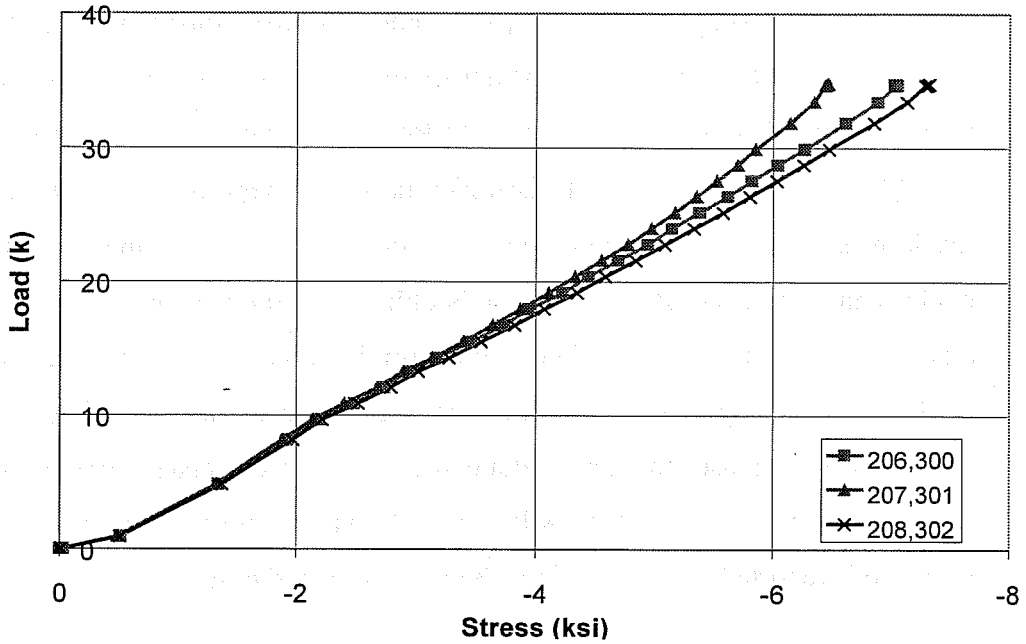

Figure 6.17 Stresses Across Width of Plate

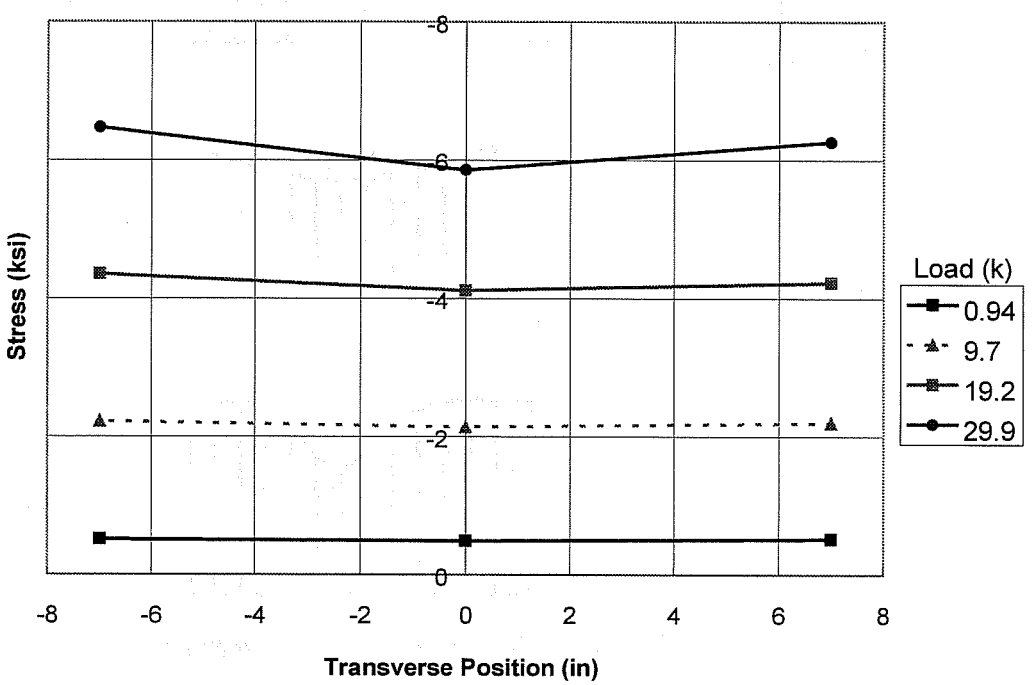

Figure 6.18 Stresses Across Plate Width

An ideal simply supported plate under uniform compression is shown in Figure 6.19. The stress distribution across the width of this plate is shown on the right as the applied load is increased. At low loads when the plate stress is below the critical stress, σ_{cr}, the plate is under uniform stress and the plate does not displace laterally. As the applied load is increased to the buckling load, the plate buckles and displaces laterally. At the buckling load the plate stress changes from a uniform stress distribution to a non-uniform distribution. The stress at the edges of the plate is higher than the stress at the center of the plate. As the load continues to increase, the stress along the edges of the plate increases and the edges start yielding. The plate will eventually yield across its entire width. This response is reported by Bleich, Timoshenko, Gere, and others.

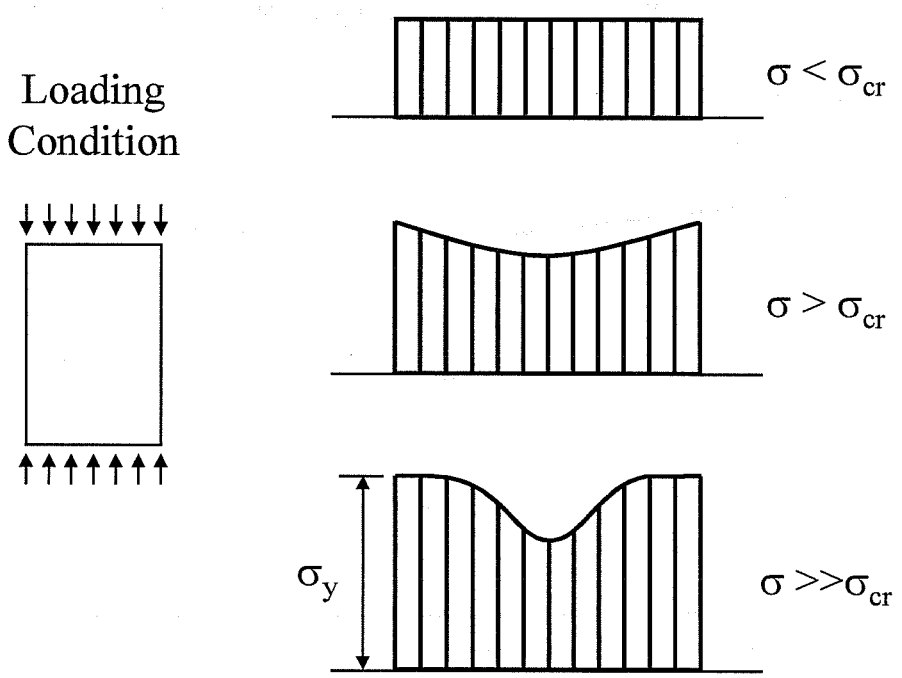

Figure 6.19 Stress Distribution Across Width of Plate

This is the same general behavior seen in the stresses of the test plate. As shown in Figure 6.18, the stresses across the width of the plate are initially uniform. As the test plate displaces significantly vertically as it buckles, the stresses in the plate become non-uniform, with lowest stresses at the middle of the plate width.

6.6.3 Unstiffened Test Conclusions

The nature of the displacement and strain data collected during the unstiffened plate test agreed with expectations. The plate response was stiff beneath the eigenvalue buckling load and softer above the buckling load. The plate displaced in the same shape as in the eigenvalue analyses, with three half-waves along the length of the plate.

6.7 Test Plate with Inadequate Stiffener

A compression plate with a small stiffener was tested. This stiffener was smaller than the "adequate" stiffener required in the AASTHO design procedure to enable use of a plate buckling coefficient of 4. The test plate with the small stiffener was tested both with the stiffener on the top surface of the test plate, "inadequate up test", and with the stiffener on the bottom surface of the test plate, "inadequate down test".

6.7.1 Inadequate Up Test Displaced Shapes

The plate and stiffener properties of the inadequate up test plate are repeated in Table 6.6. In the table, w is the stiffener spacing, t is the test plate thickness, I_s is the moment of inertia about the base of the stiffener, and P_{cr} is the ram load at which buckling occurred in the finite element analysis. Plate displacements were measured using the PDG at the same locations as in the unstiffened plate test. The center longitudinal line of potentiometers labeled E

was removed from the PDG since it conflicted with the longitudinal stiffener. The inadequate up plate was loaded and unloaded several times. A maximum load of 70 kips was applied to this test plate.

Table 6.6 Inadequate Up Test Plate Properties

Plate Thickness (in)	w/t	I_s (in^4)	P_{cr} (kips)
0.2010	72	0.106	45.0

The initial imperfection of the plate is shown in Figure 6.20. The plate was initially displaced downward at the left end of the plate, and displaced upward over the middle and right end of the plate. Due to the large magnitude of the initial imperfection, the response of the plate is not clearly seen in the absolute displacement plots. The relative plate displacements show the response of the plate to the applied load. The relative plate displacements from a load cycle to 66 kips are presented in Figure 6.21, along with the eigenvalue buckling shape.

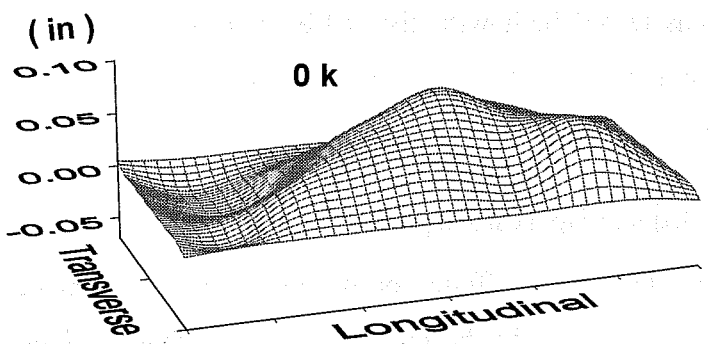

Figure 6.20 Inadequate Up - Initial Imperfection

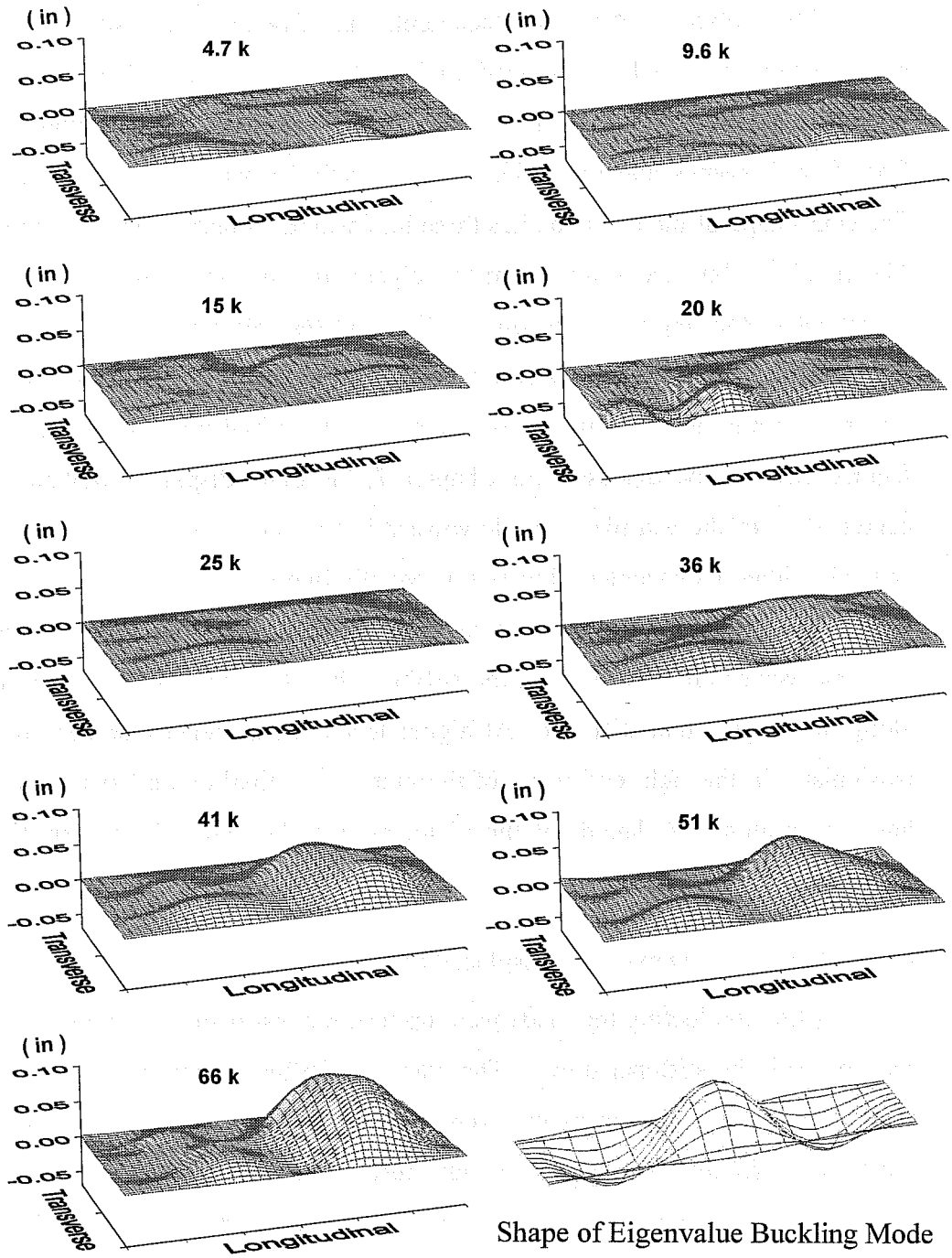

Figure 6.21 Inadequate Up Plate Test - Relative Displacement

The relative plate displacements in Figure 6.21 show that the displacements are small at low load, and the final form of the displaced shape is not apparent. At higher loads the shape of the plate displacement settles, and the final form becomes apparent. The shape is amplified as more load is applied. The final shape of the test plate has three half-waves along the length of the plate. The predicted buckled shape from the eigenvalue analysis also has three half-waves along the length of the plate. The real test plate had a complex initial imperfection. There was a large raised area over the right end panel extending towards the middle of the plate. As a result of the initial imperfection, and other factors that will be discussed in Chapter 7, the plate displaced upward in the center panel of the test plate and downward in the end panels. In the eigenvalue analysis, either displacement direction is equally likely.

The stiffener did impact the displaced shape of the plate. At low loads, the plate has waves on either side of the stiffener, but does not displace significantly along the longitudinal stiffener. At higher loads, the stiffener displaced upward, particularly in the right end panel of the plate. The final overall shape has three half-waves along the length of the plate, as was the case with the unstiffened plate.

6.7.2 Inadequate Down Test Displaced Shapes

After conducting the inadequate up test, the test plate was turned over and retested with the stiffener down. The plate and stiffener properties are shown in Table 6.7. Plate displacements were measured using the PDG at the same locations as in the inadequate up plate test. The inadequate down plate was loaded and unloaded several times. A maximum load of 80 kips was applied with this test configuration.

Table 6.7 Inadequate Down Test Plate Properties

Plate Thickness (in)	w/t	I_s (in^4)	P_{cr} (kips)
0.2010	73	0.106	47.9

The initial imperfection of the plate is shown in Figure 6.22. Though the same test plate and stiffener were used in the previous test, the shape of the initial imperfection in the inadequate down test was not a mirror image of the initial imperfection in the inadequate up test. In both tests, the plates were initially displaced upwards over the length of the plate. With the stiffener down, there were more local waves along the length of the plate than in the inadequate up test.

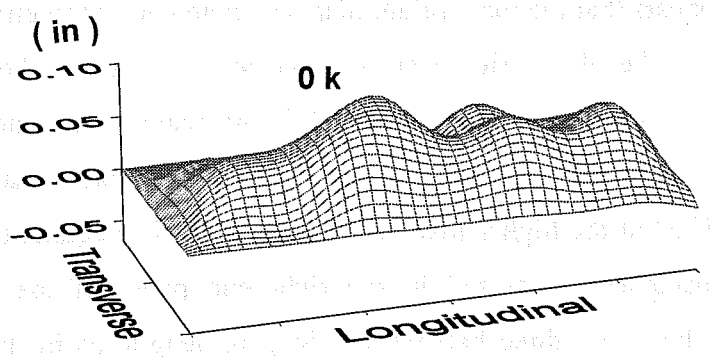

Figure 6.22 Inadequate Down - Initial Imperfection

Installation of the test plates onto the test setup affected the initial imperfection of the test plates. The test plates were bolted on all four edges to attach them to the test setup. As previously discussed, the nuts for each bolt were welded in place. The fact that the nuts were welded reduced the dimensional tolerance at each hole. Consequently, the test plates had to be worked with a spud wrench and selective tightening of bolts to pull the test plates into place. Forcing the test plates into position affected the initial imperfection of the plate. As a

result, both the inadequate up and inadequate down test plates, and the other test plates, were generally concave down along their length.

As in the previous test, due to the large magnitude of the initial imperfection, the response of the plate is not clearly seen through plots of the absolute displacements. The relative displacements from a test to 80 kips are presented in Figure 6.23. The eigenvalue buckling shape of the plate is also shown in this figure.

As in the inadequate up test, at low loads the displacements are small and the final form of the displaced shape is not apparent. At the 25 kip load level, the final form of the displaced shape becomes apparent. In the 30 kip and 35 kip load plots, it appears that the plate might displace in an anti-symmetric mode in the left end panel of the plate. However, as more load is applied, the shape at 41 kips returned to a symmetric shape in the left end panel. As load continued to be applied up to the 80 kip load level, the shape of the plate remained the same but was amplified at the higher load levels. As in the inadequate up test, the largest plate displacements occurred in the right end panel of the plate. The final displaced shape has three half-waves along its length, as in the unstiffened and inadequate up tests. The plate is depressed somewhat along the line of the longitudinal stiffener over the full length of the plate. Even in the right panel, where the plate displacements were largest, the impact of the longitudinal stiffener on the displaced shape can be seen.

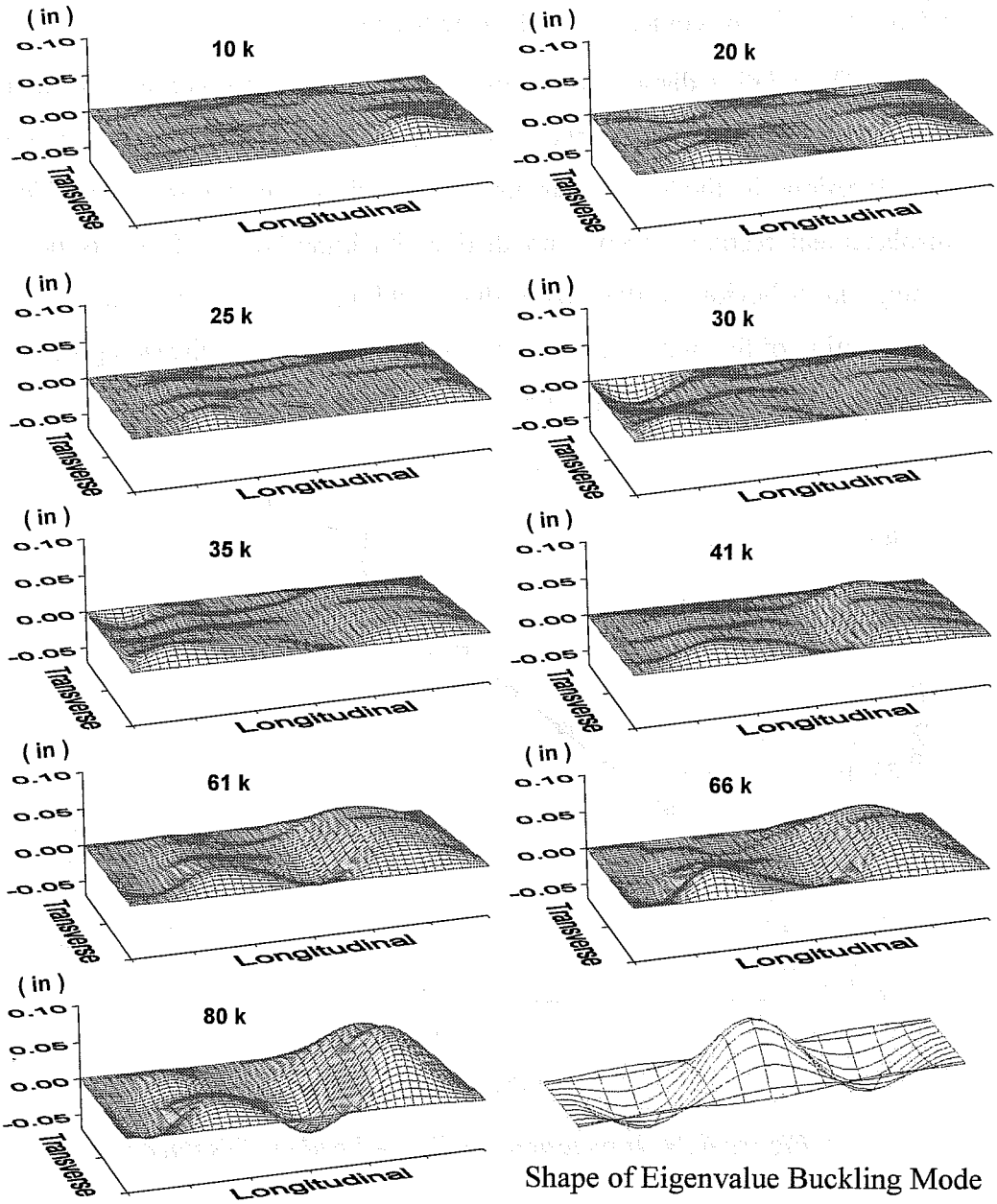

Figure 6.23 Inadequate Down Plate Test - Relative Displacement

6.7.3 Load-Displacement in Inadequate Stiffener Tests

The relative displacements measured in the inadequate up and inadequate down tests were plotted vs. the applied load. The load-displacement curves at four locations in the inadequate up test are shown in Figure 6.24. The load-displacement response shows no distinct buckling load. There is no distinct change in behavior at the eigenvalue-buckling load of 45 kips. The initial imperfection of the plate is amplified, and the plate begins displacing significantly with the application of the first increment of load.

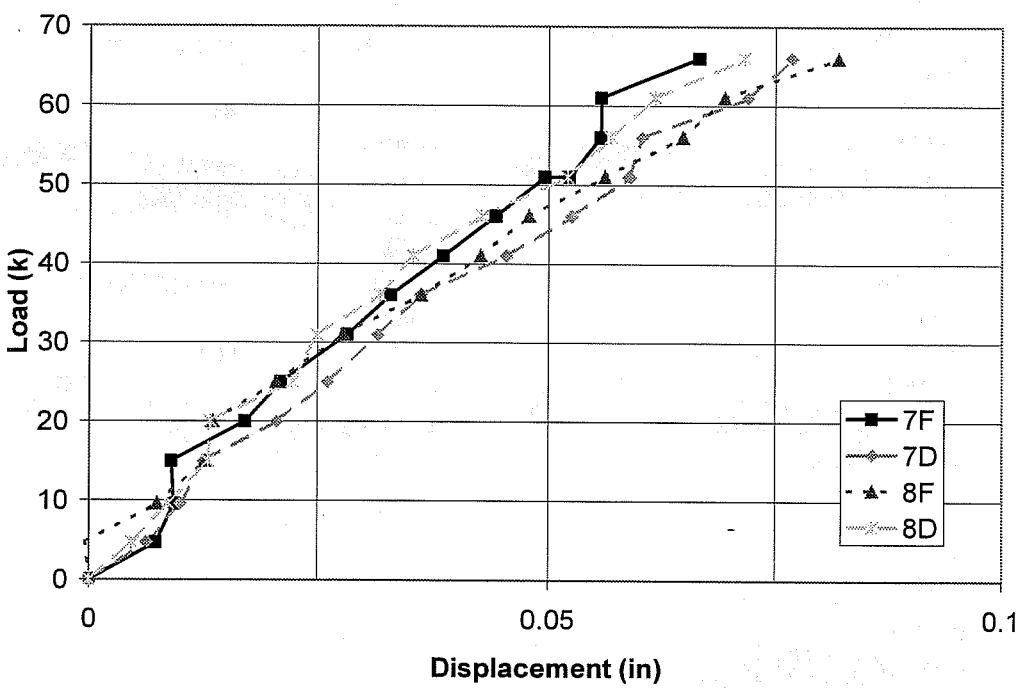

Figure 6.24 Inadequate Up Test - Load vs. Displacement

The general load-displacement response in the inadequate down test was the same as that seen in the inadequate up test. The plate began moving with the initial application of load, and no critical load was apparent in the load-displacement plots. There was no softening of the response at any specific load

level. The only significant difference between the load-displacement response of the inadequate up and inadequate down tests, is that the maximum displacement in the inadequate down test was about half that of the inadequate up test at the same applied load.

6.7.4 Strain Gage Data in Inadequate Stiffener Tests

Strain gages were installed on both sides of the test plate. No significant difference was seen in the load-stress response of the test plate with the stiffener up (inadequate up test) compared to with the stiffener down (inadequate down test). Representative stress data from the inadequate up test will be presented in this discussion.

The location of the strain gages and their labels in the inadequate up test are shown in Figure 6.25. The same strain gages were used in the inadequate down test. The averaged stresses from the gages in the inadequate up test are plotted against the applied load in Figure 6.26. The stresses increase linearly with the application of load, and the stresses are within approximately 10% of each other across the surface of the plate.

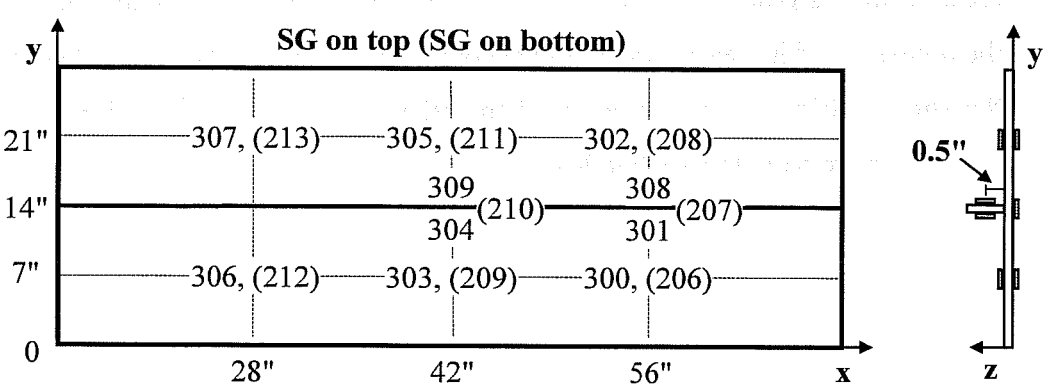

Figure 6.25 Inadequate Up Test - Strain Gage Map

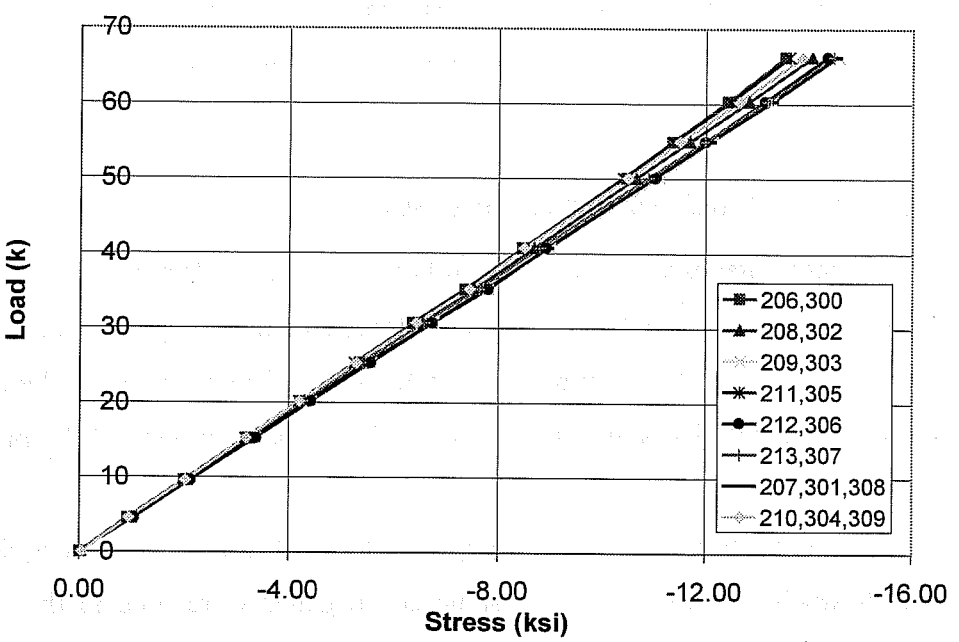

Figure 6.26 Inadequate Up Test - Average Stresses

The stresses across the width of the plate in the right end panel are shown at four load levels in Figure 6.27. The middle of the plate is at the 0 in. transverse location in this plot. The stress has a uniform distribution at low load levels. As the applied load increases, the stress becomes non-uniform. At higher load levels, the stress is higher at the location of the stiffener due to the participation of the stiffener in carrying the applied load.

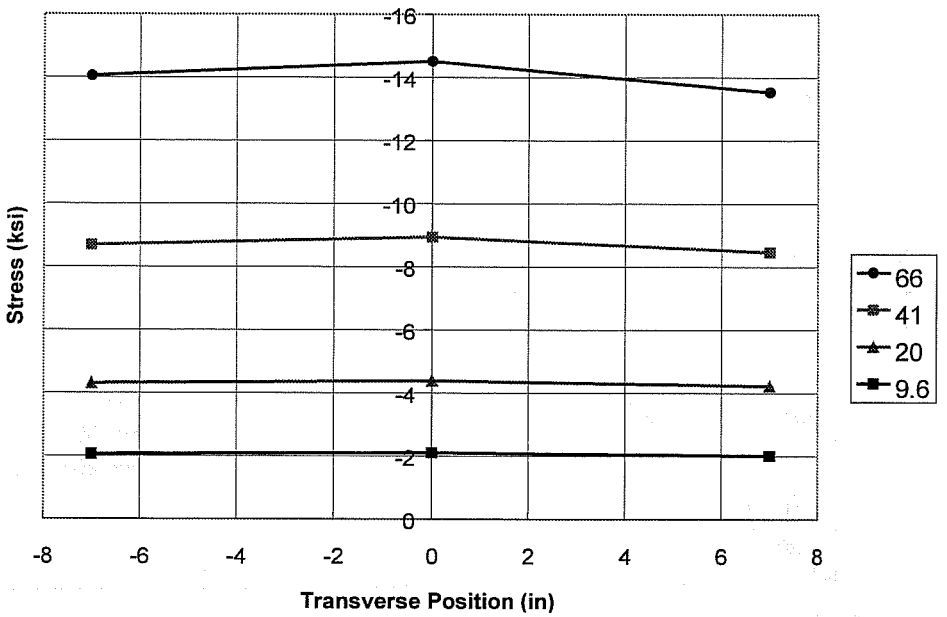

Figure 6.27 Inadequate Up - Axial Plate Stresses across Width in Center Panel

The stresses at the stiffener in the right end panel are plotted in Figure 6.28. The stresses in Gages 301 and 308, which were attached directly to the stiffener, were fairly linear up to about 40 kips of load, then become increasingly non-linear with the application of additional load. At this location, in the middle of the right end panel, the plate undergoes significant displacement. Particularly as the load is increased to the 40 kip load level and above, the plate displaces significantly upward at this location. The stiffener, which was mounted on the top of the plate surface, bends and the tensile bending stresses unload the free edge of the stiffener as the plate is loaded.

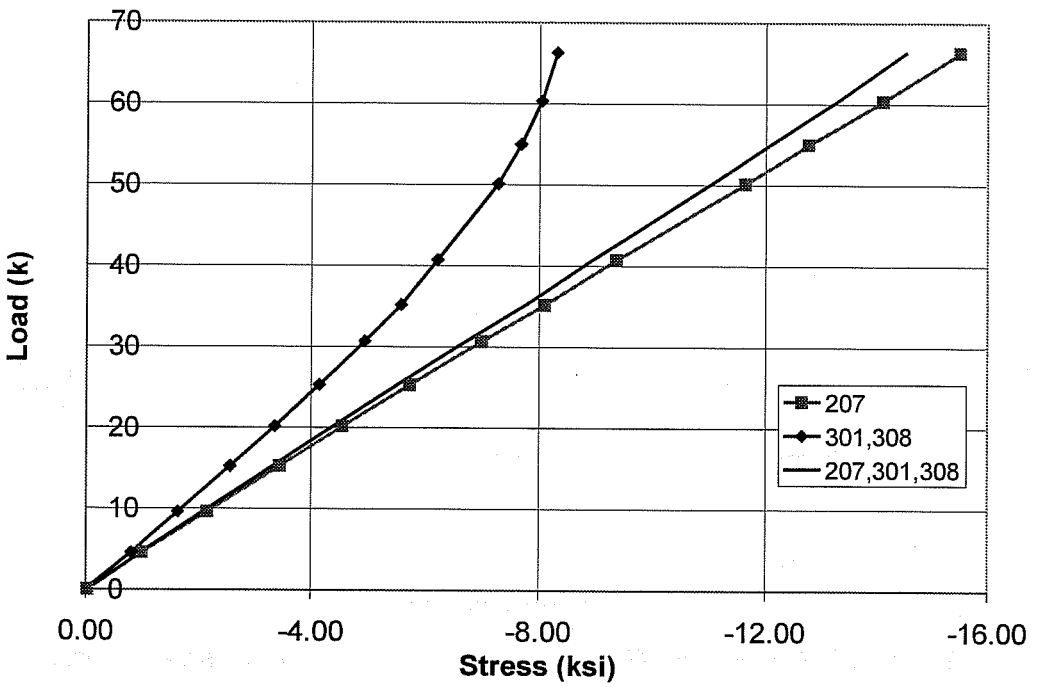

Figure 6.28 Inadequate Up Test - Stresses at Stiffener in End Panel

The stresses at the stiffener in the center panel are plotted in Figure 6.29. The relative displacement at this location, in the middle of the center panel, is much less than the displacement in the right end panel. Note that a different x-axis scale from the previous plot is used in this figure. The stresses are linear up to about the 40 kip load level. Above this load level, the stiffener is bending more significantly, and the free edge of the stiffener is loaded by the bending stresses in this location.

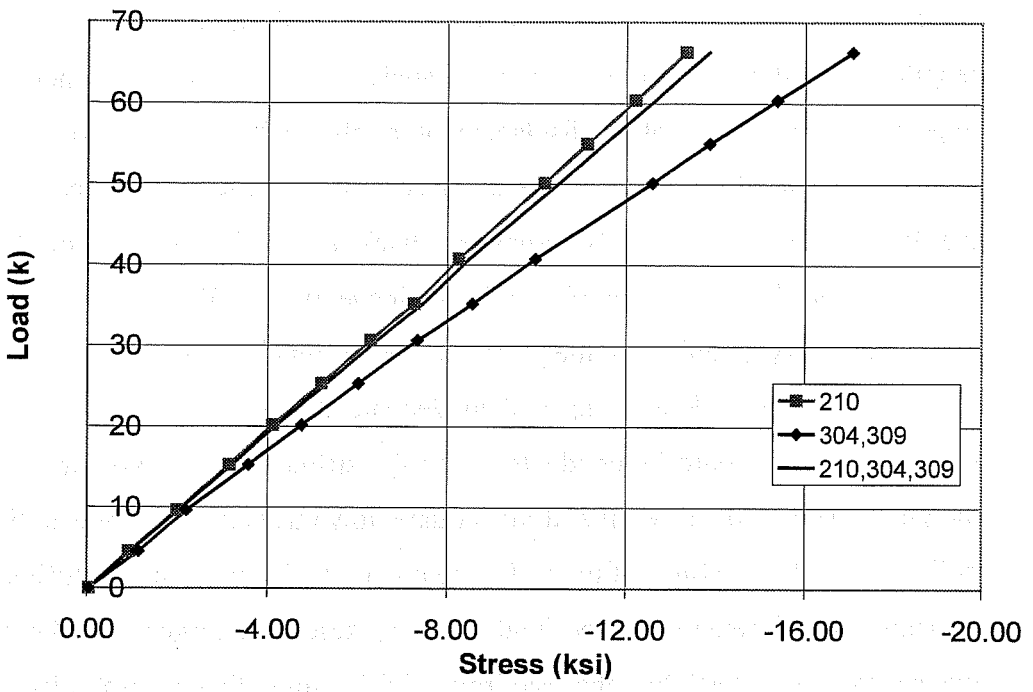

Figure 6.29 Inadequate Up Test - Stresses at Stiffener in Center Panel

The general nature of the stresses measured in the inadequate down test was the same as that presented for the inadequate up test. The plate stresses increased nearly linearly with the application of load to the test plate. The stress distribution across the surface of the plate was fairly uniform, with slightly larger stresses at the stiffener at higher load levels. As the plate bent, the free edge of the stiffener was unloaded in the center panel, due to the direction of bending and orientation of the stiffener, and the free edge of the stiffener was loaded in the right end panel.

6.7.5 Conclusions from Inadequate Stiffener Test Plates

The displaced shapes of the test plates with inadequate stiffeners were more complex than expected, due to the magnitude and complexity of the initial

imperfection of the plate. The plate did displace with three half waves along the length, as predicted by the eigenvalue analysis. The small stiffener was not expected to eliminate plate displacement at the stiffener, but did impact the displaced shape of the plate. Plate displacements were somewhat reduced along the line of the stiffener. No apparent buckling load was seen in the load-displacement plots of the test plate with an inadequate stiffener. No deterioration in the load-carrying ability of the plate was seen throughout the test.

After the inadequate up and inadequate down tests, it was decided that subsequent tests would be conducted with the stiffener on the bottom surface of the plate. The inadequate up and inadequate down tests did not show an inherent difference in the response of the test plate due to the location of the stiffener. The maximum displacements in the inadequate up test were larger than those in the inadequate down test, but the maximum initial imperfection was also slightly larger in the inadequate up test. The differences in initial imperfection and the direction of the stiffener bending can be used explain the difference in the displacements and stresses in the tests.

Philosophically, it seemed more appropriate to place the stiffener on the bottom surface of the test plate, on the inside of the box, since this most closely models the configuration used in box girder bridges. Also, with the stiffener on the bottom surface of the plate, a line of potentiometers could be placed directly above the stiffener. Furthermore, from the inadequate up test it was apparent that the stiffener deflections were much too small to be seen with the naked eye. Therefore there was no advantage to being able to see the stiffener during the tests. Consequently the steel stiffeners in subsequent tests were mounted to the bottom surface of the test plates.

6.8 Change in Displacement Measurement System

As shown in Figure 6.24, significant "noise" was apparent in the displacement plots generated from sweeping the plate surface with the PDG. As discussed at length in Chapter 4, the PDG was used during the early tests to scan the displacements along the plate surface during the test. Some error was probably introduced to the displacement measurements from slight changes in placement of the PDG. More significantly, each potentiometer demonstrated slight changes in measurement when they were read at a specific position, then allowed to fully extend, then re-read at the same position. This error became more significant as the plate displacements became smaller. Since the stiffened test plates had less displacement than the unstiffened test the displacement measuring system had to be altered. The new displacement system, discussed in Chapter 5, utilized more potentiometers that were left in place during the test. The locations of the potentiometers used in the rest of the testing program are shown in Figure 6.30. The exact positions of the transverse and longitudinal potentiometer locations are given in Table 6.8.

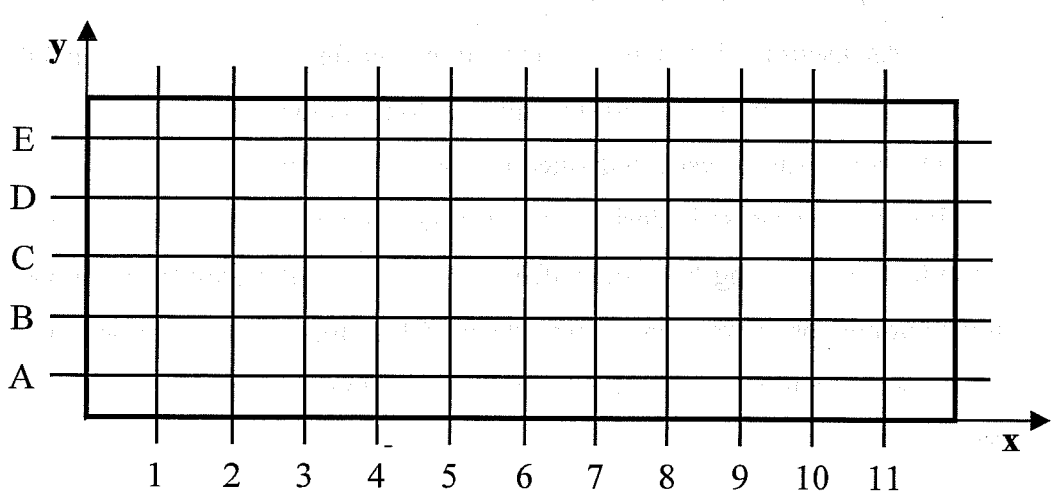

Figure 6.30 Plates with Large Stiffeners: Potentiometer Locations

Table 6.8 Longitudinal and Transverse Potentiometer Locations

Longitudinal (x)		Transverse (y)	
Label	Position (in)	Label	Position (in)
1	7	A	4
2	14	B	9
3	21	C	14
4	28	D	19
5	35	E	24
6	42	---	---
7	49	---	---
8	56	---	---
9	63	---	---
10	70	---	---
11	77	---	---

6.9 Adequate Off-Center Test

As discussed in Chapter 5, a test plate configuration was designed that had a plate stiffener mounted off the middle longitudinal line of the plate. This configuration was investigated since the buckling load was smaller and could be significantly surpassed during the testing program. However the added complexities resulting from the stiffener being off-center clouded the results, and after completion of this test it was decided that the rest of the plates would be tested with centrally located stiffeners, as is the common practice for single longitudinal stiffeners.

6.10 Adequate Test

The plate and stiffener properties of the adequate test plate are repeated in Table 6.9. As discussed, the stiffener in this test was sized so that according to the AASHTO design procedure a nodal line would form along the stiffener and the plate would buckle about the stiffener. The initial imperfection of the adequate test plate was measured using the PDG, and is presented in Figure 6.31. The plate was initially concave down across the width and along the length of the plate.

Table 6.9 Adequate Test Plate Properties

Plate Thickness (in)	w/t	I_s	P_{cr} (kips)
0.1913	76	1.44	84.3

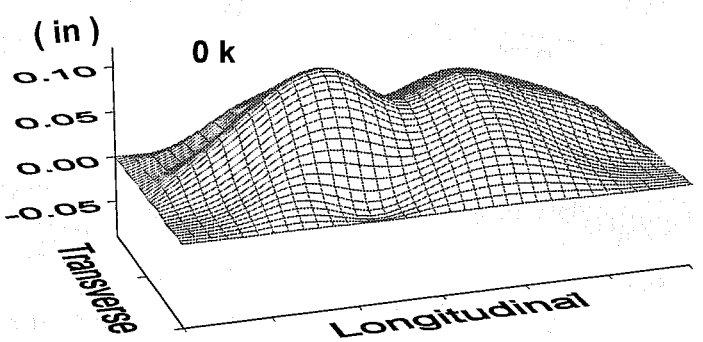

Figure 6.31 Adequate Test - Initial Imperfection

The adequate test plate was loaded and unloaded multiple times. A maximum load of 93 kips was applied to this test plate. The relative plate displacements from a test to 91 kips are presented in Figure 6.32. The eigenvalue buckled shape of the plate is also shown in the figure. The relative displacements show that the stiffener did not remain straight during the test. The maximum plate displacement occurred at the stiffener, along the middle longitudinal line of

the plate. The eigenvalue analyses, and AASHTO design procedure, indicate that a stiffener of this size will form a straight nodal line. However, in the experimental test the stiffener displaced with initial application of load, and continued to displace throughout the test.

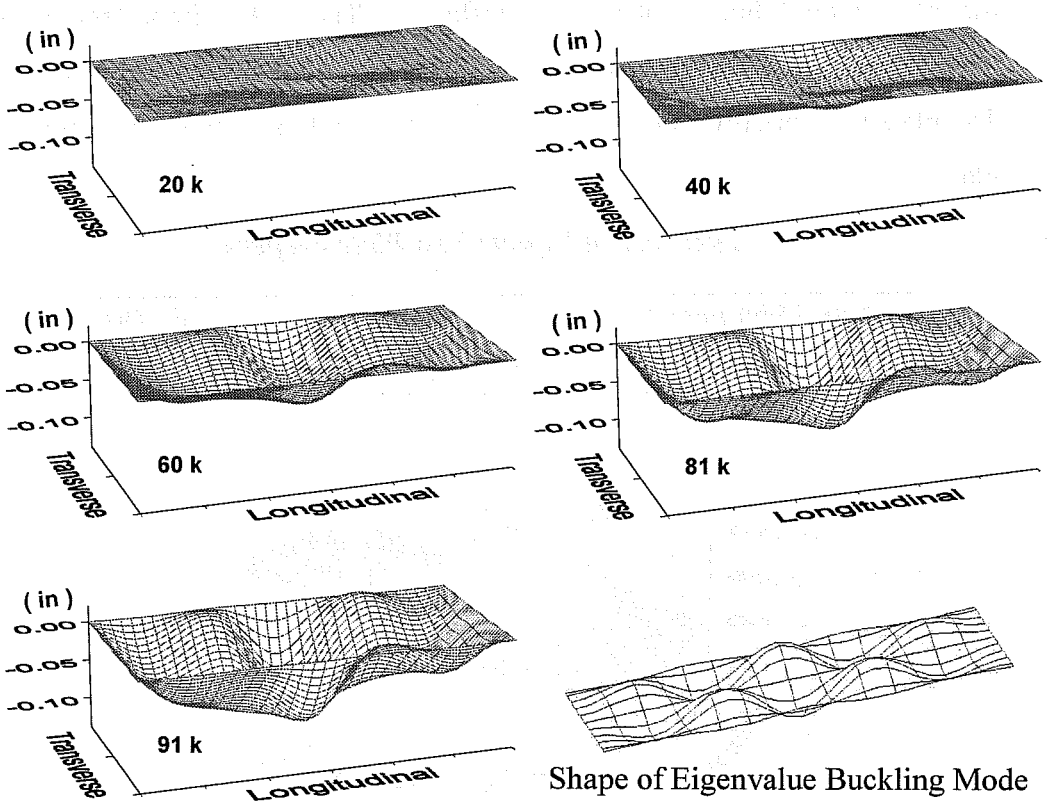

Figure 6.32 Adequate Test - Relative Displacement

The plate deflected in a symmetric shape with maximum displacement at the stiffener. There are five half-waves in the plate on either side of the stiffener. The deflected shape predicted by the eigenvalue analysis shows the stiffener remaining straight, and the plate displacing into an antisymmetric shape with five half-waves on either side of the stiffener. In the test the stiffener moved downward throughout the application of load. As the stiffener displaced, the plate

went into a symmetrical shape, instead of the anti-symmetrical shape predicted by the eigenvalue analysis.

Even though the plate was initially displaced upward, the plate moved downward, opposite the direction of the initial imperfection, throughout the test. The initial imperfection of the plate and the absolute displacement at a load of 91 kips are shown in Figure 6.33. Since the plate moved opposite the direction of the initial imperfection, the absolute displacements at ultimate load are less than the absolute displacement in the initial imperfection. The plate moved downward throughout the application of load for several reasons including the influences of overall girder bending, eccentricity of the stiffener, and second order effects. These factors will be discussed at length in Chapters 7 and 8. The combination of these factors, and particularly overall girder bending resulted in the stiffener displacing downward throughout the test.

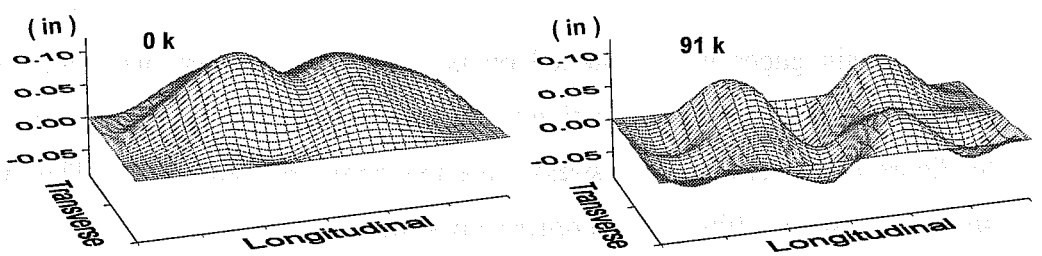

Figure 6.33 Adequate Test - Initial Imperfection and Displaced Shape

Relative plate displacements at Position 5 are presented in Figure 6.34. The plots do note show a distinct buckling load. The plate begins displacing vertically with the initial application of load, and continued moving throughout the test. No significant softening of the load-displacement response is seen at any load level in Figure 6.34.

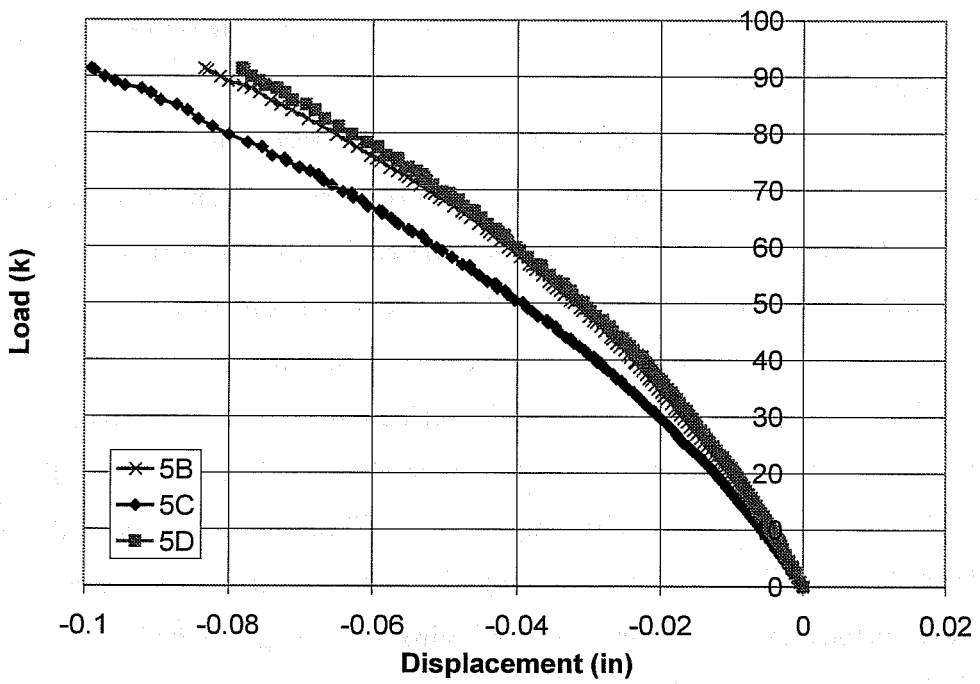

Figure 6.34 Adequate Test - Relative Displacement at Position 5

Strain gages were installed on both sides of the test plate, and on the longitudinal stiffener. The location of the strain gages and their labels are shown in Figure 6.35. The average stresses are presented in Figure 6.36. The average stresses are within 10% of each other across the plate.

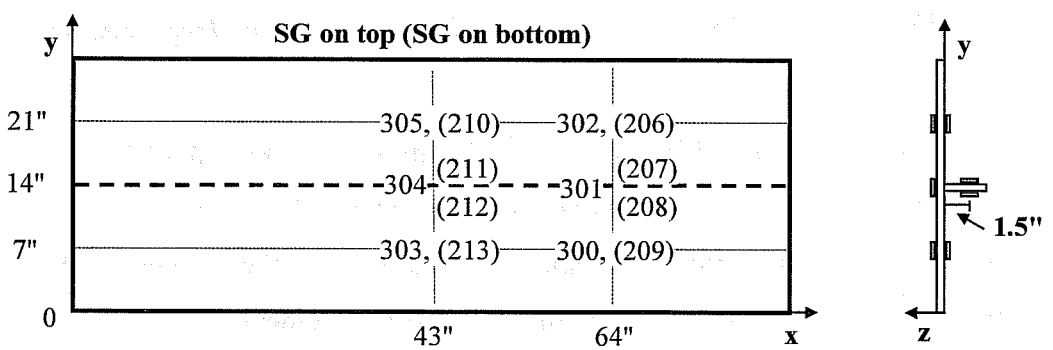

Figure 6.35 Strain Gage Map

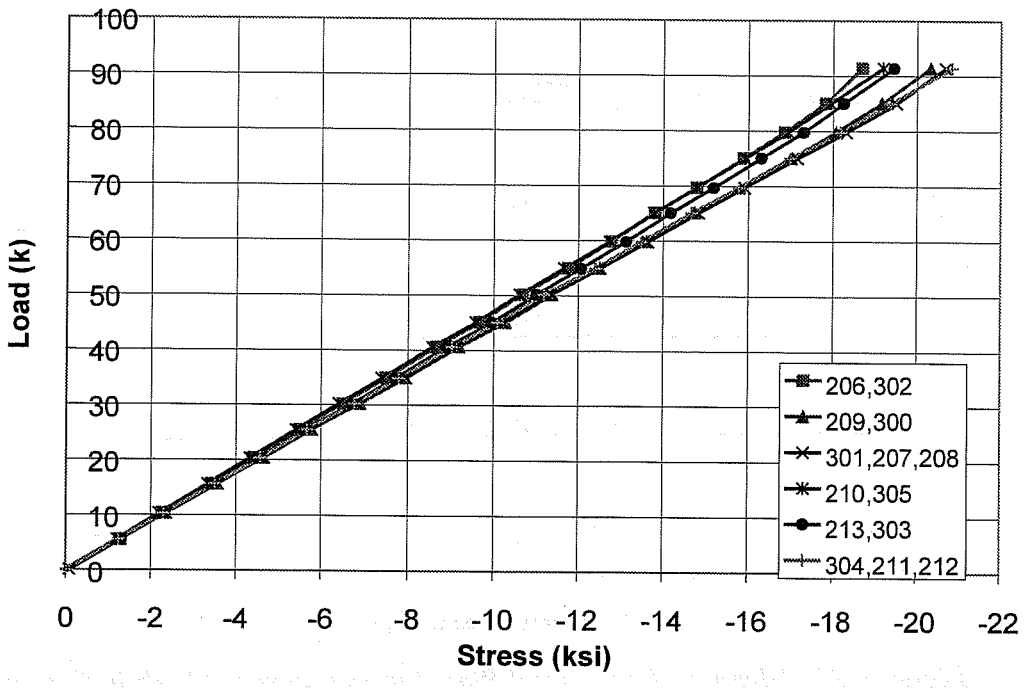

Figure 6.36 Average Stresses

The average plate stress across the width of the plate in the center panel of the plate is shown in Figure 6.37. At low load levels, there is a uniform stress distribution across the width of the plate. As more load is applied, the plate adjacent to the stiffener carries higher stresses. The stiffener was bending in a direction that resulted in compressive bending stresses in the plate adjacent to the stiffener.

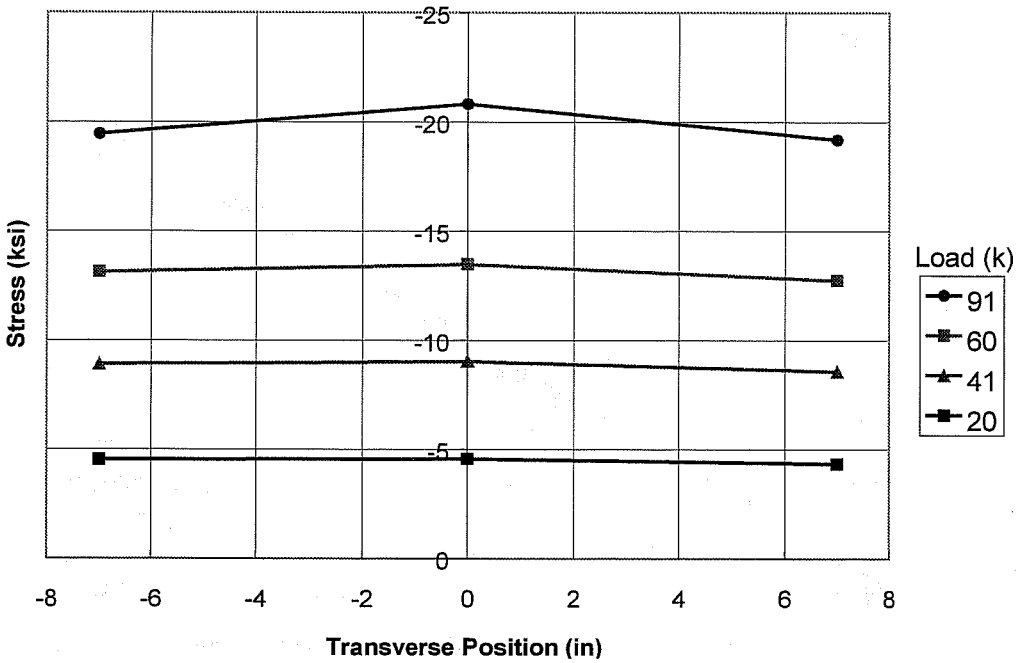

Figure 6.37 Adequate Test - Axial Plate Stresses across Width in Center Panel

The stresses at the stiffener in the center panel are plotted in Figure 6.38. The stresses confirm that the stiffener is bending. The bending of the stiffener unloads the free edge of the stiffener as the girder is loaded. As shown in the relative displacement plots the stiffener displaces downward throughout the test resulting in compressive bending stresses at the welded edge of the stiffener and tensile bending stresses at the free edge of the stiffener.

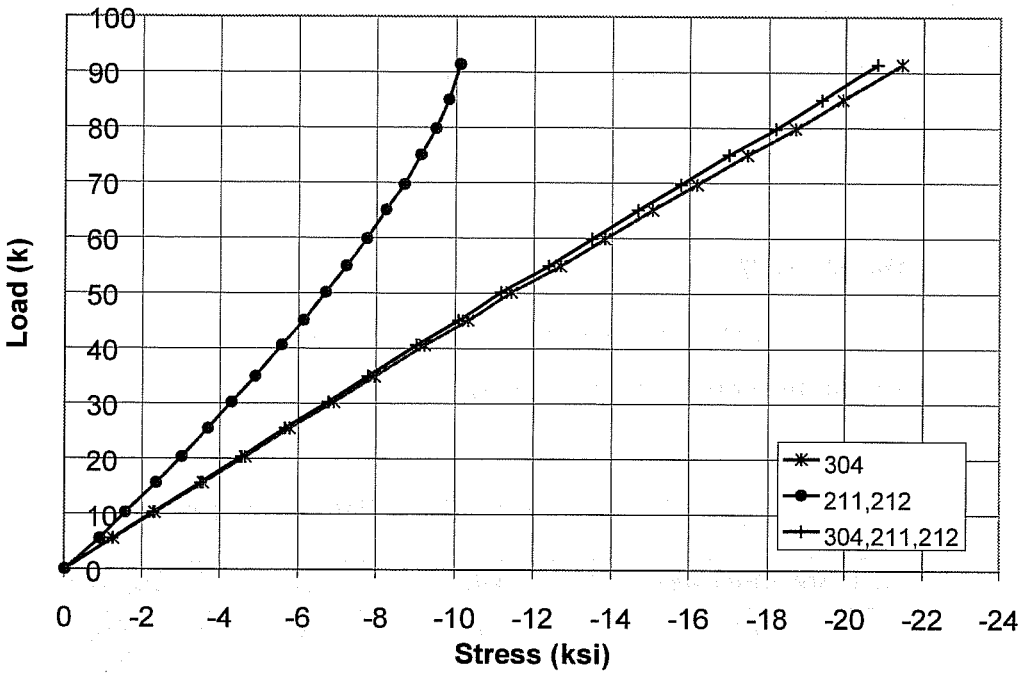

Figure 6.38 Adequate Test - Stresses at Stiffener in Center Panel

6.10.1 Adequate Test Conclusions

The nodal line that was predicted to form along the stiffener by the eigenvalue analysis procedure did not occur. The stiffener displaced downward throughout the application of load due to a variety of effects, including overall girder bending, use of an eccentric stiffener, and second order effects. These factors will be discussed at length in Chapters 7 and 8. The test plate did carry load up to the eigenvalue-buckling load, but did not respond as predicted by the eigenvalue analysis.

Since the stiffener displaced during the test, another stiffener was added to the top surface of the adequate test plate, while it was still in position on the test setup, to see if a larger stiffener moment of inertia would eliminate the

displacement. This test was conducted to see if a larger stiffener would produce a plate response more similar to the eigenvalue analysis, and the assumptions of the AASHTO design procedure.

6.11 Double Stiffener

A second stiffener was added to the top of the adequate test plate. The properties of the double test plate are shown in Table 6.10.

Table 6.10 Double Test Plate Properties

Plate Thickness (in)	w/t	I_s	P_{cr} (kips)
0.1913	76	1.61	90.7

The double test plate was loaded and unloaded several times. A maximum load of 99 kips was applied to the plate. The relative plate displacements from a test to 96 kips are presented in Figure 6.39 and the absolute plate displacements are presented in Figure 6.40. The eigenvalue buckling shape is also shown in Figure 6.39. The shapes of the relative plate displacements are very similar to those seen the adequate test. The magnitude of the relative displacements in the double test is approximately 10% less than those in the adequate test. Maximum plate displacement again occurred along the stiffener, and five half-waves developed along the length of the plate on either side of the stiffener. The eigenvalue buckling shape predicted no displacement at the stiffener, and five half-waves in the plate on either side of the stiffener.

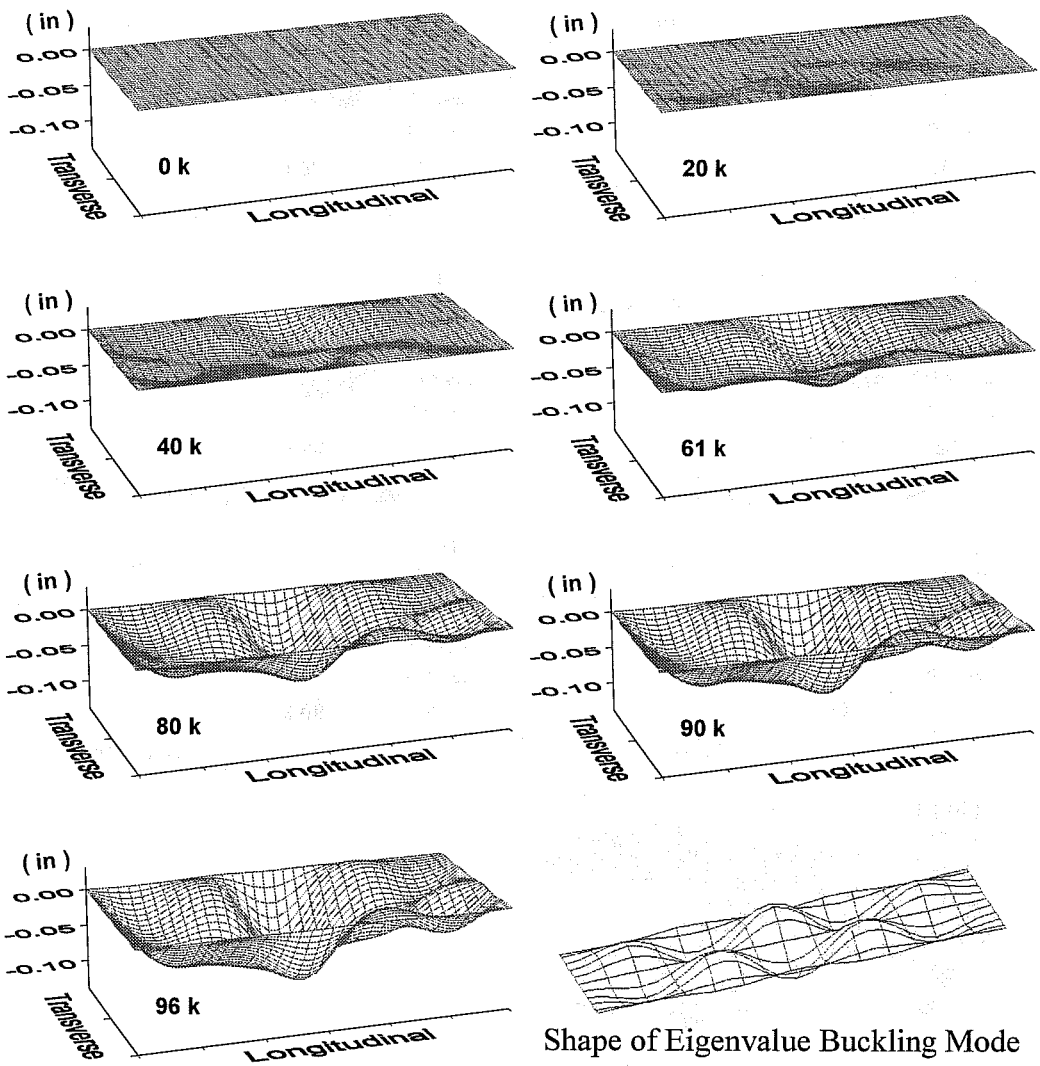

Figure 6.39 Double Test - Relative Displacement

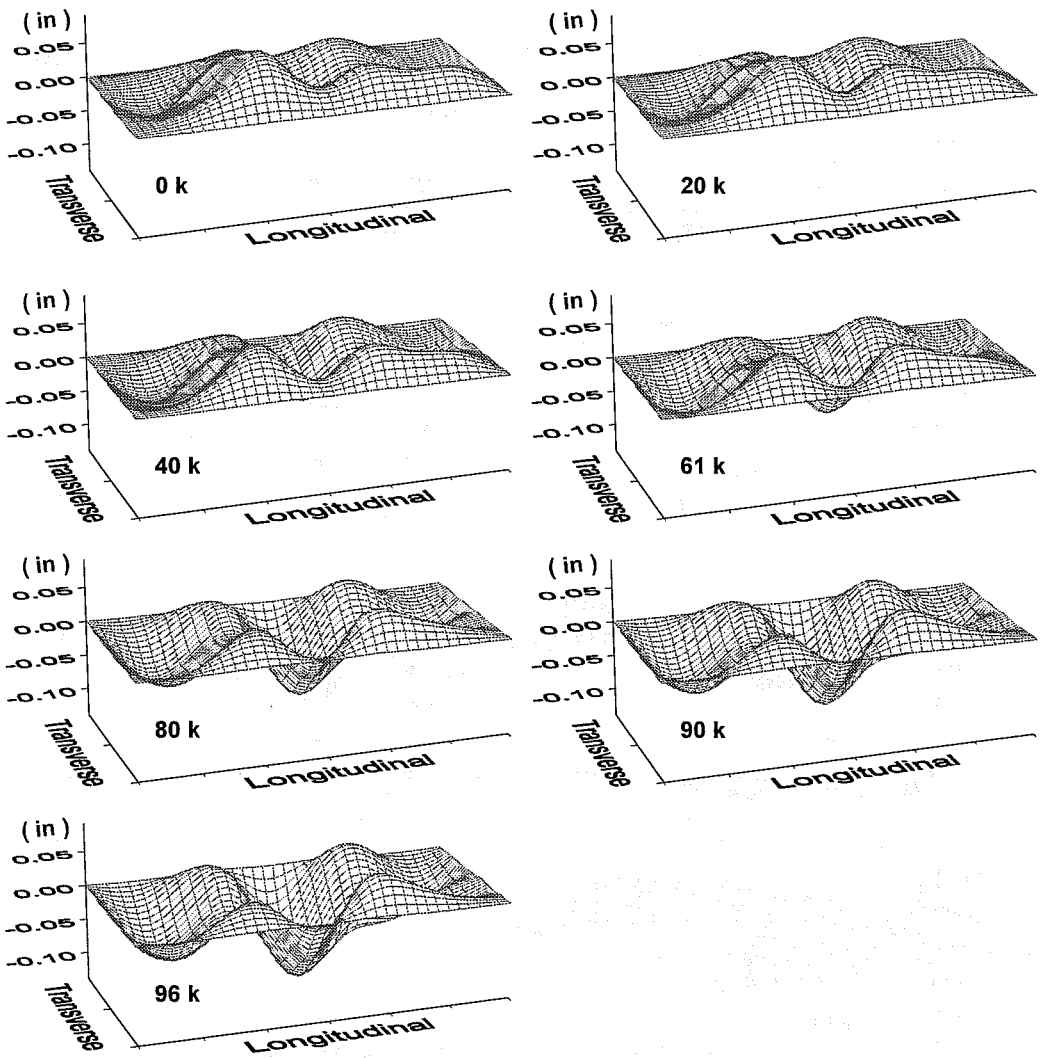

Figure 6.40 Double Test - Absolute Displacement

The initial imperfection of the plate is shown at 0 kips load in Figure 6.40. The plate was concave down over much of its length, and had positive absolute displacements across most of the length and width of the plate. As was seen in the adequate test, the relative displacements of the plate are opposite the direction of the initial imperfection. As the relative displacements show, the stiffener

moves downward throughout the test. The original stiffener on the bottom of the test plate is larger than the second stiffener added to the top of the test plate. Consequently, the effect of the eccentric stiffener, as well as overall girder bending, still tends to pull the stiffener downward throughout application of load.

Load vs. displacement plots from the double test show no noteworthy differences from the adequate test. The plots do not show a buckling load or softening of the response at a specific load level. The plate and stiffener began displacing with the initial application of load, and continued moving throughout the test.

The strain gage data collected in the double test also did not show any significant differences from that in the adequate test. The stresses were again fairly uniform across the plate's surface, particularly at lower loads. As more load was applied, and the stiffener was bending more significantly, the stresses at the plate adjacent to the stiffener were slightly higher than stresses in the plate away from the stiffener. The relative displacement of the plate shows that the stiffener was displacing downward, and bending of the stiffener contributed to the development of larger compressive stresses in the area of the plate adjacent to the stiffener.

6.11.1 Double Test Conclusions

Even with the addition of a second stiffener to the test plate, a nodal line did not form along the stiffener. The stiffener again displaced downward throughout the test. The original stiffener on the bottom of the test plate was larger than the second stiffener added to the test plate. The effects of girder bending and the eccentric stiffener again resulted in the stiffener displacing downward throughout the test. Multiple factors contributing to stiffener displacement were identified and are discussed in Chapters 7 and 8.

6.12 Angle Test

The properties and eigenvalue-buckling load of the angle test plate are shown in Table 6.11. The initial imperfection of the plate is presented in Figure 6.41. As in the previous tests, the plate was initially concave down along the length and across the width of the plate. The angle test plate was loaded and unloaded several times, to a maximum load of 125 kips. The relative plate displacements from a test to 99 kips are presented in Figure 6.42. The shape of the eigenvalue buckling mode is also shown in this figure.

Table 6.11 Angle Test Plate Properties

Plate Thickness (in)	w/t	I_s	P_{cr} (kips)
0.2018	72	0.989	122

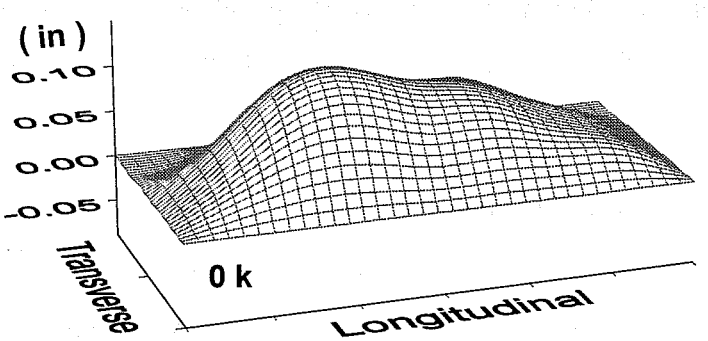

Figure 6.41 Angle Test - Initial Imperfection

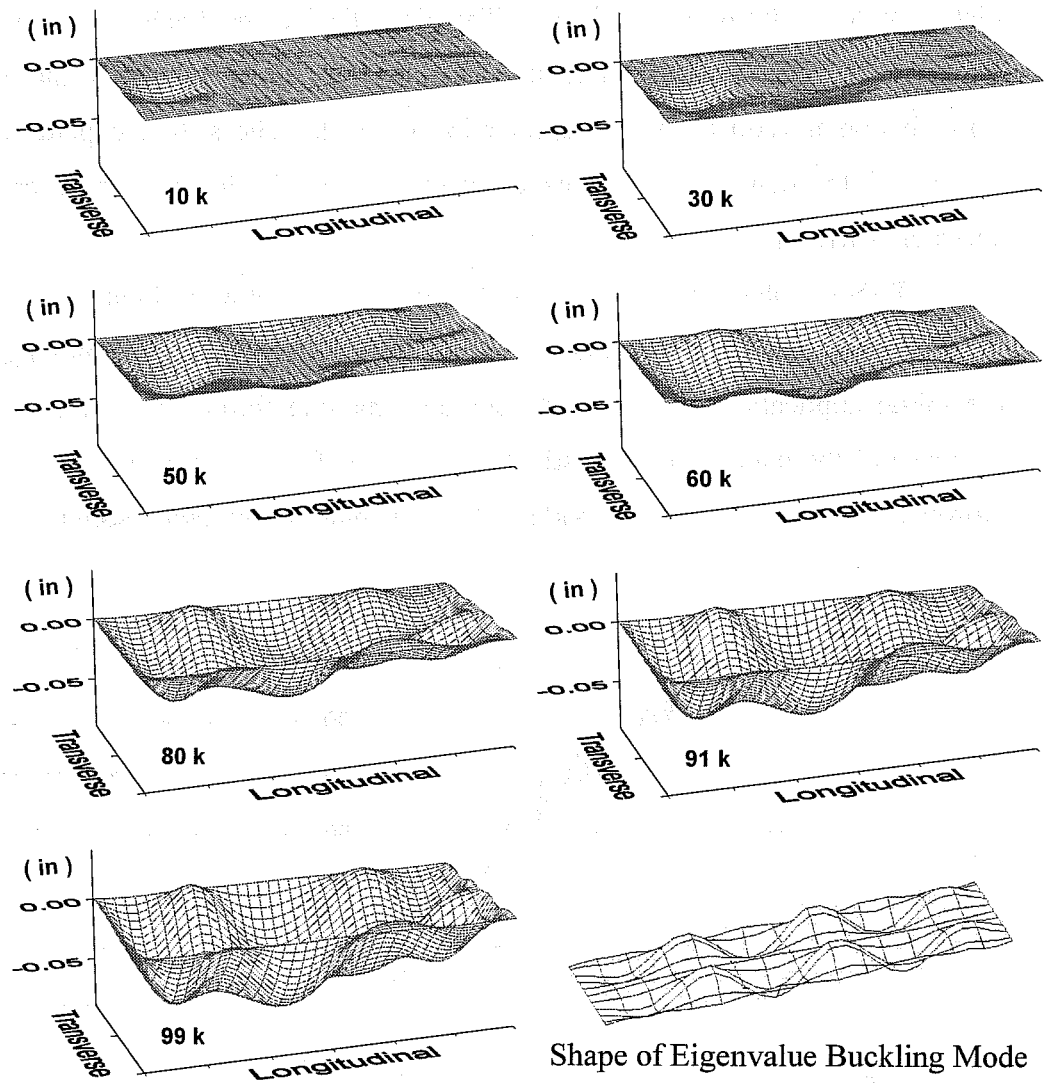

Figure 6.42 Angle Test - Relative Displacement

The shapes of the relative plate displacements in Figure 6.42 are very similar to those in the preceding two tests, but the magnitude of the displacement is less. The relative plate displacements show five half-waves on either side of the stiffener, as was seen in the adequate and double tests. The displaced shape over most of the plate is symmetric, but is anti-symmetric at the right end of the

plate next to the transverse stiffener. The plate displacement again is opposite in direction to that of the initial imperfection, or in other words the initial imperfection is reduced by the application of load. The stiffened plate moves downward throughout the test as a result of overall girder bending and the eccentric stiffener.

Relative plate displacements at Position 5 are plotted in Figure 6.43. The plots again do not show a distinct buckling load. The plate begins moving with the initial application of load, and continued moving throughout the test. The response of the plate is initially stiffer, and then softens as more load is applied. However there is not a distinct load at which the plate significantly softens.

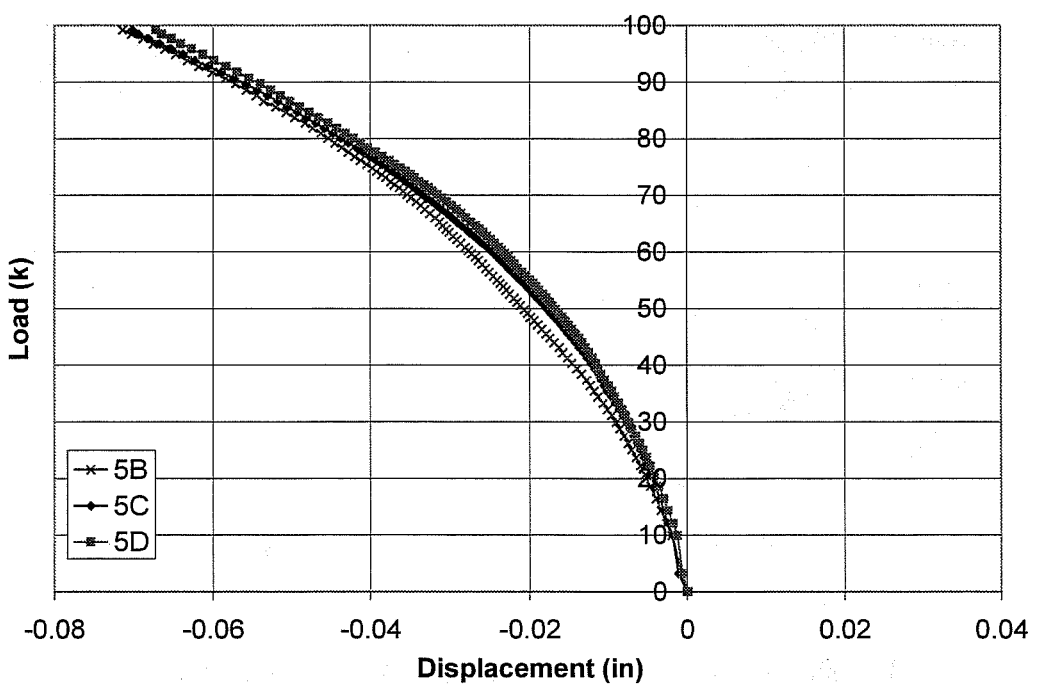

Figure 6.43 Angle Test - Relative Displacement at Position 5

No significant difference was seen in the load-stress response in the angle test compared to that in the adequate plate test. The plate stresses increased linearly with the application of load to the test setup. The stress distribution through the depth of the stiffener confirmed the fact that the stiffener was bending and displacing downward during the test, unloading the free edge of the stiffener.

The stress distribution across the width of the plate was uniform at low loads. At higher loads, the stress in the plate was slightly larger adjacent to the stiffener, due to the stiffener's participation in carrying the applied load and the compressive bending stresses generated in the plate as the stiffener displaced.

6.12.1 Angle Test Conclusions

As in the preceding tests, the stiffener did not remain straight during the test. The plate and stiffener began displacing vertically with the initial application of load, and continued moving throughout the test. The stiffener displaced downward throughout the test, reducing the initial imperfection of the plate. The magnitude of the displacement in the angle test was less than that of the adequate and double tests.

6.13 Concrete Stiffener

The final test plate had a concrete stiffener that was cast-in-place on the top surface of the test plate. As previously discussed, the stiffener was cast-in-place on the test plate to ensure the stiffener was not cracked during installation of the test plate. The properties of this test plate are shown in Table 6.12.

Table 6.12 Concrete Stiffened Test Plate Properties

Plate Thickness (in)	w/t	I_s	P_{cr} (kips)
0.1901	76	14.9	130

The initial imperfection of the test plate, after casting and curing of the stiffener, is shown in Figure 6.44. The plate was initially concave down over most of its length, but was slightly depressed at the upper left of the test plate. The plate was loaded and unloaded several times to the 50 kips load level. The plate responded elastically up to this load level, and returned to its initial condition when unloaded. The plate was then loaded to approximately 68 kips. In this test, the displacements along two transverse lines of potentiometers began showing a marked change in their load-displacement response, and the girder was unloaded. The girder was then loaded to 119 kips and then unloaded.

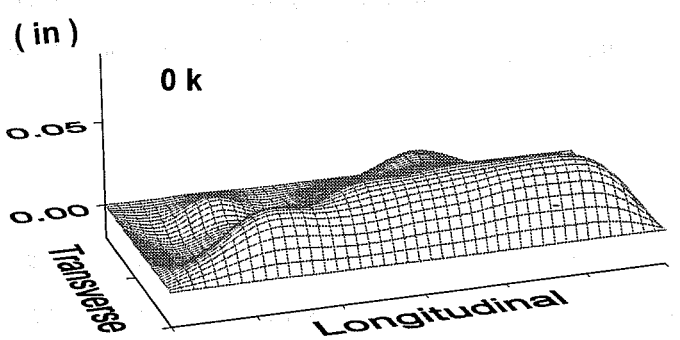

Figure 6.44 Initial Imperfection

The relative displacements from the test to 119 kips are shown in Figure 6.45. The displaced shape of the plate does not look at all like the buckled shape predicted through the eigenvalue finite element analysis. The extreme difference in the displaced shape is due to the large displacement along the stiffener. The

stiffener displaced upward throughout the test. As discussed, the plate was initially bowed up along its length and the stiffener was cast on the top surface of the plate. The initial imperfection was amplified as load was applied, since the stiffener was on the top surface of the plate and as the stiffener was bent, the plate was pulled up.

The final relative displacement of the plate at no load is also shown in Figure 6.45. Unlike previous tests, the test plate did not return to its original position after the test. The fact that the plate did not return to its initial position after testing is attributed to micro-cracking of the stiffener. There was no visible cracking of the stiffener since it was well reinforced, but the strain gages revealed that the concrete stresses exceeded the tensile capacity of the concrete, as will be discussed. The strain gages showed micro-cracking of the stiffener in the end panel of the plate when the applied load was approximately 80 kips.

Relative plate displacements at Position 5 are presented in Figure 6.46. The load displacement response at Position 5 is quite linear throughout the test. The displacements at Position 5 do not show the non-linear behavior found in the specimens with steel stiffeners. The response is dominated by bending of the large concrete stiffener. As was seen in the other tests, the plate and stiffener began moving with the initial application of load and continued displacing throughout the test.

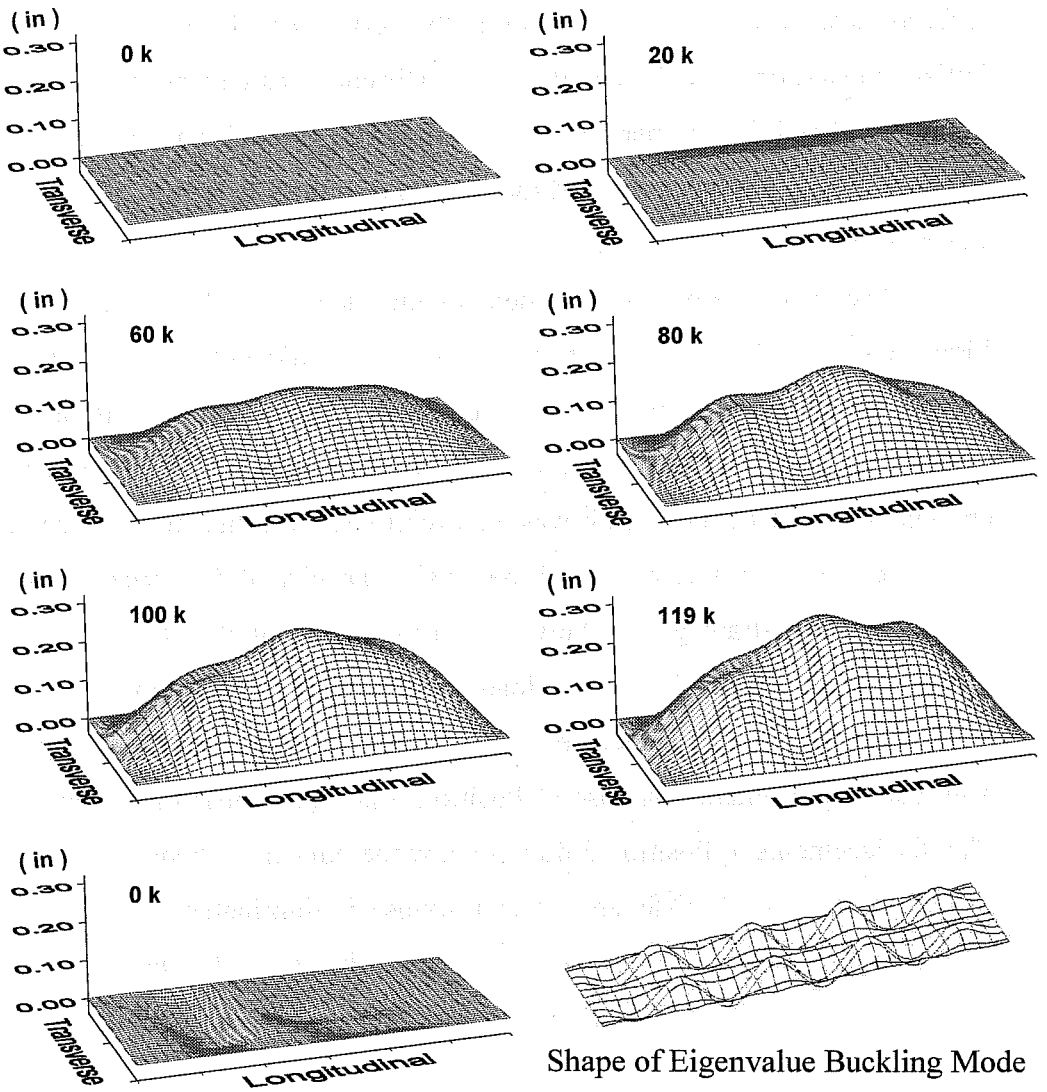

Figure 6.45 Concrete Stiffener Test - Relative Displacement

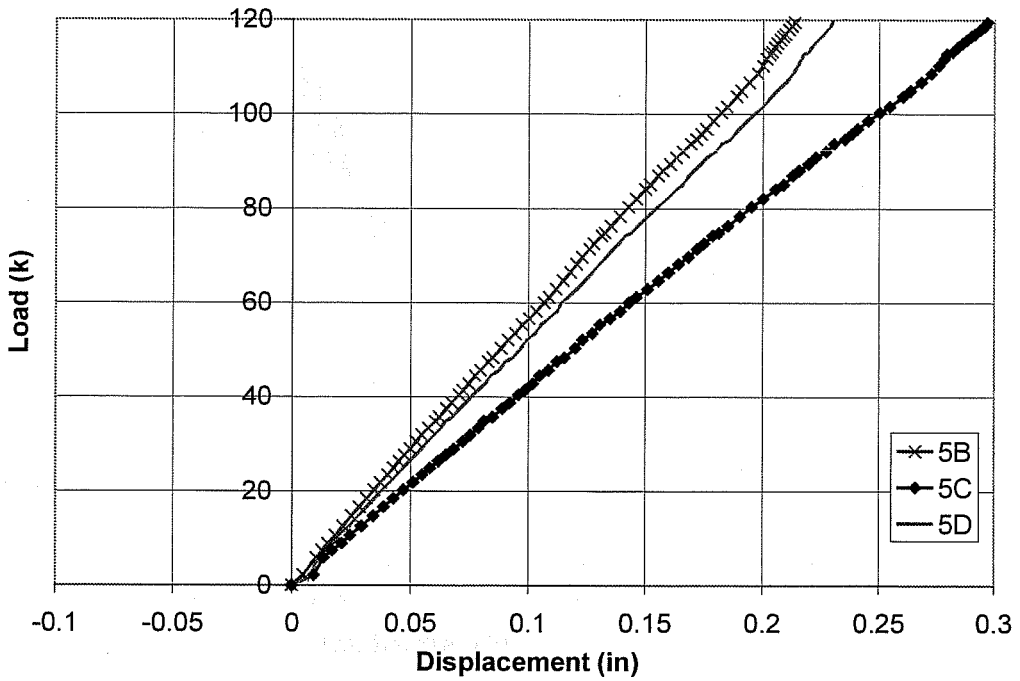

Figure 6.46 Concrete Test - Relative Displacement at Position 5

Relative displacements at Position 3 are presented in Figure 6.47. There is a marked change in the load-displacement behavior at a load of about 84 kips. The response becomes much stiffer at this transverse location, and then softens again at a load of approximately 100 kips. Micro-cracking of the stiffener occurred around 80 kips of load. After the stiffener began cracking, the plate displaced more locally in the center panel of the plate while not displacing as much in the end panel at Position 3. As this occurred, there was an apparent local stiffening of the load-displacement response in the end panel. Above the 100 kip load level, the measured strains indicate that micro-cracking was occurring both in the end panels and center panel. Above this load level the displacements in the end panel at Position 3 began growing again.

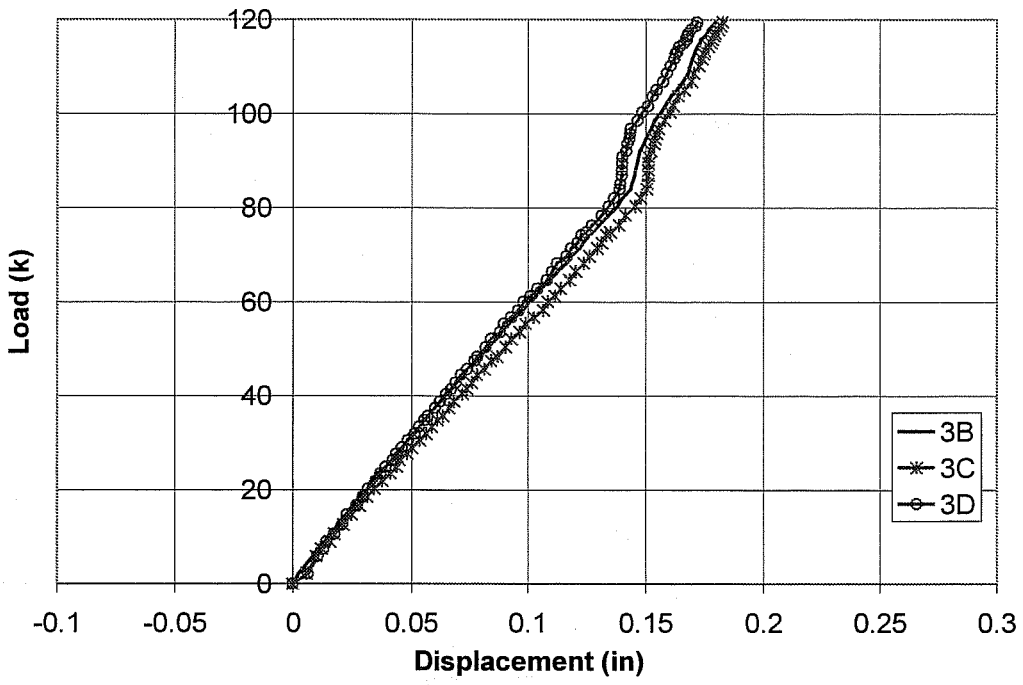

Figure 6.47 Concrete Test - Relative Displacement at Position 3

Strain gages were installed on both sides of the test plate, and on the concrete stiffener. The locations of the strain gages and their labels are shown in Figure 6.48 and Figure 6.49.

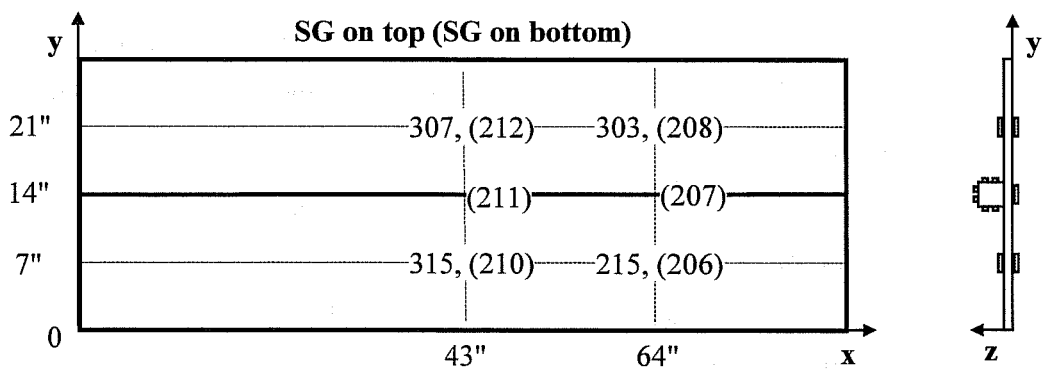

Figure 6.48 Strain Gage Map

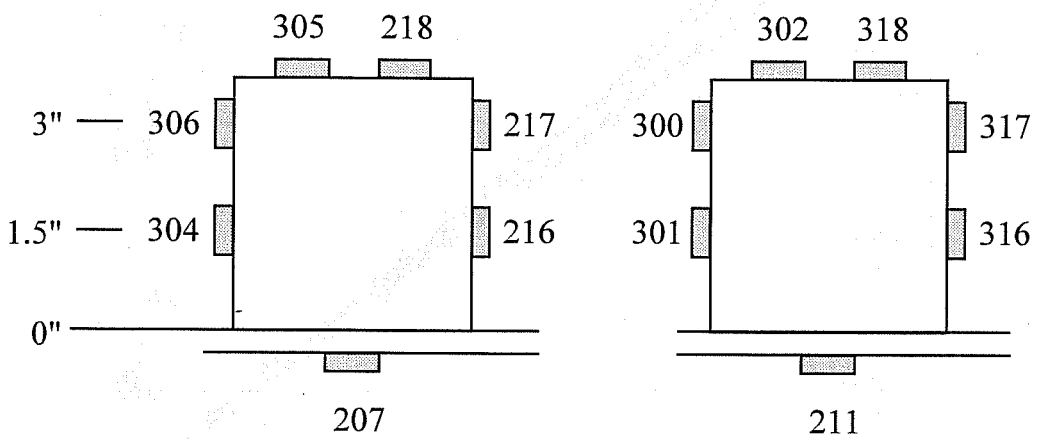

Figure 6.49 Strain Gages on Concrete Stiffener

The load-stress response of gages in the end panel is shown in Figure 6.50. The plate stresses are linear up to a load of approximately 100 kips. The stresses for just the stiffener at this location are repeated in Figure 6.51. The load-stress response is linear up to a load of approximately 80 kips. When the applied load was about 82 kips, the stiffener cracked. The concrete stiffener was mounted on the top surface of the plate, and the plate was displacing upward during the test. The top surface of the stiffener went into tension as a result of the bending, and the stiffener cracked at this location at a load of approximately 82 kips. No visible cracking was seen, since the stiffener was well reinforced. But the strain gages indicated that micro-cracking was occurring by increases in apparent tensile strain. Local changes in plate displacement response support the fact that the stiffener was cracking. The average stress on the top of the stiffener when micro-cracking began was about 640 psi. Results from split cylinder tests predicted the concrete would crack at approximately 510 psi.

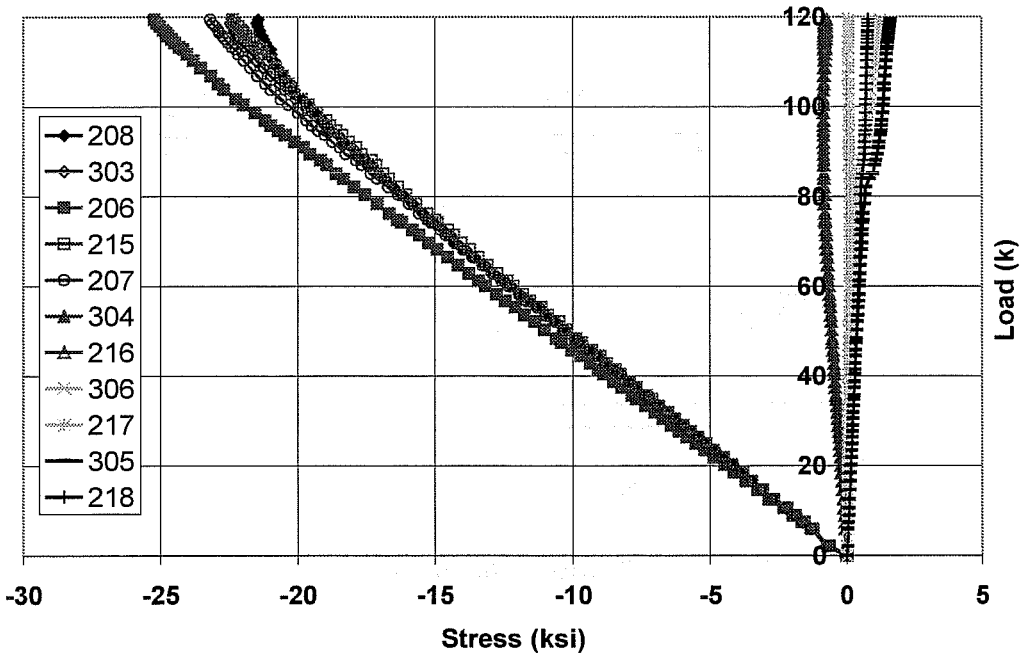

Figure 6.50 Concrete Test - Stress in End Panel

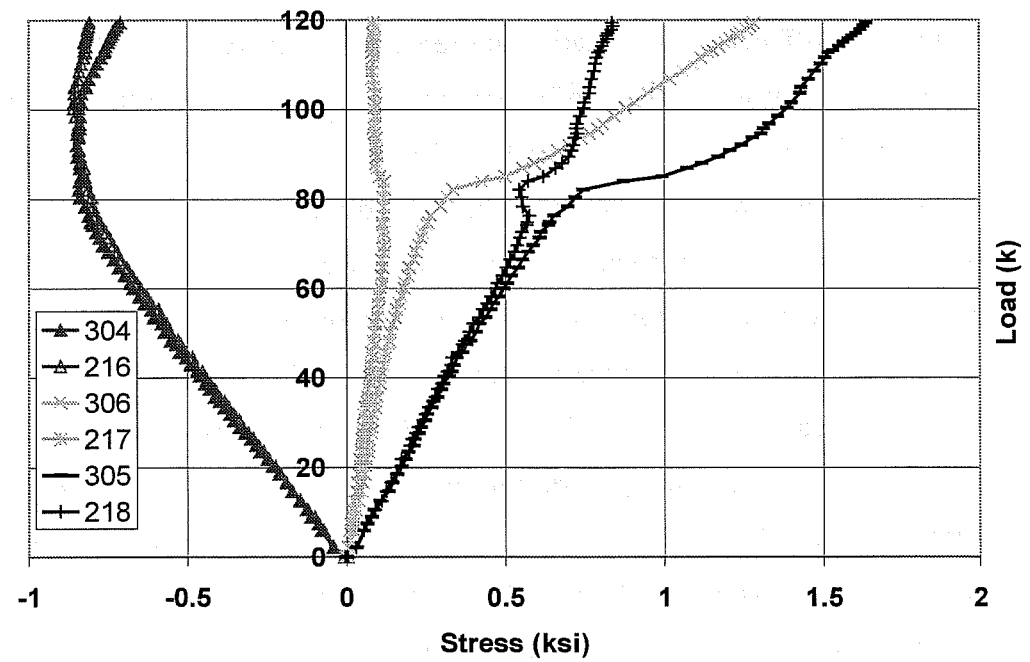

Figure 6.51 Stress in Stiffener in End Panel

The strains through the depth of the stiffener were plotted and are shown in Figure 6.52. The bottom surface of the plate is at the 0 in. vertical location, and the fee end of the stiffener is at a vertical location of 3.81 in. The strains show that the neutral axis is initially at approximately 2.9 in. The neutral axis does not begin moving until the applied load exceeds 80 kips. When the applied load was approximately 80 kips, the stiffener cracked. At this point, the neutral axis began moving down, towards the test plate. This change in strain behavior was accompanied by changes in displacement behavior, as already discussed regarding the apparent local stiffening in the end panel of the test plate.

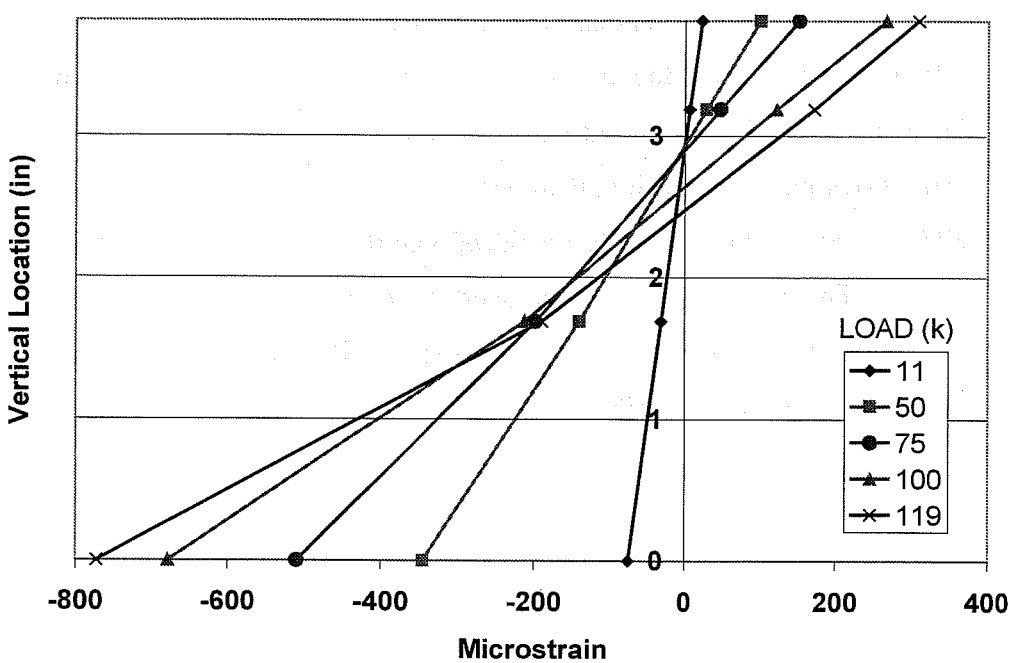

Figure 6.52 End Panel Stiffener Strains Through Depth

The load-stress response of the strain gages mounted in the center panel indicates the same general response as those in the end panel. The only notable difference is the load at which the stiffener cracked is higher at this location. The concrete gages mounted above mid-depth of the stiffener showed a marked change in behavior as the stiffener cracked at a load of about 110 kips. The stress at the top of the stiffener was approximately 630 psi when the applied load was 110 kips. Micro-cracking began in the end panel at approximately the same stress level of 640 psi.

6.13.1 Concrete Test Conclusions

As in the previous tests, the stiffener did not remain straight during the test. In this test, the situation was complicated even further by the fact that the stiffener was cast on the top surface of the plate, and the plate was initially displaced upward in the middle of the plate. Since the stiffener was not straight prior to testing, and the initial imperfection of the plate was in the direction of stiffener movement, the plate displaced significantly from the initial application of load. The bending stresses unloaded the free edge of the stiffener, and the top surface of the concrete eventually went into tension. The tensile stresses exceeded the tensile capacity of the stiffener, and the stiffener cracked.

Chapter 7

Analysis of Test Results

7.1 Displacement of Longitudinal Stiffener

The basis of the AASHTO design procedure for plates with longitudinal stiffeners is an assumption that adequate stiffeners form straight nodal lines about which the plate buckles. This is the same response seen in eigenvalue analyses of adequately stiffened plates. The results of the experimental testing program showed that the stiffeners did not remain straight under load. The stiffeners moved throughout the test, and the largest displacements occurred at the stiffeners. Several factors contributed to the stiffener movement, including initial imperfections, overall girder bending and second-order effects.

7.2 Initial Imperfections

The initial imperfections affected the response of the test plates, especially when the tendency for stiffener displacement was in the direction of the initial imperfection. The initial imperfection of each test plate was measured with the test plate installed on the box girder. Initial imperfection tolerances contained in various codes were discussed at length in Chapter 2. The initial imperfections of the test plates are compared to some of the tolerances described in Chapter 2 in the following discussion.

The impact of imperfections is directly tied to their magnitude. To be able to reuse the existing test setup, thin test plates, that would buckle elastically at relatively low buckling loads, were used. Use of the thin plates and welded stiffeners resulted in significant initial imperfections of the test plates. However, as will be shown the imperfections were well within code requirements and

proposed tolerances. Furthermore, the imperfections are comparable with those measured in previous plate research (Yen 1966a, Yen 1966b, Mueller 1967). Response of compression flanges with levels of imperfection similar to those of the test plates is consequently important and should be addressed.

7.2.1 Application of Out-of-Flatness Requirements to Test Plates

Prior to fabrication, the initial imperfection of the test plates was measured using a straightedge. The maximum deviation from the straightedge was on the order of 1/16 in. for each of the test plates. Welding of stiffeners to the test plate increased the initial imperfection of the test plate. Installation of the test plates onto the test setup also increased the out-of-flatness of the test plates. The test plates were bolted on all four edges to attach them to the test setup. As discussed in Chapter 5, the nuts for each bolt were welded in place, which reduced the dimensional tolerance at each hole. Consequently, each test plate had to be worked with a spud wrench and selective tightening of bolts to push and pull the test plate into place. Forcing the test plates into position altered the out-of-flatness of the test plates.

The initial imperfections of the test plates were compared to the tolerances of ASTM A6, the AWS D1.5 out-of-flatness requirements for webs with no intermediate stiffeners, and a tolerance of b/200 (or w/200). The prescribed tolerances are based on panel measurements. Therefore the method of checking the imperfection is as shown in Figure 7.1. For unstiffened plates the plate out-of-flatness between the webs of the box girder is measured. For stiffened plates, the plate out-of-flatness between stiffeners, or web and stiffener, is measured. The out-of-flatness of the inadequately stiffened test plates, which were expected to buckle in a mode similar to that of the unstiffened plate, were compared to both the b/200 and w/200 limit.

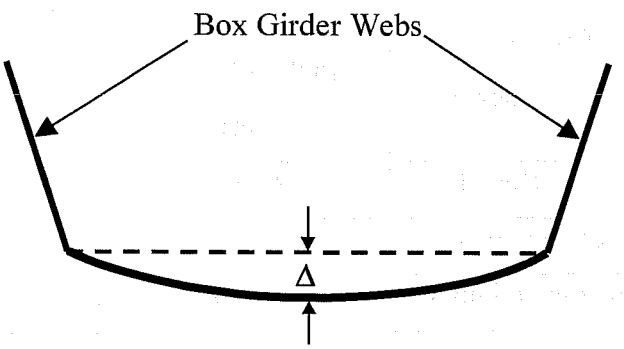

Imperfection Compared to b/200

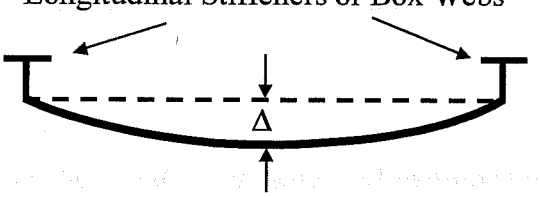

Imperfection Compared to w/200

Figure 7.1 Imperfection Tolerances

The variations from flatness of the inadequately stiffened plates are presented in Table 7.1. The maximum variation from flatness was 54% of the plate thickness and occurred in the unstiffened test.

Table 7.1 Inadequately Stiffened Test Plates - Variation from Flatness

Test Plate Stiffener	Variation from Flat (in)	Variation as % of Plate Thickness (%)
Unstiffened	0.102	54
Inadequate Up	0.086	43
Inadequate Down	0.087	43

The maximum measured out-of-flatness is shown with the ASTM A6, AWS D1.5, and the b/200 limit in Table 7.2. The maximum measured out-of-flatness was substantially less than the ASTM A6 tolerance, and significantly less than the AWS D1.5 tolerance. The out-of-flatness is about 30% less than the b/200 limit.

Table 7.2 Inadequately Stiffened Plate Out-of-Flat vs. Allowable Tolerances

Out-of-Flatness	(in)
Maximum Measured in Tests	0.102
ASTM A6	0.84
AWS D1.5	0.187
b/200 Tolerance	0.145

Some fabricators have advocated application of the ASTM A6 tolerances to the fabricated unit. The data in Table 7.2 shows that the tolerance of ASTM A6 is much more liberal than that of the other tolerances under consideration. The ASTM A6 tolerance permits very large imperfections, in this case over four times the plate thickness, for slender plates.

The variations from flatness of the stiffened test plates are presented in Table 7.3. The maximum variation from flatness was 24% of the plate thickness and occurred in the double test. The maximum out-of-flatness is shown with the w/200 tolerance in Table 7.4. The maximum measured out-of-flatness was well beneath the w/200 limit.

Table 7.3 Stiffened Test Plate Variation from Flatness

Test Plate Stiffener	Variation from Flat (in)	Variation as % of Plate Thickness (%)
Inadequate Up	0.043	21
Inadequate Down	0.042	21
Adequate	0.036	19
Double	0.046	24
Angle	0.038	19
Concrete	0.042	21

Table 7.4 Stiffened Test Plate Out-of-Flatness vs. Allowable Tolerances

Out-of-Flatness	(in)
Maximum Measured in Tests	0.046
w/200 Tolerance	0.073

7.2.2 Application of Out-of-Flatness Requirements to Houston Bridge

For comparison, the permitted variations from flatness for the bottom flange plates of a box girder bridge constructed in Houston, Texas were

computed. A WT longitudinal stiffener was used on the bottom flange in the negative moment region of this bridge. The thickest bottom flange plate was located at interior piers. The thinnest flange plates were located in the positive moment region of the bridge. The variations from flatness tolerances calculated based on the width of the plate, b, for the unstiffened plate sections are presented in Table 7.5. For the bottom flange plates with a longitudinal stiffener, the permitted variations from flatness based on stiffener spacing are presented in Table 7.6. Both tables show the permitted variations from flatness in inches and as a percentage of the plate thickness.

Table 7.5 Permitted Variation from Flatness - Plate Width Tolerance

Flange Thickness	ASTM A6		AWS D1.5 b/150		b/200	
(in)	(in)	(%)	(in)	(%)	(in)	(%)
0.75	5/8	83	0.52	70	0.39	52
1	9/16	56	0.52	52	0.39	39

Table 7.6 Permitted Variation from Flatness Between Stiffeners

Flange Thickness	w/200	
(in)	(in)	(%)
1-1/2	0.20	13
1-5/8	0.20	12
2-3/4	0.20	7.3

The smallest allowable out-of-flatness requirement is provided by the proposed w/200 limit for the 2-3/4 in. thick flange plate. The maximum

permissible variation for this plate is 7.3% of the plate thickness. The largest permissible variation is the ASTM requirement of 83% of the plate thickness for the 3/4 in. thick flange plate. The permitted variations of the test plates as a percentage of the plate thickness fall within the range of permitted variations presented in Table 7.5 and Table 7.6. The permitted variations from flatness for the stiffened bridge flanges are smaller than those of the test plates used in the experimental program, particularly for the 2-3/4 in. thick plate. However, the 2-3/4 in. plate with a longitudinal stiffener was actually designed with an inadequate stiffener, and it is questionable to apply the tolerance based on measurements between stiffeners to this case. In general, the imperfection allowance for thicker plates as a percentage of the plate thickness is somewhat smaller than that allowed for thinner plates.

7.2.3 Application of Straightness Tolerances to Longitudinal Stiffeners

For the plate stiffeners used in this study, the permitted variation in straightness, or camber, based on ASTM A6 is 1/8 in. times the length of the plate in feet divided by 5, or L/480. A more conservative limit of L/500 has been applied to longitudinal stiffeners of box girder bottom flanges, as discussed in Chapter 4. For the 84 in. long stiffeners, the L/500 tolerance results in a permitted camber of 0.168 in. The out-of-straightness of the in-place stiffeners used in the test program, are presented in Table 7.7. The maximum out-of-straightness was 0.112 in. in the angle test, which is well below the L/500 tolerance. The initial imperfections of both the plates and stiffeners are well within the prescribed tolerances.

Table 7.7 Stiffener Out-of-Straightness

Test Plate Stiffener	Variation from Flat (in)	L/500 Tolerance (in)
Inadequate Up	0.086	0.168
Inadequate Down	0.087	
Adequate	0.111	
Double	0.070	
Angle	0.112	
Concrete	0.053	

7.3 Factors Contributing to Stiffener Displacement

Several factors contributed to the stiffener displacement observed in the experimental program including initial imperfections, girder bending, and the eccentricity of boundary stresses on the stiffener.

7.3.1 Initial Imperfections

The magnitude of the test plates' initial imperfections and tolerances on these imperfection have been discussed. The tendency of an initially imperfect member in compression is for growth of the initial imperfection. All of the test plates were initially displaced upward, away from the interior of the box, over the majority of the plate. In the absence of other factors, when a compressive load is applied to the test plate and stiffener, the plate and stiffener will displace upwards, away from the interior of the box. As the stiffener bends, second order effects cause further increases in stiffener bending, increasing the displacement of the plate and stiffener away from the interior of the box girder.

7.3.2 Girder Bending

Another significant factor that contributes to the stiffener displacement is girder bending. The test plate is a component of a box girder. Bending of the girder in the test setup puts the upper portion of the girder, and the test plate, into compression. The loading applied to the test setup resulted in a uniform bending moment region in the area where the test plate was installed. When a bending moment is applied to an ideal girder section the girder will displace as shown in Figure 7.2. At mid-length of the girder, the compression plate of the girder moves down, towards the interior of the box. The stiffener will be bent as shown in the figure due to the girder bending effect. Second order effects cause the bending of the stiffener to increase, increasing the displacement of the stiffener and test plate towards the interior of the box girder.

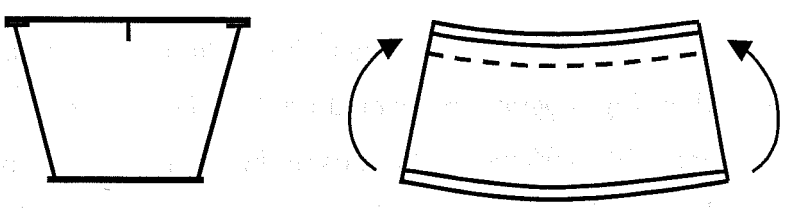

Figure 7.2 Girder Bending Effect

In a bridge girder structure, the steel compression flange is on the bottom of the box, and is in compression in the negative moment region of the structure. This situation can be pictured simply by flipping Figure 7.2 about a horizontal axis. The same resultant effect, movement of the compression flange towards the interior of the box girder, results.

An additional influence tied to the girder bending effect relates to the moment of inertia of the girder cross section. If the test plate displaces away from the interior of the box, as shown on the left in Figure 7.3, the girder moment of

inertia, I_x, is increased. If the test plate displaces towards the interior of the box, the girder moment of inertia is reduced. Displacements that result in an increase in stiffness are resisted. Thus displacement of the test plate away from the interior of the box is resisted.

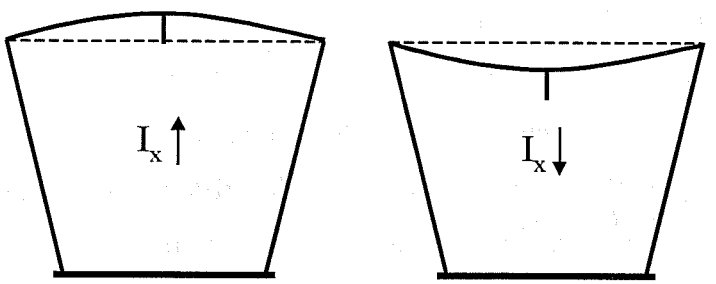

Figure 7.3 Effect of Displacement on Box Girder Moment of Inertia

7.3.3 Eccentricity of Boundary Stresses

Another factor that possibly contributed to stiffener displacement in the experimental testing program, but would not be a factor in box girder bridges, is the termination of the stiffener at the ends of the test region. In box girder bridges the longitudinal stiffener is not terminated in critical regions of the compression flange, so this effect is not a potential concern for box girder design.

The longitudinal stiffener was not continued through the transverse stiffeners that defined the boundaries of the test plate. The longitudinal stiffener was terminated at the location of the transverse stiffeners. The first picture in Figure 7.4 shows the longitudinal stiffener and test plate. The test region of the plate was located between the transverse stiffeners shown in the second picture in Figure 7.4.

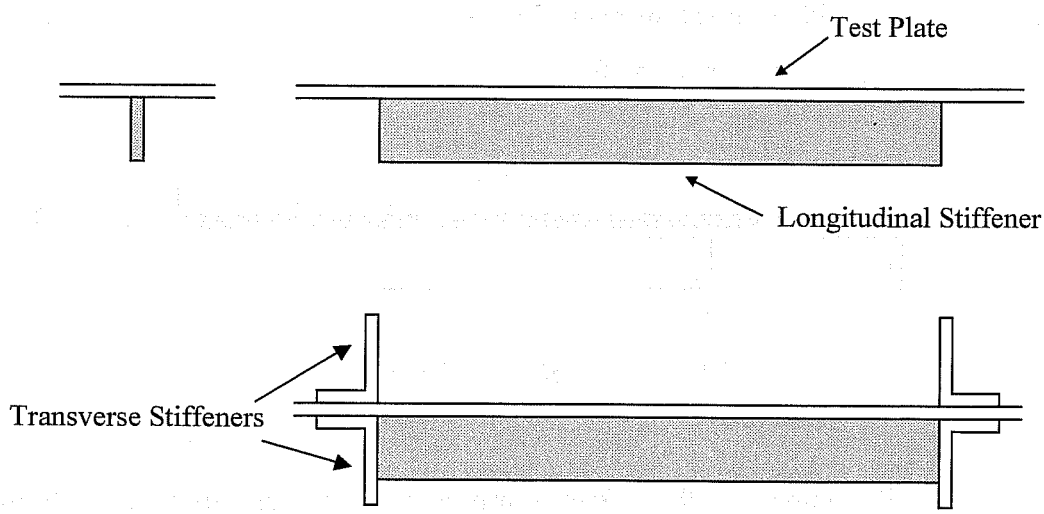

Figure 7.4 Longitudinal Stiffener Termination

There is no stress in the stiffener at the ends of the longitudinal stiffener. Away from the end of the stiffener, there are stresses in both the stiffener and plate as shown by the section cut at mid-length of the stiffener in Figure 7.5. Other factors contributing to stiffener bending were isolated from the analysis of the stiffener termination effect, so a uniform stress distribution through the stiffener is assumed. The resultant of the stresses where the stiffener is terminated acts through the middle of the plate. The resultant axial load at the cut section acts through the centroid of the cross-section. There is an eccentricity, e, between the lines of action of the two loads. This results in a moment equal to the axial load times the eccentricity about the centroid of the section. The direction of stiffener displacement from this effect depends on the orientation (up or down) of the stiffener.

For stiffeners mounted on the bottom surface of the test plate, as shown in the figure, the stiffener will tend to displace down, towards the interior of the box girder. For stiffeners located on the top surface of the test plate this effect will

result in positive curvature about the centroid of the section that will cause the stiffener to displace up, away from the interior of the box.

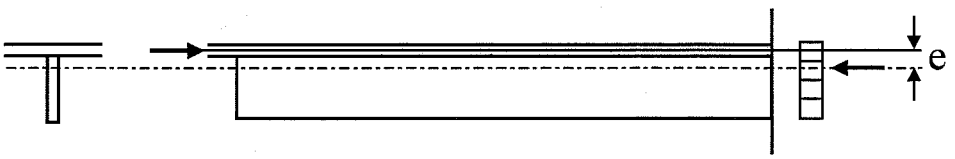

Figure 7.5 Stiffener Termination Effect

The impact of this effect is mitigated by the presence of the transverse stiffeners. Displacement of the test plates with adequate stiffeners was always such that the longitudinal stiffener was made to bear against the transverse stiffener. As the longitudinal stiffener displaced and pushed against the transverse stiffener, axial forces were applied at the end of the stiffener. This condition lessened the impact of the stiffener termination effect.

7.3.4 Combination of Factors Causing Stiffener Displacement

As has been described, a variety of factors contribute to displacement of the longitudinal stiffener. The influence of some factors tended to cause displacement of the stiffener upward, away from the interior of the box girder. The influence of other factors tended to cause displacement of the stiffener downwards, towards the interior of the box girder. Another factor that was found to contribute to displacement of the stiffener is the use of a single eccentric stiffener. This issue will be discussed in Chapter 8.

Some influences are competing factors for a given test plate. For the adequate, double and angle test plates the shape of the initial imperfection was such that the plates were initially displaced upwards, away from the interior of the girder, prior to application of load. The tendency in response to the initial

imperfection in the absence of other factors would be for the plates to displace upward under a compressive load. However, these test plates actually displaced downward when subjected to compression, due to a combination of the other factors.

The test plate with the concrete stiffener was also initially displaced upwards over most of its length. However the concrete stiffener was mounted to the top of the test plate unlike the other adequate stiffeners. The factors contributing to displacement upwards, away from the box, prevailed and the concrete stiffened test plate displaced upward under load, magnifying the initial imperfection.

7.4 Displacement Comparison

The following discussion will focus on the results from the unstiffened test and test plates with centered longitudinal stiffeners. The stiffener properties and the eigenvalue buckling loads of the test plates, are repeated in Table 7.8. The modulus of elasticity of the stiffener times the stiffener moment of inertia is normalized with respect to I_{AASHTO} in the fourth column of the table. I_{AASHTO} is the minimum moment of inertia of an adequate stiffener, k=4, based on the AASHTO LRFD Specification.

Table 7.8 Stiffener Properties

Test Plate	I_s (in^4)	EI_s ($lb \cdot in^2$)	$(EI_s)/(E_sI_{AASHTO})$	Eigenvalue P_{cr} (kips)
Unstiffened	---	---	---	19.2
Inadequate Up	0.106	3,130	0.11	45.0
Inadequate Down	0.106	3,130	0.11	47.9
Adequate	1.44	42,500	1.6	84.3
Double	1.61	47,500	1.8	90.7
Angle	0.989	29,200	1.0	122
Concrete	14.9	58,800	2.3	130

The test plates generally began displacing significantly with the initial application of load due to the variety of factors contributing to stiffener displacement discussed above. Displacements in each of the test plate panels were evaluated since the unstiffened and inadequately stiffened test plates buckled in three half waves along the length of the test plate, and the maximum displacement could occur in any panel.

The absolute values of the maximum displacements in the left end panel and right end panel are presented in Figure 7.6 and Figure 7.7 respectively. The absolute values of the maximum displacements in the center panel are presented in Figure 7.8. As discussed, the ram load applied to the test setup is used in the presentation of all test results. Though a maximum load of 125 kips was applied in the angle test, a malfunction in the data acquisition system resulted in the loss of a significant amount of the potentiometer data in this test. Consequently, data from another test to 113 kips are presented in the following comparison.

The maximum displacements occurred in the center panel in all tests of plates with adequate stiffeners. The largest displacement occurred at the stiffener. At low loads, the maximum displacement in the unstiffened test occurred in the right end panel. However, at higher loads the largest displacements in the unstiffened test also occurred in the center panel. The largest displacements in the inadequate up and inadequate down test occurred in the right end panel of the test plate.

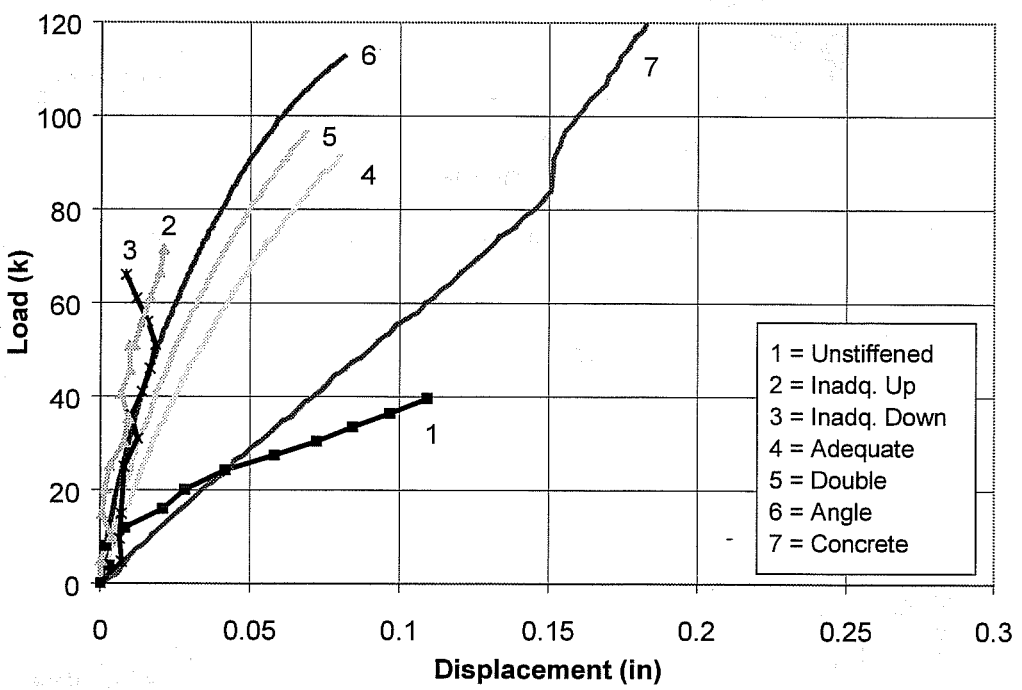

Figure 7.6 Absolute Value of Maximum Displacement in Left End Panel

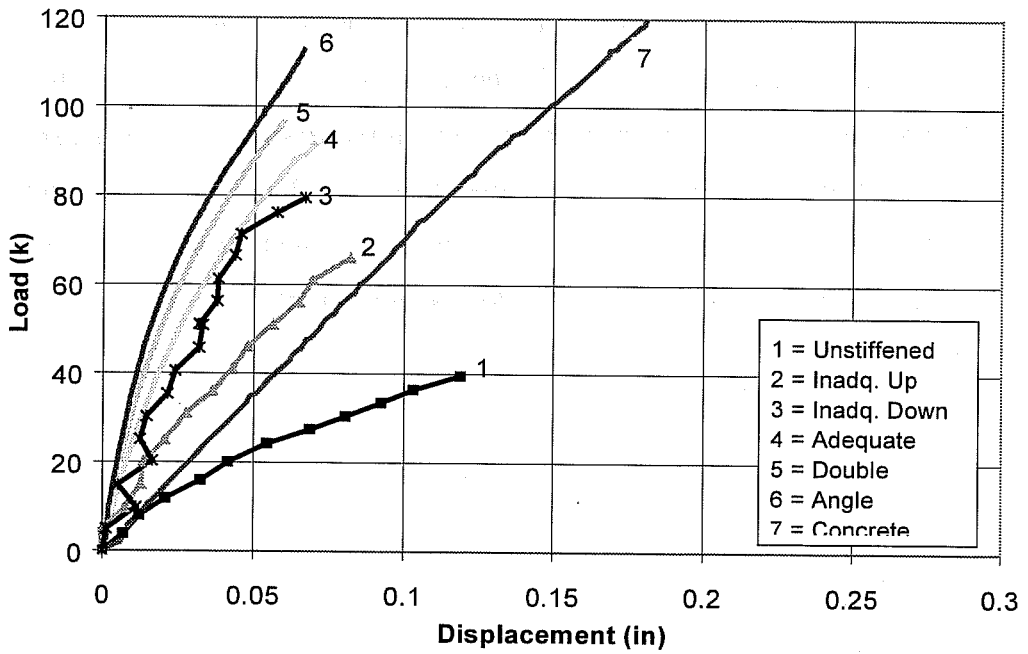

Figure 7.7 Absolute Value of Maximum Displacement in Right End Panel

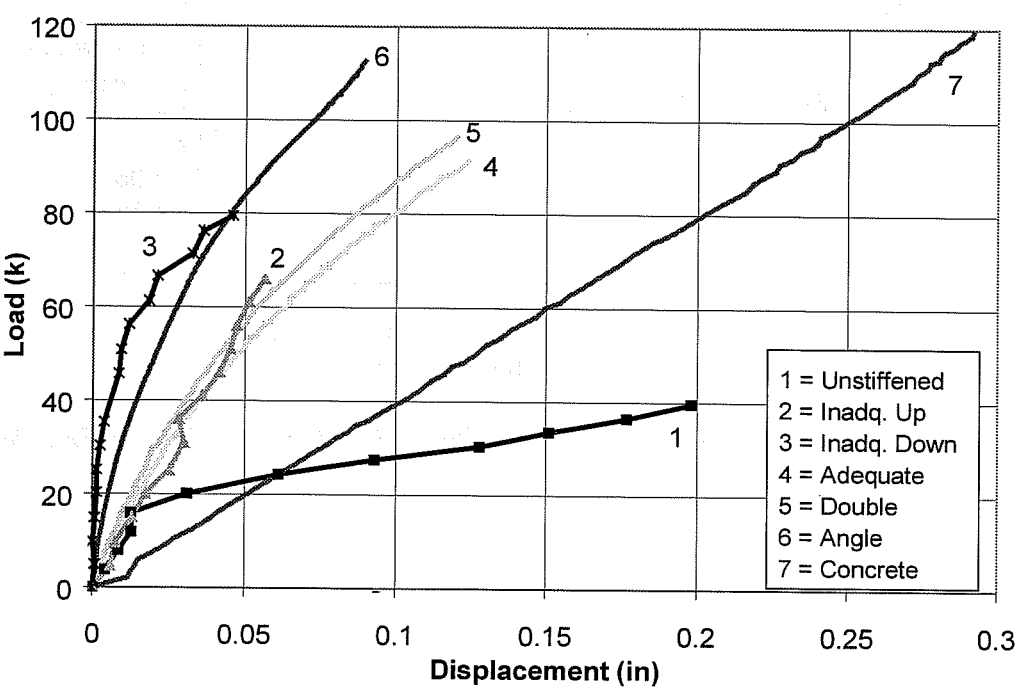

Figure 7.8 Absolute Value of Maximum Displacement in Center Panel

The maximum plate displacements in each test at 20 kips, the experimental data point closest to the buckling load of the unstiffened test plate, are presented in Table 7.9. The displacement in each test as a percentage of the unstiffened test displacement is also presented in this table. The displacement was reduced significantly in the tests with steel stiffeners. The displacements were reduced by at least half with the plate stiffeners, and were reduced over five-fold with the angle stiffener. The fact that the displacements were not reduced at this load level with the concrete stiffener will be discussed later in this chapter.

Table 7.9 Maximum Displacement at 20 kips

Test	Displacement (in)	Displacement / Unstiffened (%)
Unstiffened	0.031	100
Inadequate Up	0.014	45
Inadequate Down	0.016	52
Adequate	0.015	48
Double	0.013	42
Angle	0.005	17
Concrete	0.051	165

The displacements at 40 kips, the maximum load applied to the unstiffened plate, are presented in Table 7.10. The displacement in each test as a percentage of the unstiffened test displacement is also shown. The comparison shows the substantial reduction in displacement at higher loads accompanying the use of longitudinal stiffeners, particularly steel longitudinal stiffeners. The largest

stiffened plate displacements were seen in the concrete test, however there is still almost a 50% reduction in displacement compared to the unstiffened test at this load level. The reduction with the steel stiffeners is even more dramatic. With the steel stiffeners the displacement was at most 22% of the unstiffened test displacement.

Table 7.10 Maximum Displacement at 40 kips

Test	Displacement (in)	Displacement / Unstiffened (%)
Unstiffened	0.198	100
Inadequate Up	0.043	22
Inadequate Down	0.024	12
Adequate	0.036	18
Double	0.031	16
Angle	0.015	7
Concrete	0.103	52

7.4.1 Unstiffened Test and Concrete Test

The plots in Figure 7.6 through Figure 7.8 show that at a given load, the maximum displacements occurred in the unstiffened and concrete test. Large displacements were expected in the unstiffened test, since this was the only test plate without a longitudinal stiffener. However up to about the 25 kip load level, the test plate with the concrete stiffener had displacements that were larger than the unstiffened test plate. In the concrete test the effect of the initial imperfection and second order stiffener bending had an additive effect, resulting in large deflections.

With initial application of load, the test plate with the concrete stiffener had larger relative displacements then the unstiffened test plate. After the unstiffened test plate buckled, and the response of the plate softened, the displacements of the unstiffened plate were larger than those of the plate with the concrete stiffener.

The concrete stiffener was not straight prior to testing. The concrete stiffened test plate was initially displaced upward over most of its length, with maximum out-of-flatness along the concrete stiffener. As load was applied, the test plate immediately displaced out-of-plane. The bowed concrete stiffener did not stop the lateral displacement of the plate. The stiffener and plate displaced vertically in one half wave along the length of the plate as load was applied.

In the unstiffened plate test, the plate buckled into three half waves along its length rather than in one half wave. The three half wave shape, rather than one large half wave, meant there was less relative displacement in each panel of the plate. The displacement along the longitudinal centerline of the plate in both the unstiffened and concrete stiffened tests at a load of 20 kips are shown in Figure 7.9. The maximum displacements in both the unstiffened and concrete stiffened tests are labeled on the plot. The fact that the concrete stiffened test plate displaced in one large half wave instead of a more complex shape like the unstiffened test plate, contributed to the larger relative displacements that were measured at this load level for the concrete stiffened test plate.

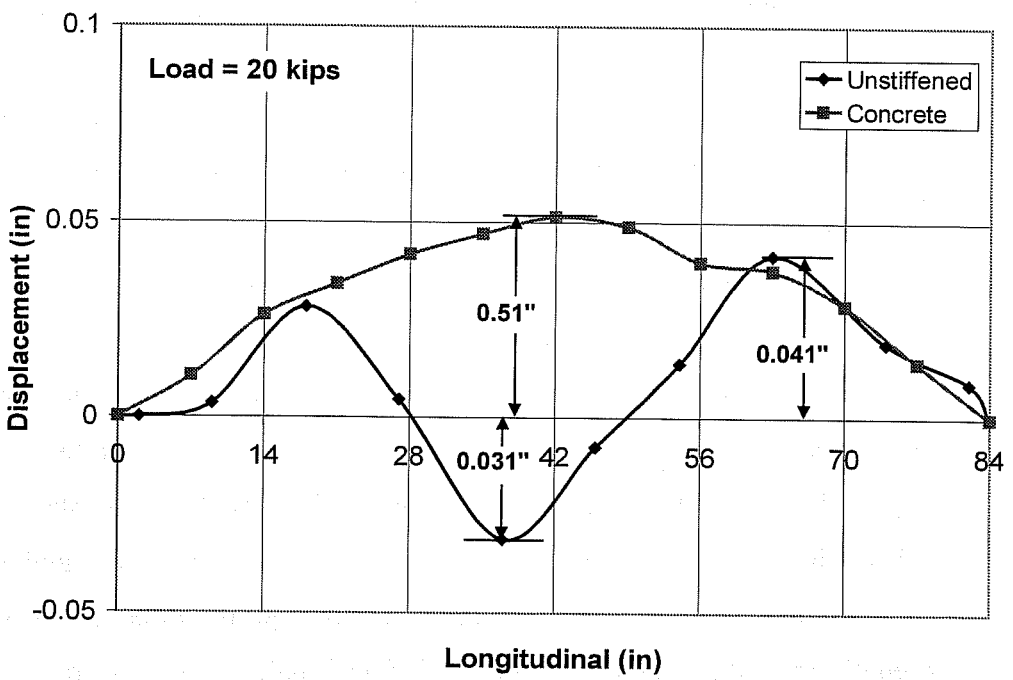

Figure 7.9 Displacements along Longitudinal Stiffener

7.4.2 Unstiffened and Inadequate Tests versus Tests with Larger Stiffeners

In the Unstiffened, Inadequate Up, and Inadequate Down tests the plate displaced in three half waves along the length of the plate. In all other tests, the plate displaced in one half wave along the length of the plate. As observed in the discussion of the unstiffened test versus the concrete stiffened test plate, larger displacements can result when the plate displaces into the less complex one half wave shape.

Referring to the displacement plots in Figure 7.6 through Figure 7.8, significantly larger displacements were expected in the inadequate stiffener tests compared to the tests with larger stiffeners. However, since the inadequate stiffened plates buckled in three half waves along the plate, and the plates with

larger stiffeners buckled in one half wave, the relative displacements in the tests with inadequate stiffeners were not greater than those for the test plates with larger stiffeners.

7.4.3 "Adequate" Steel Stiffeners

The displacements of the test plates with "adequate" steel stiffeners (adequate, double, angle tests) were included in Figure 7.6 through Figure 7.8. The largest displacements occurred in the center panel of each of these test plates. The largest deflections occurred in the adequate test, followed by the double test. The smallest plate displacements were seen in the angle test. The stiffener in the adequate test was labeled "adequate" since it was initially sized to be large enough to form a straight nodal line along the stiffener. However, in the tests, the stiffeners did not remain straight. The plates and stiffeners began displacing vertically with the initial application of load. The stiffeners displaced downward throughout the application of load.

The maximum relative displacements in the angle, double and adequate tests at a load of 91 kips are presented in Table 7.11. The displacements as a percentage of the plate thickness are also shown in the table. Comparing these results, the smallest relative displacements occurred in the angle test. The angle test had a smaller I_s than the stiffeners in either the adequate or double test, but the displacements were still smallest at each load level in the angle test. The displacement in the angle test was half of that in the adequate test at the 91 kip load level.

Table 7.11 Maximum Displacement at 91 kips

Test	Displacement (in)	Displacement as % of Plate Thickness
Adequate	0.124	65
Double	0.109	57
Angle	0.060	30

7.5 Comparison of Test Results with Large Displacement Analysis

Large-displacement FEA was done to evaluate the influence of initial imperfections and girder bending upon the behavior of the test plates. The eigenvalue-buckling load is the load at which a perfectly straight member becomes unstable and failure occurs. The eigenvalue analysis does not provide any load-displacement history and does not reveal the effects of initial imperfections. To examine the load-displacement behavior of a member, a large displacement finite element analysis (FEA) can be used.

In a large displacement analysis the load is applied to the model in discrete increments or time steps. For each time step, the load is increased slightly and a corresponding displacement is calculated based on the stiffness of the model. The routine used by the ABAQUS analysis package can account for significant changes in the geometry of the member as the load is increased. A complete load-displacement history for a model, including post-buckling behavior, can be generated using this type of analysis. The effects of initial imperfections can be studied in a large displacement analysis by including these imperfections in the model geometry.

In the following discussion, the response from finite element analyses of the unstiffened, adequate, angle and concrete stiffener tests will be compared to

the test results. As discussed in Chapter 5, the plate displacements were measured using the PDG during the first few tests. The plate displacements were measured using fixed lines of potentiometers in subsequent tests. Both methods of measuring plate displacements captured the relative displacement of the plate, and not overall girder deflection. The relative displacement of the plate, not including overall girder deflections, was also extracted from the FEA results.

7.5.1 Large Displacement Analysis of Unstiffened Test

A large displacement analysis was performed of the unstiffened test to investigate the effects of the initial imperfection of the test plate. Measured plate imperfections were added to the previously developed finite element model, and an elastic large displacement analysis was performed using the modified geometry. Geometric nonlinearity was included in the analysis.

Figure 7.10 shows the relative displacement of the plate from the finite element analysis at 21 kips and Figure 7.11 shows the measured relative displacement from the unstiffened test at 20 kips. The shape of the relative displacement from the finite element analysis is very similar in appearance to the measured displacements from the test. The magnitude of the displacement will be compared in load-displacement plots. Both the FEA and test show three distinct half-waves along the length of the plate. The largest positive displacements in both the FEA and test occurred in the right end panel, at the location of maximum initial imperfection.

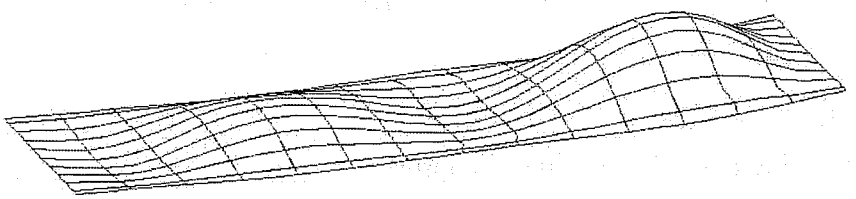

Figure 7.10 Unstiffened Test FEA - Relative Displacement at 20 kips

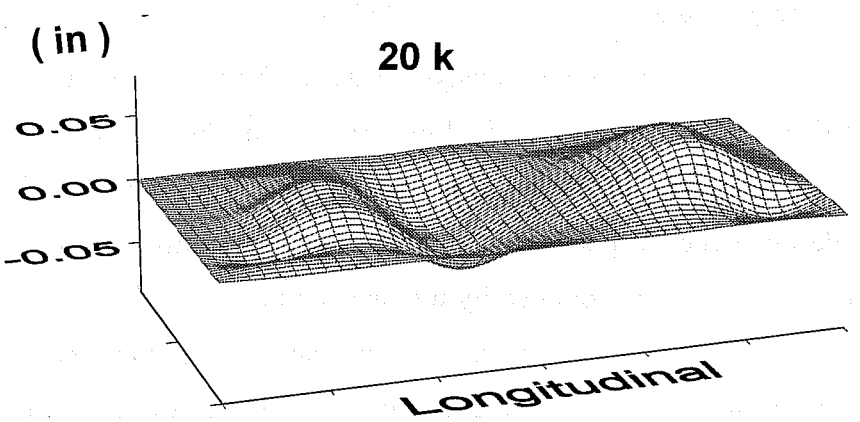

Figure 7.11 Relative Displacement from Test

The relative displacement from the FEA at 40 kips is shown in Figure 7.12 and the test displacement at 40 kips is shown in Figure 7.13. Again, the shape of the measured and FEA results are very similar in appearance. Both have a symmetric appearance, with displacement up in the end panels and down in the center panel of the test plate.

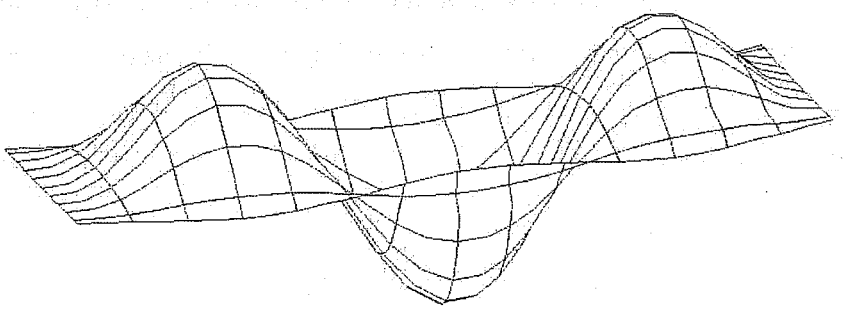

Figure 7.12 Unstiffened Test FEA - Relative Displacement at 40 kips

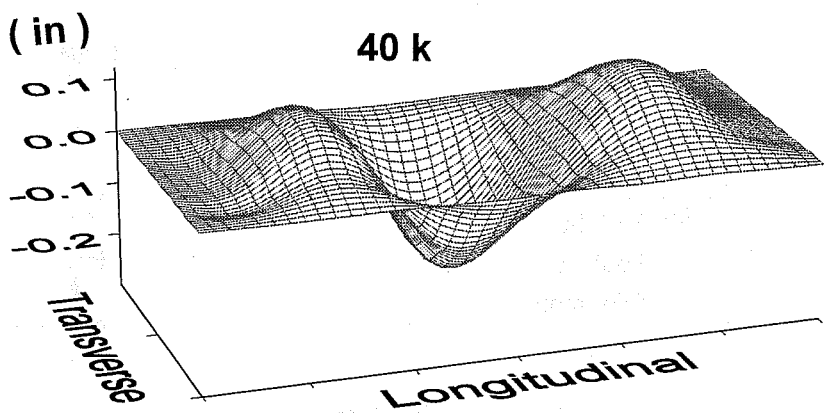

Figure 7.13 Relative Displacement from Test

The maximum measured relative displacement in the unstiffened test occurred at point 5E, which is located in the center panel of the test plate. The measured displacements and the displacements at the node in the FEM closest to this location are presented in Figure 7.14. The maximum displacement from the FEA, at the middle of the center plate panel, is also shown in this figure. The load-displacement responses from the test and FEA are similar, particularly at higher loads. In the FEA, the test plate initially began moving slightly upward, then reversed directions and moved down at the locations plotted. In the test, the

plate moved slightly downward at location 5E with the initial application of load, and continued to move downward throughout the test. As a result of this difference there is a more noticeable change in behavior above the buckling load in the finite element results.

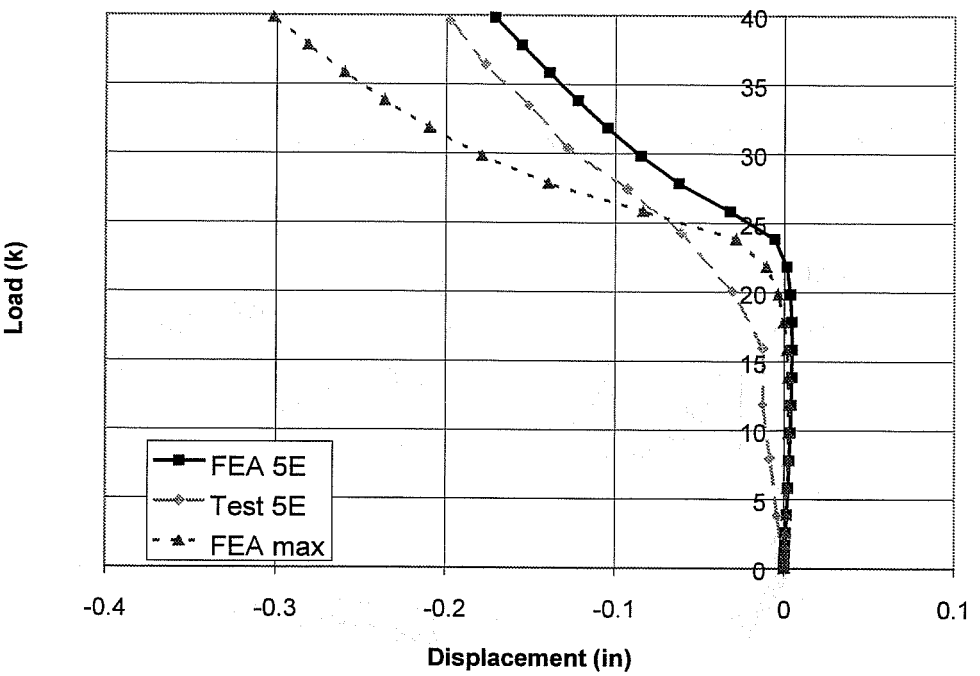

Figure 7.14 Displacement in Unstiffened Test vs. FEA

The finite element results show some softening of the response near the buckling load of 19.2 kips, particularly for the FEA max curve, but do not show significant softening until load levels of about 22 kips. The initial imperfection of the plate was reversed, resulting in initial displacement downwards at the middle of the plate. More significant softening occurred at slightly lower loads, around 20 kips, with the reversed imperfection. The finite element analysis apparently indicates a more pronounced stiffening effect because of the initial imperfection than was observed in the test. The fact that the FEA displacements are smaller

than the displacements measured in the test at location 5E may also be due to this effect.

A stress contour of the unstiffened plate at 19.8 kips is presented in Figure 7.15. All stresses in this plot are compressive, and the maximum compressive stress is shown in dark blue. The plot shows largest compressive stresses in the end panels, particularly in the left end panel. Plots at lower loads show the same general appearance with higher stresses in the end panels.

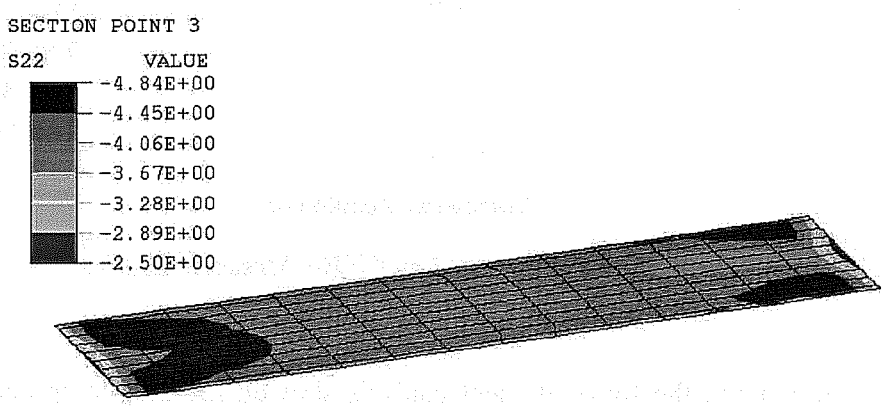

Figure 7.15 Stress Contour at 19.8 kips

The measured plate stresses at 20 kips and the stresses predicted by the finite element analysis are plotted in Figure 7.16. The legend entries in the plot identify the longitudinal location at which the stresses were recorded. There is good agreement between the measured stresses and those predicted by the finite element analysis.

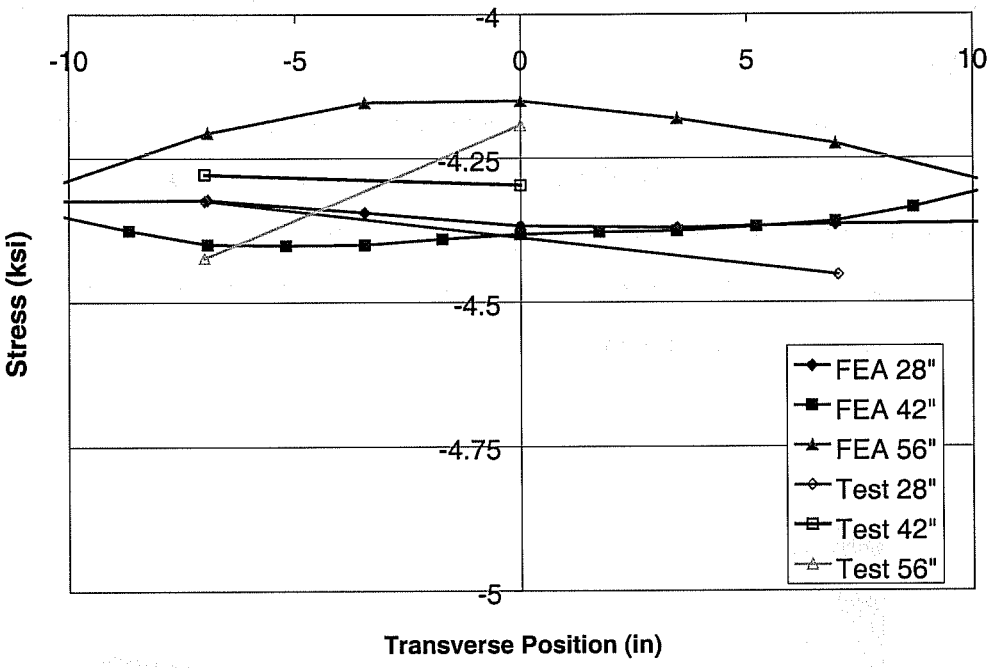

Figure 7.16 Measured and FEA Stress at 20 kips

In general, the finite element analysis showed reasonable agreement with the measured displacements from the unstiffened test. The FEA results showed softening above the eigenvalue-buckling load. Softening near the buckling load was also seen in the test. The measured stresses fall within the stress range predicted by the finite element analysis.

7.5.2 Large Displacement Analysis of Adequate Test

A large displacement analysis was also performed of the adequate test plate. Measured plate imperfections were added to the previously developed finite element model. An elastic large displacement analysis including geometric nonlinearity was performed.

Figure 7.17 shows the relative displacement of the plate from the FEA at 92 kips. The relative displacement surface plot from the adequate test at 91 kips is repeated in Figure 7.18. The shape of the relative displacement from the finite element analysis is very similar in appearance to that measured in the test. The largest displacements in both the FEA and the test occurred in the middle of the test plate at the stiffener. The stiffener displaced downward throughout the application of load to the finite element model.

The FEA surface plots show plate bowing on either side of the stiffener in five half-waves along the length of the plate. The test results also showed five half-waves developing along the length of the plate on either side of the stiffener. The relative displacements from both the FEA and tests show that the plate displaced in a symmetric shape on either side of the longitudinal stiffener.

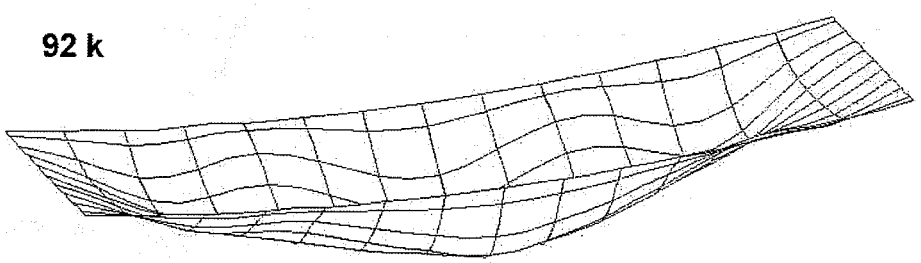

Figure 7.17 Adequate Test FEA - Relative Displacement

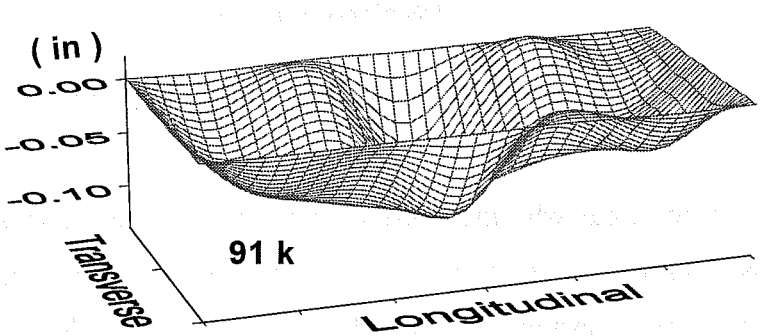

Figure 7.18 Adequate Test - Relative Displacement

The maximum displacement in the adequate test and the FEA of the adequate test occurred in the middle of the test plate at the stiffener. The measured and FEA plate displacements at this location are presented in Figure 7.19. The measured displacements in the test were significantly smaller than those predicted by the ABAQUS analysis. The FEA analysis shows more significant softening at higher loads then was observed in the actual test. No apparent buckling load was observed in the FEA results.

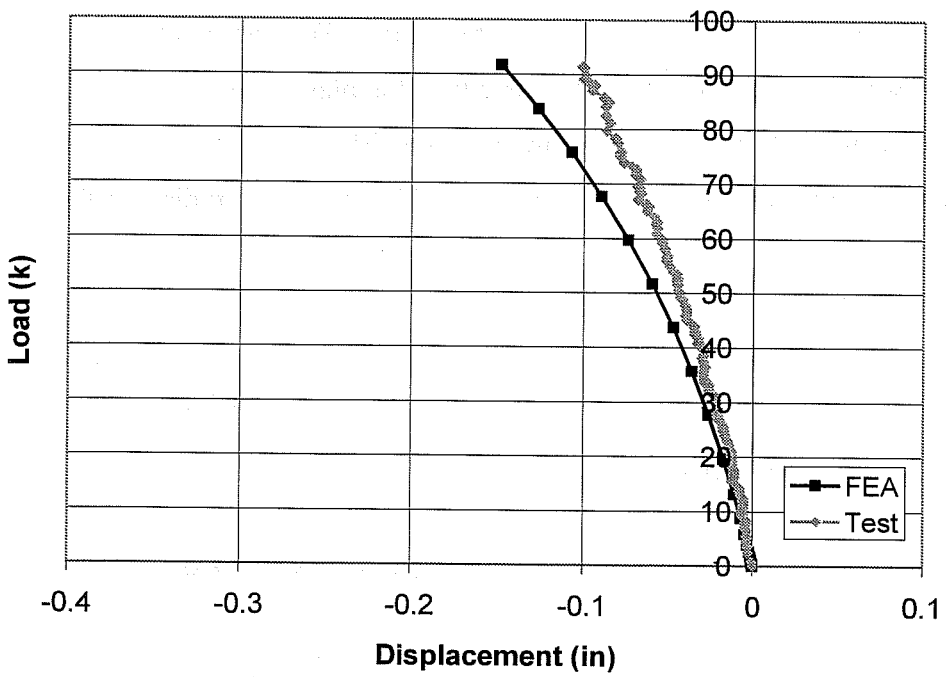

Figure 7.19 Displacement in Adequate Test vs. FEA

It is not clear why the finite element results predict larger displacement than those measured in the tests. Different approaches of attaching the test plate to the girder were evaluated, but did not significantly affect the displacement results. Another shell element, the ABAQUS S9R element, was used to model

the test plate, but this did not affect the results. The nature of the displaced shape predicted by the finite element analysis was the same as that observed in the test, but the magnitude of the predicted displacements did not show close agreement.

The plate stresses measured in the experimental tests were compared to stress contours from the finite element analysis. The FEA results show reasonable agreement with the measured stresses. There was larger variation between the FEA stresses and measured stresses than was seen in the unstiffened test, but the stress contours in the stiffened plate are more complex than that of the unstiffened test, and less point-to-point agreement was expected. The stresses measured during the test and the FEA stresses at a load of 84 kips, the eigenvalue-buckling load of the plate, are plotted in Figure 7.20. The FEA showed reasonable agreement with the measured stresses.

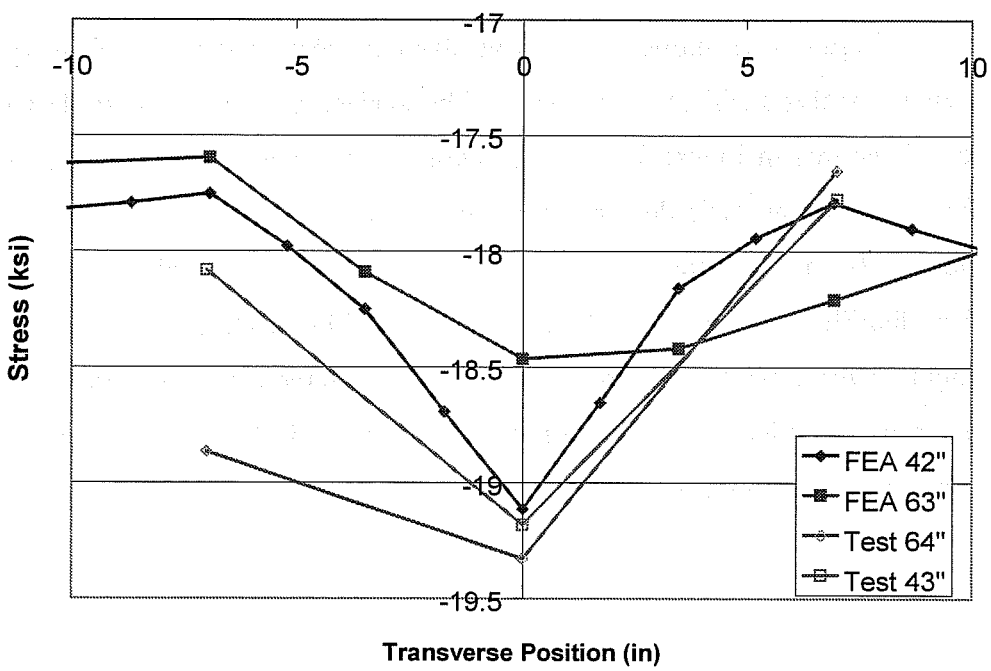

Figure 7.20 Measured and FEA Stress at 84 kips

In summary, the shapes of the relative displacement from the FEA of the adequate test agreed well with those captured in the test. The magnitude of the displacements were however larger in the FEA. The stresses in the FEA agree well with those measured in the test. The most significant point of both the test and FEA analysis is that the stiffener displaces significantly under load. The stiffener is not an unmoving nodal line. The stiffener does reinforce the centerline of the plate, and the plate does displace into waves on either side of the stiffener. But plate displacement is not zero along the stiffener.

7.5.3 Large Displacement Analysis of Angle Test

A large displacement analysis was performed of the angle test plate. Measured plate imperfections were added to the previously developed finite element model and an elastic large displacement analysis including geometric nonlinearity was performed.

Figure 7.21 shows the relative displacement of the plate from the finite element analysis (FEA) at 100 kips. The surface plot from the angle test at 99 kips is shown in Figure 7.22. The shape of the relative displacement from the finite element analysis does not show the distinct waviness of the plate on either side of the stiffener that was seen in the actual test. The relative displacement from the FEA at a load of 120 kips is shown in Figure 7.23. There are some very slight waves in the plate in the plot at 120 kips. In the test results, the waves were much more noticeable. The largest displacements in both the FEA and the test occurred in the middle of the test plate.

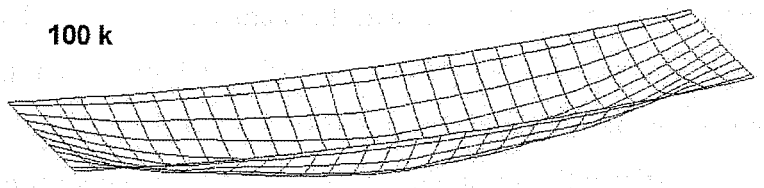

Figure 7.21 Angle Test FEA - Relative Displacement

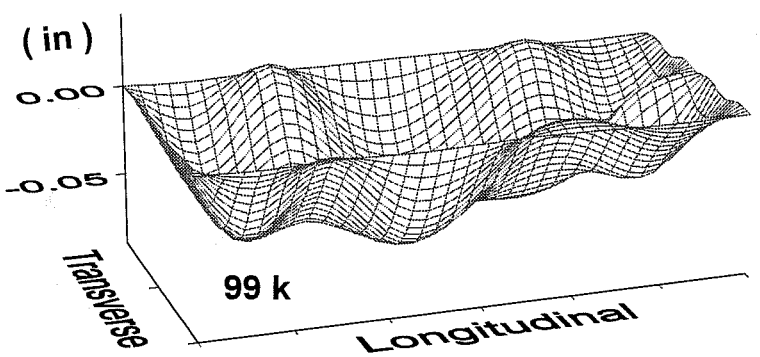

Figure 7.22 Angle Test - Relative Displacement

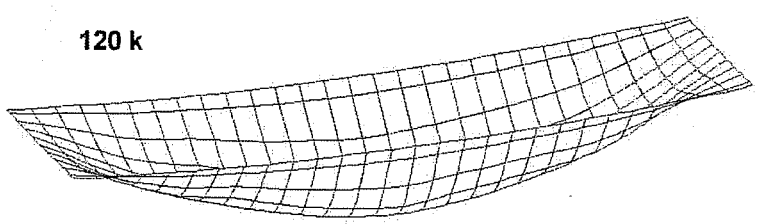

Figure 7.23 Angle Test FEA - Relative Displacement at 120 kips

The maximum test displacements and FEA plate displacements at the center of the plate are presented in Figure 7.24. The measured displacements in the test were significantly smaller than those predicted by the ABAQUS analysis. The displaced shapes predicted by the FEA analysis and the magnitude of the

displacements did not agree well with the actual test results. The response of the plate in the FEA analysis was much less stiff at all loads than the actual response measured in the test. Again, several alterations were made to the finite element model to investigate the sensitivity of the model to the connection of the test plate and other geometrical effects. Additional changes were investigated based on conversations with a finite element analysis expert. However, the changes did not result in significantly better agreement between the finite element and test displacements.

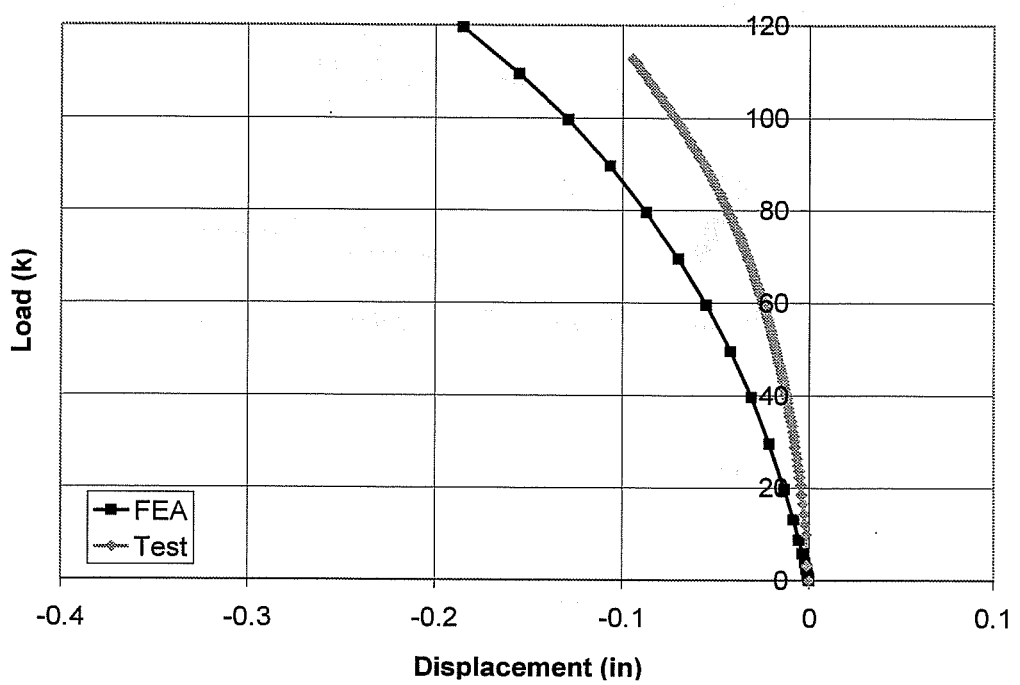

Figure 7.24 Displacement in Angle Test vs. FEA

The stress contours of the angle test plate from the FEA were compared to the measured stresses. The stresses from the FEA agree well with the stresses measured along the middle longitudinal line of the plate, at the stiffener. The stresses measured away from the middle longitudinal line do not agree as well

with the FEA results. Since the FEA displaced shape did not agree well with the measured results, the FEA stresses on either side of the stiffener also did not show as close agreement with the test results as was seen in the adequate test.

The shapes of the displacement surface plots and the magnitude of the displacements from the FEA do not agree well with the results actually measured in the test. The finite element analysis did not reveal the waving of the plate on either side of the angle stiffener, and indicated larger displacements than were observed in the test. The major point of agreement between the FEA and test was again that the stiffener did not remain straight. This point is a consideration of key interest since the current AASHTO design approach treats adequate stiffeners as if they remain straight.

7.5.4 Large Displacement Analysis of Concrete Test

A large displacement analysis of the concrete test plate was performed. Measured plate imperfections were added to the finite element model, and an elastic large displacement analysis including geometric nonlinearity was performed. The concrete was modeled as an elastic material and cracking of the concrete stiffener was not considered in the analysis.

Figure 7.25 shows the relative displacement of the plate from the finite element analysis (FEA) at 120 kips. The relative displacement from the concrete stiffener test at 119 kips is shown in Figure 7.26. The response of the plate in the FEA is consistent with what happened in the concrete test. The concrete stiffener displaced upwards and the test plate was bowed in one large half wavelength along its length. The largest displacements in both the FEA and the test occurred in the middle of the test plate. The stiffener was not straight prior to testing and the stiffener displaced throughout the application of load to the finite element model.

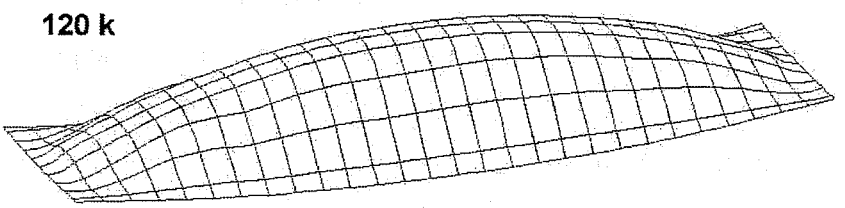

Figure 7.25 Concrete Test FEA - Relative Displacement

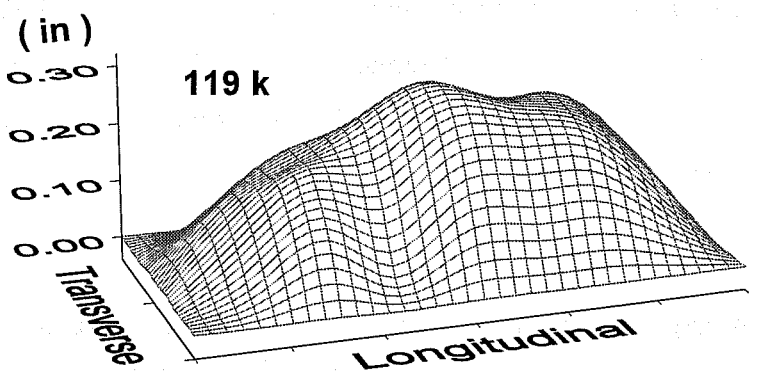

Figure 7.26 Concrete Test - Relative Displacement

The FEA surface plot does not show the waviness of the plate on either side of the stiffener as distinctly as the actual test results. The FEA results do show local plate waves in the left end panel of the plate, but they are not as prominent as the displacements measured in the test. Some differences in the displaced shape at higher loads may be due to the fact that the finite element model did not include concrete cracking.

As the FEA and test surface plots show, the maximum displacement occurred in the middle of the test plate. The measured and FEA plate displacements at this location are presented in Figure 7.27. The displacements from the FEA agree well with the measured displacements up to about 50 kips of

load, and are very close to the measured displacement up to the 60 kip load level. Above this load, the analysis predicted larger displacements than were actually measured in the test.

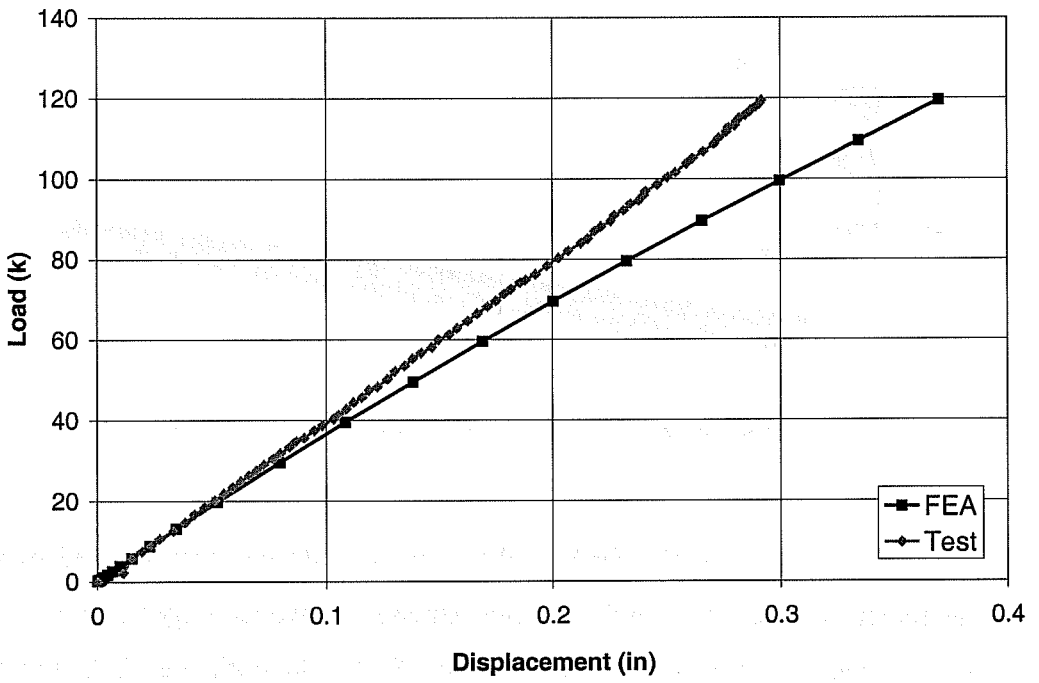

Figure 7.27 Displacement in Concrete Test vs. FEA

In the test, the strain gauges showed microcracking of the stiffener at a load of approximately 82 kips. The stress on the top surface of the concrete stiffener was 640 psi when the microcracking occurred. The FEA shows local areas where the tensile stresses in the stiffener where above 640 psi at loads as low as 60 kips. The stresses above the tensile capacity were in very local areas on the top of the stiffener, and the higher stresses did not penetrate into the stiffener at this load level. When the load applied to the FEM was 80 kips the tensile

stresses were greater than 640 psi across most of the free surface of the stiffener, as shown in Figure 7.28. Note that in this plot the maximum compressive stress is shown in blue, and the areas plotted in red are in tension. Microcracking of the stiffener was evident from the strain gages in the test when the applied load was approximately 80 kips.

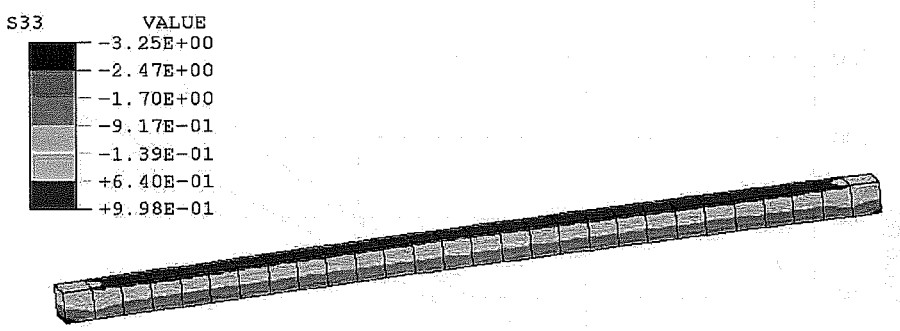

Figure 7.28 Concrete Stiffener Stresses at 80 kips

The results of the FEA of the concrete stiffened test showed reasonable agreement of measured and predicted stresses, however larger displacements at higher loads were again predicted in the FEA. In both the FEA and test the stiffener displaced throughout the test. The concrete stiffener did reinforce the longitudinal centerline of the plate, and constrained displacements at higher load s compared to an unstiffened plate. However, the fact that the stiffener was bending during the test resulted in the development of tensile stresses on the free edge of the stiffener, and cracking of the stiffener. Based on the stiffener bending seen in the tests, use of concrete stiffeners is not recommended.

7.6 General Behavior in Tests

The test plate stiffeners began displacing vertically with the initial application of load, and these displacements grew throughout the test. A nodal

line was not formed along the stiffener. In fact both the test results and finite element analysis show that the maximum displacement generally occurred at the longitudinal stiffener. No distinctive softening of the load-displacement response was seen at any particular load level in the load-displacement plots of the stiffened plates.

The applied load was not just carried axially by the stiffener and the plate. The applied load was also carried through bending of the stiffener. No deleterious plate response was seen at the eigenvalue buckling load. Some code approaches use an ultimate stress approach that results in capacities larger than the buckling load for slender plates. As shown by the test results, there was no distinct softening of the response of the stiffened plates at the eigenvalue buckling load or other factors that would indicate a significant deterioration in performance by allowing applied loads above the buckling load. There is however an increase in displacements at the higher loads, which leads to higher transverse bending stresses at the flange-web boundary and at the longitudinal stiffener. There is a potential fatigue concern at these locations for cyclically loaded structures like bridges.

The transverse bending stresses at the flange-web boundary in the finite element models of the test setup with various test plates was briefly examined. The increase in the transverse bending stress from an applied load of 0.5 P_{cr} to P_{cr} was on the order of 10 ksi. A study of fatigue behavior of welded joints subjected to variable amplitude stresses indicates that stresses above 10 ksi may potentially lead to fatigue failures (Joehnk 1982). In box girder structures with slender webs, there may be increased levels of stress from the combination of web and flange displacements. Without further study of this issue, it does not seem prudent to recommend design capacities above the eigenvalue buckling load.

For certain plate geometries, bending of the stiffener, and consequently bending of the stiffened plate, may lead to situations where yielding occurs before the eigenvalue buckling load of the plate is reached. Based on the test results of plates with stiffeners mounted on the inside of the box girder, the stiffener displaces towards the inside of the box as the girder is loaded. Tensile bending stresses are generated in the free end of the stiffener and compressive bending stresses are generated in the test plate. The potential for yielding below the eigenvalue plate buckling based approach used by AASHTO is explored using a strut based analysis approach in Chapter 8.

7.7 Amplified vs. Reduced Initial Imperfections

Although varying degrees of complexity existed in the initial shapes of the stiffeners, in general all of the test plates were initially displaced upward across the width and along the length of the plate. Consequently, the stiffeners in all cases were initially concave down along the length of the test plate. The inadequate up test plate and concrete stiffened test plate had a single stiffener mounted on the top of the test plate, while the rest of test plates had stiffeners mounted to the bottom of the test plate. With the stiffener mounted on the top of the test plate, the factors contributing to stiffener displacement away from the box overrode and the stiffeners displaced upward as the test setup was loaded. With the stiffener mounted on the bottom of the test plate, the factors contributing to displacement into the box prevailed, and the stiffener displaced downward as the test setup was loaded.

The direction of maximum displacement in the inadequate tests and the concrete stiffener test was in the direction of the initial imperfection. The initial imperfections in these tests were amplified as load was applied. The presence of these imperfections was deleterious and resulted in a softer response and larger

displacements. The direction of maximum displacement in all other stiffened plate tests was opposite the direction of the initial imperfection. The presence of the initial imperfection actually stiffened the plate response and resulted in smaller displacements for the cases where the stiffener moved towards the interior of the box.

7.7.1 Inadequate Up and Inadequate Down Tests

The shapes of the initial imperfection of the inadequate up and inadequate down test plates are shown in Figure 7.29. The relative displacements at 66 kips in the two tests are shown in Figure 7.30. The same displacement scale is used in each of these figures.

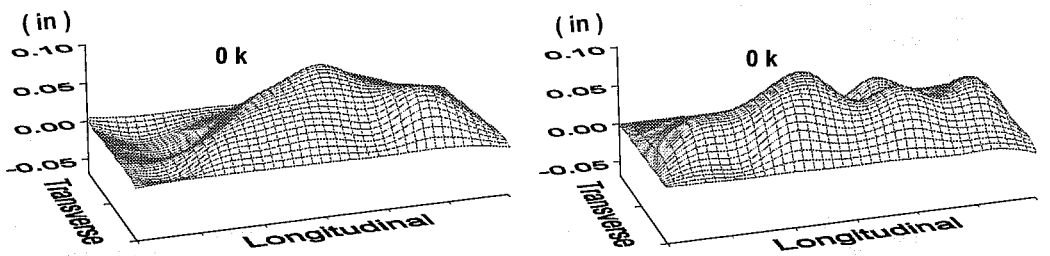

Inadequate Up ***Inadequate Down***

Figure 7.29 Initial Imperfection

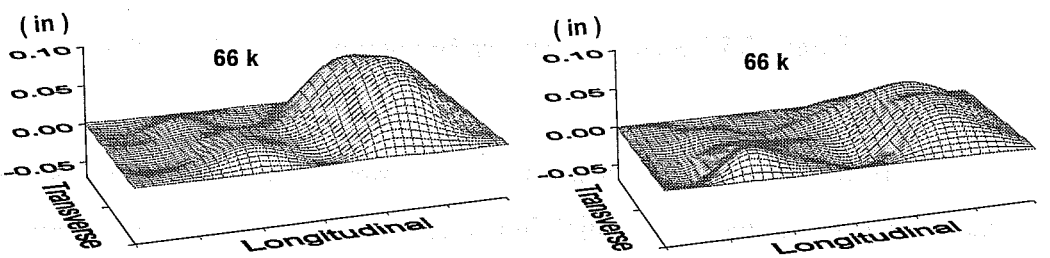

Inadequate Up ***Inadequate Down***

Figure 7.30 Relative Displacement

The maximum variations from flatness of the inadequate up and inadequate down test plates were essentially equal, as shown in Table 7.1. However, as shown in Figure 7.31, the displacements in the inadequate up test were significantly larger than the displacements in the inadequate down test. The displacement at a given load level was 50 to 90% greater in the inadequate up test.

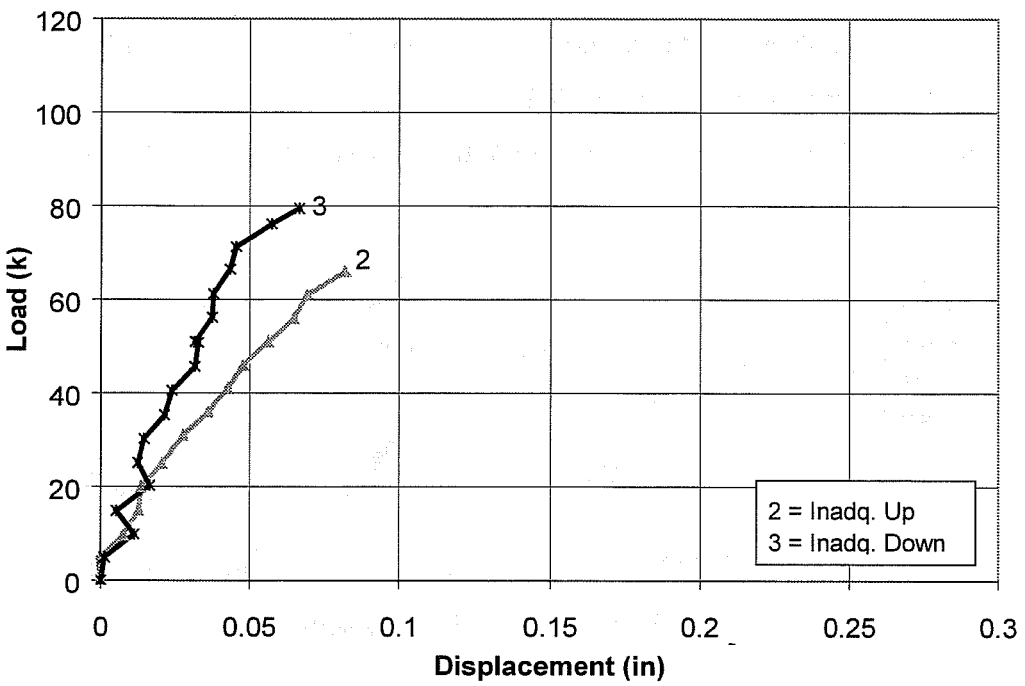

Figure 7.31 Displacement of Inadequately Stiffened Plates

In the inadequate up test, the initial imperfection was amplified. In the inadequate down test, the initial imperfection was reduced. As a result, the displacements in the inadequate up test were much larger than those in the inadequate down test.

7.7.2 Reversing Initial Imperfection in Finite Element Models

To further analyze magnified vs. reduced initial imperfections, the initial imperfections of the adequate and angle test plates were reversed and the modified FEM model was analyzed. Both the adequate and angle test plates were initially displaced upward across the width and along the length of the test plate. With the reversed imperfection, the plate was initially displaced down across the width and along the length of the test plate under no load.

The load displacement response from the analyses with the original and reversed imperfection of the adequate test is shown in Figure 7.32, and the angle test is shown in Figure 7.33. With the reversed imperfection the stiffener displacement is in the direction of the initial imperfection and the initial imperfection is amplified as load is applied to the plate. The plate response is initially softer and the displacements at each load level are larger compared to the original imperfection. Since the response is softer from the initial application of load, and there is no clear point where additional stiffness is lost, identification of a "critical" load is even less clear.

In the experimental tests, certain imperfections were reduced during the test and others were amplified. In an analysis approach that makes direct consideration of initial imperfections, imperfections that result in the worst performance, i.e. largest displacements, should be addressed.

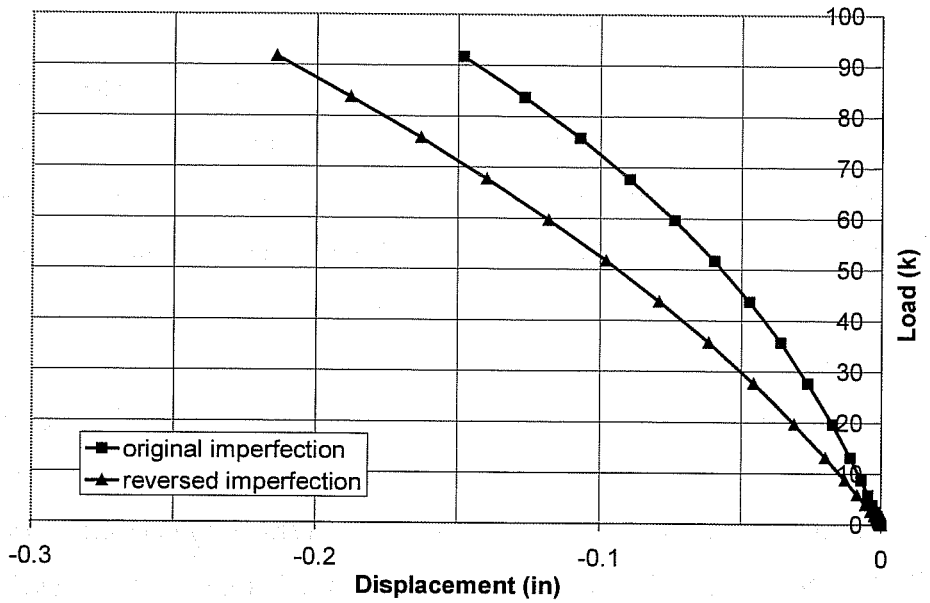

Figure 7.32 Adequate Test - Original and Reversed Imperfection

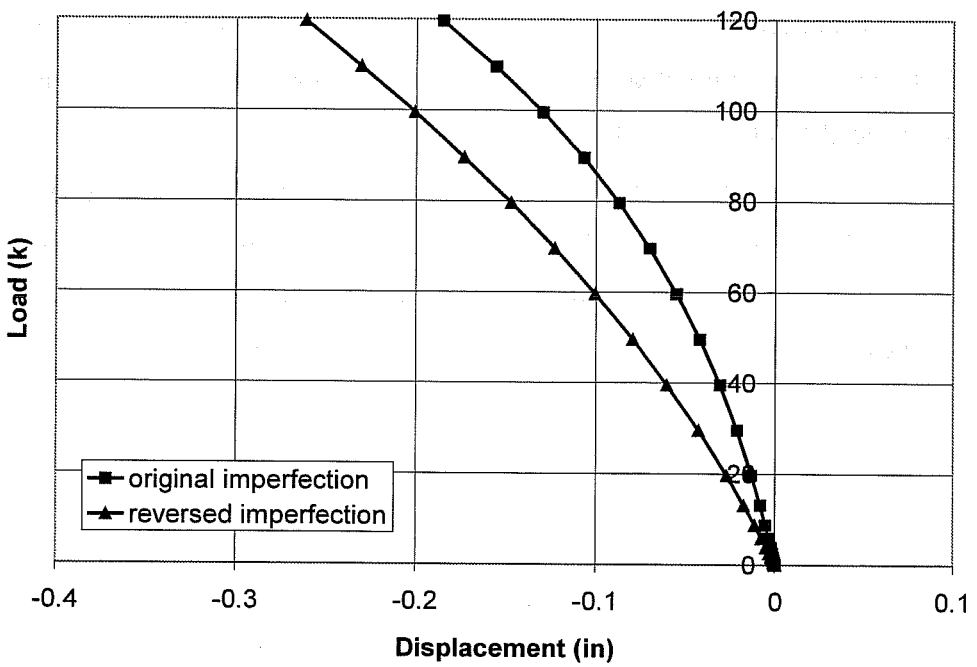

Figure 7.33 Angle Test - Original and Reversed Imperfection

7.8 Alternate Approaches for Determination of Critical Load

A recent text by Singer, Arbocz, and Weller presents a thorough discussion of methods for determination of the buckling loads in plates (Singer 1998). A substantial point of concern in plate buckling analysis is that the precise identification of the buckling load is difficult. The stable postbuckling behavior of the plates clouds the identification of the critical load. Although what can be appropriately described as plate buckling behavior was not seen in the tests of stiffened plates, approaches for determining the buckling load from experimental plate data were still investigated.

One approach used to attempt to identify the buckling load is plotting the load vs. out-of-plane displacement. The critical load is the load at which significant softening of the load-displacement response occurs. As has been discussed, for real plates with significant initial imperfection, there is generally not a load where significant softening of the response is apparent. Therefore it is difficult to identify the critical plate load. Furthermore, for slender stiffened plates where, as shown in the tests, stiffener displacement may overwhelm plate displacements, identification of a buckling load is further clouded. Several alternate methods have been developed to attempt to aid in the identification of the plate buckling load, but most of the methods involve some personal judgment and the uncertainty of the estimate increases with plate out-of-flatness.

Some methods, such as the "strain reversal method," developed based on tests of fiberglass plates, and "averaged strain method" use the load-strain response to attempt to identify the critical load of the plate (Singer 1998). Using the strain reversal method, the point at which the extreme-fiber stress on the convex side of a buckle stops increasing and starts decreasing is deemed the critical stress. The averaged strain approach uses the average of the convex and concave strains to identify the critical load. However these and other similar

strain approaches were developed based on tests of plates with very small imperfections, and the approaches have been found to be unreliable by other researchers, particularly in plates with more significant initial imperfections (Singer 1998, Fok 1984).

Other approaches focus on use of the load-deflection response of the plate, where the displacement of interest is the out-of-plane deflection of the plate. Among this type of approach are the Southwell method, modified Southwell approaches, "pivotal plot," and load vs. displacement-squared approach (Singer 1998, Fok 1984). Again, the applicability and reliability of these displacement-based approaches for plates has been questioned. The post-buckling path of a rectangular plate is different from the hyperbolic relationship of load and deflection for a column, which is the basis of the Southwell's method. The stable postbuckling nature of plates in compression have caused concern in the consistency of these load-displacement approaches. The pivotal plot method was developed by Spencer and Walker to attempt to overcome the problems associated with a nonlinear post buckling path, and makes allowance for initial imperfection, but only if the imperfections are small (Singer 1998). Furthermore, the pivotal plot has problems with computational stability, and if the pivotal points are not selected appropriately the method can lead to totally meaningless values (Fok 1984).

An approach that has been used in the determination of the web buckling load in research at the University of Texas is midspan deflection vs. lateral movement (Croce 1970). This is a modification of the load vs. displacement-squared approach. The load vs. displacement squared approach has been shown to be a satisfactory approach yielding fairly close lower bounds to P_{cr}, in some cases, but its usefulness with more significant initial imperfections is questionable. Given the concerns and uncertainties using each of the above-

mentioned methods, use of a simple technique, such as the load vs. displacement squared method, seems the best approach.

Using the load vs. displacement squared approach; the load is plotted against the square of the out-of-plane displacement. The load vs. displacement-squared plot exaggerates the load at which softening of the plate response occurs. The critical load is obtained by drawing a tangent to the load vs. displacement-squared plot as shown in Figure 7.34. The tangent to the curve is drawn prior to the postbuckling stiffening at loads well above the critical load.

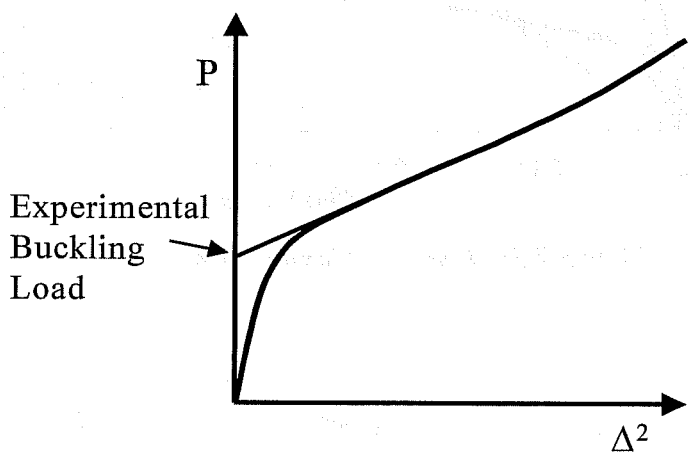

Figure 7.34 Load vs. Displacement Squared Approach

The load vs. displacement-squared approach was applied to the maximum displacements collected from the test plate results. The absolute values of the maximum measured plate displacement of each of the test plates are repeated in Figure 7.35. The maximum measured plate deflection for each of the plates tested was used to generate the load vs. displacement squared plot shown in Figure 7.36. The series labels in Figure 7.36 are the same as those used in Figure 7.35. The experimental buckling loads predicted by the tangents to the P vs. Δ^2 curves are shown in Table 7.12.

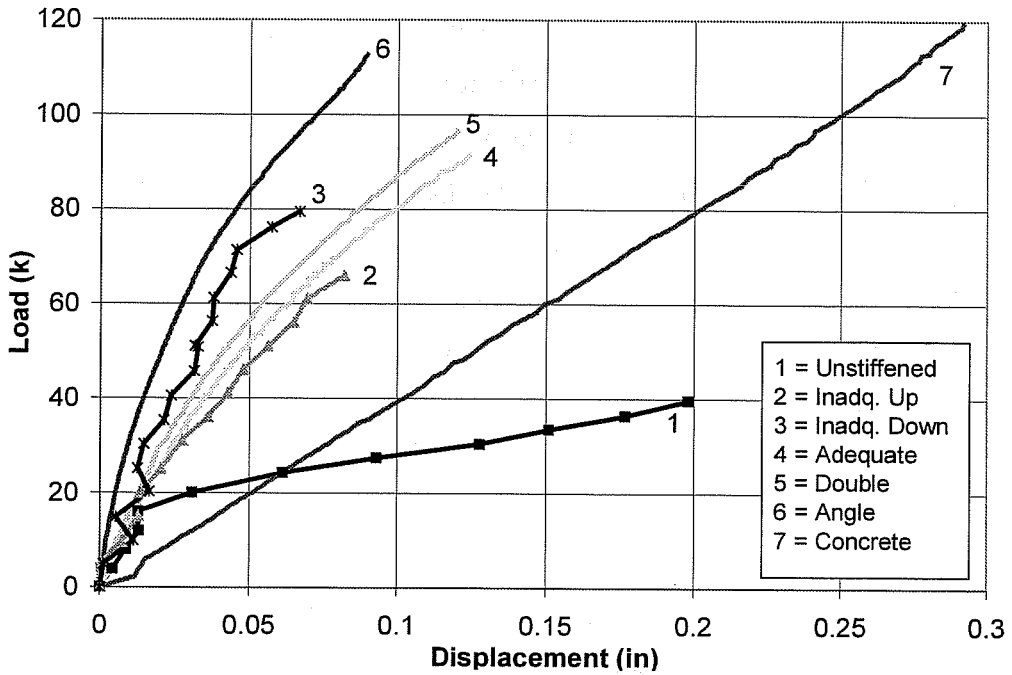

Figure 7.35 Load vs. Maximum Absolute Displacement

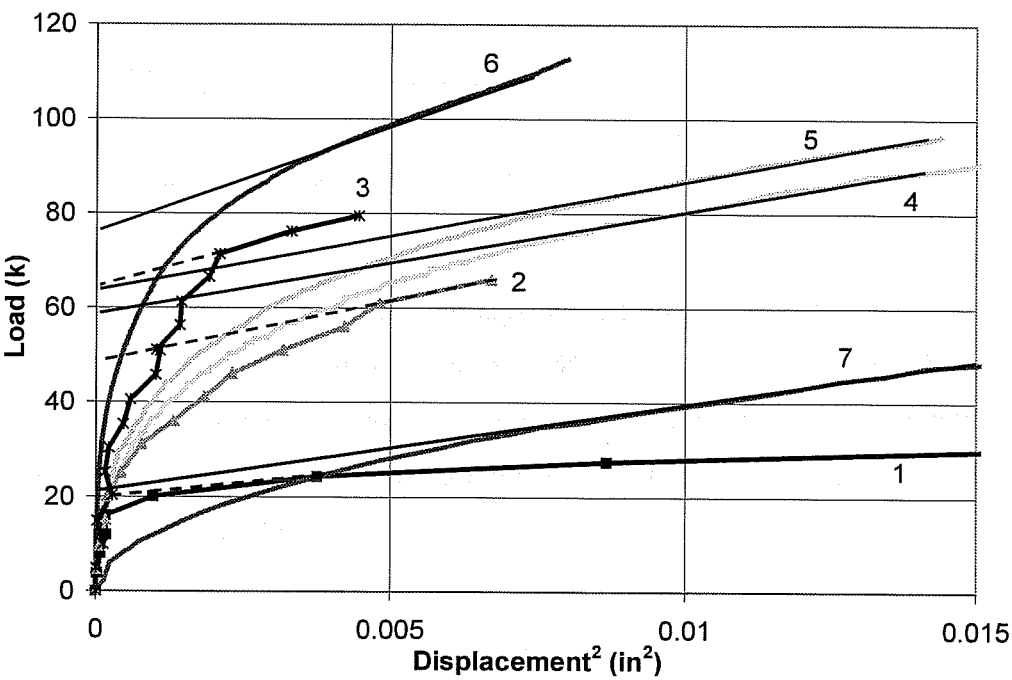

Figure 7.36 Load vs. Displacement Squared

Table 7.12 Critical Load Based on Load vs. Displacement Squared

Test Plate Stiffener	Experimental P vs. Δ^2 Buckling Load (k)	Eigenvalue Buckling Load (k)
Unstiffened	19.1	19.2
Inadequate Up	48.4	45.0
Inadequate Down	64.5	47.9
Adequate	58.5	84.3
Double	63.6	90.7
Angle	76.4	122
Concrete	20.4	130

The experimental buckling load and the eigenvalue-buckling load of the unstiffened plate are essentially equal. There is also reasonable agreement between the experimental and eigenvalue buckling load of the inadequate up test. In both of these tests, the plate displaced into three waves along the length as expected. The experimental buckling load of the inadequate down test plate is significantly larger than the eigenvalue buckling load. The response of the inadequate down test was stiffened by the initial imperfection vs. stiffener orientation, and consequently a higher experimental buckling load is predicted.

For all of the other test plates, the experimental buckling load predictions are much less than the eigenvalue buckling loads. The smallest experimental buckling load prediction was for the concrete stiffened test plate, and is less than one sixth of the eigenvalue-buckling load. The experimental buckling load predictions are not useful for the stiffened plates since no real buckling behavior

was observed in these tests. For comparison, the load vs. displacement squared approach was applied to plate displacements away from the stiffener. However since the displacement of the stiffener overwhelmed displacement of the plate between the stiffener and girder web, there was still not a meaningful buckling load using plate displacements away from the stiffener.

7.9 Other Issues

There were still several issues of concern after completion of the experimental and analytical program described thus far. These include the effect of eccentric stiffeners vs. stiffener pairs, impact of the moment gradient, and use of transverse stiffeners to control stiffener displacement. These issues will be discussed in Chapter 8. Also presented in Chapter 8 is a comparison of a strut based analysis approach to the provisions currently in AASHTO.

Chapter 8

Other Issues

8.1 Introduction

Several issues not specifically examined in the experimental tests are discussed in this chapter. The behavior of plates stiffened with pairs of stiffeners is compared to the behavior of plates with eccentric stiffeners. The impact of the moment gradient on the response of stiffened compression flanges is discussed. The behavior of plates stiffened with full transverse stiffeners, which are welded to the bottom flange, as opposed to transverse stiffener struts, which are attached only to the longitudinal stiffener and box webs, are compared. A presentation of a strut based analysis procedure is also given at the end of this chapter, and selected test results are compared to the AASHTO and strut approach capacities.

The finite element model of the test setup was used to analyze most of the effects discussed in this chapter. Consequently, the compression plate in this discussion is on the top of a box girder in positive moment, just like the test setup. The same conditions discussed apply for the bottom flange of the box in negative bending. The presentation format used thus far, with the test plate on the top a box girder in positive moment, is continued to attempt to minimize confusion.

8.2 Investigation of Stiffener Eccentricity

In the experimental tests of adequately stiffened plates, the largest displacements were recorded at the longitudinal stiffeners. The longitudinal stiffeners moved throughout the test as load was applied to the test setup. The AASHTO design procedure for adequate stiffeners is based on the assumption that the stiffeners remain straight, and form nodal lines about which the plate

buckles. This behavior was not seen in the experimental program. Several factors contributed to the stiffener movement, including initial stiffener out-of-straightness, overall girder bending, and the eccentricity of the stiffeners. In particular, the eccentricity of the stiffener was thought to have contributed significantly to the observed stiffener movement. Alternate stiffener designs with longitudinal stiffeners on both the top and bottom surface of the compression plate, and hence no cross-sectional eccentricity, were evaluated to investigate the impact of stiffener eccentricity.

Two sets of finite element models were developed to examine the influence of alternate stiffener designs on the magnitude of the stiffener movement. The first set of finite element models were of a stiffened plate loaded in uniform end compression and simply supported along its edges. Both the plate and stiffener were subjected to a uniform compressive load applied at the ends of the FEM. The second set of models was built using the FEM of the experimental test setup, with the compression plates attached to the scale box girder model. The properties of the adequate test plate were used as the basis for both sets of finite element models. The initial imperfection of the adequate test plate, which is repeated in Figure 8.1, was included in both sets of FEM.

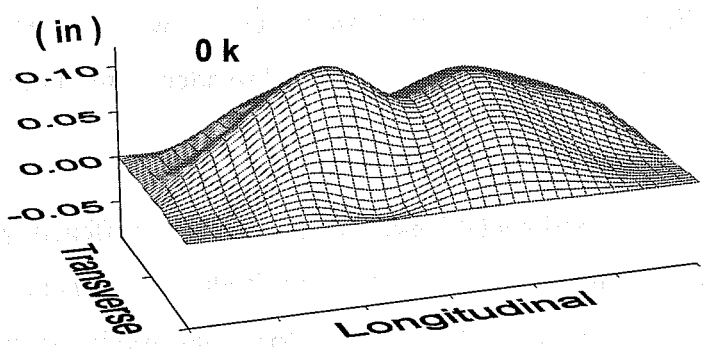

Figure 8.1 Initial Imperfection

The first set of finite element models of the stiffened plates under uniform compression did not include the effects of girder bending. This set of analyses examined only the influence of the initial imperfection on the response of the stiffened plate with alternate stiffener designs. Three stiffener alternates were evaluated in the analysis of the stiffened plates under uniform compression. The three stiffener designs are shown in Figure 8.2. The first stiffener pair in Figure 8.2 was designed to provide the same I_s, stiffener moment of inertia, as the single plate stiffener. The second stiffener pair was designed to provide the same total stiffener area as the single plate stiffener.

The first stiffener in Figure 8.2 is a single plate stiffener with an I_s of 1.3 in^4, as shown in the figure. As has been discussed, the moment of inertia of a single stiffener is calculated about an axis parallel to the flange plate and taken at the base of the stiffener. The axis about which the moment of inertia was calculated is shown by a dashed line in the figure with the single plate stiffener.

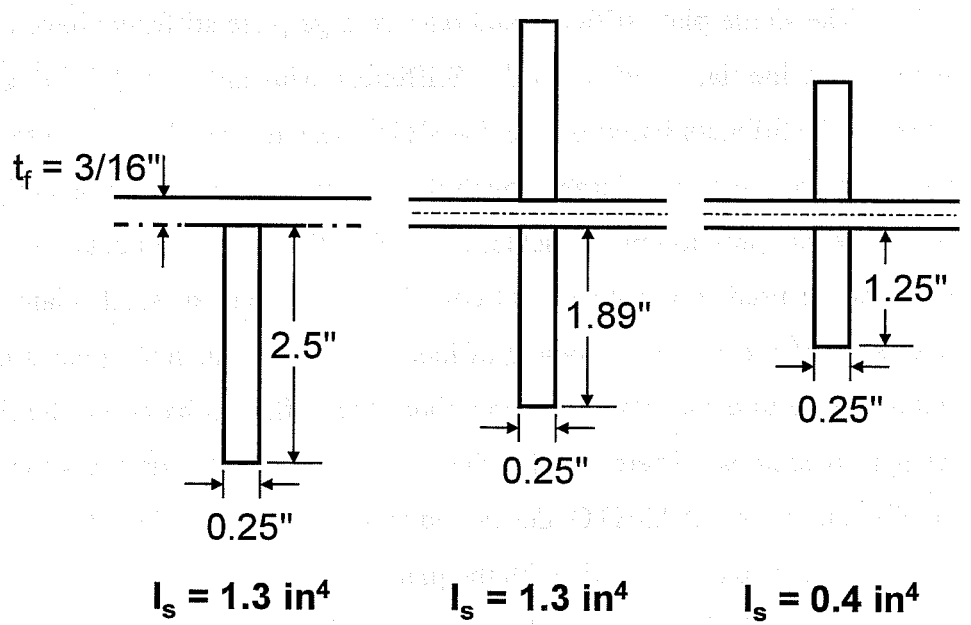

Figure 8.2 Stiffener Alternatives

The other stiffener designs shown in the figure have two plate stiffeners of equal size mounted to both the top and bottom surface of the compression plate. The moment of inertia of the stiffener pairs was calculated about the mid-thickness of the compression plate, shown by the dashed lines in the figures with two plate stiffeners. Pairs of stiffeners, on either side of the plate element, are often used for the transverse stiffeners of plate girder webs. The AASHTO LRFD Specification contains information for calculating the moment of inertia of transverse stiffeners for both single stiffeners and stiffener pairs in Section 6.10.8.1.3. For single stiffeners, the moment of inertia of the transverse stiffener is taken about the edge in contact with the web. This is the same approach used for calculation of the moment of inertia of a single longitudinal stiffener. For transverse stiffener pairs, the moment of inertia is taken about the mid-thickness of the web. Similarly, with the pair of longitudinal stiffeners, the moment of inertia was calculated about the mid-thickness of the compression plate.

The single plate stiffener and pair of large plate stiffeners have a stiffener moment of inertia, I_s, of 1.3 in^4. Stiffeners with an I_s of 1.3 in^4 qualify as "adequate" stiffeners based on the AASHTO design procedures. These adequate stiffeners are sized to be large enough that the stiffener will form a straight nodal line. The compression plate buckles about the stiffener and a buckling coefficient of 4 can be used in the AASHTO equations. The pair of small plate stiffeners have an I_s of 0.4 in^4. The moment of inertia of the pair of small plate stiffeners is not adequate to cause plate buckling about the stiffeners based on the AASHTO design procedures. Therefore, for the pair of small plate stiffeners the buckling coefficient in the AASHTO design equations would be less than 4 and the stiffener is expected to buckle with the plate.

Large displacement analyses of the plate in compression, with elastic material properties and nonlinear geometry, were performed. The shapes of the

relative displacement of the plates are shown in Figure 8.3. The displaced shapes were generated at the same applied load using the same displacement magnitude. The load-displacement response at the longitudinal stiffener in the middle of the plate is shown in Figure 8.4. The load in this figure was normalized with respect to P_{ref}, the eigenvalue-buckling load of the plate with the centerline nodes fixed against out-of-plane movement.

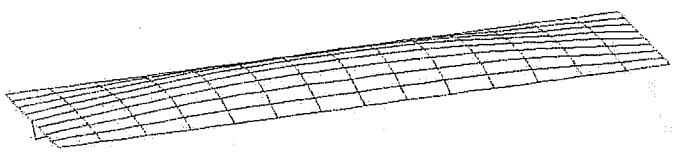

Single Plate Stiffener, $I_s = 1.3\ in^4$

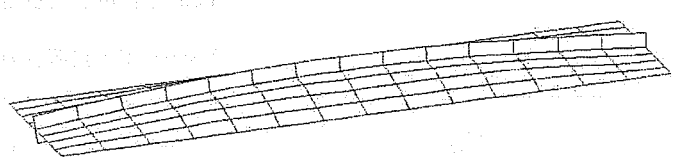

Two Plate Stiffeners, $I_s = 1.3\ in^4$

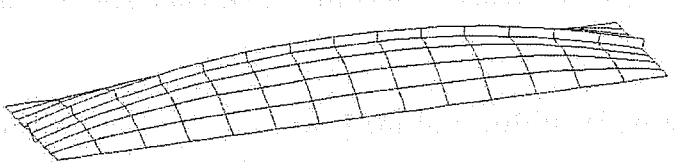

Two Plate Stiffeners, $I_s = 0.4\ in^4$

Figure 8.3 Stiffened Plate under Uniform End Compression

The load-displacement plot in Figure 8.4 shows very similar responses for the two stiffener designs with an I_s of 1.3 in^4 up to the level of P_{ref}. The initial stiffness is the same for the designs with the same I_s. Above P_{ref}, when the test plate is bending significantly, the design with the single plate stiffener shows

larger displacements at a given load. The design with the pair of large plate stiffeners does a better job of controlling displacements at higher loads when bending is more significant than does the eccentric stiffener.

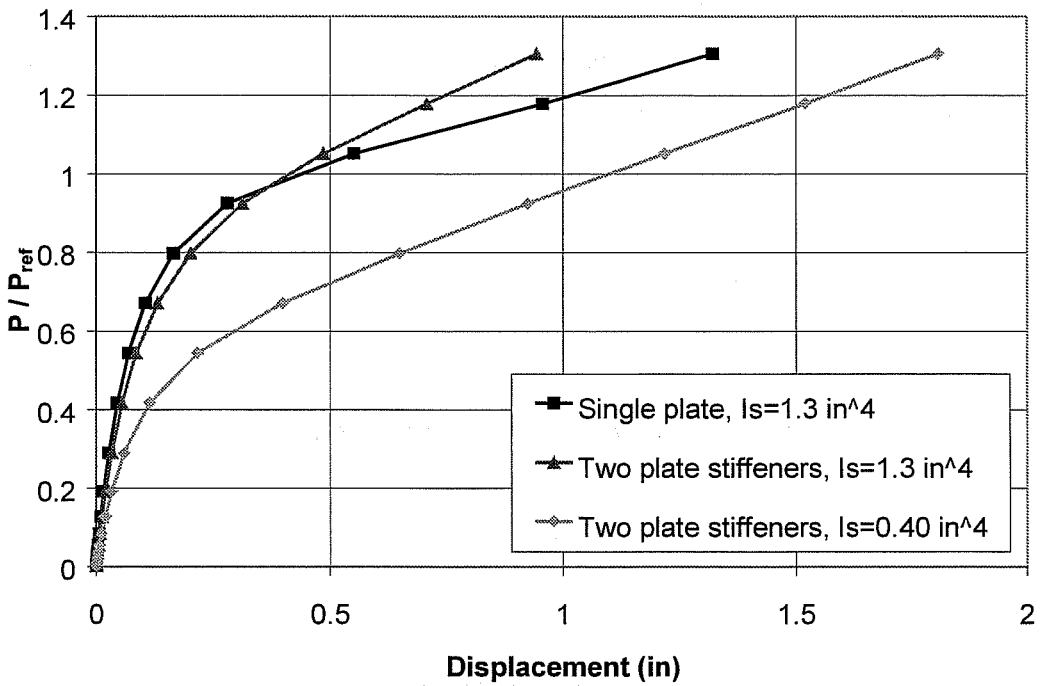

Figure 8.4 Load-Displacement of Stiffened Plate under Uniform Compression

The initial stiffness of the plate with the small pair of plate stiffeners is less than that of the plates stiffened with the other stiffener designs. As shown in Figure 8.4, with the small pair of plate stiffeners there are larger displacements at all load levels than with the other stiffener designs. The small pair of plate stiffeners provide the same total stiffener area as the single plate stiffener, but less than 1/3 the stiffener moment of inertia of the other two stiffener designs. Larger displacements occurred at all load levels with the smaller stiffener moment of inertia.

The stiffener design alternates presented above were also analyzed using the finite element model of the experimental test setup. In this model the compression plate is attached to the girder, and is subjected to a compressive load as well as girder bending. The compression flange is on the top surface of the box in the FEA models of the test setup. A fourth stiffener design was included in this analysis. This stiffener had a tee shape and the same I_s as the single plate stiffener and the larger pair of plate stiffeners, as shown in Figure 8.5. A tee shaped stiffener was included in this set of analysis since it was felt that the stiffener displacement due to overall girder bending might be worse with the tee shaped stiffener. The centroid of the tee stiffener is closer to the flange of the tee, not at the mid-height of the web like a plate stiffener. The line of action of the load in the stiffener is therefore further away from the compression plate with a tee stiffener than with a plate stiffener of the same height, as shown in Figure 8.6. To investigate any differences that might exist with a tee stiffener versus a plate stiffener, a tee stiffener was included in this set of finite element models.

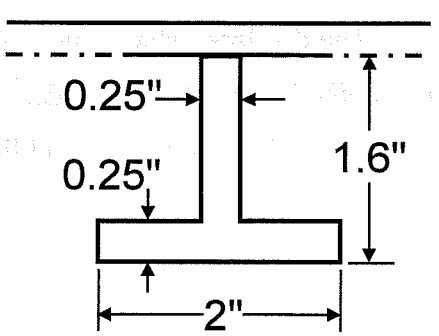

$I_s = 1.3\ in^4$

Figure 8.5 Tee Stiffener

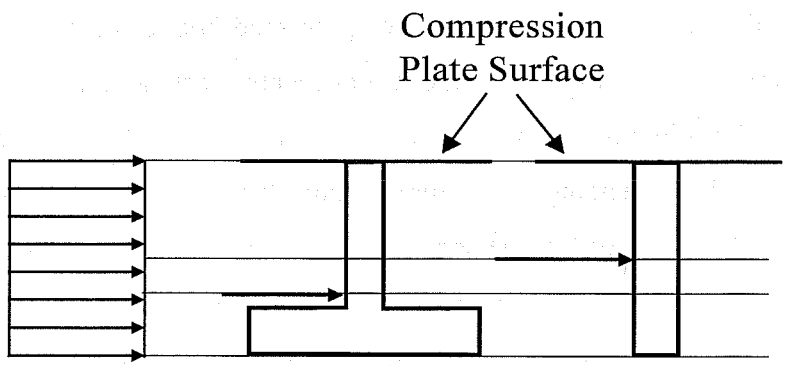

Figure 8.6 Line-of-Action of Load in Stiffener

The initial imperfection of the adequate test plate was input to the finite element model. As was previously discussed, this initial imperfection was actually reduced under load in the experimental tests. This means that the movement of the compression plate due to overall girder bending was opposite the direction of movement due to the initial imperfection. The initial imperfection and girder bending effects are not additive in this case. The displaced shapes of the plates with each of the four stiffener alternates are presented in Figure 8.7. The displaced shapes were generated at the same applied load and using the same displacement magnitude. The load at which the plots were generated was just above the eigenvalue buckling load of the test plate with the single plate stiffener.

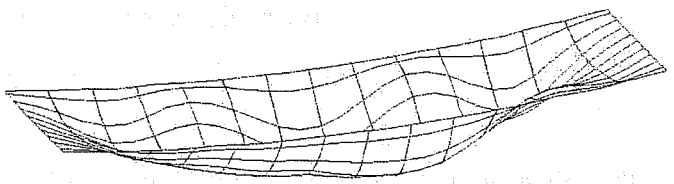

Single Plate Stiffener, $I_s = 1.3\ in^4$

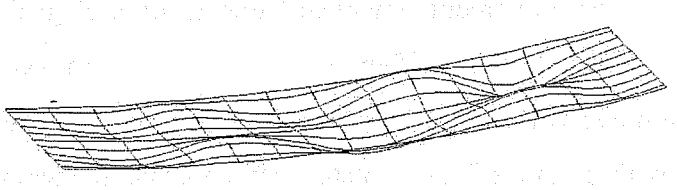

Two Plate Stiffeners, $I_s = 1.3\ in^4$

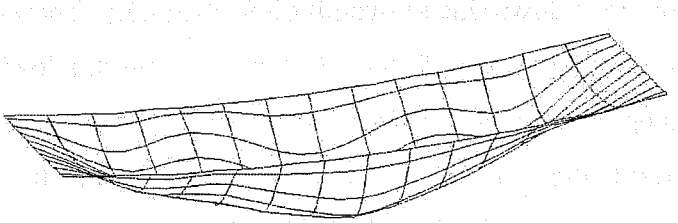

Tee Stiffener, $I_s = 1.3\ in^4$

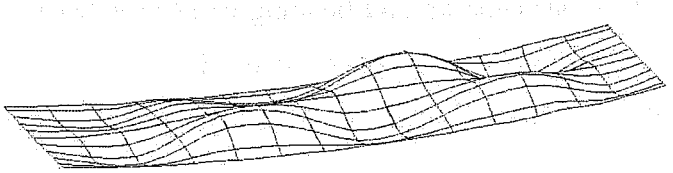

Two Plate Stiffeners, $I_s = 0.4\ in^4$

Figure 8.7 Displaced Shape of Plates in Test Setup Finite Element Model

The load-displacement response at the longitudinal stiffener in the middle of the plate is shown in Figure 8.8. The eigenvalue buckling load of the test plate with the single plate stiffener is 84 kips. The curves in this figure show that larger displacements were generated with the eccentric single plate and single tee

stiffeners. As was predicted, the largest displacements occurred with the single tee stiffener. Significant displacements also were seen with the single plate stiffener.

For the plate with a pair of small plate stiffeners, the tendency for movement upward, in the direction of the initial imperfection, was greater than the tendency for movement downward due to overall girder bending. For the plate with the small pair of stiffeners the tendency for movement due to the initial imperfection overwhelmed the tendency for movement due to girder bending. For the plate with a pair of large plate stiffeners the tendency of the stiffener to displace upward due to the initial imperfection was approximately the same as the tendency to move down due to overall girder bending. Therefore the stiffener was fairly straight up to a load of about 70 kips. Above this load, the combination of plate bending and girder bending overwhelmed the tendency of the stiffener to move upward due to the initial imperfection, and the stiffener displaced downward with the application of additional load.

With the eccentric single plate stiffener and tee stiffener, the movement due to overall girder bending and bending due to the eccentricity of the stiffener dominated the response. The plates with single eccentric stiffeners displaced downward throughout the application of load to the FEM.

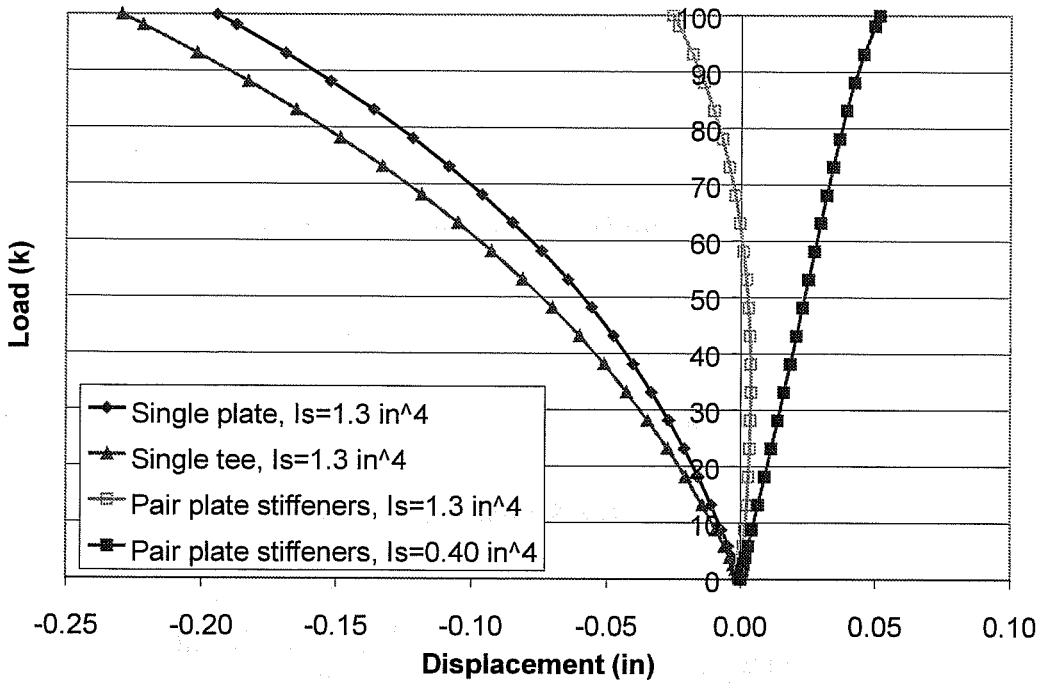

Figure 8.8 Load-Displacement of Stiffened Plate in Test Setup FEM

The initial imperfection from the adequate test was reversed, and the finite element analysis of the plate in the girder model was repeated. With the reversed imperfection the plate was initially displaced down in the middle of the plate with respect to the edges of the plate. With this initial imperfection, the tendency for stiffener movement from the initial imperfection was additive to the tendency for movement from bending. The displaced shapes of the plates with the reversed imperfection for each of the four stiffener alternates are presented in Figure 8.9. The displaced shapes were generated at the same applied load using the same displacement magnitude. The load at which the plots were generated was just above the eigenvalue buckling load of the test plate with the single plate stiffener.

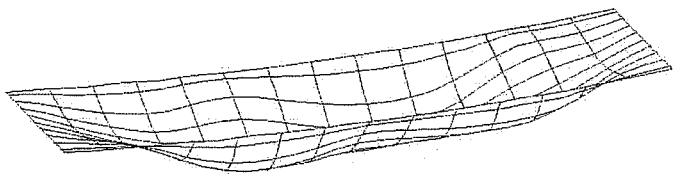

Single Plate Stiffener, $I_s = 1.3\ in^4$

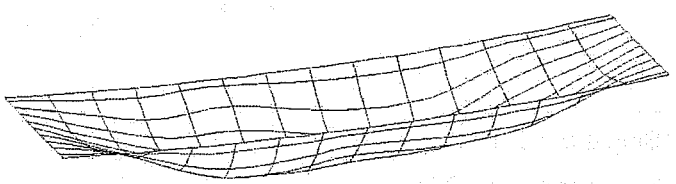

Tee Stiffener, $I_s = 1.3\ in^4$

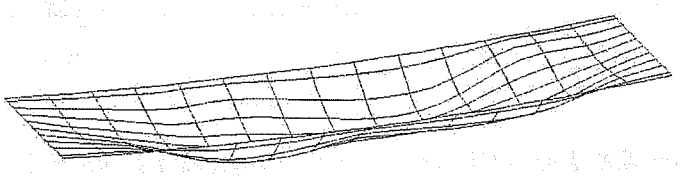

Two Plate Stiffeners, $I_s = 1.3\ in^4$

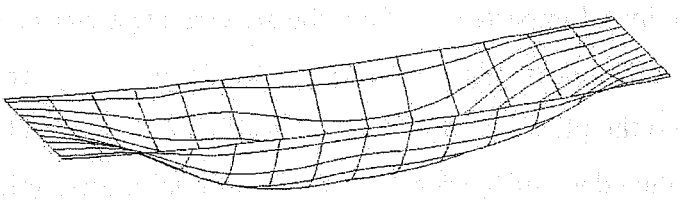

Two Plate Stiffeners, $I_s = 0.4\ in^4$

Figure 8.9 Displaced Shape of Plates in Test Setup Finite Element Model - Reversed Initial Imperfection

The load-displacement response at the longitudinal stiffener in the middle of the plate for each of the stiffener alternatives is shown in Figure 8.10. The eigenvalue buckling load of the test plate with the single plate stiffener is 84 kips.

Note that the scale in this figure is larger than that used in Figure 8.8. Much larger stiffener displacements resulted because of the additive effects of the initial imperfection and bending. The largest displacement was seen for the stiffener pair with an I_s of 0.4 in^4. Larger displacements were expected for this stiffener pair since its I_s was significantly smaller than the I_s of the other stiffeners. With the initial application of load, the plates with the stiffener pairs exhibited a stiffer response than the plates with single stiffeners. The eccentric stiffeners are more sensitive to the influence of girder bending and moved more with the initial application of load.

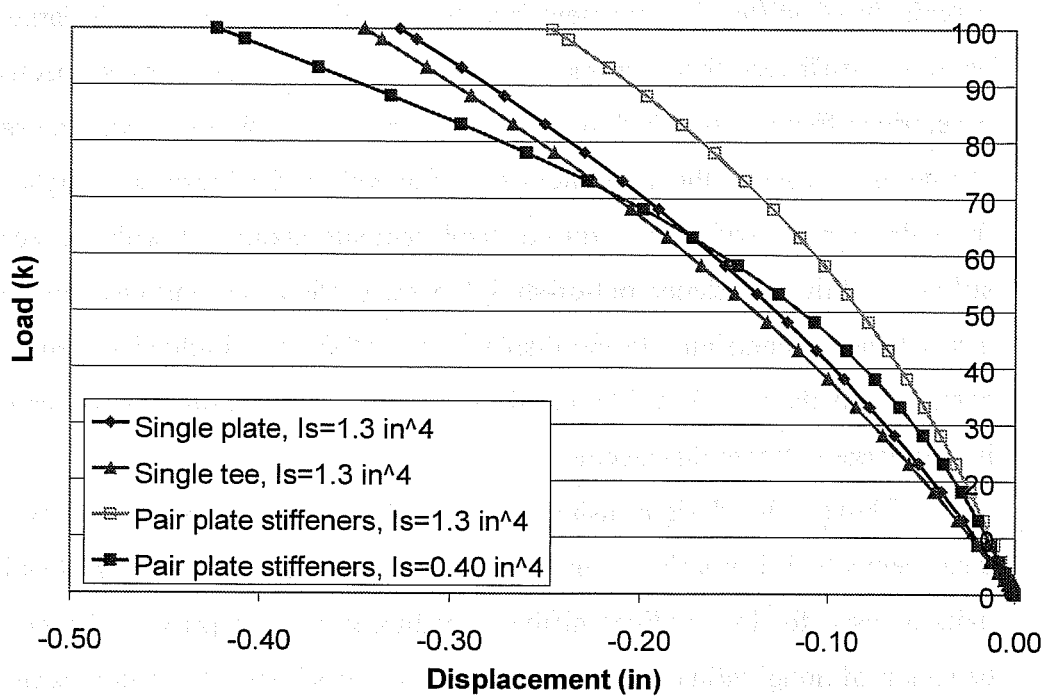

Figure 8.10 Load-Displacement of Stiffened Plate in Test Setup FEM - Reversed Initial Imperfection

At higher loads, the pair of large plate stiffeners displaced the least. The next smallest displacement was with the single plate stiffener followed by the single tee. The larges displacements were seen with the small pair of plate stiffeners. Again, the pair of large plate stiffeners was less sensitive to overall girder bending in particular, and stiffener bending in general, since the line of action of the stiffener force is closer to the centerline of the plate with pairs of plate stiffeners. Therefore with the pair of plate stiffeners that provided a significant I_s, the magnitude of the displacement was reduced compared to the eccentric stiffeners with the same I_s.

The study of the stiffener alternatives discussed above confirmed that the magnitude of stiffener movement due to overall girder bending is larger with eccentric stiffeners than for pairs of plate stiffeners. As was suspected, the eccentric stiffeners displaced more than a pair of plate stiffeners with the same I_s. Furthermore, even without the inclusion of overall girder bending, at higher loads the pair of plate stiffeners reduced displacements compared with the eccentric stiffener. Initial stiffener out-of-straightness, stiffener eccentricity, and overall girder bending contribute to the displacement of the longitudinal stiffener of the compression flange. Additive initial imperfection and bending effects can result in very large stiffener displacements.

Though the designs using pairs of plate stiffeners result in lower final displacements, it is not the recommendation of this dissertation that plate stiffener pairs be used for longitudinal stiffeners of box girder compression flanges. The behavior of longitudinal stiffener pairs was investigated to better explain the behavior seen in the experimental program, and to further investigate the response of plates in compression. As shown in Figure 8.10, use of stiffener pairs reduces the magnitude of the displacements but will not eliminate stiffener displacements.

Often box girder sections are chosen based on their aesthetic appeal, rather than economic or structural concerns. The clean, closed shape of the box section is attractive to the public. Placement of stiffeners on the outside of the box section would detract from their appearance, as well as complicate handling of the boxes prior to construction. Sections of box girder bridges are stored with the bottom flange resting on the ground during fabrication and prior to erection. Mounting a stiffener to the outside surface of the bottom flange would require blocking up the section during storage to ensure the stiffener was not damaged. Handling of the girder would also require greater care to ensure exterior stiffeners were not damaged. The more important consideration however is still aesthetics. Aesthetic considerations simply do not allow placement of bottom flange longitudinal stiffeners on the outside of the box section. An investigation of stiffener pairs was done to help clarify the factors contributing to the behavior seen in the experimental testing program, but use of stiffener pairs for longitudinal stiffeners is not a recommended alternative.

8.3 Impact of Moment Gradient in Negative Moment Region

One factor not investigated in the testing program that may potentially influence the behavior of the steel compression flange of box girder bridges is the steep moment gradient that typically exists in the negative moment region. The box girder bridge section is generally chosen for longer span structures. In longer span structures, the moment from the uniform dead load, rather than moment from live loading, generally dominates at the pier. In the negative moment region of continuous bridges under uniform loading, there is a steep moment gradient near the pier as shown in Figure 8.11. The largest negative moment occurs at the piers, and the magnitude of the negative moment decreases at sections away from the pier. For non-haunched box girders with uniform section properties, the bottom

flange compressive stress is subsequently also greatest at the pier, and decreases away from the pier section. The highest stress, at the pier section, is used for the design of the bottom flange element in that area. However the compressive stress in the bottom flange away from the pier section may be much less than that at the pier section. This stress gradient in the bottom flange is not considered in design.

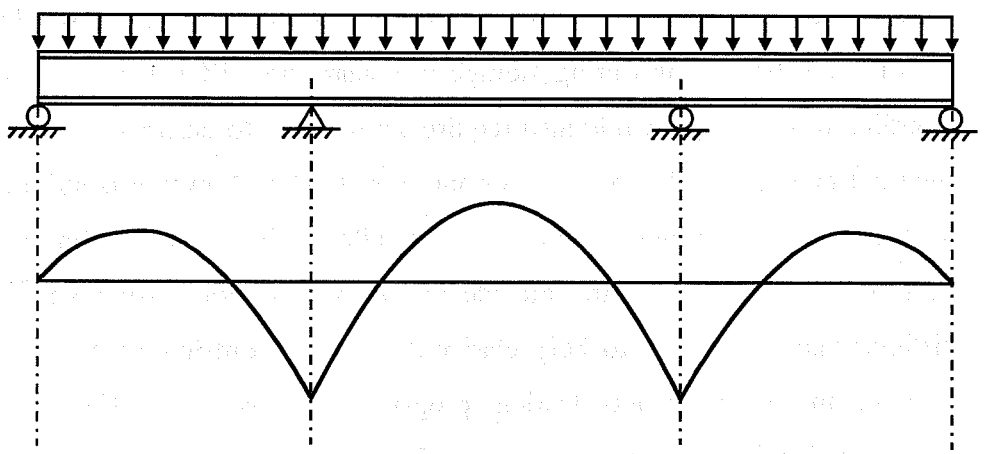

Figure 8.11 Three Span Continuous Bridge - Bending Moment

When large box girder structures with deep boxes are designed, it is not uncommon to use haunched girder profiles, with deeper sections at the interior piers and shallow sections in the positive moment regions. A photo of the Storrow Drive Connector Bridge, which has a haunched profile, is shown in Figure 8.12. With the haunched profile the negative bending moment will again have a steep gradient near the pier, but the bending stresses in the bottom flange will not vary as sharply along the length of the girder. The compressive stress in the bottom flange is reduced through the use of the deeper section at the piers. The compressive stress in the bottom flange will be more uniform with use of the haunched profile.

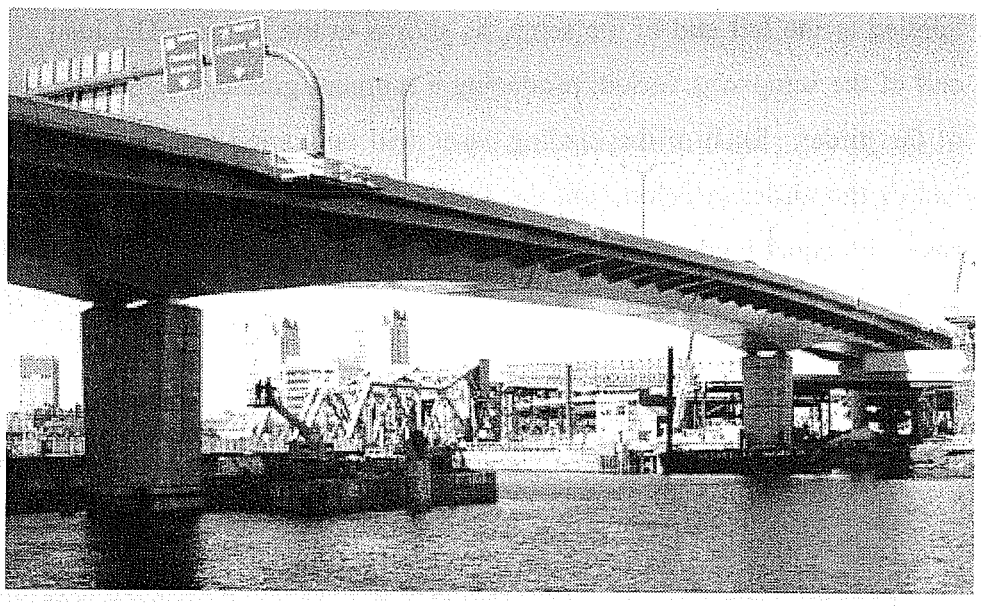

Figure 8.12 Haunched Girder - Storrow Drive Connector Bridge (TEC 2001)

Box girder profiles typically used for non-signature bridges in Texas and across the United States do not include haunches. The compressive stress in the bottom flange varies with distance from the pier due to the moment gradient, as discussed above. During the experimental testing program significant movement of the longitudinal stiffeners was observed. It was thought that with a moment gradient along the test plate, and lower stresses at one end of the test plate, the response of the plate might be different. The impact of the moment gradient on the behavior of the steel compression flange was examined using the finite element model of the adequate test plate.

Both eigenvalue and large displacement analyses were performed. Elastic material properties and nonlinear geometry were used in the large displacement analyses. The measured initial imperfections of the adequate test plate were included in each of the large displacement analyses. Four different loading configurations were considered, and are shown in Figure 8.13. A load of P was

applied to the left end of the setup, as shown in the figure. The load at the right end of the setup was varied, producing a moment gradient across the center span of the girder. Each of the loading cases will be named using the load at the left end of the girder, a colon, and the load at the right end of the girder. Thus, the case with equal loads on the ends of the girder is P:P, and the second loading case in Figure 8.13 is P:0.9P.

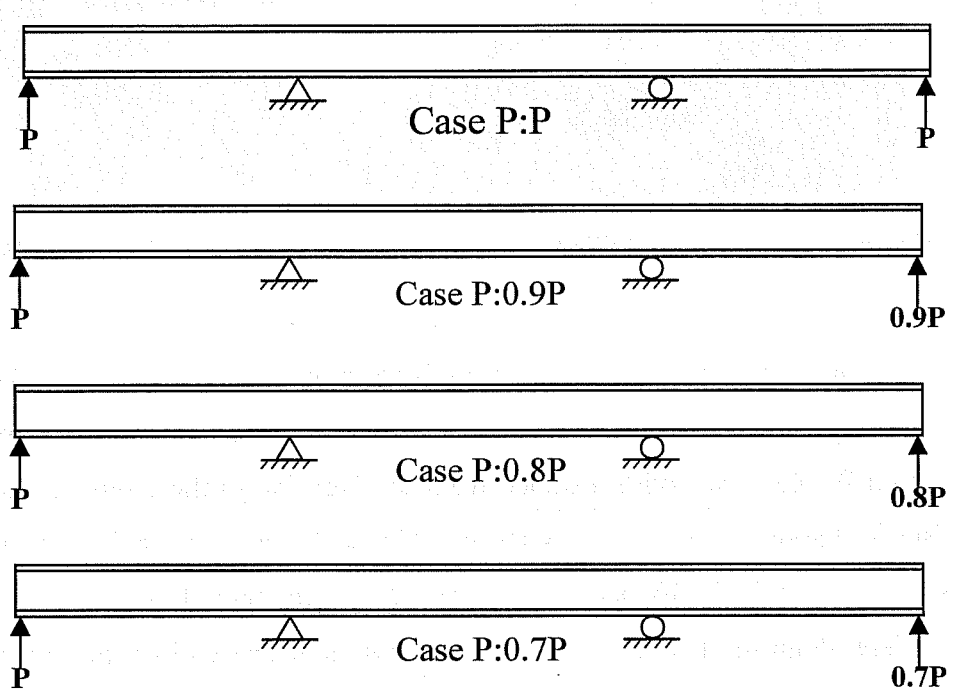

Figure 8.13 Loading Cases

With a load of P on the left end of the girder and 0.9P on the right end, the bending moment at the left support is M and the moment at the right support is 0.9M. The proportion of the moment at the left support to that at the right support is the same as the proportion of the load at the left end to the load at the right end.

The eigenvalue-buckling loads for each of the load cases are shown in Table 8.1. The eigenvalue-buckling load was increased with the presence of the moment gradient. This response indicates that when a lower load is applied at the right end of the girder, a larger load can be applied to the left end of the girder before the buckling load of the compression plate is reached.

Table 8.1 Eigenvalue Buckling Load

Load Case	**Eigenvalue Buckling Load $P_{cr} = P$ (kips)**
P:P	84.3
P:0.9P	88.3
P:0.8P	91.8
P:0.7P	95.1

Large displacement analyses were also completed for each of the load cases. The displaced shapes for the P:P and P:0.7P load cases are shown in Figure 8.14. The displaced shape of the plate with equal loads on the ends of the girder was very similar to the displaced shape with unequal loads. The stiffener still moved, as was observed in the experimental tests, however, the magnitude of the displacement at a given load was reduced with the presence of the moment gradient. The load-displacement histories at two points, shown in Figure 8.15, are presented in Figure 8.16 and Figure 8.17.

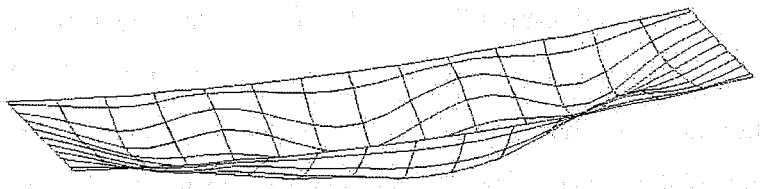

Load Case - P:P

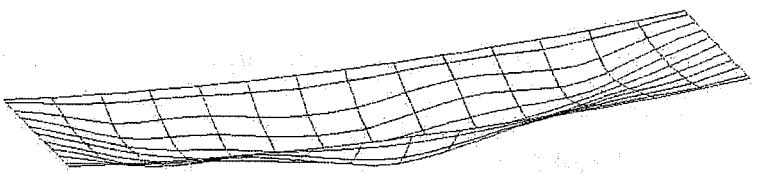

Load Case - P:0.7P

Figure 8.14 Displaced Shape of FEA Compression Plate, P=100kips

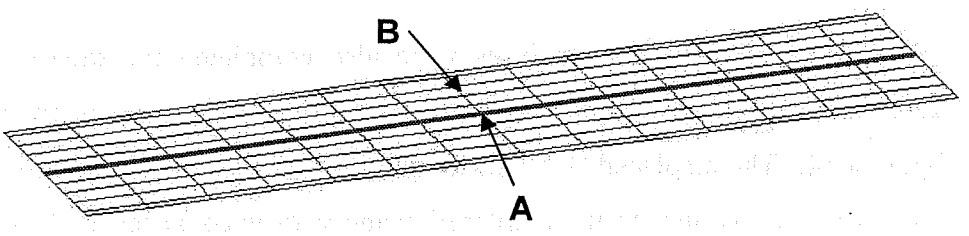

Figure 8.15 Load-Displacement Plot Locations

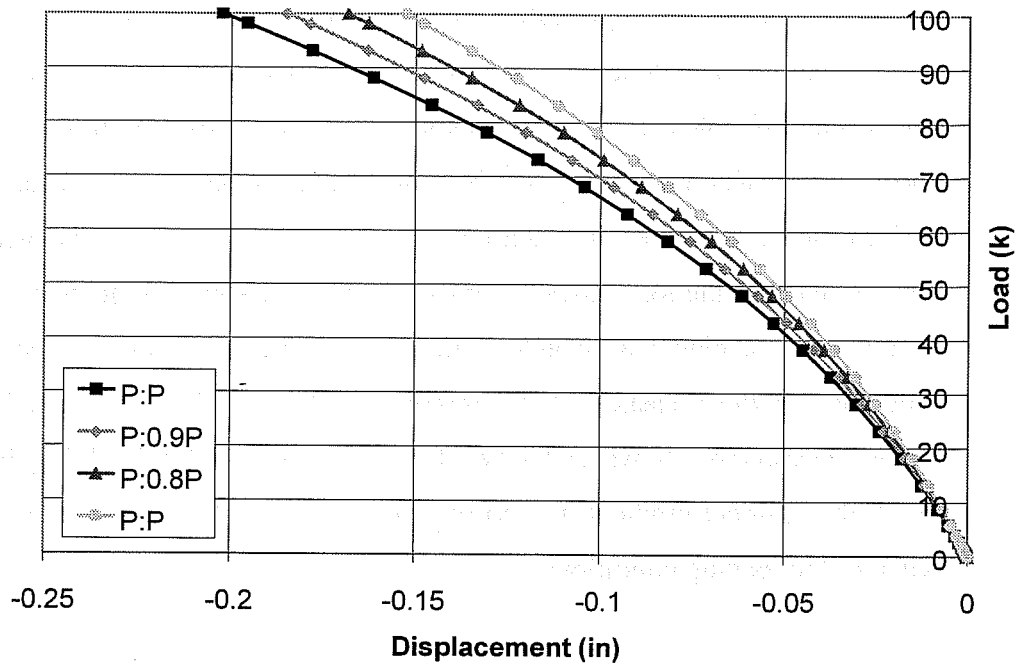

Figure 8.16 Load-Displacement at Location A

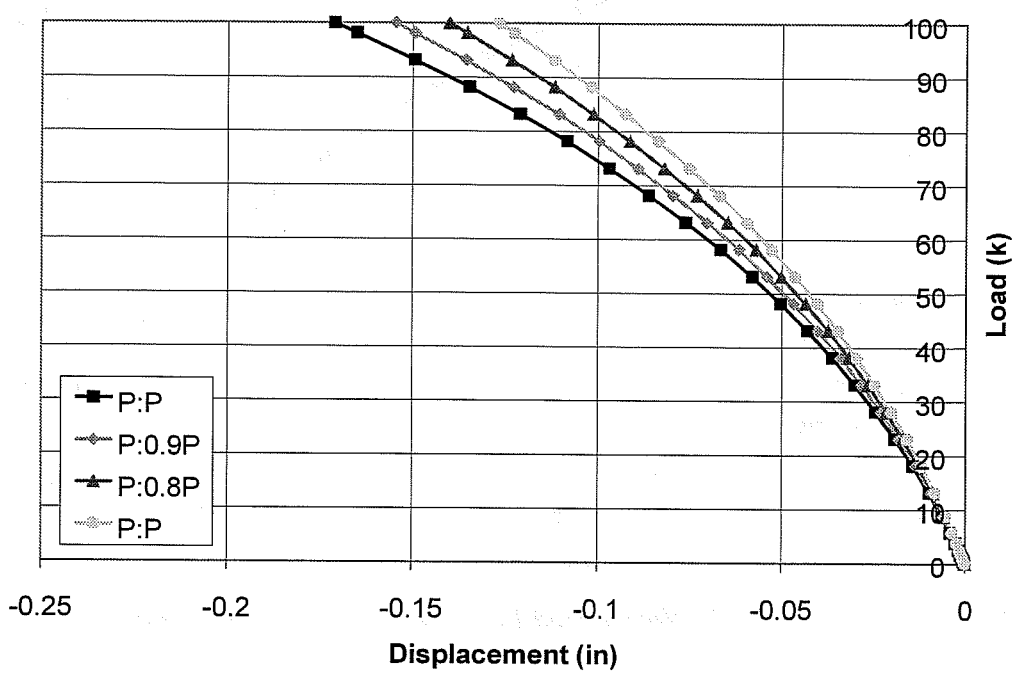

Figure 8.17 Load-Displacement at Location B

As described, the eigenvalue-buckling load was increased due to the presence of the moment gradient. The values of P_{cr} for the different load cases were presented in Table 8.1. The load-displacement data presented in Figure 8.16 was normalized with respect to the buckling load for each load case. This normalized plot is presented in Figure 8.18. The normalized load-displacement response for each of the load cases is almost identical. Using an eigenvalue based design approach, a higher allowable load could be permitted due to the larger buckling load in the presence of the moment gradient. The normalized load-displacement response shows that when the higher eigenvalue buckling load is used with the moment gradient, the normalized response of the plate is the same with each of the loading conditions.

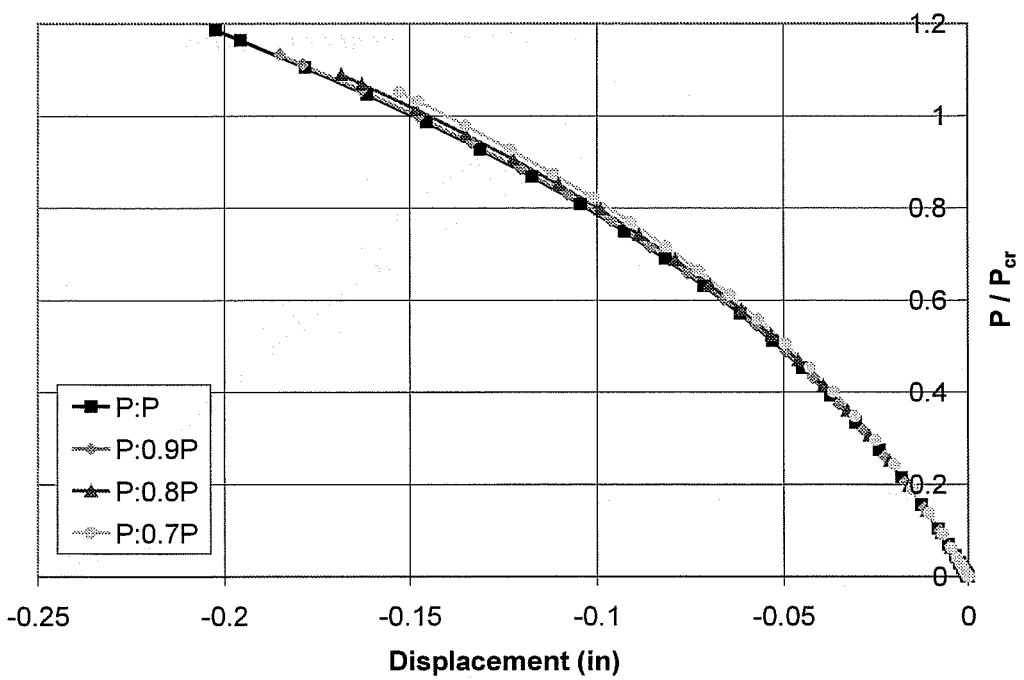

Figure 8.18 Normalized Load-Displacement at Location A

The stresses obtained from the large displacement analysis were also examined. A stress contour of the plate for the P:P case is presented in Figure 8.19 and the same contour for the P:0.7P case is shown in Figure 8.20. Both of these plots are at a load of P=83 kips, just below the eigenvalue buckling load, with the same scale. With the moment gradient, the stress at the right end of the plate is reduced compared to the P:P case. This seems reasonable, since smaller loads are applied at the right end of the girder, and a smaller bending moment is generated at the right support, and consequently smaller compressive stresses are generated in the right end of the plate.

With the moment gradient, the highest stressed areas of the plate are localized to the left end of the plate. However, these local areas are as highly stressed as is seen in the equal load case. At a given load, P, the maximum stress in the plate is comparable whether or not there is a moment gradient, but only a very small local area of the plate is highly stressed in the presence of the moment gradient.

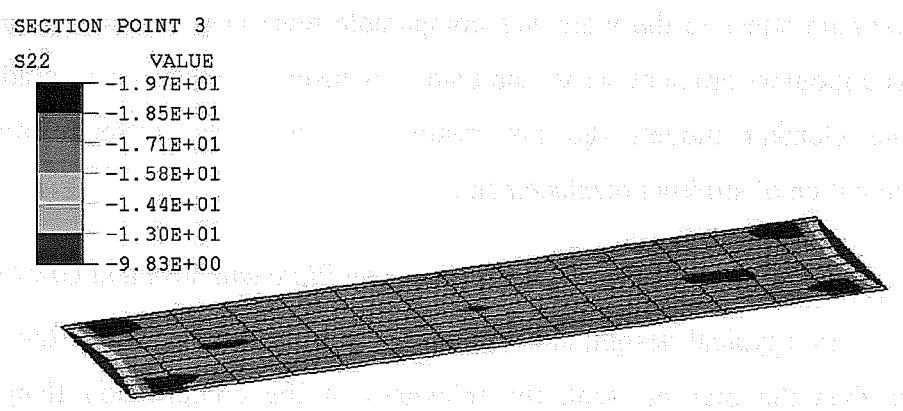

Load Case - P:P

Figure 8.19 Axial Plate Stress, P=83 kips

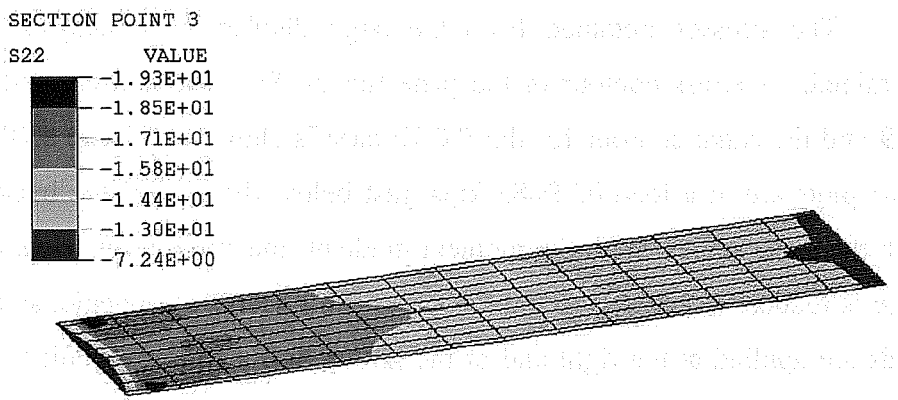

Load Case - P:0.7P

Figure 8.20 Axial Plate Stress, P=83 kips

In summary the presence of the moment gradient results in larger eigenvalue buckling load predictions, and smaller displacements at a given load. However, there was still significant stiffener displacement with the moment gradient. The normalized load-displacement response of the plate is the same for the equal loading case and for the load cases producing a moment gradient. The maximum stress in the plate was comparable regardless of whether or not there was a moment gradient across the plate. Inclusion of the moment gradient in the finite element models did not result in a markedly different response or elimination of stiffener displacement.

8.3.1 Impact of Reduced Plate Thickness on Plate with Moment Gradient

In a typical design, at a section away from the pier where the moment is less than the pier moment, the thickness of the compression flange plate is reduced. A reduced plate thickness was input over part of the test plate in the finite element model for the P:0.7P loading case to examine the influence of this reduced thickness on the overall behavior of the plate. The thickness of the plate

was reduced 15% from 0.1913 in. to 0.1626 in. on the right end of the plate shown in Figure 8.21. The reduced plate thickness used was chosen using the member plate stresses from the FEA at the reduced section and the AASHTO design equations for slender plates with a buckling coefficient of 4.

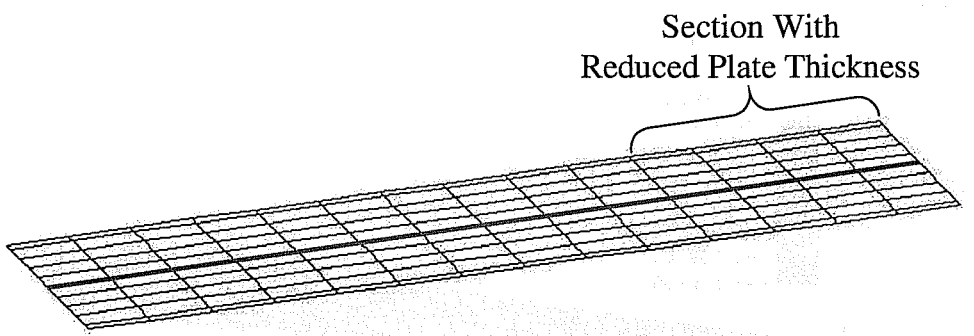

Figure 8.21 Reduced Plate Thickness

The inclusion of the reduced plate thickness had very little impact on the displacements of the plate. The displaced shape of the plate was the same with the reduced thickness section, and the maximum displacement was increased less than 1% with inclusion of the reduced plate section. The stress contours for the P:0.7P load case and for the P:0.7P load case with the reduced plate thickness are shown in Figure 8.22.

The stresses in the right end of the plate are higher in the second plot in Figure 8.22 since the thickness of the plate was reduced in this area. The transverse membrane action supporting the plate over the width of the plate was more significant to the plate behavior than the longitudinal membrane action. Though the plate section is reduced in the right section of the plate, this reduction did not affect the response of the plate away from the reduced section. Since the plate thickness at the critical section was not decreased, the membrane action

across the width of the plate at the critical section remained the same, and the stresses and displacements at the critical section were unchanged. There was no negative impact on the critical section due to the reduction in plate thickness away from the critical section. The practice of reducing the flange thickness away from the critical section of the plate does not seem to adversely affect other areas of the plate.

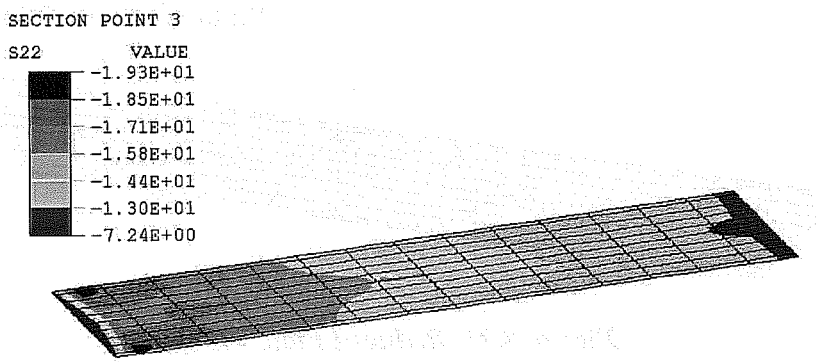

Load Case - P:0.7P

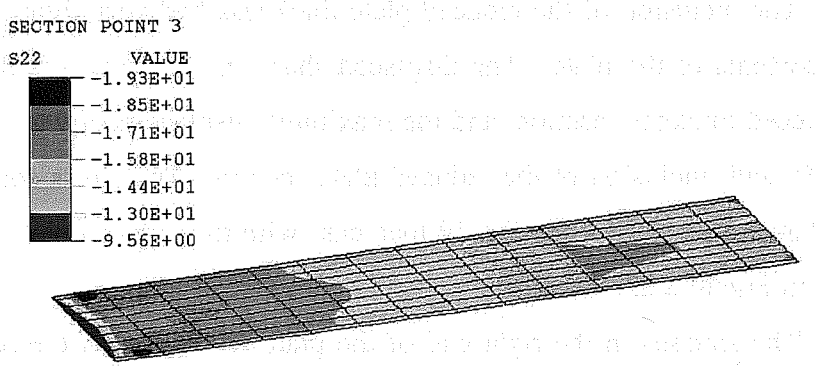

Load Case - P:0.7P, Reduced Plate Thickness in Right Section

Figure 8.22 Axial Plate Stress, P=83 kips

8.4 Transverse Stiffeners

A key observation from the experimental testing program is that AASHTO "adequate" longitudinal stiffeners do not remain straight when the box girder is loaded. The stiffeners are initially not straight, and under uniform compression of a stiffened plate, the tendency is for the initial out-of-straightness of the stiffener to increase. Overall girder bending and local bending of the bottom flange, also result in stiffener movement, particularly with eccentric stiffeners.

As was observed in the experimental program, and verified in the subsequent finite element analysis, the stiffeners moved significantly during the application of load to the girder section. The longitudinal stiffeners displaced vertically throughout the application of load to the test setup. Substantial movement of the stiffener was not expected and is not desired. The analysis procedure used in AASHTO for adequate stiffeners includes a plate buckling coefficient of 4 and is based on the assumption that the stiffeners remain straight and form nodal lines about which the plate will buckle. There was no expectation of or consideration of large stiffener displacements in the formulation of the design equations used in the AASHTO specifications. Furthermore, secondary bending stresses result at panel boundaries from out-of-plane deflections of the flange, similarly to the effect of out-of-plane web deflections described by Yen and Mueller, which creates a fatigue concern (Yen 1966a).

To control displacement of the longitudinal stiffener, transverse stiffeners can be added to the bottom flange. Fully welded transverse stiffeners that are connected to the bottom flange, longitudinal stiffener, and webs of the box girder are typically used in large European box girder designs. Displacement of the longitudinal stiffener can also be controlled by using a transverse stiffener that is not connected to the flange plate, but is connected to the webs of the box and the

longitudinal stiffener. A transverse stiffener such as this can be incorporated into the interior cross-frames of the box girder.

Internal cross-frames, such as the K-frame shown in Figure 8.23, are provided to control distortion of the box section. Close spacing of the K-frames provides better control of the distortion of the box section (Fan 1999). A low strut can be included in the internal cross-frame, as shown in Figure 8.24. The low strut of the diaphragm is connected to the webs of the box and to the longitudinal stiffener. This transverse stiffener strut controls vertical displacement of the longitudinal stiffener at the point of attachment.

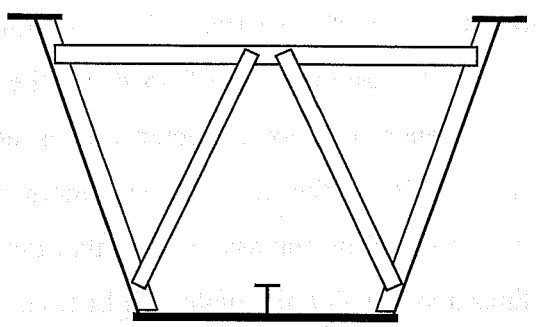

Figure 8.23 Internal Cross-Frame

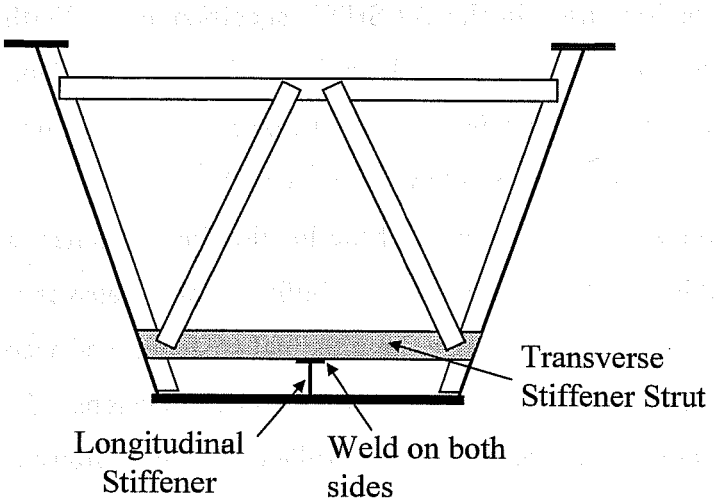

Figure 8.24 Transverse Stiffener Strut

In the study by Fan and Helwig, interior cross-frames were provided at 10 ft. and 20 ft. spacings and the width of the bottom flange element was 80 in. (Fan 1999). If a transverse stiffener strut is included at each cross-frame, the resulting aspect ratio, a/b, of the bottom flange plate would be 1.5 for the 10 ft. cross-frame spacing and 3 for the 20 ft. cross-frame spacing.

Adding a transverse stiffener strut to the internal cross-frames of box girder sections should not require extensive additional material or fabrication costs. There is already extensive welding required at the internal cross-frame location, and the transverse stiffener strut can be installed at the same time as the interior cross-frame. The transverse stiffener will control stiffener displacement at the internal cross-frame locations and significantly reduce the length of the unsupported longitudinal stiffener.

Transverse stiffener struts were used in a box girder bridge constructed in Houston, Texas. The designer included a transverse stiffener in every other interior cross-frame in the negative moment region. The resulting aspect ratio, a/b, of the bottom flange plate in this bridge was about 2. The AASHTO design capacity of this bottom flange was not increased by the inclusion of these transverse stiffener struts. However, stiffener displacement, such as that observed in the experimental program of this research, would be controlled by inclusion of these transverse stiffener struts.

The finite element model of the adequate test plate was used to examine the impact of transverse stiffeners. A single transverse stiffener was added to the FEM, positioned at the middle of the center span of the girder, at mid-length of the longitudinal stiffener. Both a fully connected transverse stiffener and a transverse stiffener strut, as shown in Figure 8.25, were studied. The fully connected transverse stiffener was attached to the webs of the girder, the longitudinal stiffener, and the compression plate. The transverse stiffener strut

was attached only to the webs of the box girder and to the longitudinal stiffener. The transverse stiffeners were sized using the guidelines in the ASD portion of the AASHTO Standard Specification in Section 10.39.4.4.2.

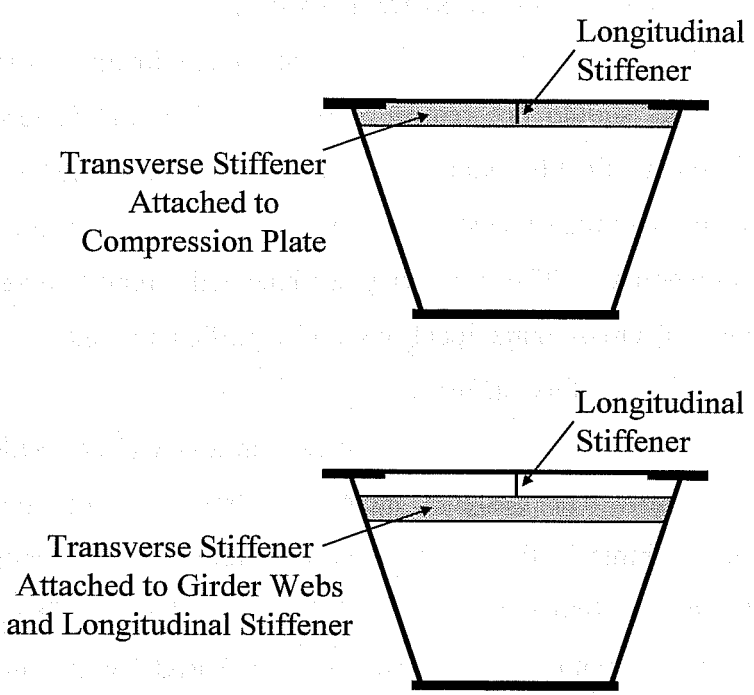

Figure 8.25 Finite Element Models with Transverse Stiffeners

The displaced shape of the plate with the full transverse stiffener and the transverse stiffener strut are shown in Figure 8.26. The displacement of the stiffener is substantially reduced with the transverse stiffener, and local plate displacements in some areas are larger than the stiffener displacements. The load displacement response of the test plates with no transverse stiffeners, full transverse stiffeners, and transverse stiffener struts are show in Figure 8.27 and Figure 8.28. Figure 8.27 shows the displacement at mid-length of the stiffener, where the transverse stiffener was positioned. Figure 8.28 shows the

displacement at the quarter point of the stiffener, at the middle of the new unsupported stiffener length, between the original transverse stiffener defining the end of the test plate and the transverse stiffener added at midspan.

At the transverse stiffener location, there was a very dramatic reduction in displacement. There was slight longitudinal stiffener displacement at the transverse stiffener due to bending of the transverse stiffener, but the magnitude of this displacement was very small. Displacement at the quarter point of the longitudinal stiffener was also significantly reduced by the addition of a transverse stiffener. The displacement was reduced about fourfold at this location.

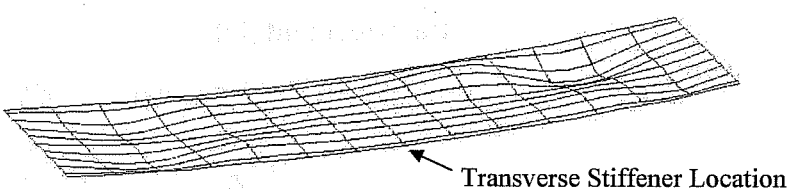

Full Transverse Stiffener

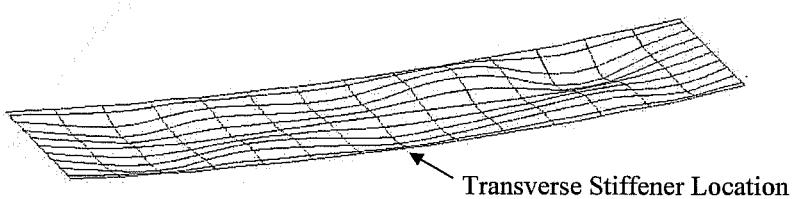

Transverse Stiffener Strut

Figure 8.26 Displaced Shape of Compression Plate with Transverse Stiffener

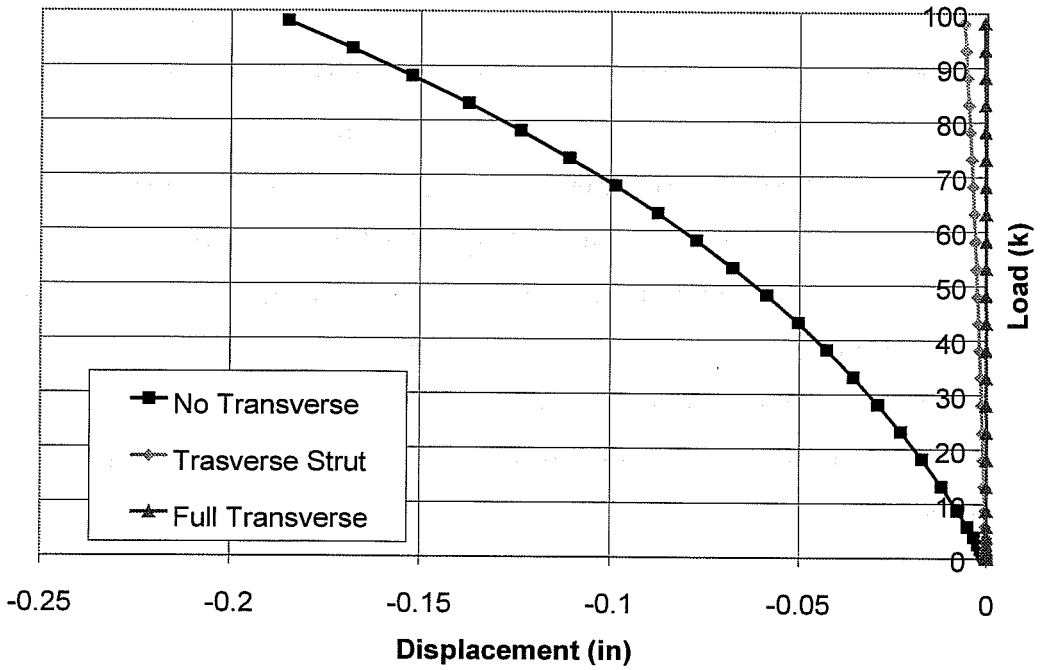

Figure 8.27 Displacement at Mid-Length of Stiffener

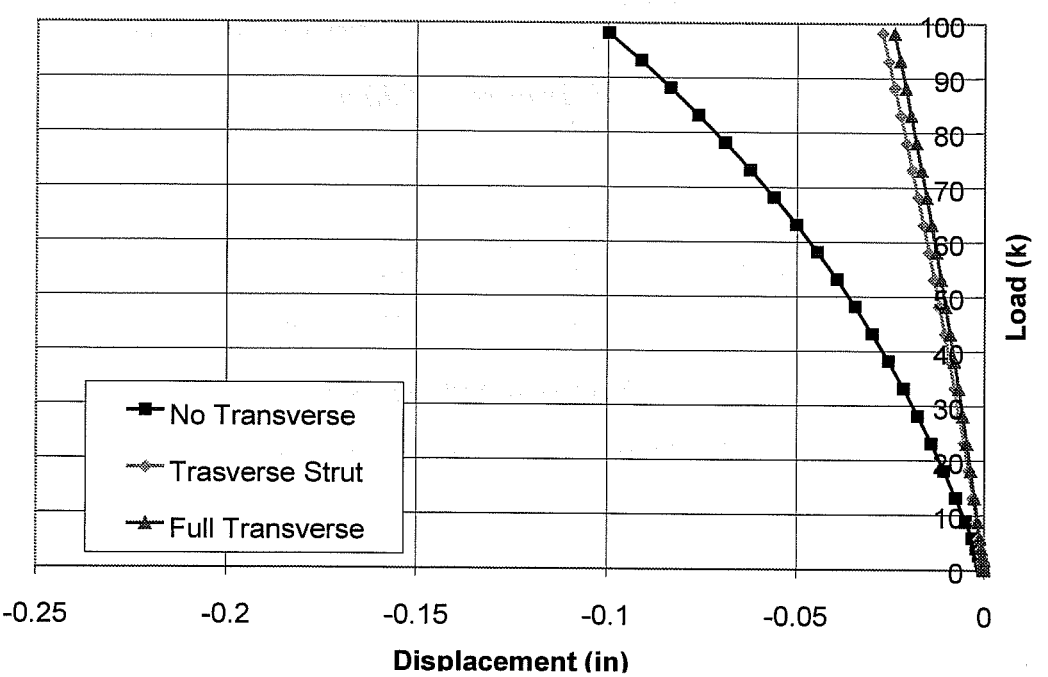

Figure 8.28 Displacement at Quarter Point on Longitudinal Stiffener

Comparing the full transverse stiffener, which was connected to the compression plate, and the transverse stiffener strut, there was a slightly larger reduction in displacement with the full transverse stiffener. However this slight reduction in displacement is not significant enough to justify use of the full transverse stiffener. With a fully welded transverse stiffener, two transverse stiffener pieces have to be used on either side of the longitudinal stiffener. These transverse stiffener sections must be welded at both ends of the transverse stiffener to the webs of the box girder and to the longitudinal stiffener. The transverse stiffener also has to be welded to the flange of the box girder. Using the transverse stiffener strut, a one-piece stiffener can span between the webs of the box. Much less welding is required to attach the stiffener strut to just the webs and longitudinal stiffener. Furthermore, welding the full transverse stiffener to the compression flange creates another poor fatigue detail, which is not desired.

The stresses generated in the adequate test plate with the full transverse stiffener and the transverse stiffener strut were compared. There was a slight decrease in the plate stress at the location of the transverse stiffener with the full transverse stiffener, but the plate stresses away from the transverse stiffener were the same for the full transverse stiffener and the transverse stiffener strut. There was no advantage in terms of design stress using a full transverse stiffener.

There does not seem to be any significant advantage to use of a full transverse stiffener instead of the transverse stiffener strut. The transverse stiffener strut controlled displacement of the longitudinal stiffener as was desired. Addition of the transverse stiffener strut should not cause a significant increase in material or fabrication costs, and will limit the undesired stiffener displacement observed in the experimental testing program.

8.5 Strut-Based Analysis Approach

As discussed, the stiffeners of the test plates tested in the experimental program did not form straight nodal lines. The maximum displacement actually occurred at the longitudinal stiffener. The basis of the AASHTO design equations for slender flanges is that adequate stiffeners remain straight, and that the plate buckles about the stiffener. This response was not seen in the experimental tests. The stiffeners displaced significantly in the tests. An alternate analysis approach that has been proposed for analysis of stiffened plates is use of a strut-based approach. The stiffener and associated plate width are treated as a column strut with an applied axial load. Consideration for the possibility of plate buckling between the stiffeners should also be included in design equations based on strut-based approaches.

The design approach used by Wolchuk in the Proposed Specifications for Steel Box Girder Bridges is a strut-based approach that makes allowance for plate buckling between the stiffeners. A key aspect of strut-based approaches is establishment of the strut length. The approach used by Wolchuk is based on the recommendations of Dwight and Little (Dwight 1973). Dwight et al present an approximate expression for the half-wavelength of the plate in the absence of transverse stiffeners. The length of the half-wavelength is

$$L_o = 2b\sqrt{r/t} \qquad (8.1)$$

where b is the plate width, r is the radius of gyration of the stiffener strut, and t is the plate thickness. A reduction factor, which takes into account the transverse bending stiffness of the plate, is applied to the smaller of the half-wavelength of the plate and transverse stiffener spacing to determine the strut length. The strut length, L, presented in the Proposed Design Specifications for Steel Box Girder Bridges is

$$L = \frac{L_o}{\sqrt{1 + \frac{[2 + (L_o/b)^2](L_o/b)^2}{18(r/t)^2}}} \tag{8.2}$$

A strut-based analysis of several stiffened plates was performed. The capacity determined from this analysis will be referred to as the capacity of the "strut approach" in the following discussion. A yield strength of 50 ksi was assumed in all of the analyses. Both slender plates and plates that fall into the transition region of the AASHTO design equations were analyzed. An initial imperfection of L/500, where L is the strut length, was assumed. This level of imperfection corresponds to typical stiffener tolerance limits presented in Chapter 3. The strut was analyzed as a column of length L with initial imperfections. Calculation of the maximum stress in a column with initial imperfections is discussed in mechanics of materials texts. The maximum stress in the column is given by the Perry Robertson formula:

$$\sigma_{max} = \frac{P}{A} + \frac{M_{max} c}{I} = \frac{P}{A}\left[1 + \frac{\Delta_o c}{r^2(1 - \frac{P}{P_e})}\right] \tag{8.3}$$

where P is the axial load, A is the cross-sectional area, M_{max} is the maximum bending moment, c is the distance from the centroidal axis to the concave side of the column, I is the moment of inertia, Δ_o is the initial imperfection, r is the radius of gyration of the strut, and P_e is the Euler buckling load of the pin-ended strut. Based on the response seen in the experimental tests, and subsequent finite element analysis, the compression flange side of the strut, as opposed to the stiffener side of the strut, is the concave side of the column, and therefore c will

be the distance from the outer surface of the compression flange to the centroid of the strut. The maximum absolute deflection at the middle of the strut is given by:

$$\Delta = \frac{\Delta_o}{1 - \frac{P}{P_e}} \tag{8.4}$$

The maximum stress in the strut was limited to the yield stress. The impact of residual stresses was included by using a design plate stress equal to the yield stress minus the assumed residual stress. Maximum permitted stresses of 50 ksi, assuming no residual stress, and 40 ksi, assuming a residual stress of 10 ksi, were used in the calculations. The capacity of the plates was also calculated using the AASHTO design equations and the Wolchuk strut capacity presented in the Proposed Design Specifications for Steel Box Girder Bridges. A FEM of the stiffened plate was also analyzed using ABAQUS. A plate length of L_o was used in the finite element model, and an initial imperfection of $L_o/500$ was included. The same failure criteria used in the strut approach, maximum compressive plate stress of 40 ksi and 50 ksi, was applied to the FEA.

Sample strut approach calculations for an 84 in. wide by 1.5 in. thick plate stiffened with a WT 12x42 are presented. The plate was not stiffened transversely. The longitudinal stiffener selected was sized to produce a plate buckling coefficient of 4 in the AASHTO capacity equations. The geometry and section properties of the stiffener strut are shown in Figure 8.29. An associated plate width of w, b/2, as recommended by Wolchuk, was assumed to act with the stiffener to form the column strut.

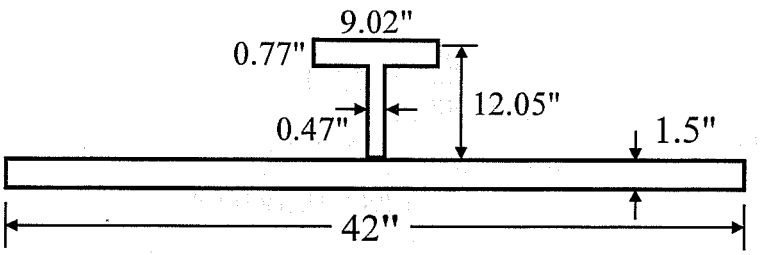

c = 2.221 in
I_x = 1098 in^4
A = 73.33 in^2
r = 3.870 in

Figure 8.29 Stiffener Strut of 84 in. x 1.5 in. Plate Stiffened with WT 12x42

$$\sigma_{max} = \frac{P}{73.33\,in^2}\left[1 + \frac{\frac{L}{500}(2.221\,in)}{(3.870\,in)^2\left(1 - \frac{PL^2}{\pi^2(29000\,ksi)(1098\,in^4)}\right)}\right] \tag{8.5}$$

The half-wavelength of the stiffened plate is

$$L_o = 2(84)\sqrt{3.870/1.5} = 269.8\,in \tag{8.6}$$

The reduced strut length is

$$L = \frac{269.8}{\sqrt{1 + \frac{[2 + (269.8/84)^2](269.8/84)^2}{18(3.870/1.5)^2}}} = 188.0\,in \tag{8.7}$$

As will be shown, the capacity of the stiffener strut is significantly influenced by its length. For comparison, both the half-wavelength, L_o, of the stiffened plate and the reduced strut length, L, were used to calculate the axial capacity of the strut. As noted, maximum permissible stresses of 50 ksi and 40 ksi were assumed. Lengths of 188.0 in., L, and 269.8 in., L_o, and σ_{max} of 50 and 40 ksi were substituted in Equation (8.5), and the strut capacity, P, was calculated. For a maximum stress of 50 ksi and a strut length of 188.0 in,

$$50\,\text{ksi} = \frac{P}{73.33\,\text{in}^2}\left[1 + \frac{\frac{188\,\text{in}}{500}(2.221\,\text{in})}{(3.870\,\text{in})^2\left(1 - \frac{P(188\,\text{in})^2}{\pi^2(29000\,\text{ksi})(1098\,\text{in}^4)}\right)}\right] \tag{8.8}$$

Solving the above equation yields a strut load P of 3365 kips. The capacity of the stiffened plate is calculated using the strut stress times the total area of the flange including longitudinal stiffeners.

$$\text{Plate Capacity} = \frac{3365\,\text{k}}{73.33\,\text{in}^2} = 45\,\text{ksi} \tag{8.9}$$

A summary of the plate configurations and results for four stiffened plates is presented in Table 8.2 and Table 8.3. Table 8.2 contains the plate geometry, plate slenderness, longitudinal stiffener used, AASHTO plate buckling coefficient for the given configuration, reduced strut length, L, and the half-wavelength of the plate, L_o. Table 8.3 contains the FEA results, and the capacities calculated using the AASHTO design equations, the Wolchuk strut chart, and the strut approach presented above.

Table 8.2 Plate Properties and Stiffener

CASE #	Plate bxt (in x in)	b/t	Stiffener	AASHTO k	L (in)	L_o (in)
1	60x0.5	120	0.5″x3″ Plate	2.1	86	130
2	60x0.5	120	WT4x9	4	136	195
3	84x1.5	56	WT6x17.5	2	116	175
4	84x1.5	56	WT12x42	4	188	270

Table 8.3 Stiffened Plate Capacity

CASE #	Finite Element Analysis Length = L_o		AASHTO	Wolchuk	Strut Approach Length = L		Strut Approach Length = L_o
	σ_{max} 50 ksi (kips)	σ_{max} 40 ksi kips	(kips)	(kips)	σ_{max} 50 ksi (kips)	σ_{max} 40 ksi kips	σ_{max}=50 ksi kips
1	23	21	15	N/A	15	14	7
2	33	29	29	21	28	27	14
3	42	34	46	32	38	32	21
4	46	37	49	41	45	36	33

8.5.1 Impact of Strut Length

Comparing the strut approach results for a maximum plate stress of 50 ksi with strut lengths of L and L_o, respectively, show the significant impact of the strut length on the capacity of the strut, particularly for slender plates. For the slender plate in Cases 1 and 2, the capacity calculated using the longer L_o length is approximately half that of the capacity calculated using a length of L. For the stockier plates, Cases 3 and 4, the capacity is also significantly less using the longer strut length, L_o.

A reduced length is used to take into account the additional stiffness from transverse bending of the plate. For the remainder of this presentation the strut approach capacities calculated using the reduced strut length, L, will be used. This reduced strut length showed better agreement with the finite element results using the actual plate length, L_o, for the strut length.

8.5.2 Comparison of FEA and Strut Approach (Strut Length L)

For σ_{max} of both 50 and 40 ksi, the strut approach gives conservative capacity estimates compared to the FEA. For the slender plates listed in Case 1 and 2, the strut approach is very conservative compared to the FEA results. The strut approach capacities for the slender plates are 10 to 35% less than the FEA results. For the stockier plates in Cases 3 and 4, capacity estimates using the strut approach are conservative, but show reasonable agreement with the FEA capacity. For the stocky plates the strut approach capacities are 2 to 10% less than the FEA results.

Comparing the FEA and strut approach capacities with maximum stresses of 50 ksi and 40 ksi, respectively, the impact of the residual stresses on the capacities of the slender plates is much less significant than the impact of residual stresses on the stockier plates. As discussed, residual stresses were included by reducing the maximum stress of the strut. A residual stress of 10 ksi, which has been reported as a conservative upper bound of expected compressive residual stress (FHWA 1980), was assumed.

The slender plate capacity, Cases 1 and 2, is reduced by 10% or less by inclusion of residual stresses. However, the capacity of the stockier plates, Cases 3 and 4, is reduced by 15 to 20% by the inclusion of residual stresses. As discussed in Chapter 3, residual stresses have been thought to have a significant impact on the capacity of stockier plates that fall into the inelastic region of the AASHTO design equations. The FEA and strut calculations for Cases 3 and 4 support the assertion that residual stresses significantly influence the capacity of such plates.

8.5.3 *Wolchuk Capacity*

The plate capacity was also calculated using the Wolchuk chart presented in the Proposed Design Specifications for Steel Box Girder Bridges. The design chart proposed by Wolchuk does not cover the slender flange with small stiffener configuration of Case 1. For Case 2, the Wolchuk capacity is significantly less than that obtained using the strut approach. The Wolchuk capacity chart indicates very low capacities for slender column struts.

For Cases 3 and 4, the Wolchuk capacity falls between the capacities of the strut approach using a design stress of 50 and that predicted using a stress of 40 ksi. The Wolchuk capacity is based on multiple residual stress levels, the combined effect of which has less impact on the design capacity than the 10 ksi assumed in the strut approach presented here.

8.5.4 *AASHTO Capacity*

The plate capacity was also calculated using the AASHTO design equations. The capacity indicated by the AASHTO equations is analogous to that of the strut approach for the slender plates in Cases 1 and 2. The capacity indicated by AASHTO is unconservative compared to the FEA and strut approach for the stockier plates in Cases 3 and 4, particularly for higher levels of residual stress.

8.5.5 *FEA and Strut Approach Deflections*

The maximum relative deflection of the plate using the strut approach was calculated using Equation (8.4), the initial imperfection of the strut, and the strut capacity presented in Table 8.3 for a σ_{max} of 40 ksi. The deflections from the strut approach, and the FEA are presented in Table 8.4. The deflections are normalized with respect to the plate thickness, t. An initial imperfection of $L_o/500$ was used

in the finite element analysis, and an initial imperfection of L/500 was used in the strut approach.

For the slender plates in Cases 1 and 2, the strut approach overestimates the deflection compared to the FEA results. The deflections calculated using the strut approach are about 12% higher than the FEA. For the stocky plates, the strut approach underestimates the deflection compared to the FEA. The deflections from the strut approach calculations are 10 to 15% less than that of the FEA. In general, the strut approach deflections showed reasonable agreement with the FEA results. The strut deflections were within 15% of that obtained from the finite element analysis. The strut approach may either underestimate or overestimate deflections depending on the geometry of the plate.

Table 8.4 FEA and Strut Approach Relative Deflection (σ_{max} = 40 ksi)

CASE #	Finite Element Analysis Length = L_o Δ/t	Strut Approach Length = L Δ/t
1	3.2	3.6
2	2.6	3.0
3	0.23	0.21
4	0.13	0.11

8.5.6 Conclusions of Strut Analysis Investigation

In summary, the behavior observed in the experimental tests did not agree with assumptions that form the basis of the AASHTO equations for stiffened plate behavior. Consequently, particularly for larger stiffeners, it seems appropriate to use an analysis approach other than the bifurcation plate buckling approach

currently forming the basis of the AASHTO equations. Use of an analytical approach that includes the effects of initial imperfections, residual stresses, and stiffener displacement is appropriate. The analytical approaches recommended in British specifications and by Wolchuk in the Proposed Design Specifications for Steel Box Girder Bridges use a strut-based analysis approach.

A strut design approach using the Perry-Robertson formula was evaluated. Stiffened plates of different slendernesses and with different stiffeners were modeled as struts and analyzed as initially imperfect columns. The strut calculations indicate conservative capacities compared to finite element results. The strut approach was very conservative for slender plates, but showed closer agreement for the stockier configurations more commonly used for bottom flanges of box girder bridges.

The AASHTO equations indicated conservative capacity estimates compared to the FEA for the slender flanges analyzed, but unconservative capacity estimates for the stockier flanges. The fact that the AASHTO design procedure does not include the possibility of stiffener displacement for adequate stiffeners may lead to unconservative capacity estimates in compression flange designs.

8.6 AASHTO and Strut Approach Capacities of Test Plates

The capacities of the inadequate, adequate, and angle test plates were calculated using the AASHTO LRFD design equations and the strut approach presented above. A σ_{max} of 40 ksi was assumed in the strut approach. A reduced strut length was used in the strut approach calculations based on an L_o equal to the transverse stiffener spacing of 84 in. Both an initial imperfection of L/500 and the stiffener imperfection measured in each test, shown in Chapter 7, were included in the strut calculations. The AASHTO and strut approach capacities are

presented in Table 8.5, along with the maximum stress applied to the plate during the test. Note that the maximum load applied to the plate during the test did not produce failure. No significant loss in performance was seen for any of the stiffened plates at the maximum load levels applied during the testing program.

Table 8.5 Test Plate Design Capacity

Test Plate	AASHTO LRFD (ksi)	Strut Approach (ksi)		Maximum Stress Applied in Test (ksi)
		Δ_o = L/500	Measured Δ_o	
Inadequate	9.8	9.0	8.9	17.7
Adequate	18.2	20.7	21.2	20.2
Angle	20.3	16.0	16.1	26.9

The strut approach capacities using a Δ_o of L/500 and the measured Δ_o are analogous for each test. The largest disparity, in the adequate test, resulted in less than 3% difference in the calculated capacities.

For the inadequate test plate, the strut approach indicates about 10% less capacity than the AASHTO equations. In the testing program, the inadequate test plate carried much higher stresses than the capacities indicated by either the AASHTO or strut approach. For the adequate test plate, the strut approach indicates about 13% higher capacity than the AASHTO equations. A maximum stress of 20.2 ksi, which is less than the strut approach capacity, was applied to the adequate test plate in the test. However, FEA analysis indicates that the adequate test plate could easily carry stresses up to and above that indicate by the strut approach calculations.

The maximum stress applied to the angle test plate was much larger than the capacity indicated by either the AASHTO or strut approach. For the angle test, the strut approach calculations indicate a capacity about 22% less than that of the AASHTO equations. The reason why the strut approach calculations indicate such a low capacity for the angle test plate is because of the angle stiffener configuration. The angle stiffener provided less stiffener moment of inertia than that of the plate stiffener used in the adequate test, but had a larger cross-sectional area. Consequently, the radius of gyration of the strut, r, using the angle stiffener was smaller than that of the adequate stiffener, and the distance from the centroidal axis to the compressive side of the strut, c, was greater with the angle stiffener. A smaller r and larger c both lead to higher calculated strut stresses, and subsequently lower indicated capacities for the angle test plate using the strut approach. In the formulation of a design procedure using a strut approach the likely configuration of longitudinal stiffeners must be considered.

8.7 Conclusions

The results of the analyses presented in this chapter show that plates with eccentric stiffeners respond differently than plates with stiffener pairs. The eigenvalue analysis procedures do not reveal the impact of eccentricity on adequate stiffeners, since the stiffeners are assumed to remain straight. Use of stiffener pairs showed better displacement control than eccentric stiffeners, but external stiffeners should not be used for longitudinal stiffeners of box girders. Analytical approaches such as the strut-based approach can include the stiffener eccentricity directly.

Inclusion of a moment gradient increased the eigenvalue buckling load of the plates studied. The moment gradient reduced displacement of the longitudinal

stiffener, but did not eliminate stiffener displacement or significantly change the overall response of the plate configurations studied.

Inclusion of transverse stiffener struts is an effective means of controlling displacement of the longitudinal stiffener. Transverse stiffener struts should be included at every internal cross-frame in the negative moment region. No significant advantage is seen with a transverse stiffener that is also welded to the bottom flange, and additional fabrication costs and fatigue concerns result from inclusion of fully welded transverse stiffeners.

A strut approach was described, and the capacity obtained using the strut approach was compared to the capacity given by AASHTO design equations and finite element analysis. The strut approach and AASHTO equations indicate conservative capacity estimates for the slender plates analyzed. The AASHTO equations indicated unconservative capacities compared to the FEA for the stockier plates analyzed. Thus, the AASHTO equations may be unconservative for certain plate geometries. The strut approach indicated close, but conservative, capacity estimates for the stockier plates analyzed.

Chapter 9

Summary and Conclusions

9.1 Summary

The design equations contained in the bridge specifications of the American Association of State Highway and Transportation Officials for compression flanges of box girder bridges are different in form than other bracing-design equations, and equations contained in other box girder specifications. The development of the design equations in AASHTO was researched and is recorded in this dissertation. The design equations for slender plates are based on elastic buckling theory with some simplifying assumptions. The capacity of stocky plates is limited by the yield stress of the plate, and the design of plates which are neither slender nor stocky is given by a transition equation.

The basis of the AASHTO equations for slender flanges was verified using eigenvalue finite element analysis. During the analytical investigation, it was discovered that alternate stiffener designs, utilizing torsionally rigid stiffeners, could result in significant increases of the elastic buckling strength of the stiffened plates. An experimental program was developed to experimentally test the performance of plates with torsionally weak stiffeners, typical of the current stiffener design used in the United States, as well as torsionally stiff longitudinal stiffeners. Plates with both steel and concrete longitudinal stiffeners were tested.

The results of the experimental testing program showed that the behavior of the stiffened plates did not agree with the predictions of the eigenvalue analysis and the assumptions that form the basis of the AASHTO design equations for

plates with adequate stiffeners. The basis of the AASHTO procedure for adequate stiffeners, enabling use of a plate buckling coefficient of 4, is that the stiffeners form straight nodal lines about which the plate will buckle. The experimental program showed that the stiffeners did not remain straight, and in fact the largest displacements generally occurred at the stiffeners. Several factors contributed to stiffener movement, including the initial imperfection of the stiffener, overall girder bending, the use of a single eccentric stiffener, and second order bending effects of the stiffener.

The capacity given by the AASHTO equations underestimates the strength of slender compression flanges. As shown by the test results, the full cross section of the plate, including the plate and stiffener, participates in carrying the compressive and bending stresses in the stiffened plate. The fundamental assumption of the AASHTO design approach, that the stiffeners form straight nodal lines, was not evidenced in the tests. The stiffener moved throughout application of load to the test setup. Linear elastic buckling theory does not allow for inclusion of the factors contributing to stiffener movement, such as initial stiffener imperfection, second order bending effects, and stiffener eccentricity. Consequently the AASHTO design approach, which is based on elastic buckling theory, does not give accurate predictions of the capacity of the stiffened plates.

Due to the displacement of the stiffener, and the resulting impact on the behavior of the stiffened plate, the extensive increase in performance indicated by eigenvalue analyses for the torsionally rigid stiffeners was not realized. Particularly with the soft concrete stiffener, large displacements, which were at times in excess of that of the unstiffened plate at the same load, were recorded. Use of the steel angle stiffener did result in smaller displacements at a given load, however, at this time no increase in the design capacity of plates with torsionally stiff longitudinal stiffeners is recommended. The behavior of the stiffened plates

tested did not match the assumptions of the eigenvalue analysis, and consequently it is recommended that another analysis approach be used to develop a new set of design equations.

To control the stiffener displacements observed in the experimental program, use of transverse stiffener struts in all internal cross-frames in the negative moment region is recommended. Stiffener displacement between transverse stiffeners still occurs, but the magnitude of the overall stiffener displacement is reduced. The design equations contained in the AASHTO ASD for flanges stiffened longitudinally and transversely can be utilized for design of these compression flanges at this time. The provisions of the AASHTO LFD and LRFD do not recommend use of or include design equations for flanges stiffened both longitudinally and transversely. The basis of the LFD and LRFD equations, which assumes that adequate longitudinal stiffeners remain straight, was not supported by the results of experimental tests. The direction of the LFD and LRFD specification approach in eliminating consideration of transverse stiffeners is not prudent. Neither the LFD nor LRFD specification include recommendations for inclusion of transverse stiffeners or design provisions for transverse stiffeners. The experimental program and subsequent finite element analysis show that there are many factors contributing to displacement of the stiffener. Inclusion of transverse stiffener struts in internal diaphragms in the negative moment region does not require substantial increase in material or fabrication costs, and effectively controls longitudinal stiffener displacement at the location of the transverse stiffener.

It is hoped that a future research effort will address development of new design equations for the AASHTO specifications using an analysis approach other than that forming the basis of the current design equations. Of the analysis approaches currently available, use of a strut-based approach seems most

attractive for development of new design provisions. Such a formulation can include the effects of stiffener imperfection and eccentricity that were found to be very important during this research. The strut-based approach should also make consideration of the potential for plate buckling between stiffeners. The impact of overall girder bending on the stress distribution in the stiffener should be considered in the development of the provisions. The basis of the provisions presented in the Proposed Design Specifications for Steel Box Girder Bridges should provide a good starting point for this work. However, a numerical presentation of capacity rather than a graphical presentation, such as that contained in the Proposed Design Specifications for Steel Box Girders, is recommended. Furthermore, given the fact that the Proposed Designs Specifications have not been adopted by AASHTO, the new set of design equations must not be unnecessarily complicated and the basis of the approach must be clearly stated and documented.

9.2 Conclusions

The results of this study indicate that:

1. The current AASHTO design provisions yield a conservative estimate of the capacity of the slender flanges tested.
2. The current formulation of the AASHTO equations for flanges stiffened only longitudinally severely underestimates the capacity of flanges with small longitudinal stiffeners. Small longitudinal stiffeners in this case are stiffeners that currently result in a buckling coefficient less than 2 in the AASHTO equations. The current formulation can indicate stiffened plate capacities that are less than that of an unstiffened plate of the same geometry. New design equations were developed that agree well with the current

requirements for larger stiffeners, and provide rational solutions for plates with smaller stiffeners.

3. The assumptions of the eigenvalue/elastic buckling theory approach that is the basis of the current AASHTO design provisions do not agree with the observed experimental behavior of the stiffened compression flanges tested. The AASHTO design approach assumes the large stiffeners form straight nodal lines. This behavior was not seen in the experimental program.
4. The presence of initial imperfections in the plate, and particularly initial out-of-straightness of the stiffener, significantly affected the load-displacement response of the stiffened plates tested. Tolerances of plate and stiffener initial imperfections were researched and are presented. Imperfection tolerances for bottom flanges should be included in AASHTO and AWS specifications.
5. Stiffener eccentricity contributed to increased displacements due to girder bending and second order effects.
6. The stiffener displacements observed in this research program can be limited using transverse stiffener struts attached to the interior cross-frames of box girder sections in the negative moment region. For the resulting flanges, stiffened both longitudinally and transversely, smaller longitudinal stiffener sizes are "adequate" to produce a buckling coefficient of 4 when multiple longitudinal stiffeners are used, as indicated by the ASD provisions, finite element analysis performed during this dissertation research, and recent results by Yoo et al (Yoo 2001).
7. Use of a torsionally stiff steel longitudinal stiffener resulted in smaller displacements at a given load than a torsionally weak stiffener with a

comparable stiffener moment of inertia. No negative performance issues specific to torsionally rigid steel stiffeners were observed. Positive aspects of torsionally rigid steel stiffeners include stabilization of a larger plate width in the neighborhood of the stiffener, increased fabrication ease, and reduced stiffener displacement. Use of closed stiffener shapes is recommended.

9.3 Future Research Needs

A key aspect of the AASHTO equations is that an optimum or adequate stiffener size results in the stiffener forming a straight nodal line. Using a stiffener that is larger than the adequate size is not accompanied by an increase in capacity compared to that of a plate with an adequate stiffener. As shown in experimental tests and subsequent finite element analysis, the stiffener does not actually remain straight due to a variety of factors, including stiffener imperfection, overall girder bending, stiffener eccentricity and second order effects. Consequently stiffeners larger than an "adequate" stiffener can produce a larger stiffened plate capacity. An analysis approach capable of incorporating factors such as stiffener imperfection, stiffener eccentricity, bending effects and residual stresses should be used to develop new provisions which agree with the actual response of the stiffened plate under load.

Use of a strut-based approach, with consideration of plate buckling between the stiffeners, appears to be a reasonable alternative for the stiffened plate designs typically used for compression flanges of box girder structures constructed in the United States. These structures typically have few longitudinal stiffeners and may not be realistically modeled by orthotropic plate approaches that treat the stiffened plate as a grillage and other approaches that smear the stiffeners across the plate.

The lack of acceptance by the engineering community of the strut-based approach presented in the Proposed Design Specifications for Steel Box Girder Bridges must be kept in mind in the development of new provisions. The proposed design requirements should be clear and their basis well documented. Furthermore, the requirements should be presented in numerical equations, not a graphical format, so that they can be easily codified in spreadsheets and software packages. The fundamental inadequacies in the assumptions forming the basis of the AASHTO provisions warrant the production and adoption of new equations.

9.3.1 Single Box Systems

There is significant resistance to moving to larger, more heavily stiffened boxes. Design of these box girders demands more rigorous attention and requires use of more sophisticated analyses and more rigorous design procedures. Fabrication of these boxes is more complex, and challenges the state-of-the-art of steel box bridge fabrication. Fabricators and DOT personnel are not anxious to undertake design and construction of larger box girders with more slender panel elements. However, greatest economy will most certainly be achieved through using a minimal number of girders. Fabricators have reported that the cost per pound of box girders is higher than that of I-girders, but through a lower overall box weight with a single larger box, and subsequent reductions in substructure costs, the box girder section can become more economically competitive. Single box cross sections with one pier shaft can be utilized, especially for the flyover ramps where boxes are currently seeing significant application in Texas. Use of a single box is possible based on the significant torsional stiffness of the section, and the subsequent ability to use larger overhangs.

Texas is making extensive use of box girders because of the increased importance of bridge aesthetics. The bridge sections being designed use multiple

boxes, and the resulting designs are not necessarily economically competitive, but are selected because aesthetic concerns override. It will be difficult to encourage designers, fabricators, and Departments of Transportation to move to more sophisticated, single box bridge cross sections, such as those used in Europe. But by moving to more sophisticated designs, and by further exploiting the available benefits of the box girder design, it should be possible to make box girders economically, as well as aesthetically, attractive.

References

AASHO 1969 — *AASHTO Standard Specifications for Highway Bridges*, American Association of State Highway Officials, Washington, DC 1969.

AASHTO 1996 — *AASHTO Standard Specifications for Highway Bridges*, 16th Edition, American Association of State Highway and Transportation Officials, 1996.

AASHTO 1998 — *AASHTO LRFD Bridge Design Specifications*, Second Edition, American Association of State Highway and Transportation Officials, 1996.

AASHTO 1998b — *AASHTO LRFD Bridge Construction Specifications*, First Edition, American Association of State Highway and Transportation Officials, 1998.

ABS 2001 — *Rule Requirements for Materials and Welding 2001, Part 2,* American Bureau of Shipping, Houston, TX, 2000.

AISC 1943 — *Steel Construction, A Manual for Architects, Engineers and Fabricators of Buildings and Other Steel Structures*, American Institute of Steel Construction, Fourth Edition, New York, NY, 1943.

AISC 1994 — *AISC Load and Resistance Factor Design Specification for Steel Buildings*, Manual of Steel Construction, American Institute of Steel Construction, 1994.

Alinia 2001 — Alinia, MM, Box Girders: Constant Depth, April 26, 2001, http://www.aku.ac.ir/faculty1/aliniamm/Structural%20Slides/beams/Box%20girders%20constant%20depth.htm.

ASCE 1974 — ASCE-AASHTO Task Committee on Flexural Members, "Steel Box-Girder Bridges - Ultimate Strength Considerations," *ASCE Journal of the Structural Division*, Vol. 100, No. ST12, Dec. 1974, pp. 2433-2448.

ASTM A6-01 — *ASTM A6/A 6M-01 Standard Specification for General Requirements for Rolled Structural Steel Bars, Plates, Shapes and Sheet Piling,* American Society for Testing and Materials, 2001.

ASTM 1946 — *ASTM Standards, Part I-A Ferrous Metals*, American Society for Testing Materials, Philadelphia, PA 1947.

ASTM A6-58 — ASTM A6-58 *General Requirements for Delivery of Rolled Steel Plates, Shapes, Sheet Piling, and Bars for Structural Use,* American Society for Testing and Materials, 1958.

AWS 1947 — *Standard Specifications for Welded Highway and Railway Bridges*, Fourth Edition, American Welding Society, New York, 1947.

AWS 1956 — *Standard Specifications for Welded Highway and Railway Bridges*, Fifth Edition, American Welding Society, New York, 1956.

AWS 1972 — *AWS Structural Welding Code*, AWS D1.1-72, American Welding Society, Miami, FL 1972.

AWS D1.5 — *AWS Bridge Welding Code*, ANSI/AASHTO/AWS D1.5-96, American Welding Society, 1996.

AWS D1.1 — *AWS Structural Welding Code - Steel*, AWS D1.1:2000, 17th Edition, 2000.

Bleich 1952 — Bleich, Friedrich, "Buckling Strength of Metal Structures," McGraw-Hill Book Company, Inc., New York, 1952.

Blodgett 1966 — Blodgett, Omer W., "Design of Welded Structures", The James F. Lincoln Arc Welding Foundation, Cleveland, Ohio, June 1966.

Chen 1999 — Chen, Brian Scott, "Buckling of U-Shaped Girders with Top-Flange Lateral Bracing, Thesis presented to The University of Texas at Austin, in partial fulfillment of the degree of Master of Science in Engineering, May 1999.

Chen 2000 — Chen, Brian S., Survey of Box Girder Fabricator, December 14, 2000.

Corrado 1965 — Corrado, J.A., J.A. Mueller, and B.T. Yen, "Fatigue Tests of Welded Plate Girders in Bending", Fritz Engineering Laboratory Report No. 303.9, Lehigh University, Bethlehem, PA, May 1965.

Dwight 1973 — Dwight, J.B., G. H. Little, and N. A. Rogers, "An Approach to Stiffened Steel Compression Panels", CUED / C-Struct / Tr.32 (1973).

ECCS 1986 — Dubas, P. and E. Gehri, editors, *Behaviour and Design of Steel Plated Structures*, European Convention for Constructional Steelwork, Applied Statics and Steel Structures, 1986.

Fan 1999 — Fan, Z. and T. Helwig, "Behavior of Steel Box Girders with Top Flange Bracing," *Journal of Structural Engineering*, American Society of Civil Engineers, Vol. 125, No. 8, 1999, pp. 829-837.

FloorPro 2001 — Ytterberg Scientific, Inc., May 1, 2001, http://www.flatfloors.com.

Fok 1984 — Fok, Wing-Chau, "Evaluation of Experimental Data of Plate Buckling," *Journal of Engineering Mechanics*, Vol. 110, No. 4, April 1984, pp. 577-588.

Ford 2000 — Ford, Elizabeth Michelle, "Stiffness Requirements for Longitudinally Stiffened Compression Flanges," Thesis Submitted to Graduate Faculty of Auburn University in Partial Fulfillment of the Requirements for the Degree of Master of Science, June 10, 2000.

Fukumoto 1974 — Fukumoto Yuhshi, Tsutomu Usami, and Yoshio Okamoto, "Ultimate Compressive Strength of Stiffened Plates," Specialty Conference on Metal Bridges, American Society of Civil Engineers, November 12 and 13, 1974, pp. 201-218.

Gilbertsen 1980 — Gilbertsen, N.D. and J.P. Moehle, "Experimental Study of Small-Scale R/C Columns Subjected to Axial and Shear Force Reversals," Civil Engineering Studies, Structural Research Series No. 481, University of Illinois, Urbana, July, 1980.

Ghavami 1994 — Ghavami, K., "Experimental Study of Stiffened Plates in Compression up to Collapse," *Journal of Constructional Steel Research*, Vol. 28, 1994, 197-221.

Gilmer 2001 — Gilmer, Heather, Personal Correspondence, 2001.

Hall 1997 — Hall, Dan H., "Why Steel Box Girders?," Reprinted from *Modern Steel Construction*, No. 6, April 1997.

HKS 1995 — *ABAQUS/Standard User's Manual*, Version 5.5, Pawtucket, RI, 1995.

Hutchison 2001 — *The Hutchinson Family Encyclopedia*, April 26, 2001, http://ebooks.whsmithonline.co.uk/encyclopedia/82/M0015582.htm.

J. Muller 1996 — "Steel/Composite Optimization Study, Phase II - Concept Design Alternates CC-3320 (Draft)," prepared by J. Muller International Bridge Engineering Consultants, American Iron and Steel Institute - Transportation Structures Committee, August 1996.

Joehnk 1982 — Joehnk, John Michael, "Fatigue Behavior of Welded Joints Subjected to Variable Amplitude Stresses," Thesis presented to The University of Texas at Austin, in partial fulfillment of the degree of Master of Science in Engineering, August 1982.

Johnson 1986 — Johnson, RP and RJ Buckby, *Composite Structures of Steel and Concrete*, Volume 2, 1986.

Kasparova 1983 — Kasparova, Helena, Vladmir Kristek, and Miroslav Skaloud, "On Some Stability Problems of Steel Box Girder Bridges," *Acta Technica CSAV*, Vol. 29, No. 6, 1983, pp. 716-734.

Korol 1984 — Korol, R.M., Thimmhardy, E.G., and M.S. Cheung, "Field Investigation of Out-of-Plane Deviations for Steel Box Girder Bridges," *Canadian Journal of Civil Engineering*, Vol. 11, No. 3, Sep. 1984, pp. 377-386.

Kumarasena 2001 — Kumarasena, Sena T. and Raymond J. McCabe, "Designing Boston's Storrow Drive Connector Bridge: Steel Alternatives Chosen for Cost and Constructability," HNTB Corporation, April 27, 2001, http://bridges.hntb.com /downloads/Storrow%20Article.pdf.

Maeda 1975 — Maeda, Yukio and Takashi Hikasa, "Analysis of Buckling of Stiffened Plates with Residual Stresses," 1975, pp. 299-309.

Mattock 1967 — Mattock, A. H., "Commentary on Criteria for Design of Steel-Concrete Composite Box Girder Bridges," (unpublished), 1967.

Mueller 1967 — Mueller, J.A. and B.T. Yen, "Girder Web Boundary Stresses and Fatigue," Fritz Engineering Laboratory Report No. 327.2, Lehigh University, Bethlehem, PA, July 1967.

NORSOK 1998 — *Design of Steel Structures*, NORSOK STANDARD N-004, Norwegian Technology Standards Institute, Oslo, Norway, Rev. 1, December 1998.

Ontario 1991 — *Ontario Highway Bridge Design Code*, Third Edition, Ontario Ministry of Transportation, Quality and Standards Division, 1991.

Parsanejad 1970 — Parsanejad, Siamak and Alexis Ostapenko, "Fatigue Strength of Unsymmetrical Plate Girders," Fritz Engineering Laboratory Report No. 328.15, Lehigh University, Bethlehem, PA, May 1970.

Sen et al 1999 — Sen, R., S. Stroh, J. Olbinska, S. Hassiotis, and G. Mullins, "Development of a New Concept for Florida's Bridges," Volume I, Florida Department of Transportation, Contract BB 522, Tampa, Florida, January 1999.

Singer 1998 — Singer, J., J. Arbocz, and T. Weller, *Buckling Experiments: Experimental Methods in Buckling of Thin-Walled Structures*, Vol. 1, John Wiley and Sons, West Sussex, England, 1998.

Skaloud 1984 — Skaloud, Miroslav, and Marie Zornerova, "Effect of Residual Stresses on the Stability Problem of Longitudinally Stiffened Compression Flanges," *Acta Technica CSAV*, Vol. 29, No. 2, 1984, pp. 242-253.

Tamura 1993 — Tamura, Todd T., "Development of a Field Method to Measure Out-of-Flatness of Structural Steel Plates," Master's Thesis, The University of Texas at Austin, August 1993.

TEC 2001 — The Engineering Center, June 3, 2001, http://www.engineers.org/acec/hntb.html.

Thimmhardy 1988 — Thimmhardy, Eugene G., and Korol, Robert M., "Geometric Imperfections and Tolerances for Steel Box Girder Bridges," *Canadian Journal of Civil Engineering*, Col. 15 No. 3, June 1988, pp. 437-442.

Timoshenko 1961 — Timoshenko, Stephen and James Gere, *Theory of Elastic Stability*, Second Edition, Mc-Graw Hill Book Company, Inc., New York, NY, 1961.

TxDOT 1993 — *TxDOT Standard Specifications for Construction of Highways and Bridges*, Texas Department of Transportation, March1, 1993.

Wolchuk 1980 — Wolchuk and Mayrbaurl Consulting Engineers, "Proposed Design Specifications for Steel Box Girder Bridges," Report No. FHWA-TS-80-205, Federal Highway Administration, Washington, DC, January 1980.

Wolchuk 1981 — Wolchuk, R., "Design Rules for Steel Box Girder Bridges," *International Association for Bridge and Structural Engineering Proceedings P-41/81*, Zurich, Switzerland, May 1981

Yen 1966a — Yen, B.T. and J.A. Mueller, "Fatigue Tests of Large-Size Welded Plate Girders," Fritz Engineering Laboratory Report No. 303.10, Lehigh University, Bethlehem, PA, June 1966.

Yen 1966b — Yen, B.T. and J.A. Mueller, "A Summary Report on the Behavior of Thin-Web Plate Girders Under Repeated Loading," Fritz Engineering Laboratory Report No. 303.13, Lehigh University, Bethlehem, PA, August 1966.

Yen 1986 — Yen B.T., T. Huang, D. Wang, C.K. Chuang, and J.H. Daniels, "Composite Compression Bottom Flange for Steel Box Girders," Fritz Engineering Laboratory Report No. 489.3, Lehigh University, Bethlehem, PA, January 1986.

Yen 1986b — Yen, B. T.; T. Huang, D. Wang, C.K. Chuang, J.H. Daniels, "Steel Box Girders with Composite Bottom Flanges," *Official Proceedings - 3rd Annual International Bridge Conference*, Pittsburgh, PA, 1986, p 79-86.

Yoo 2001 — Yoo, Chai Y., Byung H. Choi, and Elizabeth M. Ford, "Stiffness Requirements for Longitudinally Stiffened Box Girder Compression Flanges," Submitted for Publication in *Journal of Structural Engineering*, American Society of Civil Engineers, Manuscript #ST/2000/022319, 2000.

Vita

Reagan Sentelle Herman was born in Charlotte, NC on February 6, 1971, to David B. and Jane O. Sentelle. She graduated from A. C. Reynolds High School, Asheville, North Carolina, in 1989, and entered North Carolina State University in Raleigh, North Carolina in fall of the same year. She graduated Summa Cum Laude with the degree of Bachelor of Science from North Carolina State University in May 1993. She married Jerry Wayne Herman on July 31, 1993. In August 1993 she entered The Graduate School at The University of Texas. Under the supervision of Dr. James O. Jirsa, she completed a thesis entitled "Consolidation of Concrete with Epoxy-Coated Reinforcement," and received the degree of Master of Science in Engineering in December 1995. She then began her doctoral work.

Permanent address: 1720 Wells Branch Pkwy #5104
Austin, TX 78728

This dissertation was typed by the author.